Report 41164R02

ADAPTIVE FULL-SPECTRUM SOLAR ENERGY SYSTEMS

Cross-Cutting R&D on adaptive full-spectrum solar energy systems for more efficient and affordable use of solar energy in buildings and hybrid photobioreactors

Semi-Annual Technical Progress Report

April 1, 2002 – August 31, 2002

Byard D. Wood, Project Director
Mechanical Engineering Department
Mail Stop 312
University of Nevada, Reno
Reno, NV 89557

Jeff D. Muhs, Principal Investigator
Oak Ridge National Laboratory
2360 Cherahala Blvd.
Bldg. NTRC, MS 6472
Knoxville, TN 37932

PREPARED FOR

NATIONAL ENERGY TECHNOLOGY LABORATORY
THE UNITED STATES DEPARTMENT OF ENERGY

DOE Award Number DE-FC26-01NT41164
Energy Crosscutting Science Initiative
Office of Energy Efficiency and Renewable Energy

Date Published – September 2002

ABTRACT

This RD&D project is a three year team effort to develop a hybrid solar lighting (HSL) system that transports day light from a paraboloidal dish concentrator to a luminaire via a large core polymer fiber optic. The luminaire can be a device to distribute sunlight into a space for the production of algae or it can be a device that is a combination of day lighting and florescent lighting for office lighting. In this project, the sunlight is collected using a one-meter paraboloidal concentrator dish with two-axis tracking. The secondary mirror consists of eight planar-segmented mirrors that direct the visible part of the spectrum to eight fibers (receiver) and subsequently to eight luminaires. This results in about 8,200 lumens incident at each fiber tip. Each fiber can illuminate about 16.7 m^2 (180 ft^2) of office space. The IR spectrum is directed to a thermophotovoltaic array to produce electricity. This report describes eleven investigations on various aspects of the system. Taken as a whole, they confirm the technical feasibility of this technology.

PREFACE

This report is a joint effort between Oak Ridge National Laboratory and the University of Nevada, Reno, as such it satisfies the reporting requirements for the University and ORNL as the M&O for this project. Although this report emphasizes the results of the second half of Budget Period 1, it details all of the progress during Budget Period 1.

TABLE OF CONTENTS

LIST OF FIGURES

PARTICIPATING ORGANIZATIONS

Organization	Abbreviation	Principal Investigator
University of Nevada, Reno	UNR	Byard Wood
Oak Ridge National Lab P.O. Box 2009, MS-8058 Oak Ridge, TN 32831	ORNL	Jeff Muhs
Honeywell Technology Center 3660 Technology Drive Minneapolis, MN 55418	Honeywell	Robert Schnell
JX Crystals, Inc. 1105 12th Avenue NW, Suite A2 Issaquah, WA 98027	JXC	Lewis Fraas
Ohio University Dept. of Mechanical Engineering 248 Stocker Center Athens, OH 45701-2979	OU	David Bayless
Rensselaer Polytechnic Institute Lighting Research Center 21 Union Street Troy, NY 12180-3352	RPI	Nadarajah Narendran
Science Application International Corporation 9455 Towne Centre Drive San Diego, California 92121	SAIC	Robin Taylor
3M Company 3M Corporate Process Technology Center St. Paul, MN 55144-1000	3M	Jennifer Sahlin
TVA Public Power Institute 1101 Market Street, MR 2T Chattanooga, TN 37402-2801	TVA	David Dinse
University of Arizona Department of Agricultural and Biosystems Engineering 507 Shantz Building Tucson, AZ 85721	UA	Joel Cuello
University of Wisconsin Solar Energy Lab 1500 Johnson Dr. Madison, WI 53706	UW	William Beckman

The contributions of each of these individuals in the preparation of this report are gratefully acknowledged.

EXECUTIVE SUMMARY

This RD&D project is a three year team effort to develop a hybrid solar lighting (HSL) system that transports day light from a paraboloidal dish concentrator to a luminaire via a large core polymer fiber optic. The luminaire can be a device to distribute sunlight into a space for the production of algae or it can be a device that is a combination of day lighting and florescent lighting for office lighting. In this project, the sunlight is collected using a one-meter paraboloidal concentrator dish with two-axis tracking. The secondary mirror consists of eight planar-segmented mirrors that direct the visible part of the spectrum to eight fibers (receiver) and subsequently to eight luminaires. This results in about 8,200 lumens incident at each fiber tip. The IR spectrum is directed to a thermophotovoltaic array to produce electricity. This report describes the technical progress during budget period 1 (August 2, 2001 through August 31, 2002).

The goals of this project are to:

1. Determine technical feasibility of using full-spectrum solar energy systems to enhance the overall sunlight utilization in buildings and biomass production rates of photobioreactors. This will be accomplished by developing a benchmark prototype system.

2. Determine the commercial viability of using full-spectrum solar energy systems to enhance the overall sunlight utilization in buildings and biomass production rates of photobioreactors. This will be accomplished by determining those characteristics that characterize performance efficiency, reliability, durability and ultimately minimum cost potential.

3. Demonstrate the HSL technology in a building application and a photobioreactor application. The emphasis in developing the demonstration systems will be to meet performance objectives at minimum cost.

During Budget Period 1, the project team has made significant progress towards understanding of the basic principles that govern the design of hybrid solar lighting systems. The R&D to date has been directed towards establishing the technical feasibility of the proposed concept. The research thus far has shown that the proposed concept is technically feasible. Accomplishments to date are:

1. For the design proposed, the optical fiber must transport approximately 8,000 -10,000 lumens of daylight. The primary candidate for the large-core optical fiber is the 12mm 3M LF 120B polymer light fiber manufactured by 3M Company. The fiber is comprised of a crosslinked methacrylate-type polymer core. Experiments have shown that it is capable of transporting up to 12,000 lumens.

2. For the proposed/collector receiver, a high quality concentrating mirror that could supply the required lumens to eight fibers was commercially available. This concentrator was used to build a benchmark prototype collector/receiver to accelerate determining the technical feasibility process. The receiver consists of eight planar mirrors that reflect the sun light to the eight fibers. The prototype has been constructed and tested with satisfactory performance. The mirror's physical description is 46.5 in. diameter formed glass mirror with 16.5 in. focal length (f/D = 0.35) with enhanced aluminum coating.

3. A prototype 2 ft x 4 ft x 4 in. luminaire has been designed and built for the photobioreactor application. Preliminary experiments have shown satisfactory performance.

4. A hybrid luminaire that consists of two 4 ft T-8 florescent light tubes and one day light diffuser in the form of a 4 ft straight rod has been built to demonstrate the concept. The diffuser rod is

commercially available from 3M (Part #: LF-180-EX-D-1M). Total optical efficiency of Hybrid Luminaire was measured to be 58.4% for fiber optic sources and 85% for fluorescent sources. A significant amount of fiber optic loss was attributed to the fiber-to-rod coupling (≈20% loss). Team experience with other coupling issues suggests that this loss can be reduced significantly. ORNL has been experimenting with a Fresnel diffuser that is approaching the same efficiency as that for fluorescent lighting.

5. The team has developed excellent ray trace computational capabilities that allow the evaluation of optical designs for the collector/receiver with turn-around times in the order of a few days.

6. A thermal management model has been developed to evaluate fiber temperatures in the entrance region for the fiber. Calculations have shown that IR filters are effective in maintaining fiber tip temperatures below fiber deformation temperatures. The critical entrance length is less than 3 cm. Experiments with the prototype collector receiver have shown that a 3 cm quartz rod placed in front of the fiber prevents the fiber tip from reaching deformation temperatures.

7. The thermophotovoltaic array uses Gallium Antimony cells. The measured conversion efficiency on a single 1.0 m^2 cell was 15.3%. The use of an AR coating should increase it to 17.8%.

8. An adaptive, full-spectrum solar energy system model using performance data from the prototype components has been developed using the system simulation program TRNSYS. Some preliminary calculations have been completed. In Madison, WI, a single hybrid lighting unit (1.8 m^2) can supply 29% of the annual lighting needs for a floor area of 200 square meters (2153 square feet or 179 ft^2 per fiber) and in Reno, NV that same unit will provide 51% of the lighting demand. The figures are based on annual beam normal radiation in Madison, WI, and Reno, NV, a 50 % occupancy schedule, and an illumination level of 500 Lux (typical of office space). The area was selected by specifying the best day of the year as having no excess lighting. The best days in Reno and Madison differ only slightly with Reno having about 5% more beam. However, Reno has many more clear days than does Madison.

9. Characterizing the losses when two fibers are joined together is an important part of technical feasibility. A variety of connections have been investigated. Thus far the minimum loss occurs when the mating ends are machined polished with the face perpendicular to the fiber longitudinal axis with an index matching medium applied at the interface. The losses for this connection are less than 3%.
10. Ray tracing calculations show that the tracking accuracy in both the altitude and azimuth directions must be +/- 0.125 degrees. Two tracking mechanisms were tested: WattSun and SolarTrak. The WattSun system uses sun seeking sensors and the SolarTrak uses a clock system. On clear days, both tracking systems worked within specifications. For less than clear days the WattSun tracker was unacceptable while the SolarTrak worked well.

11. A Lab-Scale Hybrid Solar Photobioreactor has been built at Ohio University. The significant accomplishments include:
    - Candidate Organisms Evaluated
    - Candidate Growth Surfaces Tested
    - Alternative Growth Enhancement / Harvesting Methods Tested
    - One Solar Collector and 8 Light Distribution Panels have been installed at the pilot-scale bioreactor site

PROJECT DESCRIPTION

This project is part of the FY 2000 Energy Efficiency Science Initiative that emphasized Cross-Cutting R&D in Solicitation No.: DE-PS36-00GO10500. It is a three year research project that addresses key scientific hurdles associated with adaptive, full-spectrum solar energy systems and associated applications in commercial buildings and new hybrid solar photobioreactors. The goal of this proposal is to demonstrate that full-spectrum solar energy systems can more than double the affordability of solar energy in commercial buildings and hybrid solar photobioreactors used in CO_2 mitigation and compete favorably with existing alternatives.

The proposed research has the potential to provide potential energy-savings of 0.3 Quads and carbon reductions of 45 MtC per year by 2020, as well as economic benefits totaling over $15 billion in the United States alone. Adaptive, full-spectrum solar energy systems represent a new, systems-level approach to solar energy that holds the promise of dramatically improving its end-use efficiency and affordability in two ways. First, it more efficiently uses different portions of the solar spectrum simultaneously for multiple end-use applications such as solar lighting and distributed power generation, e.g., combined solar light and power. Second, it continually optimizes solar energy end-use efficiency by adapting to real-time changes in end-use needs and external factors such as real-time electricity prices, solar availability, and ancillary services. In order to realize the above benefits, key scientific hurdles must be addressed. Accordingly, the research team will:

1. Determine technical feasibility and economic viability of using full-spectrum solar energy systems to enhance the overall sunlight utilization in buildings and biomass production rates of photobioreactors. (Demonstrate a 2X – 5X improvement in solar energy end-use efficiency.)

2. Design solar collector/receiver with large-core optical fiber light distribution system that efficiently delivers the visible portion of direct sunlight to multiple remote locations for illumination purposes while simultaneously converting the IR portion of the solar spectrum into electricity using ideally-suited infrared thermophotovoltaics.

3. Develop intelligent control strategies that continuously-optimize energy-efficiency in buildings through the integration of sensor data, dynamic end-use requirements, and other relevant building and solar meteorology information

SCOPE OF WORK

The key scientific hurdles are being addressed in a three phase effort, viz.:

Phase I. Assess Technical Feasibility
Determine technical feasibility of using full-spectrum solar energy systems to enhance the overall sunlight utilization in buildings and biomass production rates of photobioreactors. This will be accomplished by developing a benchmark prototype system that can evaluate the solar lighting technology that was outlined in the original proposal.

Phase II. Assess Commercial Viability
Determine the commercial viability of using full-spectrum solar energy systems to enhance the overall sunlight utilization in buildings and biomass production rates of photobioreactors. This

will be accomplished by determining those characteristics that characterize performance efficiency, reliability, durability and ultimately minimum cost potential.

Phase III. Assess System Affordability
Demonstrate the HSL technology in a building application and a photobioreactor application. The emphasis in developing the demonstration systems will be to meet performance objectives at minimum cost.

PROGRESS TOWARDS PROJECT OBJECTIVES

The emphasis during budget period 1 has been on establishing the technical feasibility of the proposed lighting system. The research team has completed a number of investigations which clearly show that this unique lighting system is technically feasible. A brief summary of each investigation is given below and the details are provided in technical papers that have been drafted and included in the Appendices to describe the progress towards establishing technical feasibility.

Benchmark Collector Receiver: A prototype collector/receiver has been designed and fabricated and tests have begun at ORNL. Using funding from this project and other funds, ORNL has built a 1.0 m^2 parabolic concentrator with a receiver that can illuminate eight fibers. (See Figures 1-4) This design will produce about 8,200 lumens per fiber. This is the energy from about 0.08 square meters of sunlight (1000W/ m^2 of sunlight is equal to 100klumens/m^2.). By design this is also the amount of day lighting needed for a single luminaire.

Two Axis Tracker: As part of the design and development effort for the "Hybrid Lighting System," Oak Ridge National Laboratory (ORNL) scientists have evaluated two potential candidate tracking systems for the solar collector. The first system, the WattSun Solar Tracker, built by Array Technologies utilizes a patented, closed loop, optical sun sensor to sense the sun's position and track it. The second tracking system, SolarTrak Controller, built by enhancement Electronics, Inc. is a micro controller-based tracking system. The SolarTrak micro controller-based Tracker's sun position is determined by computing the celestial bearing of the sun with respect to the earth using the local time, date, latitude, longitude and time zone rather than sensing the relative bearing of the sun with optical receptors. This system connects directly to the mechanical system hardware supplied by Array Technologies. Both the WattSun Solar Tracker and the SolarTrak Controller were mounted on the prototype "Hybrid Lighting" mechanical system (array) hardware. A simple switch allowed independent testing of each system.

Upon completion of the evaluation of the two systems, the WattSun Solar Tracker controller was found to be unacceptable for use with our prototype hybrid lighting system. The SolarTrak Controller has performed well to date and provides suitable tracking accuracy for use with our prototype "Hybrid Lighting System". After a six-month evaluation period at ORNL and three months of operation at the Ohio University Photobioreactor Test Facility, the benchmark collector/receiver and tracker have met the design requirements.

Details of this investigation are given in Appendix A. [Tracking Systems Evaluation for the "Hybrid Lighting System", D.L. Beshears, G.J. Capps, D.D. Earl,, J.K. Jordan, L.C. Maxey, J.D. Muhs, ORNL and T.M. Leonard, Enhancement Electronic, Inc.]

Fig. 1. Full-Spectrum Collector/Receiver Mounted on roof at ORNL

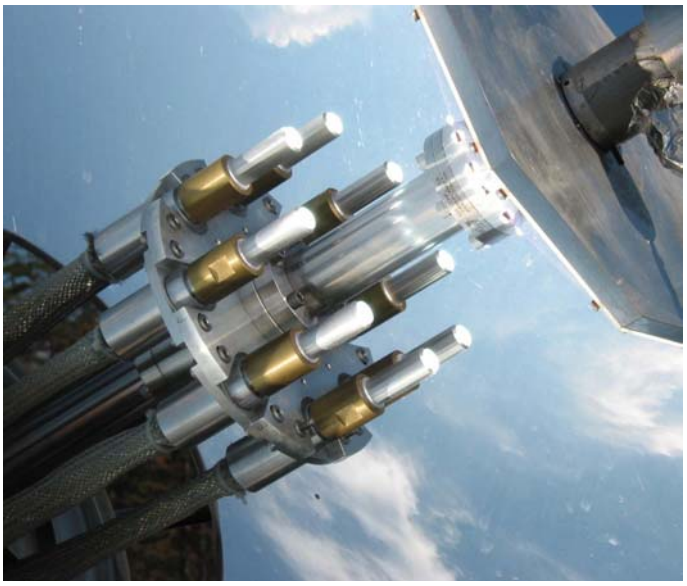

Fig. 2. Secondary Mirror and Fiber Optic Assembly

Fig. 3. Demonstration of fiber optic transporting day light from roof mounted collector/receiver

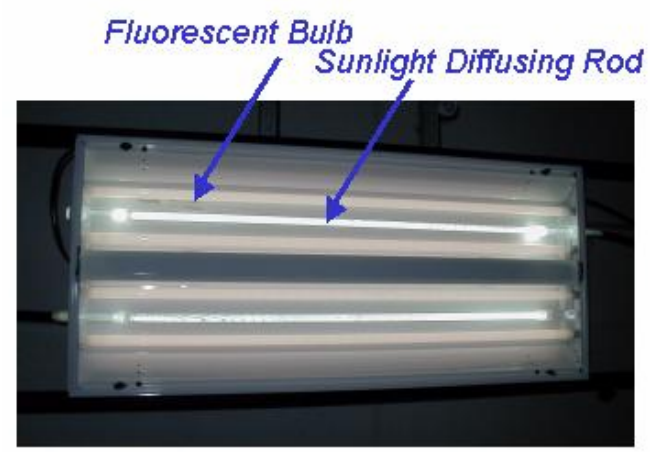

Fig. 4. Luminaire Accommodating Two Sunlight Diffusing Rods

IR Spectrum Receiver: The receiver utilizes the majority of the solar spectrum by splitting the infrared (IR) and visible energy for two different end uses. The visible light is directed toward the large core optical fibers while the IR energy is directed towards the thermophotovoltaic array for electrical power generation. The major concern is that the optics will provide uniform irradiance of the IR energy on the thermophotovoltaic (TPV) array. The benchmark full-spectrum collector/receiver and prototype TPV array have been built, so the work performed here is to match the two systems together for optimal performance. The design consists of a non-imaging system for the IR flux incident on the TPV array mounted behind the secondary mirror. Results of the ray-tracing analysis of the different systems tested are presented. A non-imaging square tube provides the best uniformity of the IR flux at +/- 9%.

Details of this investigation are given in Appendix B. [Optical Design of an Infrared Non-Imaging Device for a Full-Spectrum Solar Energy System, Dan Dye and Byard Wood, UNR; Lewis Fraas, JX Crystals, Inc. and Jeff Muhs, ORNL]

Performance of TPV: The sun's spectrum can be divided into visible light and infrared where the sunlight can be used for plant growth(1) or building interior lighting(2) and the IR can be converted to electricity using low bandgap GaSb photovoltaic cells. In this system, the solar radiation is collected by the parabolic mirror which then reflects and concentrates the solar radiation onto the selective spectral reflector where the solar radiation is divided into two spectral components: the photosynthetically active radiation (PAR) spectra (light: 400 nm - 700 nm); and non-PAR spectra (IR: > 700 nm). The PAR component is directed to low loss optical fiber. The PAR spectra are transmitted to the plant growth chamber where the light distribution panel spreads uniform light over the plants at an optimum intensity for plant growth. The IR spectra is converted to electric power by low bandgap photovoltaic (PV) cells.

The performance characterization tests using the GaSb cell for with the IR solar spectra have been investigated. The experiments were conducted at Physical Sciences Inc.'s solar laboratory in San Ramon, CA. JX Crystals provided the cells. A 20 inch parabolic mirror reflects the solar radiation to the PV cell module near the focal point of the mirror. The cold mirror installed at the PV cell module reflects the PAR to the aperture of a 10-meter lightguide which transmits the light inside the building. Emission of the PAR from the other end of the lightguide in the building is visible light. The IR spectra is converted into electric power by the GaSb cell placed behind the cold mirror in the PV cell module.

A representative outdoor measurement was made on 11/7/2001 of the efficiency and power density for a water-cooled GaSb cell. The results were: Isc = 8 Amps, Voc = 0.49 V, P(IR) = 17.85 W, Imax = 7.2 Amps, Vmax = 0.38 V, Pmax = 7.2x0.38 = 2.74 W, FF = (7.2x0.38)/(8x0.49) = 0.7, Efficiency = 2.74/17.85 = 15.3%

Details of this investigation are given in Appendix C [Electricity from Concentrated Solar IR in Solar Lighting Applications, Lewis M. Fraas & James E. Avery, JX Crystals, Issaquah, WA, Takashi Nakamura, Physical Sciences Inc., San Ramon, CA, 29th IEEE Photovoltaic Specialist Conference]

Optical Fiber Alignment at Receiver: Paraboloidal mirrors are the preferred reflector choice. This is due to the fact that an ideal paraboloid can transform the highly parallel rays from the sun into an un-aberrated, well-focused spot. To maintain high transmission efficiency, the focused spot must be smaller than the entrance aperture of the optcal fiber. To achieve optimum performance in systems requiring relatively small focused spot sizes, both the quality of the mirror and the quality of optical system alignment must be well controlled.

This system uses multiple fibers or waveguides with a single paraboloid, the focus of the paraboloid must be segmented into several separate focal points directed into individual fibers. Each waveguide entrance aperture must be accurately collocated with its designated focal point so that the image that is formed on the fiber will have the fewest possible aberrations and thus, the smallest possible focused spot size.

Two methods for aligning individual optical waveguides in a multi-aperture paraboloidal collection system were investigated. The first method employs a commercially available collimation tester to incrementally improve the alignment. The second, a deterministic method, employs a cube corner retro-reflector and an easily constructed imaging system to reliably align the fibers to their respective segments of the parent paraboloid. The image of the focused spot formed by the light that is returned from the retro-reflector reveals alignment information that is easily interpreted to enable pitch, yaw and focus errors to be systematically removed. This ensures that the alignment of the system is optimized to reduce aberrations prior to final adjustment of the system "on-sun".

Details of this investigation are given in Appendix D. [A Deterministic Method for Aligning Multiple Optical Waveguides to a Paraboloidal Collector, L.C. Maxey and B.J. Hilson, ORNL]

Large Core Optical Fiber Transmission: Transmission studies of 3M optical light guide, type LF120C with nominal 12.6 mm core diameter, were performed to characterize the material for use in solar lighting applications, in particular for the transport of sunlight from a collector to discrete lighting fixtures (luminaires). The light guide properties studied included: total transmission (in lumens) per unit length, transmission as a function of input angle and wavelength, transmission as a function of bend radius, and transmission through two bends. The preliminary value for total transmission is 96.6 % per meter. Angular input begins to drop significantly at angles greater than 25 degrees. Wavelength transmission has significant minima at about 643 and 750 mm. Losses through bends are much greater for light input at large angles.

Details of this investigation are given in Appendix E. [Characterization of Transmission Properties of 3M LF120C Plastic Optical Light Guide, M.R. Cates, S.L. Jaiswal, L.C. Maxey, D.D. Earl, ORNL]

Large Core Optical Fiber Connections: Although the concept of transmitting the sun's light through an optical fiber for illumination is simple, lighting systems based on this approach will be somewhat more complex. The sun's light must first be collected and launched into a fiber. From there, it must be transmitted, perhaps divided and ultimately allowed to flow into a luminaire for useful distribution into the area to be lighted.

The deployment of efficient hybrid lighting systems will require the ability to connect all of the various subsystem components in a way that minimizes any degradation of luminous efficiency. When the sun's energy is collected and launched into a fiber, any subsequent connection of that fiber to another system component (e.g. another fiber, a splitter or a luminaire) will cause some of the light to be lost. The quality of the systems that are ultimately deployed will directly depend on the ability to connect all of the components in a way that wastes as little of the collected light as possible. Several connections of two fibers have been investigated. The best connection has a measured light attenuation of less than 3%.

Details of this investigation are given in Appendix F. [Efficient Optical Couplings for Fiber-Distributed Solar Lighting, L.C. Maxey, M.R. Cates, and S.L. Jaiswat, ORNL]

Thermal Management of Fiber at Entrance Region: The secondary mirror consists of eight planar-segmented mirrors that direct the visible part of the spectrum to eight fibers (receiver) and subsequently to eight luminaires. This results in about 8,200 lumens incident at each fiber tip. This investigation is concerned with predicting the radial and axial temperature distribution in the entrance region of the fiber in light transmission. Thermal management of the plastic optical fibers is crucial to prevent melting or deformation of the fiber. Several filtering techniques have been investigated to minimize the effect of IR portion of the solar spectrum at the fiber entrance tip surface as well as the whole-spectrum absorption of solar energy inside the fiber. According to the analysis results, the use of fused quartz glass attachment was proven to be cheaper, more cost effective and feasible among other proposed solutions. In the present study, SMARTS v2.9 program, was used to predict the terrestrial direct normal solar spectral irradiance. Ray tracing software TracePro was used to describe the incident radiation at the fiber tip and as it passes through the fiber. A 3-D thermal model was developed using ANSYS v6.1, an FEA software. Depending on the mirror/filter specifications, the first 8 mm of the fiber was found to be critical based on 5 m/s air speed across the lateral surface of fiber. Modes of heat transfer taken into account included thermal conduction, convection and radiation on the first 5 cm of the polymethylmethacrylate (PMMA) core and Teflon-FEP cladding fiber.

Details of this investigation are given in Appendix G. **[**Thermal Management of the Polymethylmethacrylate (PMMA) Core Optical Fiber for use in Hybrid Solar Lighting, Murat Tekelioglu and Byard D. Wood, Univ. Nevada, Reno]

Hybrid Luminare: A prototype hybrid solar luminaire has been developed and evaluated. This investigation describes the performance of the luminaire designed to blend light from a fiber optic solar source with electric fluorescent lamps. The luminaire design studied involves a commercially-available fluorescent luminaire that had been modified to include optical elements for efficiently dispersing two fiber optic solar light sources. Quantitative measurements of the hybrid luminaire's optical efficiency and spatial intensity distribution/deviations are discussed. The effects of static differences and dynamic fluctuations in spatial intensity distribution are qualitatively discussed and potential design improvements examined.

Details of this investigation are given in Appendix H. [Performance of a New Hybrid Solar Lighting Luminaire Design, Dennis D. Earl, Curt L. Maxey and Jeff D. Muhs, ORNL and Robert R. Thomas, Pennsylvania State University]

Chromaticity of Collected and Transmitted Light: A computational model capable of accurately predicting the chromaticity values of collected and fiber-optically distributed sunlight has been developed. The seamless integration of solar and electrical illuminants into a single Hybrid Lighting System requires the careful color matching of two spectrally different sources. Due to the high variability of solar spectra with time, day, year, and location, combined with the significant absorption effects associated with collection and distribution optics (mirror coatings, fiber optic transmission, etc.) an extensive chromaticity model is required to predict the final output spectrum and color values (CRI, CCT, and CIE x-y, u-v, u'-v' values) of collected and distributed sunlight. This report characterizes the spectral properties of unmodified direct sunlight in North America, evaluates the spectral modification of sunlight due to a proposed solar collector design, and evaluates the severity of color shifting due to the fiber optic transport of sunlight. The effects of fiber optic launch angles on spectral shifting are examined using data known about the current Hybrid Lighting Solar Collector design and transport optical fibers. The color matching between fluorescent and unfiltered sunlight is addressed and the design of a filter

to improve color matching between solar and electric illuminants is discussed. Conclusions related to the applicability and energy efficiency of the final system are presented.

Details of this investigation are given in Appendix I. [Modeling and Evaluation of Chromatic Variations in a Hybrid Solar/Electric Lighting System, D.D. Earl and J.D. Muhs, ORNL]

Daylight and Productivity – A Literature Review: No studies to date have demonstrated a relationship between daylighting and productivity, but this does not mean a mechanism does not exist. Light is not restricted to vision in its ability to affect people. There are three routes through which light (including daylight) might affect productivity: the visual system, the circadian photobiological system, and the perceptual system.

The visual and the circadian photobiological systems are essentially discrete systems, each with its' own unique set of physiological processes. Each system is essentially consistent, with normal variation, in its functioning among the human population. This consistent functioning allows for direct investigation of the underlying mechanisms of these systems.

We have a good understanding of how light affects the visual system. Quantitative models have been developed allowing the prediction of lighting conditions on visual performance. While our knowledge of the visual system is fairly complete, our understanding of the circadian system is in its infancy. We know that light is the primary stimulus for synchronizing the daily rhythm of the system to its surroundings and that the sensitivity of the system changes over the course of the day. We also know that light must actually enter the eye for it to be effective, and that the quantity of light required for proper functioning of the circadian system is much greater than the quantity of light required by the visual system. Whereas daylight offers nothing unique to the circadian system, it may offer an efficient means of maintaining circadian rhythmicity in the built environment (offices, factories, etc.). This is especially likely during the winter months when availability to daylight is limited on the commute to and from work

Unlike the other two systems, the perceptual system is not simply a function of certain physiological events. It is inherently complex and unique to each individual in a population. The perceptual system, being idiosyncratic to individual experience, temperament, education, etc., responds to many variables in many combinations. It does not readily lend itself to scientific investigation, except in the most general sense. This means that the interpretations of lighting installations are unique to each individual in a population. This individuality makes a systematic study of daylighting's effect on productivity via the perceptual system quixotic.

The distinct requirements of the visual system and the circadian system can be served by electric lighting through proper specification of the characteristics of that light (quantity, spectrum, spatial distribution, timing and duration). Daylight can, however, provide a practical source of light able to serve both the visual and circadian system in a highly efficient manner. This is a complex issue.

Details of this investigation are given in Appendix J. [Daylighting and Productivity Review: A Literature Review, Charles Fay, RPI]

Results from an experimental hybrid solar lighting system installed in a commercial buildings: A physical description of the HSL system components along with preliminary results from an experimental system deployed in a commercial building in Knoxville, TN are provided in Appendix K. A total lumen distribution efficiency of over 50% was

recorded for the initial prototype having optical fibers an average of 6 m (19.5 ft) in length. The total electrical power displacement of the 1 m^2 HSL proof-of-concept prototype is estimated to be between 522 – 2350 watts per 1000 W/m^2 of incident solar radiation depending on the type of electric lights being used in conjunction with the solar lighting system. By adding the reductions in heat gain associated with reduced electric lamp use and predicted performance improvements achieved by a system redesign, the electrical power displaced in a commercial prototype could rise to between 702 – 3160 W (peak)/m^2 not including any additional electrical power that can be generated using the otherwise wasted IR energy. The color temperature of the distributed sunlight emerging from the optical fibers is approximately 5100^oK and the chromaticity values in uniform color space (u'v') are approximately (0.2010, 0.4977). These values match well with modeled results and will vary slightly depending on the day, time, atmospheric conditions, and system configuration.

Details of this investigation are given in Appendix K. [Results from an experimental hybrid solar lighting system installed in a commercial buildings, Jeff Muhs, Duncan Earl, Dave Beshears, and Curt Maxey, ORNL]

CONCLUSIONS

During Budget Period 1, the project team has made significant progress towards understanding of the basic principles that govern the design of hybrid solar lighting systems. The R&D to date has been directed towards establishing the technical feasibility of the proposed concept. The research thus far has not identified any barriers that suggest the proposed concept is not technically feasible. In fact, the results support the concept as summarized in the following statements:

1 For the design proposed, the optical fiber must transport approximately 8,000 -10,000 lumens of daylight. The primary candidate for the large-core optical fiber is the 12mm 3M LF 120B polymer light fiber manufactured by 3M Company. The fiber is comprised of a crosslinked methacrylate-type polymer core. Experiments have shown that it is capable of transporting up to 12,000 lumens. (In earlier communications the fiber has been identified as a PMMA which it is not. There are a whole class of methacrylate monomers, methyl methacrylate being one of them. PMMA is a homopolymer of methyl methacrylate monomer. Large core fibers would be rigid if they were made solely of methyl methacrylate. Instead, various monomers in this family (or other chemical classes) can be copolymerized to adjust the mechanical properties as well as the reaction kinetics. The 3M polymer is crosslinked so that it will not melt when heated.)

2 For the proposed/collector receiver, a high quality concentrating mirror that could supply the required lumens to eight fibers was commercially available. This concentrator was used to build a benchmark prototype collector/receiver to accelerate determining the technical feasibility process. The receiver consists of eight planar mirrors that reflect the sun light to the eight fibers. The prototype has been constructed and tested with satisfactory performance. IR filters in front of the fiber tips were used to minimize the IR irradiance incident upon the fiber. The mirror's physical description is 46.5 in. diameter formed glass mirror with 16.5 in. focal length (f/D = 0.35) with enhanced aluminum coating.

3 A prototype 2 ft x 4 ft x 4 in. luminaire has been designed and built for the photobioreactor application. Preliminary experiments have shown satisfactory performance.

4 A hybrid luminaire that consists of two 4 ft T-8 florescent light tubes and one day light diffuser in the form of a 4 ft straight rod has been built to demonstrate the concept. The diffuser rod is commercially available from 3M (Part #: LF-180-EX-D-1M). Total optical efficiency of Hybrid Luminaire was measured to be 58.4% for fiber optic sources and 85% for fluorescent sources. A significant amount of fiber optic loss was attributed to the fiber-to-rod coupling (≈20% loss). Team experience with other coupling issues suggests that this loss can be reduced significantly. ORNL has been experimenting with a Fresnel diffuser that is approaching the same efficiency as that for fluorescent lighting.

5 The team has developed excellent ray trace computational capabilities that allow the evaluation of optical designs for the collector/receiver with turn-around times in the order of a few days.

6 A thermal management model has been developed to evaluate fiber temperatures in the entrance region for the fiber. Calculations have shown that IR filters are effective in maintaining fiber tip temperatures below fiber deformation temperatures. The critical entrance length is less than 3 cm. Experiments with the prototype collector receiver have shown that a 3 cm quartz rod placed in front of the fiber prevents the fiber tip from reaching deformation temperatures.

7 The thermophotovoltaic array uses Gallium Antimony cells. The measured conversion efficiency on a single 1.0 m^2 cell was 15.3%. The use of an AR coating should increase it to 17.8%. This suggests that the 100 series connected gallium antimony cells on a rectangular grid (14.7 x 10.5 mm) can produce 177 W. Preliminary estimates suggest that this energy is sufficient for operating the tracking system.

8 An adaptive, full-spectrum solar energy system model using performance data from the prototype components has been developed using the system simulation program TRNSYS. Some preliminary calculations have been completed. In Madison, WI, a single hybrid lighting unit (1.8 m^2) can supply 29% of the annual lighting needs for a floor area of 200 square meters (2153 square feet or 179 ft^2 per fiber) and in Reno, NV that same unit will provide 51% of the lighting demand. The figures are based on annual beam normal radiation in Madison, WI, and Reno, NV, a 50 % occupancy schedule, and an illumination level of 500 Lux (typical of office space). The area was selected by specifying the best day of the year as having no excess lighting. The best days in Reno and Madison differ only slightly with Reno having about 5% more beam. However, Reno has many more clear days than does Madison.

9 Characterizing the losses when two fibers are joined together is an important part of technical feasibility. A variety of connections have been investigated. Thus far the minimum loss occurs when the mating ends are machined polished with the face perpendicular to the fiber longitudinal axis with an index matching medium applied at the interface. The losses for this connection are less than 3%. (See page 4 Maxey et al. Paper #4 listed below.)

10 Ray tracing calculations show that the tracking accuracy in both the altitude and azimuth directions must be +/- 0.125 degrees. Two tracking mechanisms were tested: WattSun

and SolarTrak. The WattSun system uses sun seeking sensors and the SolarTrak uses a clock system. On clear days, both tracking systems worked within specifications. For less than clear days the WattSun tracker was unacceptable while the SolarTrak worked well.

11 A Lab-Scale Hybrid Solar Photobioreactor has been built at Ohio University. The significant accomplishments include:
- Candidate Organisms Evaluated
- Candidate Growth Surfaces Tested
- Alternative Growth Enhancement / Harvesting Methods Tested
- 1 Solar Collector and 8 Light Distribution Panels have been installed at pilot-scale bioreactor site

12 In a comprehensive review of the published literature, no studies were found detailing daylighting's effect on visibility tasks. There is no evidence that any particular lamp type is better than any other in its effects on people.

13 In terms of HSL technology development, the areas that need increased development are:
- Uniform distribution of the day light in the hybrid luminaire and the photobioreactor luminaire,
- Service life of the high efficiency fiber connectors,
- Design options that will allow a relaxation of the high accuracy tracking requirements,
- Optical fibers with lower transmission losses,
- Improved uniformity of IR energy on TPV array,
- Low cost concentrating collector/receiver.

PUBLICATIONS RESULTING FROM THIS RESEARCH

Infrared Photovoltaics for Combined Solar Lighting and Electricity for Buildings, L.M. Fraas, JX Crystals, Inc., 17th European Photovoltaic Solar Energy Conference in Munich, Germany in October 2001. (This paper is available from the Project Web Site www.energy.unr.edu/lighting.)

Full Spectrum Hybrid Lighting for Commercial Buildings, G.O. Schlegel, B.D. Wood, J.D. Muhs, S.A. Klein, and W.A. Beckman, 2002 Right Light 5 Conference in Nice, France. Paper Number RL5#51. (This paper is available from the Project Web Site www.energy.unr.edu/lighting.)

DISTRIBUTION

NETL AAD Document Control
James Brodrick, DOE
Joel S. Chaddock, NETL
Peter Grandillo, NETL

David J. Bayless, Ohio University
William Beckman, University of Wisconsin

Clinton Berry, TN Dept. of Economic & Community Dev. Energy Division
Joel L. Cuello, University of Arizona
Roger Davenport, Science Applications International Corporation
David R. Dinse, TVA Public Power Institute
Lewis Fraas, JX Crystals Inc
Jason B. Keyes, JX Crystals Inc.
Sandy Klein, University of Wisconsin
Dave McNeil, Nevada Energy Office
Jeff Muhs, Oak Ridge National Laboratory
Nadarajah Narendran, Rensselaer Polytechnic Institute
Jennifer Sahlin, 3M
Robert Schnell, Honeywell Laboratories
Robin W. Taylor, Science Applications International Corporation

This report is posted on web site www.energy.unr.edu/lighting

APPENDICES

Each appendix is a self contained report that contributes to the determination of the technical feasibility of Adaptive Full Spectrum Solar Energy Systems. As indicated below, most of these papers have been prepared and have been submitted simultaneously for consideration at the March 2003 ASME International Solar Energy Conference.

APPENDIX A
Tracking Systems Evaluation for the "Hybrid Lighting System", D.L. Beshears, G.J. Capps, D.D. Earl,, J.K. Jordan, L.C. Maxey, J.D. Muhs, ORNL and T.M. Leonard, Enhancement Electronic, Inc., Submitted for consideration at the March 2003 ASME International Solar Energy Conference

APPENDIX B
Optical Design of an Infrared Non-Imaging Device for a Full-Spectrum Solar Energy System, Dan Dye and Byard Wood, UNR; Lewis Fraas, JX Crystals, Inc. and Jeff Muhs, ORNL, Submitted for consideration at the March 2003 ASME International Solar Energy Conference

APPENDIX C
Electricity from Concentrated Solar IR in Solar Lighting Applications, Lewis M. Fraas & James E. Avery, JX Crystals, Issaquah, WA, Takashi Nakamura, Physical Sciences Inc., San Ramon, CA, 29th IEEE Photovoltaic Specialist Conference. (Note: The work in this paper was not funded by this project. However, the PV cell that was tested is identical to those used in this project and therefore has relevance to this project.)

APPENDIX D.
A Deterministic Method for Aligning Multiple Optical Waveguides to a Paraboloidal Collector, L.C. Maxey and B.J. Hilson, ORNL, Submitted for consideration at the March 2003 ASME International Solar Energy Conference

APPENDIX E
Characterization of Transmission Properties of 3M LF120C Plastic Optical Light Guide, M.R. Cates, S.L. Jaiswal, L.C. Maxey, D.D. Earl, ORNL, Submitted for consideration at the March 2003 ASME International Solar Energy Conference

APPENDIX F
Efficient Optical Couplings for Fiber-Distributed Solar Lighting, L.C. Maxey, M.R. Cates, and S.L. Jaiswat, ORNL, Submitted for consideration at the March 2003 ASME International Solar Energy Conference

APPENDIX G
Thermal Management of the Polymethylmethacrylate (PMMA) Core Optical Fiber for use in Hybrid Solar Lighting, Murat Tekelioglu and Byard D. Wood, Univ. Nevada, Reno, Submitted for consideration at the March 2003 ASME International Solar Energy Conference

APPENDIX H
Performance of a New Hybrid Solar Lighting Luminaire Design, Dennis D. Earl, Curt L. Maxey and Jeff D. Muhs, ORNL and Robert R. Thomas, Pennsylvania State University, Submitted for consideration at the March 2003 ASME International Solar Energy Conference

APPENDIX I
Modeling and Evaluation of Chromatic Variations in a Hybrid Solar/Electric Lighting System, D.D. Earl and J.D. Muhs, ORNL, Submitted for consideration at the March 2003 ASME International Solar Energy Conference

APPENDIX J
Daylighting and Productivity Review: A Literature Review, Charles Fay, RPI, Subagreement Deliverable August 2002

APPENDIX K
Results from an experimental hybrid solar lighting system installed in a commercial buildings, Jeff Muhs, Duncan Earl, Dave Beshears, and Curt Maxey, ORNL, Submitted for consideration at the March 2003 ASME International Solar Energy Conference

APPENDIX A

TRACKING SYSTEMS EVALUATION FOR "HYBRID THE LIGHTING SYSTEM"

D. L. Beshears, G. J. Capps, D. D. Earl, J. K. Jordan, L. C. Maxey, and J. D. Muhs
Oak Ridge National Laboratory
Oak Ridge, Tennessee

T. M. Leonard
Enhancement Electronics, Inc.
Tijeras, New Mexico

ABSTRACT

As part of the design and development effort for the "Hybrid Lighting System," Oak Ridge National Laboratory (ORNL) scientists have evaluated two potential candidate-tracking systems for the solar collector. The first system, the WattSun Solar Tracker, built by Array Technologies utilizes a patented, closed loop, optical sun sensor to sense the sun's position and track it. The second tracking system, SolarTrak Controller, built by Enhancement Electronics, Inc. is a micro controller-based tracking system. The SolarTrak micro controller-based Tracker's sun position is determined by computing the celestial bearing of the sun with respect to the earth using the local time, date, latitude, longitude and time zone rather than sensing the relative bearing of the sun with optical receptors. This system connects directly to the mechanical system hardware supplied by Array Technologies. Both the WattSun Solar Tracker and the SolarTrak Controller were mounted on the prototype "Hybrid Lighting" mechanical system (array) hardware. A simple switch allowed independent testing of each system.

Upon completion of the evaluation of the two systems we found the WattSun Solar Tracker controller to be unacceptable for use with our prototype hybrid lighting system. The SolarTrak Controller has performed well to date and provides suitable tracking accuracy for use with our prototype "Hybrid Lighting System". After a six-month evaluation period at ORNL, the first prototype "Hybrid Lighting System" was installed at Ohio University as part of an "Enhanced Practical Photosynthetic CO2 Mitigation." This document will highlight the results of the tracker investigation and outline the remaining issues to be addressed, to provide a suitable tracking system for our "Hybrid Lighting" collector.

INTRODUCTION

As part of the design and development effort for the "Hybrid Lighting System" ORNL scientists have evaluated two potential candidate-tracking systems for the solar collector. The first system, the WattSun Solar Tracker, built by Array Technologies utilizes a patented, closed loop, optical sun sensor to sense the sun's position and track it. The second tracking system, the SolarTrak Controller, built by Enhancement Electronics, Inc. is a micro controller-based tracking system. The SolarTrak micro controller-based system determines sun position by computing the celestial bearing of the sun with respect to the earth using the local time, date, latitude, longitude and time zone rather than sensing the relative bearing of the sun with optical receptors. This system connects directly to the mechanical system hardware (which will be referred to as the array) supplied by Array Technologies. Both the WattSun Solar Tracker and the SolarTrak Controller were mounted on the array and used a simple switch to allow independent testing of each system.

The collector alignment along with the tracking accuracy is critical to the performance of the "Hybrid Lighting System". In order to better understand the issues of alignment and tracking accuracy, ZEMAX ray-tracing software was used to optically model and analyzed the complete Hybrid Lighting Solar Collector system. The sensitivity of the modeled solar collector to various internal misalignments was analyzed and acceptable alignment tolerances determined. These same tolerances apply to both the alignment of the collector as well as the tracking accuracy. Five alignment parameters were identified as critical

to the proper operation of the solar collector. These alignment parameters are shown in Figure 1:

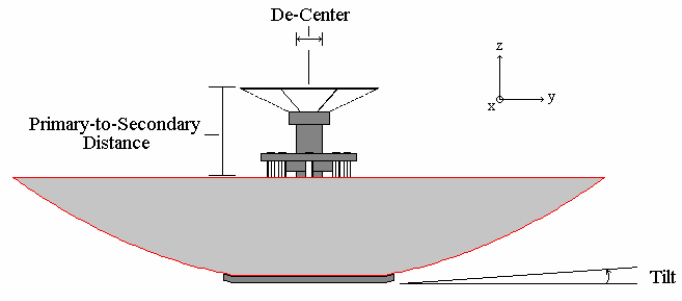

- X-Tilt = X-Axis Tilt of Primary Mirror Axis Relative to Secondary Axis
- Y-Tilt = Y-Axis Tilt of Primary Mirror Axis Relative to Secondary Axis
- X-De-Center = Offset in the X-Axis Between Secondary Center and Primary Center
- Y-De-Center = Offset in the Y-Axis Between Secondary Center and Primary Center
- Prim-to-Sec Distance = Distance Between Secondary and Primary Mirror

Figure 1. Critical Internal Alignment Parameters

If each of the alignment parameters in Figure 1 is perfectly adjusted (zero alignment errors), and the collector is properly tracking the sun, then the sunlight collected by the solar collector will be precisely focused into the center of each of the eight fiber optic cores (see Figure 2a). However, if the alignment parameters are not perfectly adjusted, as is typically the case, the focused sunlight will be off-center to the core of the optical fiber (see Figure 2b) and may even miss the fiber core altogether.

To compensate for these misalignments, the eight optical fibers are mounted in movable holders that can move ±4 mm in any direction. Unfortunately, this limited fiber mobility provides only marginal compensation for misalignments, and thus, imposes a relatively high tolerance on the five alignment parameters identified in Figure 1. Using the ZEMAX model of the solar collector, the alignment tolerances needed to insure the complete capture of focused sunlight into all eight optical fibers was computed. If a misalignment caused any portion of the focused sunlight to exceed the reach of the fiber optic cores, the misalignment was deemed unacceptable. Given these conditions, the acceptable alignment tolerances were calculated from the model and provided in Table 1.

Parameter	Tolerance
X-Tilt	±0.125°
Y-Tilt	±0.125°
X-De-Center	±3.0 mm
Y-De-Center	±3.0 mm
Prim-to-Sec Distance	±2 mm

Table 1. Acceptable Alignment Tolerances

To meet these desired tolerances, the assembly of the solar collector was performed in a laboratory setting and the placement/orientation of the collector's components were precisely measured with a Faro SpaceArm 3D digitizer (See Figure 3).

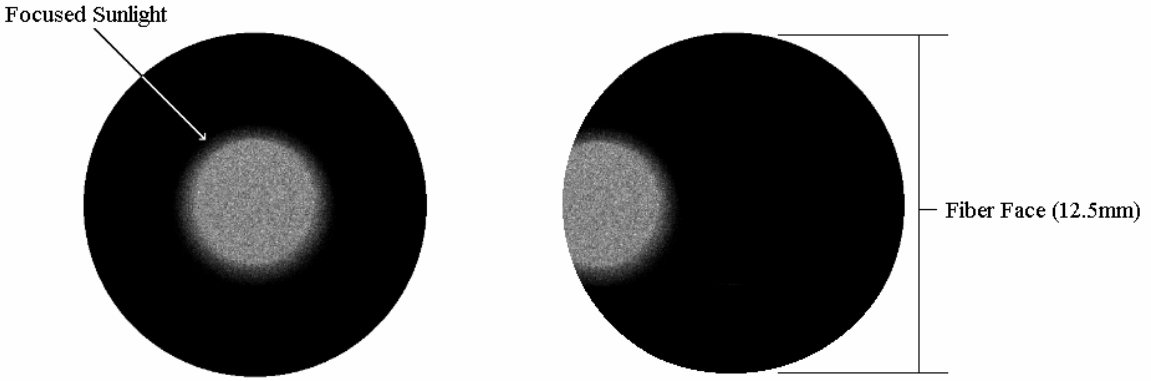

Figure 2a) Collection of Sunlight Under Ideal Alignment Conditions, b) Collection of Sunlight When Internal Misalignments Present

Figure 3. Measurement and Alignment of Collector Optics

After assembly, the errors on the various alignment parameters were measured and summarized in Table 2.

Parameter	Error
X-Tilt	+0.089°
Y-Tilt	-0.209°
X-De-Center	0.1 mm
Y-De-Center	0.5 mm
Prim-to-Sec Distance	-1.55 mm

Table 2. Final Measured Alignment Errors

Due to the crude and limited adjustments available during assembly, one of the five acceptable alignment tolerances was not met. However, it was determined that, because of the relatively small errors experienced in the other alignment parameters, this error would only result in a small (< 5%) decrease in the final efficiency of the solar collector. Therefore, the re-alignment of the solar collector was not attempted. In order for the tracking system to meet these same tolerances, the tracking system must be able to track the sun well enough to meet the X- and Y-tilt tolerances outlined in Table 1.

WattSun Solar Tracker Evaluation

General Description

The WattSun Solar Tracker, built by Array Technologies, utilizes a patented, closed loop, optical sun sensing system to sense the sun's position and track it. The optical sun sensor consists of a square post machined to a cone tip with four individual optical sensors. Figure 4 shows a photo of the optical sun sensor with the individual optical sensors mounted at approximately 45 degrees to the face of the square post. The optical sun sensor is mounted such that its axis is parallel to the center axis of the solar collector. When the cone tip is pointed toward a light source (the sun) the controller circuitry sums the signals from the four individual sensors. The closed loop system feeds information to the controller electronics about the direct component of sunlight available, the diffuse amount of sunlight, the total amount of sunlight as well as the differential amount of sunlight on the opposing sensors. The control electronics then provides a signal to the azimuth-elevation motors to move the optical sun sensor until the individual optical sensors balance.

Test Set-Up

The test set-up consisted of the WattSun Tracker Mechanism with a frame attached to provide a sun pointer mechanism to allow us to monitor the tracking accuracy of the overall system using the WattSun optical sun sensor. The overall WattSun Tracker system mechanism is shown in Figure 5.

Figure 6 shows a close-up view of just the collector-mounting frame along with the pinhole-mounting frame, the sun pointer grid mounting, and the optical sun sensor arrangement. An aluminum plate is mounted on the pinhole-mounting frame with a 1 mm pinhole in the center. The pinhole projects sunlight onto a 1.5 X 1.5 inch grid paper 26.5 inches below the pinhole. The optical sun sensor is mounted such that its apparent centerline is parallel to the sunlight projected through the pinhole and onto center of the grid paper. This allows one to monitor the tracking ability of the WattSun tracker and determine the tracking error projected over the 26.5 inch light path.

Wattsun Tracker Array with Optical Sun Sensor Test Results

The tracker system was evaluated under various sun conditions; bright sunny days with clear conditions, slightly hazy days with few clouds, partial overcast days and overcast days. We found that the WattSun Tracker with the optical sun sensor performed reasonably well only on days with bright sun and clear conditions. On days with hazy or cloudy conditions, when the system's metal frame did not project a strong shadow, or there was not enough light to project a sun spot via the sun pointer, the system would not consistently or accurately track the sun. In fact, the system would often search during cloudy or hazy times and then if the sun came out from behind a cloud, the sun spot projected by the sun pointer would be off considerably from were it should be.

Furthermore, because the system seeks to balance the signal from the individual sensors opposite one another on the optical sun sensor, partial sky shadowing effects from building's in the near vicinity of the tracker or dark clouds in a portion of the sky would cause the system not to track properly. These problems cause the WattSun optical sun sensor to be unacceptable for use on our hybrid lighting system which requires that the axis of the primary and secondary mirrors be precisely aligned with the sun at all times in order for the system to operate efficiently.

Figure 4. Optical Sun Sensor device used to provide feedback to the electronics control system.

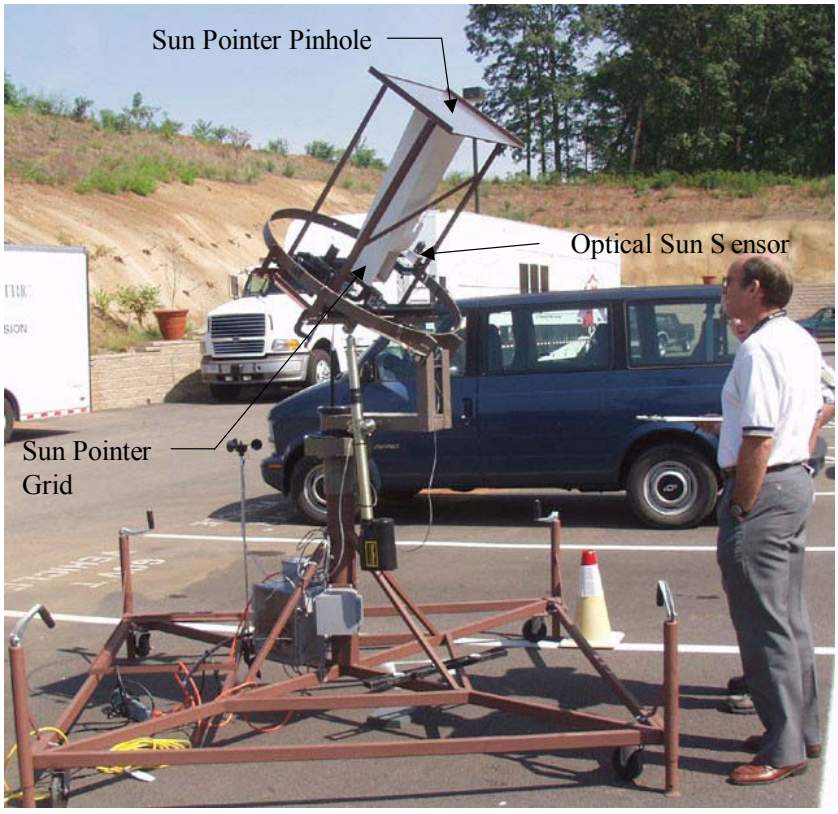

Figure 5. Overview of the WattSun Tracker with a frame added to provide a sun pointer for monitoring overall system tracking accuracy.

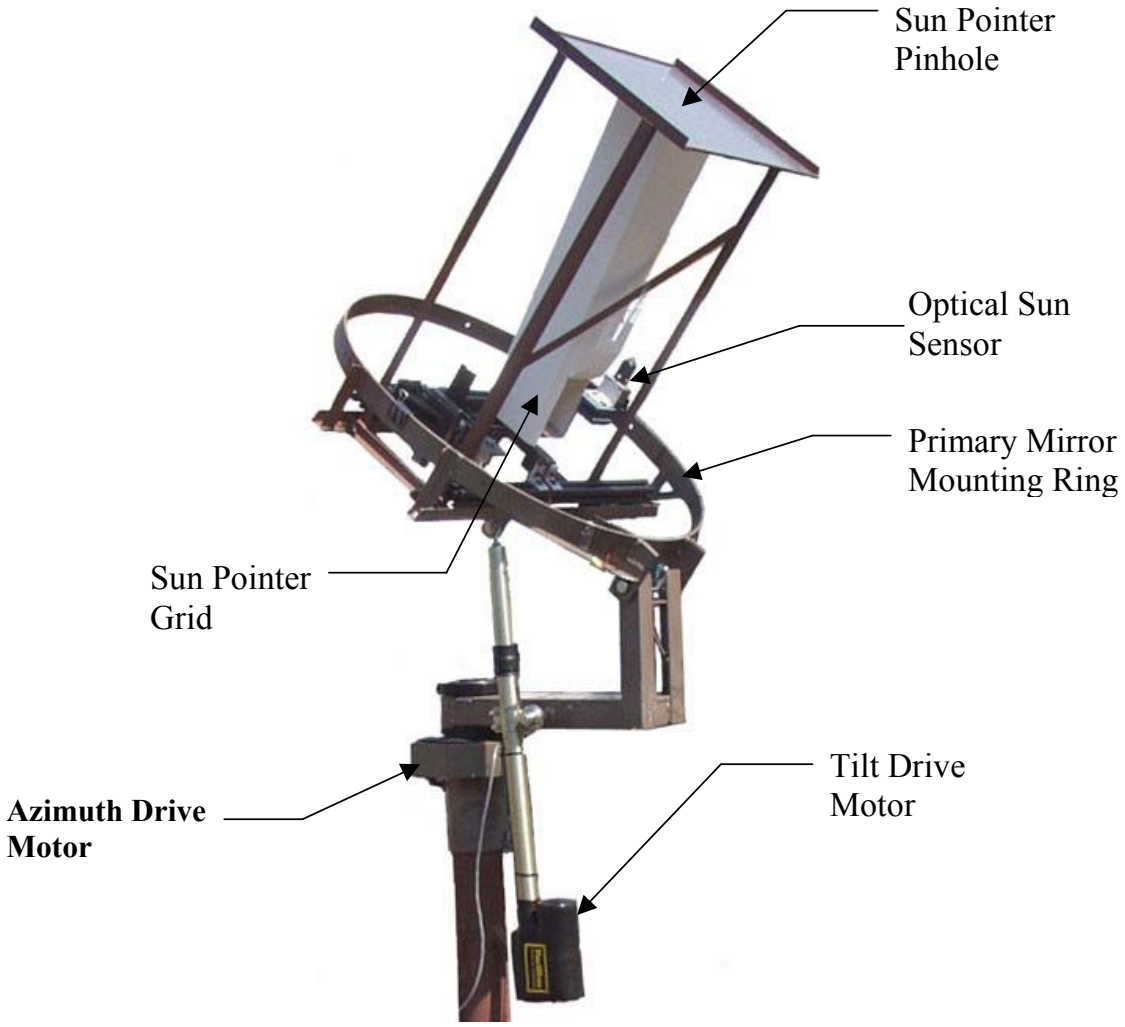

Figure 6. Close-up view of the collector mounting ring along with the pinhole mounting frame, the grid paper mounting, and the optical sun sensor arrangement.

In order to fully evaluate the WattSun optical sun sensor and attempt to quantify its accuracy we performed two types of tests under bright, sunny, clear conditions. The tests were performed to determine the accuracy of the WattSun optical sun sensor under ideal conditions. The WattSun tracker system has two modes of operation: 1) manual, which allows one to manually move the tracker via a joystick type arrangement, and 2) automatic, which uses the optical sun sensor to sense the position of the sun and serve as a feedback to automatically track the sun. The first series of tests performed consisted of:

1) placing the WattSun Tracker in the automatic mode and noting the position of the projected sunspot,
2) switching the system to manual and moving the tracker until the sunspot was misaligned approximately 1 inch in a given direction,
3) switching it back to automatic and allowing it the reposition the sun spot and noting the degree of misalignment of the new position, and finally,
4) this process was repeated five times for each direction, (east, west, north, south, southeast, southwest, northeast, and northwest) and the amount of misalignment or error were noted.

The spot size of the projected sunspot was approximately 0.25 inches and the maximum error recorded for the center movement was +/- 0.40 inches in the X direction and +/- 0.35 in the Y direction. This corresponds to an angular error of +/- 0.75 degrees in the X direction and +/-0.86 degrees in the Y

direction. Referring to the Acceptable Alignment Tolerances outline in Table 1 of the introduction, the misalignment due to tracking with the optical sun sensor is unacceptable.

The second series of tests consisted of allowing the system (again under ideal, bright, sunny conditions) to track the sun during a period from 11 am (once there was no building shadowing effect) until 5:15 pm. During this period, the position of the sunspot was noted at regular time interval. Under these ideal conditions, the system was able to maintain the center point of the projected sunspot to within +/- 0.25 inches in the X direction and +/- 0.25 inches in the Y direction. This corresponds to an angular error of +/- 0.54 in the X direction and +/- 0.54 in the Y direction. Again referring to the Acceptable Alignment Tolerances outline in Table 1 of the introduction, the misalignment due to tracking with the optical sun sensor is unacceptable.

Although it appears that the WattSun tracking controller would work well for applications for which it was designed such as positioning a large panel of photovoltaic solar cells, the solar panel application does not require the precision alignment of our hybrid lighting system. Even under ideal conditions the error manifest in the WattSun optical sun sensor are unacceptable for maintaining the focused spot within the target 12mm (approximately 0.50 inches) fiber diameter for the required 8 fibers.

Solartrak Controller Evaluation

General Description

Where the WattSun controller uses a remote sensor module for closed-loop feedback sensing and control described earlier, the SolarTrak is an open-loop system. The SolarTrak Controller, built by Enhancement Electronics, Inc. is a micro controller-based tracking system. This micro controller-based SolarTrak Controller's sun position is determined by computing the celestial bearing of the sun with respect to the earth using the local time, date, latitude, longitude and time zone rather than sensing the relative bearing of the sun with optical receptors. It uses an embedded microprocessor to derive the computed position of the sun (Request Position) and drive the motor to control the physical orientation (the Array Position) of the mechanical system. The computerized controller calculates the Request Position based on the precise position on the earth (latitude and longitude), the date, and the time of day. It then drives the azimuth and elevation actuators to cause the Array Position to coincide with the calculated Request Position. The embedded processor is a Motorola 68HC11 and the software is written in assembly language, adapted from code originally developed at Sandia National Laboratories, Albuquerque.

The SolarTrak controller can be programmed and calibrated at the unit by means of manual controls and a small display mounted directly on the controller card. In addition, it can be controlled remotely through separate software running on an IBM-compatible computer connected with an RS-232 cable.

The computer maintains an internal clock that must be synchronized to an external time source. A software procedure provides for correcting drift in the internal clock. The latitude, longitude, and certain physical parameters are input into the controller at time of installation. These parameters describe the physical dimensions of the elevation actuator geometry and the gear ratios of the drive mechanisms. A calibration procedure is provided to correct the computed tracking position for errors introduced by any vertical misalignment of the mounting post. A Reference Offset value is also determined during calibration to allow the computer to orientate the coordinate system of the Array with the coordinate system of the Earth.

The controller monitors the actual Array Position by counting pulses (turncounts) from magnetic reed switches mounted in the drive gearboxes of both the azimuth and elevation actuators. Once each morning, the system does a Reference Check. It returns both axes of the array to fixed reference points provided by limit switches mounted on the Array, calculates the current position of the Sun in the sky, corrects the calculation with the calibration factors, determines the desired machine coordinates, and drives the axis motors to position the Array. As the Array is moved, it accumulates turncounts from the reed switches to monitor the actual position of the physical Array hardware. The controller monitors the Array Position continuously and makes small adjustments throughout the day.

Test Set-Up

The test set-up for the evaluation of the SolarTrak Controller was somewhat different from that of the WattSun Solar Tracker tests with the optical sun sensor. As outlined earlier, the two systems were mounted on the prototype "Hybrid Lighting" array with simple switches to allow independent testing of each system. Enhancement Electronics, Inc. furnished the SolarTrak controller and software. Enhancement Electronics provided electrical diagrams for wiring of the system to the existing Array Technology array. By the time the SolarTrak controller evaluation began the primary and secondary mirrors had been assembled and a new sun pointer system was required to be built into the "Hybrid Lighting" assembly. Figure 7 shows a picture of the assembled Hybrid Lighting System" illustrating the components of the reflective sun pointer. Figure 8 is a schematic illustrating the principle of the sunspot pointing device. The light enters through the pinhole orifice and travels through the secondary support tube to a mirror mounted at the bottom of the support tube mounting plate and then returns to a grid mounted on the back side of the orifice pinhole where it is viewed via a camera. As the system tracks throughout the day the sunspot position was monitored and recorded. Below the quantification of error for this sunspot pointing device is illustrated in Figure 9.

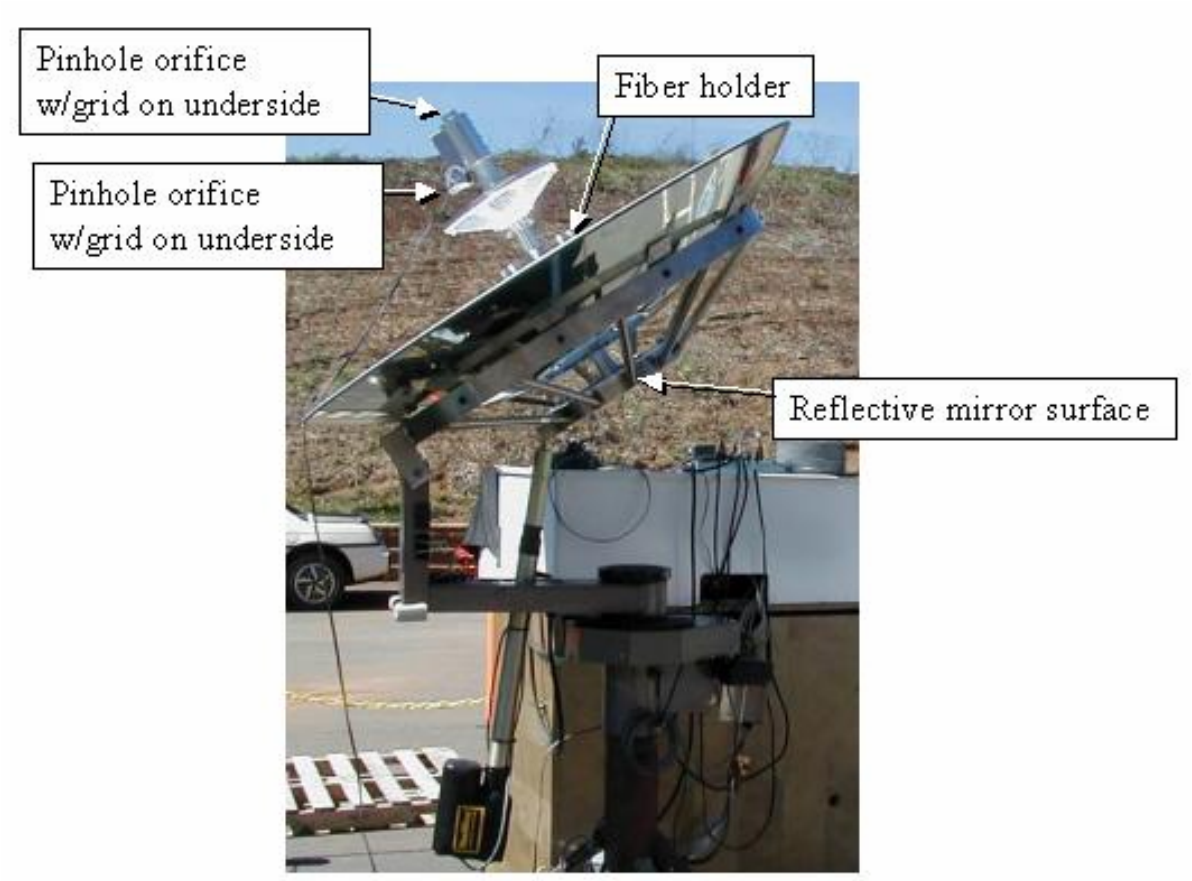

Figure 7. Assembled "Hybrid Lighting System"

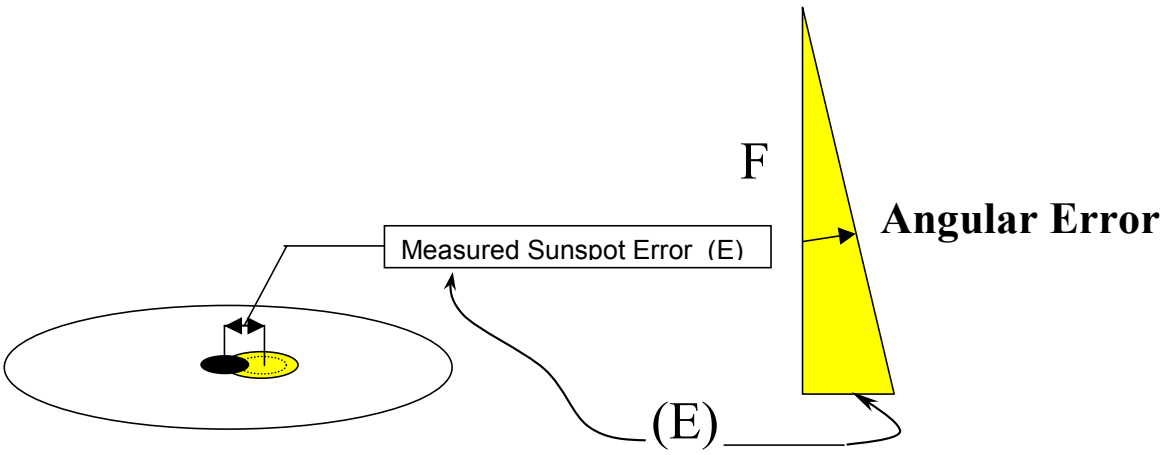

Figure 9. Quantification of Error for sunspot pointing device.

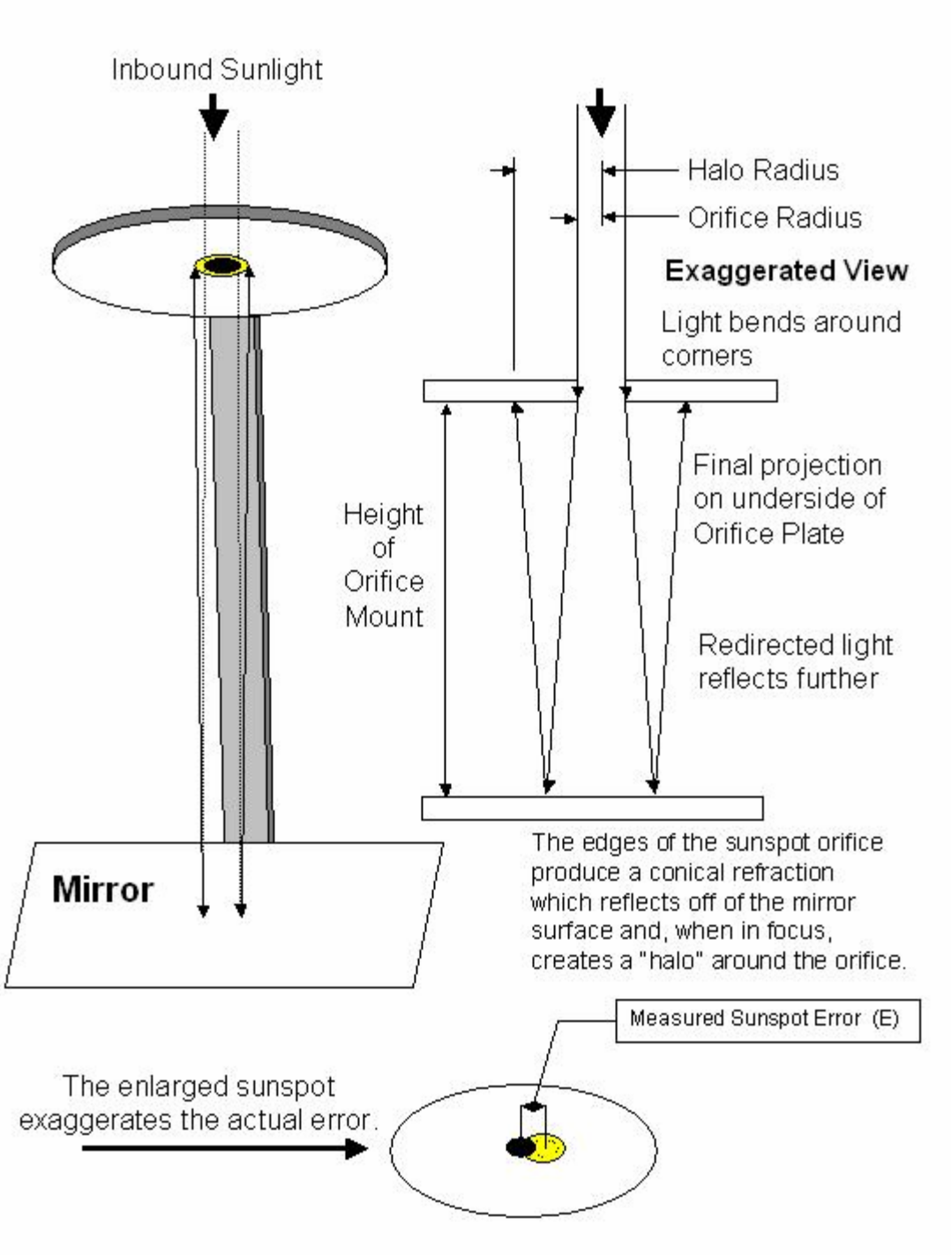

Figure 8. Reflected Sunspot Pointing Device

Requirements:
Measure 'Height of Orifice Mount' (**H**), Focal length = **F = 2 * H**

2. Measure Error (**E**), from center of the sunspot to the center of the pinhole

*** Any Consistent Units will do ***

Angular Error = Arc TAN (E / F)

WattSun TRACKER ARRAY WITH SolarTrak CONTROLLER TEST RESULTS

The tracker system was evaluated under various sun conditions; bright sunny days with clear conditions, slightly hazy days with few clouds, partial overcast days and overcast days. As expected, the SolarTrak controller was unaffected by sun conditions. We tested the programming and control of the SolarTrack Controller using the remote computer interface. The remote computer interface provided easier access to parameters and calibration data than the onboard controller display. Physical Array parameters were entered into the controller along with the latitude and longitude (as determined from GPS readings) and the Coordinated Universal Time (CUT) obtained from a US government time source. The steel frame of the tracker was positioned in an asphalt area with a clear view of the sky and indexing marks allowed it to be returned to the same orientation after it is moved into position for the day. The tracker frame was adjusted with the corner screw jacks until the vertical alignment of the azimuth axis was as close as could be determined with a bubble level, and the turn count of each jack recorded to provide for consistent realignment.

Using the sun pointer described above, we tested the calibration procedure and made observations of the tracking performance. The maximum error recorded for the center movement was +/- 0.109 inches in the X direction, and +/- 0.094 inches in the Y direction. This corresponds to an angular error of +/- 0.120 degrees in the X direction and +/-0.103 degrees in the Y direction. Referring to the Acceptable Alignment Tolerances outline in Table 1 of the introduction, the misalignment due to tracking with the SolarTrak controller is within the acceptable limits.

A second test involve setting up the tracker with a single fiber to collect light from one-eight of the collector and focus it into a large core fiber mounted in the fiber holder (See Figure 7). The intensity of the light entering the fiber was reduced by a factor of approximately 60 to assure that no damage to the fiber would occur that could bias the test results. The output of this large core fiber was monitored over the course of the day using a Labsphere, Inc., Integrating Sphere. Figure 10, top plot, shows the fiber output in lumens as a function of time with the system being monitored from approximately 11:00am until 4:15pm. The bottom plot shows how the intensity of the sun varied over the same time period as measured using an Eppley Laboratory, Inc., Eppley Radiometer (sometimes referred to as a NIP sensor). As can be seen, the SolarTrak Controller performed well tracking the sun throughout the day, providing an output that varied only with the intensity of the sun and did not vary due to misalignment of the system.

Advantages

The SolarTrack computerized controller has many advantages when compared to the WattSun photovoltaic-based controller, including:

- Consistent operation under varied environmental conditions. Note that the WattSun controller exhibited inconsistent tracking under some circumstances, such as with hazy skies and sky views with contrasting elements from certain types of clouds or adjacent objects.
- Greater tracking precision.
- Adaptability. A computerized controller is inherently adaptable by modifying the software routines to incorporate enhanced tracking algorithms, add features, and accommodate specific issues discovered during development.
- Easily interfaced with external control hardware, for example, switches and weather sensors.
- Networkable. A simple RS-232 network allows a central remote location to monitor and control multiple units.

Possible Enhancements

We have identified several areas where the SolarTrack controller may or should be enhanced to meet specific "Hybrid Lighting" needs:

- Evaluate electrical loads of the axis actuator motors and optimize drive electronics.
- Incorporate a GPS chip to synchronize to an atomic clock and provide latitude /longitude coordinates.
- Provide for automatic self-calibration using feedback from an optical sensor.
- Provide user-interface improvements and operation under MS NT and Windows2000
- Simplify electronics to reduce eventual deployment costs.
- Enhance precision by adding an additional magnetic sensor to double the turncount resolution.
- Evaluate and enhance the calibration software if needed.

CONCLUSIONS

The Hybrid Lighting System requires precise, accurate tracking under all sun conditions. The collector tracking accuracy is critical to the performance of the "Hybrid Lighting System". The SolarTrak computerized controller is far superior to the WattSun controller in applications such as the "Hybrid Lighting System." The SolarTrak Controller performed well tracking the sun throughout the day, providing an output that varied only with the intensity of the sun and did not vary due to misalignment of the system. The misalignment due to tracker error was well within the Acceptable Alignment Tolerances outlined in Table 1 of the introduction.

The WattSun tracking controller with the optical sun sensor performs reasonably well under bright sunny conditions although even under these ideal conditions it did not meet the stringent requirements of our "Hybrid Lighting System." Although the WattSun tracking controller would work reasonably well for applications for which it was designed, it

was unsatisfactory for tracking control for our "Hybrid Lighting System." In solar panel applications, for which the WattSun tracking controller was designed, the alignment precision is less stringent.

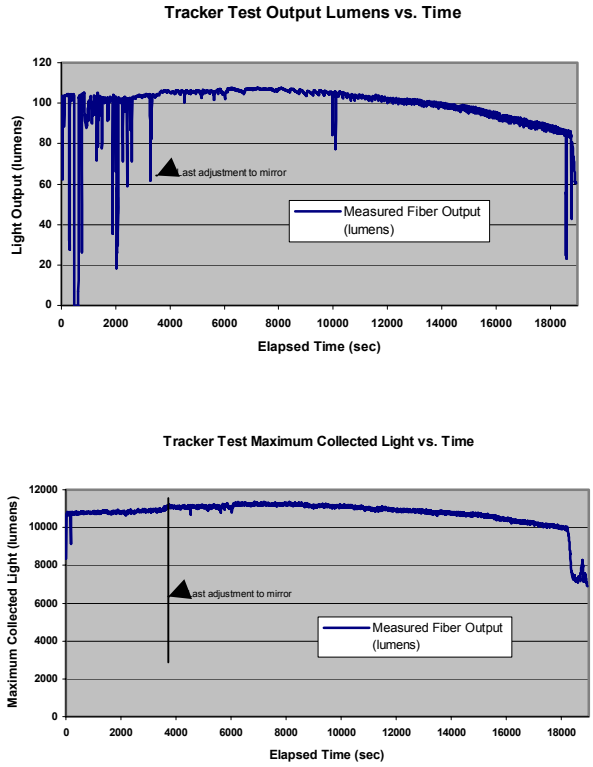

Figure 10. Maximum Collected Light compared to the Fiber Output

ACKNOWLEDGMENTS

Research at ORNL was sponsored by the Energy Efficiency and Renewable Energy Office of the U.S. Department of Energy and the Public Power Institute of the Tennessee Valley Authority. The authors wish to acknowledge the support of Leesa Laymance as Project Assistant, John Turner for his system design efforts, and Mike Jenkins for fabrication of specialized test and development hardware.

This document has been prepared by the Oak Ridge National Laboratory, Oak Ridge, Tennessee 37831-6472, Managed by UT-BATTELLE for the U.S. DEPARTMENT OF ENERGY under contract DE-AC05-00OR22725.

REFERENCES

1. J. D. Muhs, "Hybrid Solar Lighting Doubles the Efficiency and Affordability of Solar Energy in Commercial Buildings", CADDET Energy Efficiency Newsletter December 2000, p. 6.
2. J. D. Muhs, "Design and Analysis of Hybrid Solar Lighting and Full-Spectrum Solar Energy Systems", *Solar 2000, July 16-21, 2000,* American Solar Energy Society.
3. D. D. Earl, J. D. Muhs, "Preliminary Results on Luminaire Designs for Hybrid Solar Lighting Systems", *Solar 2001, April 21-25, 2001,* American Solar Energy Society.

APPENDIX B

OPTICAL DESIGN OF AN INFRARED NON-IMAGING DEVICE FOR A FULL-SPECTRUM SOLAR ENERGY SYSTEM

Dan Dye, University of Nevada, Reno
Mailing Address:
Mechanical Engineering
Mail Stop 312
University of Nevada, Reno
Reno, NV 89557
PH: (775) 784-6735
FAX: (775) 784-1701
Email: dye@unr.edu

Byard Wood, University of Nevada, Reno
Mailing Address:
Mechanical Engineering
Mail Stop 312
University of Nevada, Reno
Reno, NV 89557
PH: (775) 784-6931
FAX: (775) 784-1701
Email: bdwood@unr.edu

Lewis Fraas, JX Crystals, Inc.
Mailing Address:
1105 12th Avenue NW, suite A2
Issaquah, WA 98027
PH: (425) 392-5237
FAX: (425) 392-7303
Email: lfraas@jxcrystals.com

Jeff Muhs, Oak Ridge National Laboratory
Mailing Address:
P.O. Box 2009, MS-8058
Oak Ridge, TN 32831
PH: (865) 946-1281
FAX: (865) 946-1292
Email: um4@ornl.gov

Keywords: non-imaging; thermal photovoltaic; infrared; full-spectrum

ABSTRACT

A solar collector/receiver system for a full-spectrum solar energy system is being designed by a research team lead by Oak Ridge National Laboratory and the University of Nevada, Reno. [1,2] This solar energy system is unique in that it utilizes the majority of the solar spectrum by splitting the infrared (IR) and visible energy for two different end uses. The visible light will be used for day lighting and the IR energy for electrical power generation.

This paper is concerned with the optics that will provide uniform irradiance of the IR energy on the thermal photovoltaic (TPV) array. The benchmark full-spectrum collector/receiver and prototype TPV array have been built [3], so the work performed here is to match the two systems together for optimal performance. The design consists of a non-imaging system for the IR flux incident on the TPV array mounted behind the secondary mirror. Results of the ray-tracing analysis of the different systems tested are presented.

INTRODUCTION

The benchmark full-spectrum solar collector/receiver system built at Oak Ridge National Laboratory has demonstrated effective collection and transfer of the visible portion of the solar spectrum. The visible portion of the solar spectrum is separated from the IR and concentrated for transmittance of the day light via fiber optics to hybrid luminaries or photobioreactors. The IR spectrum is concentrated and will be directed onto a thermal photovoltaic (TPV) array for electric power generation.

The collector/receiver is a modified Cassegrain system that uses a large parabolic mirror and a secondary mirror comprised of multiple planar segments, as

shown in Fig. 1. The secondary mirror's segments are coated with a cold mirror coating that lets IR energy pass through while reflecting the visible light.

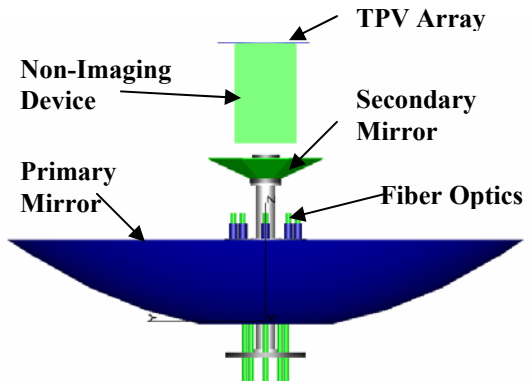

Figure 1. Full-Spectrum Collector/Receiver

The spectral response of the primary and secondary mirrors is shown in Figures 2 and 3. The primary mirror is coated with an enhanced aluminum coating that is highly reflective from the visible out through the IR spectrum. The secondary mirror transmissivity has not been documented beyond 0.9 microns, but is believed to be approximately 95% transmissive beyond 0.8 microns. The IR energy that passes through the secondary mirror is concentrated at the focal point of the primary mirror. This is the problem with the IR optics of the collector/receiver system.

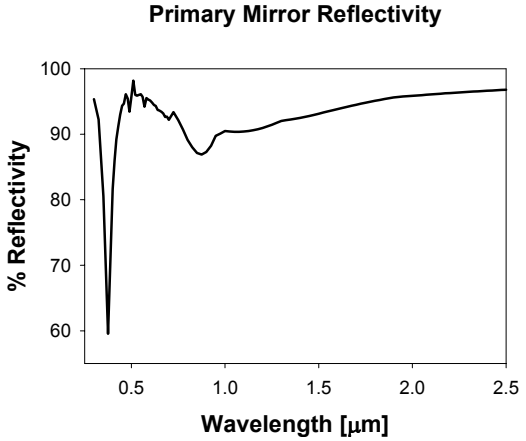

Figure 2. Primary Parabolic Mirror Spectral Response

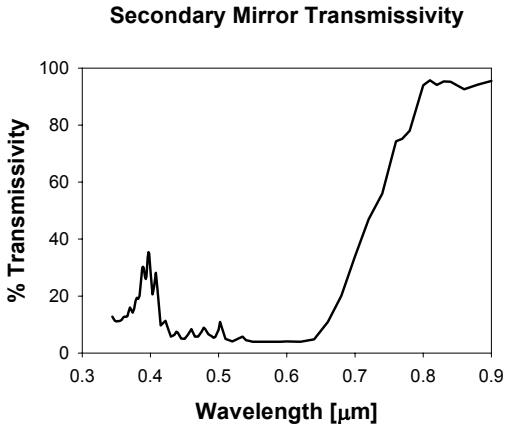

Figure 3. Secondary Mirror Spectral Response

ANALYSIS

The TPV array requires uniform flux in order to function properly, so a non-imaging device is required to de-focus and distribute the flux evenly on the array. The key is to break up the rotational symmetry of the flux, so a cylinder or circular funnel does not work well. A solid square-shaped refractive non-imaging device was investigated as recommended in the literature [4]. However, due to the short f/d of the prototype collector/receiver, excessive reflection losses were expected so hollow total internal reflecting (TIR) systems were investigated. The tube will have an IR-reflective inner surface. For analysis, a 95% reflective inner surface was assumed. Five different geometries have been analyzed here, four of which are shown in Figure 4. The fifth geometry, a cylindrical funnel, produced similar results to the cylinder.

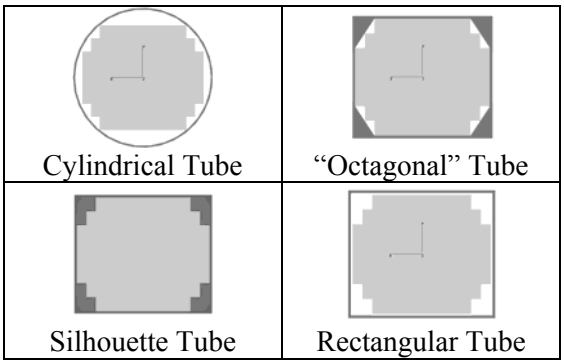

Figure 4. Non-Imaging Geometries Investigated

The TPV array is comprised of 100 Gallium Antimonide (GaSb) cells that are responsive from $0.7 < \lambda < 1.8$ μm. The active area of the array is approximately 180 cm^2. The cells are mounted on a thin dielectric applied to a metal substrate in shingle fashion, as shown in Figure 5. The cells are wired in series, so maximum power output will be reached when all cells receive equal amounts of IR energy.

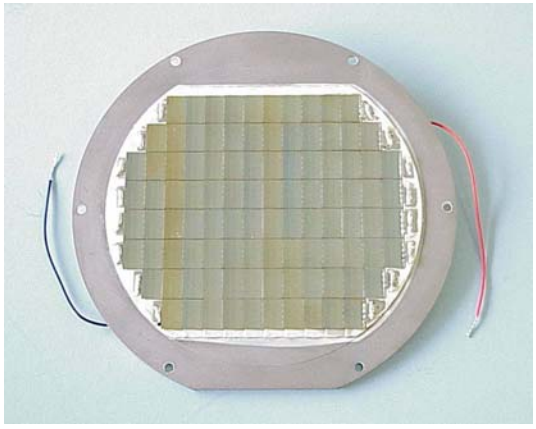

Figure 5. 100 Cell GaSb TPV Array

The analysis was performed using TracePro version 2.4, a ray-tracing optical design program that geometrically traces photons. A solid model of the collector/receiver system with the surface reflectivity and transmissivity properties shown in Figures 2 and 3 was built within TracePro. The solar spectrum at Air Mass 1.0, as shown in Figure 6, is used as the ray source in the analysis. The wavelengths are entered individually with the corresponding irradiance values to accurately represent the direct normal solar radiation.

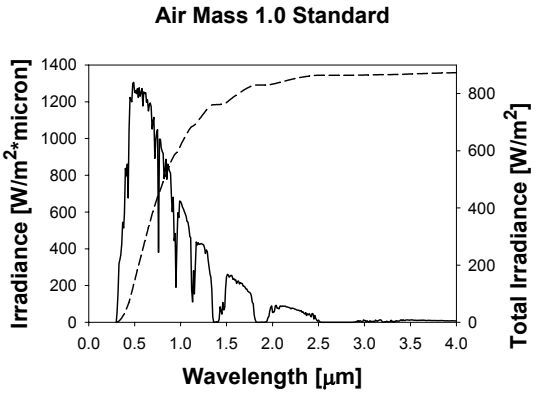

Figure 6. Solar Irradiation Data

The non-imaging device to be investigated is placed at the antenna of the parabolic dish, directly behind and in the shadow of the secondary mirror. The TPV array is moved down the non-imaging device away from the focal point in 0.254 cm (0.1 in.) increments. A Scheme program was written that runs TracePro through these iterations and saves the results in text files, which are later analyzed. The whole analysis is setup and ran for approximately 50 hours on a 1.6 GHz Pentium 4 with 512 mb ram, for each non-imaging device tested. The incident flux on each cell of the TPV array is accounted for and the results are compared to determine which tube geometry and array location provides the least amount of flux variation across the array surface.

RESULTS

A comparison of the absolute flux variation of the four configurations investigated is presented in Figure 7. Of the four systems, three behave as an exponentially decaying function. Only the cylinder exhibits a significant rise in the absolute flux variation after a minimum is reached. This is due to the fact that the other three geometries break up the rotational symmetry of the flux, while the cylinder does not.

Of the four geometries, the simple rectangular tube produces the lowest flux variation of 18.7% (+7.9, -10.8). The average flux value at this point is 2.39W,

while the low is 2.14W and the high is 2.58W. Figure 8 shows the results of the ray tracing analysis of the rectangular tube. The lowest flux variation is reached at 63.5 cm (25.0 in.) from the dish, approximately 23 cm (9 in.) past the focal point.

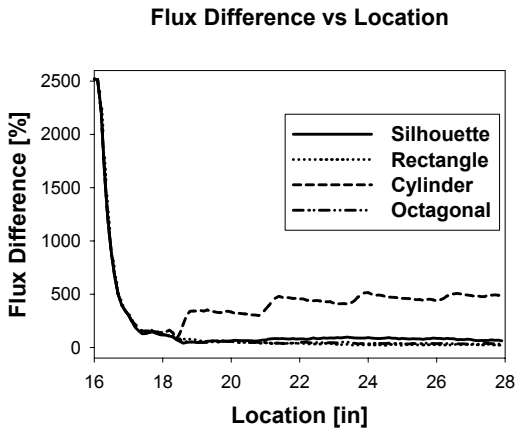

Figure 7. Comparison of the Four Configurations Investigated

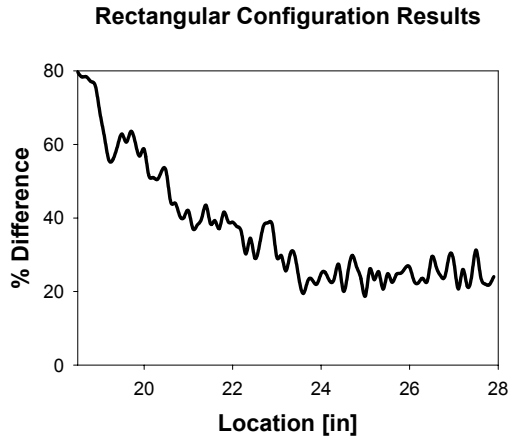

Figure 8. Ray Tracing Results

Three dimensional flux maps are shown in Figure 9. The flux profile is seen to flatten out as the array is moved away from the focal point. The downside of the rectangular tube is that there are losses at the four corners of the TPV array. Future iterations of the TPV array and non-imaging system will be tailored towards the rectangular tube.

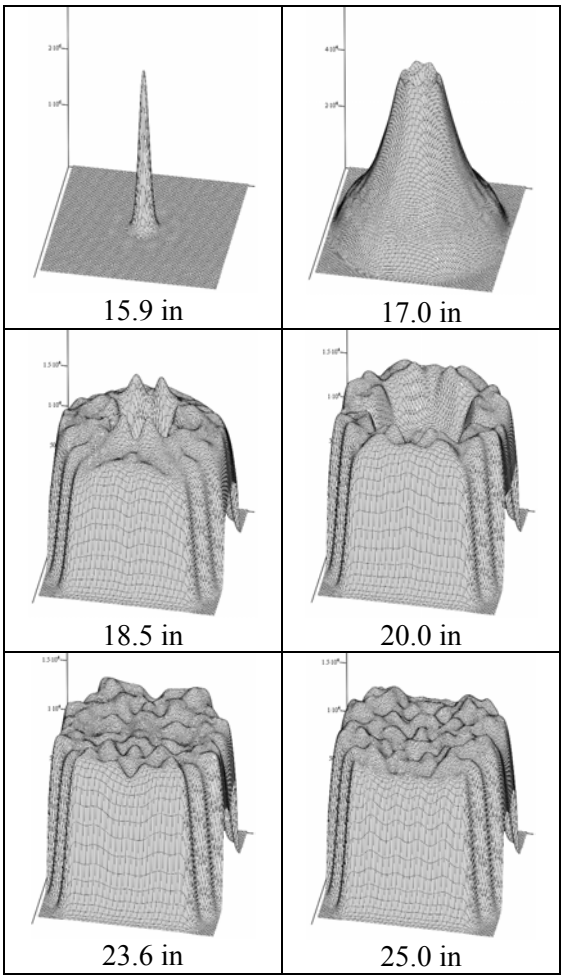

Figure 9. Flux Distributions at Different Locations in the Rectangular Non-Imaging Device

CONCLUSIONS AND RECOMMENDATIONS

A simple, yet effective, non-imaging device has been shown that can reduce the flux from a 2525% flux variation across the TPV array at the focal point of the primary mirror down to an 18.7% flux variation within a very short distance. This IR energy system, in combination with the visible lighting system to be used for day lighting or photobioreactors, can better utilize the solar spectrum than standard day lighting systems or photovoltaic cells alone.

Future iterations of the non-imaging device and TPV array will produce better matched

systems. A simple alternative to the current TPV array is an array with less cells and a rectangular shape. This would obviously have fewer losses due to space at the corners, and possibly a shorter tube length would reduce the losses in the non-imaging device as well.

ACKNOWLEDGEMENTS

This project is funded in part by:
Cooperative Agreement
DE-FC26-01NT41164

Thanks also go to Oak Ridge National Laboratory and all team members involved in this project.

REFERENCES

[1] J. Muhs, "Design and Analysis of Hybrid Solar Lighting and Full-Spectrum Solar Energy Systems," American Solar Energy Society, SOLAR2000.

[2] J. Muhs, "Hybrid Solar Lighting Doubles the Efficiency and Affordability of Solar Energy in Commercial Buildings," CADDET Energy Efficiency Newsletter, No. 4, pp. 6-9 (2000).

[3] L.M. Fraas, W.E. Daniels, J. Muhs, "Infrared Photovoltaics for Combined Solar Lighting and Electricity for Buildings," Proceedings of 17th European Photovoltaic Solar Energy Conference, (2001)

[4] J.J O'Gallagher and R. Winston, "NonImaging Solar Concentrator with Near Uniform Irradiance for Photovoltaic Arrays," Nonimaging Optics: Maximum Efficiency Light Transfer VI, Proceedings of SPIE Vol. 4446 (2001)

APPENDIX C

ELECTRICITY FROM CONCENTRATED SOLAR IR IN SOLAR LIGHTING APPLICATIONS

Lewis M. Fraas & James E. Avery, JX Crystals, Issaquah, WA
Takashi Nakamura, Physical Sciences Inc., San Ramon, CA
29th IEEE Photovoltaic Specialist Conference

The sun's spectrum can be divided into visible light and infrared where the sunlight can be used for plant growth(1) or building interior lighting(2) and the IR can be converted to electricity using low bandgap GaSb photovoltaic cells. Physical Sciences Inc. (PSI) has been developing the Solar Lighting System for space based plant growing as schematically shown in Figure 1. In this system, the solar radiation is collected by the parabolic mirror which then reflects and concentrates the solar radiation onto the selective spectral reflector where the solar radiation is divided into two spectral components: the photosynthetically active radiation (PAR) spectra (light: 400 nm < λ < 700 nm); and non-PAR spectra (IR: λ > 700 nm). The PAR component is directed to low-loss optical fiber or lightguide cables. The PAR spectra are transmitted to the plant growth chamber where the light distribution panel spreads uniform light over the plants at an optimum intensity for plant growth. The IR spectra is converted to electric power by low bandgap photovoltaic (PV) cells.

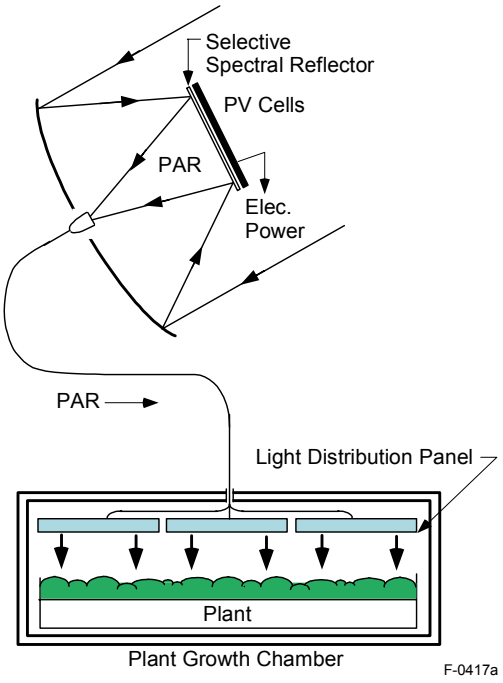

Figure 1. Schematic representation of the Light pipe solar lighting system for space IR based plant growing

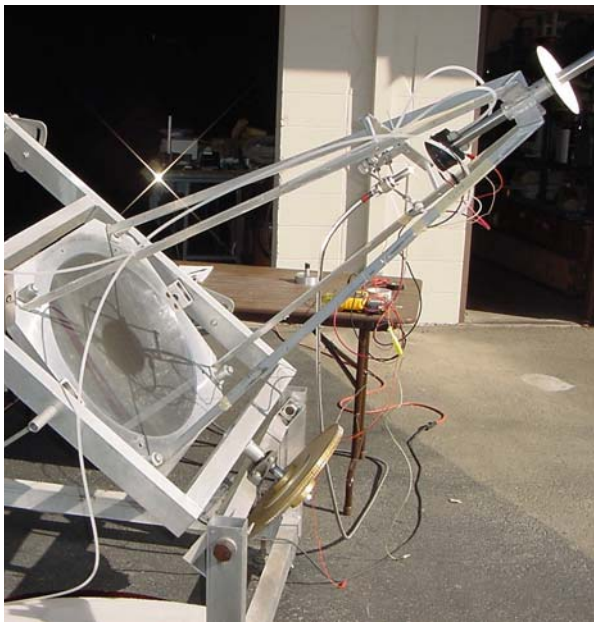

Figure 2. Experimental facility for GaSb cell performance characterization tests for solar spectra

In this paper we will discuss results of the performance characterization tests using the GaSb cell for with the IR solar spectra. The experiments were conducted at PSI's solar laboratory in San

Ramon, CA using the experimental system shown in Figure 2 for outdoor testing. JX Crystals provided the cells. As shown in the photo, a 20 inch parabolic mirror reflects the solar radiation to the PV cell module near the focal point of the mirror. The cold mirror installed at the PV cell module reflects the PAR to the aperture of a 10-meter lightguide which transmits the light inside the building. Emission of the PAR from the other end of the lightguide in the building is visible. The IR spectra is converted into electric power by the GaSb cell placed behind the cold mirror in the PV cell module. Figures 3 shows the solar spectra separated by the cold mirror.

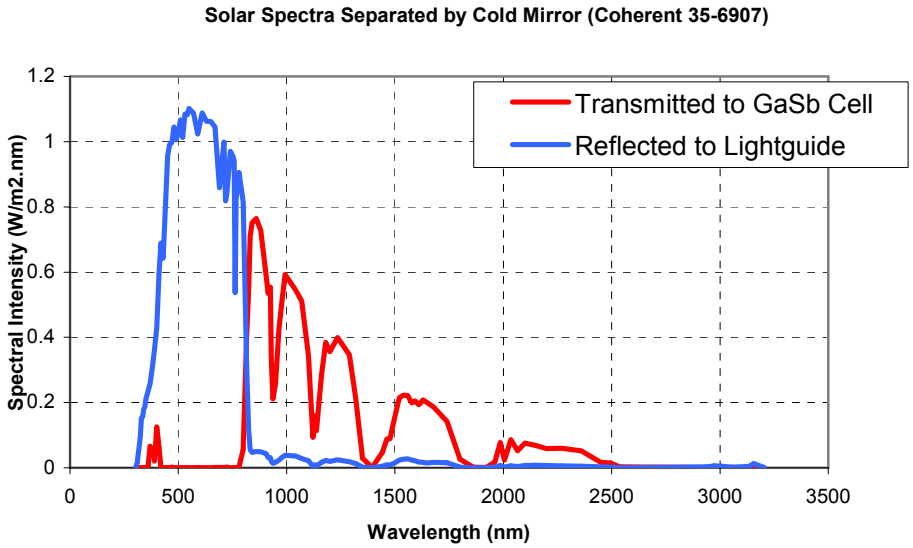

Figure 3. Solar spectra reflected by the cold mirror at the PV cell module

A representative outdoor measurement was made on 11/7/2001 of the efficiency and power density for a water-cooled GaSb cell. The resultant current vs. voltage curve for a 1 cm^2 cell is shown in Figure 4. Also noted is a calorimeter measurement of the incident IR power density.

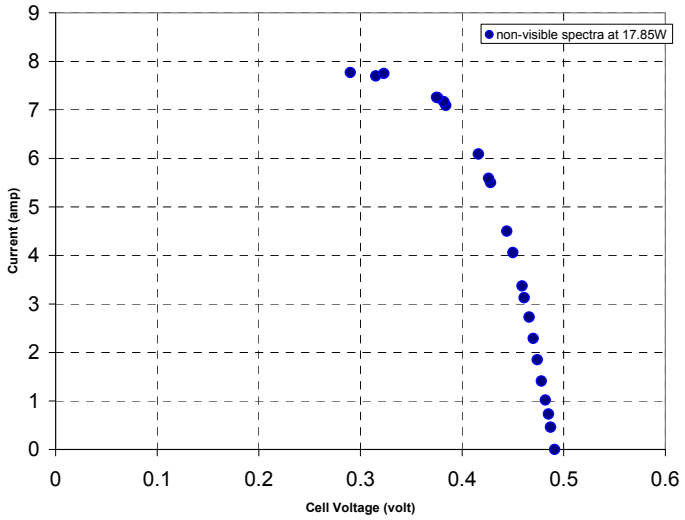

Figure 4: Outdoor illuminated current vs. voltage for 1 cm^2 GaSb cell.

The data from Figure 4 can be summarized as follows.

Isc = 8 Amps	Voc = 0.49 V	P(IR) = 17.85 W
Imax = 7.2 Amps	Vmax = 0.38 V	**Pmax = 7.2x0.38 = 2.74 W**
FF = (7.2x0.38)/(8x0.49) = 0.7		**Efficiency = 2.74/17.85 = 15.3%**

These outdoor data are consistent with projections based on indoor flash test data combined with quantum efficiency data as the following discussion shows. GaSb cells are typically fabricated for TPV applications. The GaSb cells measured here were TPV cells with antireflection (AR) coatings tuned to 1.5 microns. However, improved AR coatings can be designed specifically for this application as shown in Figure 5.

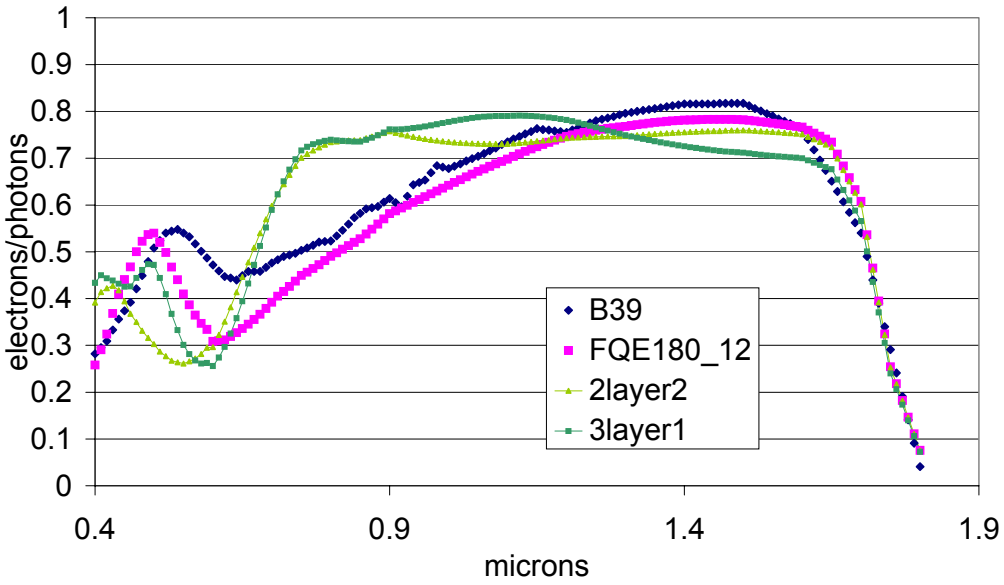

Figure 5: GaSb cell external spectral response given various AR coating designs.

Referring to Figure 5, the B39 QE is a measured curve for a typical GaSb TPV cell. The FQE180_12 curve is consistent with an internal QE of 90% from 0.8 to 1.7 microns and a grid shading of 12% and a 180 nm Silicon Nitride AR coating. This curve is consistent with a standard TPV cell where the AR is set to peak at 1.5 microns. The remaining curves are for potential improved AR coatings for the solar lighting case. When these curves are convolved through the IR filter function, we get the following currents. The FQE180_12 current is
22.1 ma/cm^2 and the 3layer current is 25.4 ma/cm^2.

Using these calculated Isc values from the various QEs and: given 1 sun IR power=490 mW/cm2
Then for Case 1: 3layer AR
The Efficiency = (0.7 x 0.49 V x 25.4 mA/cm2) / 490 mW/cm2 = 17.8%
And for Case 2: FQE180_12
The Efficiency = (0.7 x 0.49 V x 22.1 mA/cm2) / 490 mW/cm2 = 15.5%
The FQE180_12 data are more representative of the measured cell and the data is in very good agreement. However, with a simple improvement in the cell AR coating the cell efficiency can be raised to 17.8%. Note also that the electric power produced by a 1 cm^2 GaSb cell is a remarkable 2.74 W.

APPENDIX D

A DETERMINISTIC METHOD FOR ALIGNING MULTIPLE OPTICAL WAVEGUIDES TO A PARABOLOIDAL COLLECTOR

L. C. Maxey
Oak Ridge National Laboratory
Oak Ridge, Tennessee

B. J. Hilson
Oak Ridge Institute for Science and Education Participant
411 Baucom Deese Road
Monroe, NC 28110

ABSTRACT

For solar lighting systems employing fiber optic waveguides[1,2], to conduct the collected light, paraboloidal mirrors are the preferred reflector choice. This is due to the fact that an ideal paraboloid can transform the highly parallel rays from the sun into an un-aberrated, well-focused spot. To maintain high transmission efficiency, the focused spot must be smaller than the entrance aperture of the fiber optic waveguide. To achieve optimum performance in systems requiring relatively small focused spot sizes, both the quality of the mirror and the quality of optical system alignment must be well controlled.

In systems employing multiple waveguides with a single paraboloid, the focus of the paraboloid must be segmented into several separate focal points directed into individual fibers. Each waveguide entrance aperture must be accurately co-located with its designated focal point so that the image that is formed on the fiber will have the fewest possible aberrations and thus, the smallest possible focused spot size.

Two methods for aligning individual optical waveguides in a multi-aperture paraboloidal collection system are described. The first method employs a commercially available collimation tester to incrementally improve the alignment. The second, a deterministic method, employs a cube corner retro-reflector and an easily constructed imaging system to reliably align the fibers to their respective segments of the parent paraboloid. The image of the focused spot formed by the light that is returned from the retro-reflector reveals alignment information that is easily interpreted to enable pitch, yaw and focus errors to be systematically removed. This ensures that the alignment of the system is optimized to reduce aberrations prior to final adjustment of the system "on-sun".

INTRODUCTION

A paraboloidal mirror is uniquely suited for the collection of sunlight for distribution via optical waveguides. It represents the mathematically perfect solution to the energy concentration challenge. That is to say, it is the only shape that can perfectly reflect parallel rays to form an un-aberrated focused spot. The sun, because of its finite size and great distance, can be considered a source of parallel rays. And the introduction of sunlight into optical waveguides requires the ability to form a well-focused spot at the waveguide entrance aperture.

The quality of the mirror and the alignment of the optical system both have a significant influence over the ultimate size of the focused spot. The minimum spot size that can be realized by a given mirror is determined by the degree to which the mirror represents a perfect paraboloid. Irregularities in the paraboloidal shape of the mirror, as well as any roughness or fine structure in the reflective surface, will cause light to stray from the intended point of focus. This results in a larger than optimum spot size and a degradation in optical performance. The physical imperfections in the paraboloid will determine the limit of the best performance that can be achieved with a particular mirror. Actually obtaining that level of performance requires that the mirror be perfectly aligned into the collection system. Any misalignment will create aberrations that further increase the spot size and decrease performance.

A solar tracker employing fiber optic waveguides is shown in Fig. 1. As the light reflected from the paraboloidal mirror converges, it intercepts an assembly of plane mirrors. These mirrors (see Fig. 2.) divide and fold the collected light to form eight individual focused spots. A large core (12mm) optical waveguide is positioned at each of the focused spots to receive and conduct the collected light.

Fig. 1. Solar tracker and collector system partially populated with four waveguides

Fig. 2. Collection optics close up, showing segmented planar secondary mirrors

A solar collection system of this type could be constructed with little regard for the axis of the paraboloid. Conceivably such a system might even function well enough to get light into all of the waveguides. The system as a whole would, however, function with diminished performance. If the optical axis of the paraboloid were pointed a few degrees away from the sun, it would still concentrate the light but the alignment aberrations would produce (relatively) large and asymmetric focused spots.

Paraboloidal collector alignment – practical considerations

In order to appreciate the importance of properly aligning the paraboloidal primary mirror in a waveguide-distributed solar lighting system, the relationship of that alignment to the cost and performance of the system must be understood. Within such a system, the characteristics of the primary mirror, the solar tracking system and the waveguides for distribution of the collected sunlight are mutually interdependent. The collection of light into a fiber optic waveguide requires a mirror capable of producing a focused spot that will fit within the entrance aperture of the selected waveguide. In addition, the accuracy of the tracking system must be such that the focused spot remains within the aperture of the waveguide throughout the tracking process.

The interdependent nature of the system components has significant practical (and financial) implications. For example, assume it is possible to obtain a "perfect" solar tracking system for use with a convenient diameter of commercially available optical waveguide. The paraboloidal primary mirror for use in such a system could contain imperfections as long as it was of sufficient quality to collect the light into a spot the size of the entrance aperture of the waveguide. Since the cost of the mirror increases with the degree of accuracy of the paraboloidal surface, this would set an economic baseline.

However, real solar trackers are not perfect. They are constructed with mechanical drive mechanisms that may have slack or backlash in them, and they are controlled by feedback systems with gain and dead-band control limitations or by pre-programmed algorithms with finite inaccuracies. Thus, in a real tracking system the focused spot will move around relative to the aperture of the waveguide during the tracking process. To ensure that the focused light remains within the aperture of the waveguide, a better (more expensive) paraboloidal mirror may be necessary. Alternately, a lager (more expensive) waveguide might be chosen to accommodate the tracking system deviations. To keep the costs of the mirror and waveguide within manageable bounds, a more accurate (more expensive) tracker might have to be developed.

Whatever balance in performance is finally distributed among the three interdependent components, it is clear that any degradation in performance of one element will affect the requirements of the other two, as well as the overall system cost. It is for that reason that the alignment of the paraboloidal primary mirror is of such importance. Ultimately, the performance of the paraboloidal mirror is only as good as the quality of its alignment within the complete solar collection system.

The challenge of aligning the paraboloid is that neither the optical axis nor the focal point can be directly measured by any mechanical means. Their locations can only be inferred through tedious physical measurements of the paraboloid's surface. With some manufacturing processes, such as single point diamond turning, it is easy to incorporate fiducial reference features for accurately locating the axis and focal

point. Due to cost constraints, however, mirrors produced through (relatively) inexpensive replication processes are more likely candidates for use with solar lighting systems. With such mirrors, it is usually necessary to optically locate the focus and axis of the paraboloid.

Methods for optically locating the paraboloidal focus

Upon first consideration, the process of locating the focal point of a paraboloid may seem trivial. In principal, given a source of parallel rays, one need only adjust the paraboloid relative to the parallel rays, until an un-aberrated image is obtained. This general method is actually known as a "star test" and is widely used in amateur astronomy and optical testing[3]. The location of the best focus of that image is the focal point of the paraboloid, and the axis is the line that passes through that focus and is parallel to the rays from the source.

There are several challenges associated with using the star test method. Choosing a good source of parallel rays, for alignment of a large paraboloidal mirror, is not trivial. The source should be large enough to illuminate a representative portion of the aperture of the paraboloid and must not have any detectable divergence or convergence. Precisely adjusting the angular position of the mirror relative to the source of parallel rays can be an engineering challenge in itself, further complicating the overall alignment challenge. Evaluating the quality of the focused spot is non-trivial, requiring high resolution to reveal subtle alignment cues in the image. Even after an un-aberrated focus is obtained, however, identifying its position in a way that is useful for the alignment of the subsequent components may be difficult.

There is an alternate approach to locating the focus of a paraboloid that essentially reverses the approach used in the star test. Instead of beginning with a distant source of parallel rays, a point source is placed near the focus of the paraboloid. The location of the point source is then adjusted until the reflected rays from the paraboloid form an un- aberrated parallel beam. There are advantages to this method that make it very attractive. One advantage to this approach is that it is relatively simple to move the point source relative to the paraboloid. The need to precisely tip and tilt the mirror relative to a parallel source is eliminated. Another advantage to this method is that the apparatus that is used to position the point source provides an un-ambiguous reference, clearly marking the location of the focal point of the paraboloid.

The challenge with this method is that it is more difficult to observe aberrations in a parallel beam than it is to detect them in a focused spot. Two methods are described for locating the focus of a paraboloidal mirror by using a point source located near the focus. These methods require relatively simple hardware for detecting the aberrations in a parallel beam of light. The first method employs a commercially available collimation tester to incrementally improve the alignment. The second of the two methods uses a beamsplitter to sample the light returned from a retroreflector. The latter method builds upon a novel approach developed previously[4,5], to enable the aberrations to be very systematically interpreted to deterministically correct the alignment.

Alignment strategy

In the system shown in Figs. 1 and 2, the mechanical mounting assembly that holds the waveguides in place allows for about 5mm of adjustment laterally in two dimensions (see Fig. 3.) The vertical position of the waveguide can be adjusted to place its aperture at the height of the folded focal point from the paraboloid. It was determined that, using these available adjustments, each waveguide could be individually aligned to the best-fit parabolic surface of its respective octant of the mirror. Although local variations in the mirror might cause the individual best-fit paraboloids to have different optical axes, the aggregate should coincide with the axis of the parent mirror.

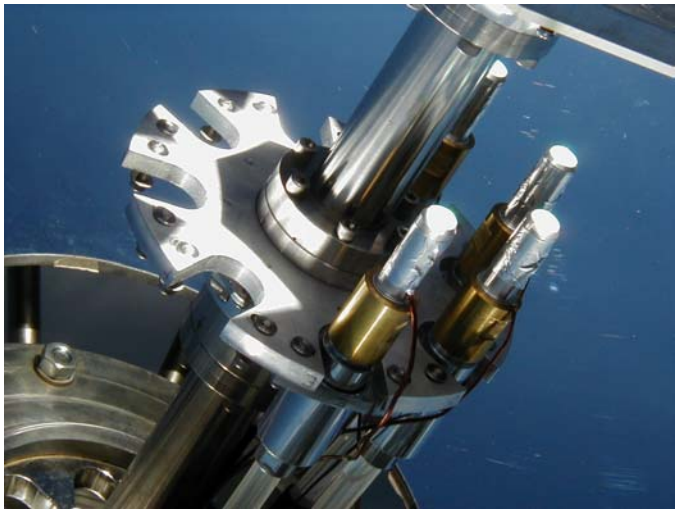

Fig. 3. Close up of waveguide mounting structure showing slotted positioning mechanism (pitch adjustment slots visible at edges of round clamping nuts)

The alignment of each waveguide holder would be achieved by placing a fiber optic "point source" in an adapter designed to fit the mounting hardware for the waveguides. The location of the point source, mounted in the waveguide holder, would be adjusted until the aberrations in the collimated beam reflected from the paraboloid were removed. The adjustments would then be locked down and the height of the point source location recorded. After removing the point source, the waveguide would then be placed into the holder and is input aperture adjusted to the measured height.

After aligning the individual waveguides, the mirror would be pointed toward the sun. The azimuth and elevation would be adjusted to achieve a "best fit" of the multiple focused spots to the entrance apertures of the waveguides. This would, in effect, arrive at the average agreement in the location of the optical axis, accounting for any variations among the individual segments. Minor adjustments of selected waveguide positions would then ensure the foci were centered within the apertures of all of the waveguides.

Alignment procedure

To implement the alignment strategy, a single mode optical fiber was used for a point source. The end of this optical fiber was mounted in the center of an aluminum rod of the same diameter as the large core optical fiber waveguides. This enabled the point source to easily be secured into the mounting structures for the waveguides. A low-power helium neon laser was focused onto the opposite end of the single mode fiber using a microscope objective in a three-axis translation mount. The light from the fiber formed a diverging beam that illuminated the central portion of the collection area of the paraboloid octant being aligned.

The position of the point source was adjusted using the translation slots provided in the waveguide mounts. These are two orthogonal pairs of slots, one pair on the mount itself and one pair in the plate to which it is attached. Together they enable about 5mm of travel in the two axes. Movement of the mount radially in and out is referred to as "yaw" adjustment and the transverse adjustment is referred to as "pitch" adjustment. These refer to the influence that the two adjustments have on the beam direction. In both cases, pitch and yaw, the adjustment produces a deflection similar to that which would result from rotating the mirror about its associated (pitch or yaw) axis as illustrated in Fig. 4. It is important to note that the adjustment for each segment has the same pitch and yaw nomenclature and that the frame of reference is tied to the individual mirror segment, without regard for where it is (e.g. 9 o'clock position versus 12 o'clock position) within the collector assembly.

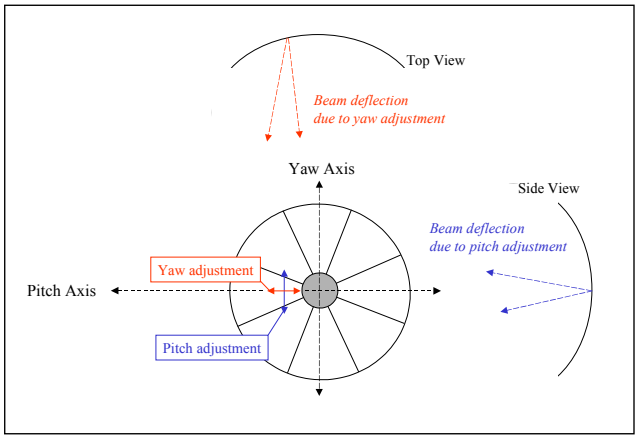

Fig. 4. Schematic representation of parabolic collector illustrating axis definitions, pitch and yaw adjustment axes and associated beam deflections

The first method for identifying and eliminating aberrations in the collimated beam used a shear plate collimation tester (or shear plate interferometer). A shear plate interferometer is a simple device for evaluating the collimation of a laser beam[6]. It uses a thick glass plate to shear the incoming beam with respect to itself, producing an overlap region as shown in Fig. 5. It incorporates an imaging screen upon which interference fringes are formed and a reference line is incorporated into the imaging screen so that the collimation can be evaluated (see Fig. 6). When the fringes are parallel to the reference line, the light is collimated. If the light is either converging or diverging, the interference fringes will cross at an angle to the reference line. The sign of the slope indicates whether the beam is converging or diverging. The collimation of a beam is only evaluated along one axis (the shear axis along the reference line) at a time. When a beam contains astigmatic aberrations, the shear plate may show it to be perfectly collimated in one axis but will reveal defocus when the shear plate is rotated to analyze another axis.

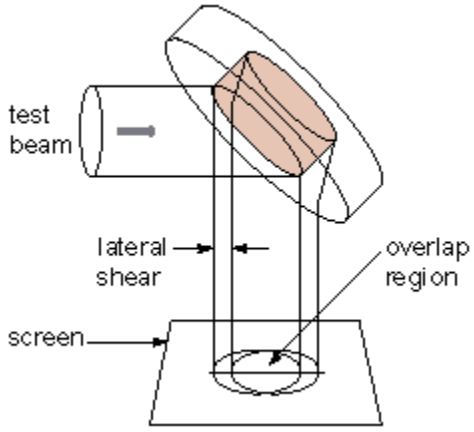

Fig. 5. Schematic representation of shear plate *Source*: "Theory and uses of shear plates," http://photon.bu.edu/PRIDE/SC570/labs /lab1/theory.htm

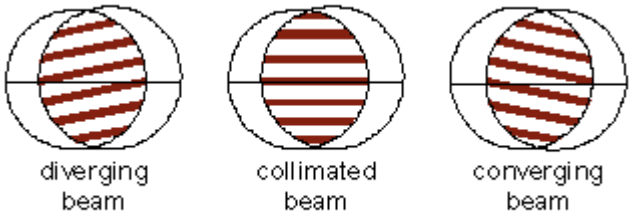

Fig. 6. Shear plate interferograms showing divergent, collimated, and convergent beams *Source*: "Theory and uses of shear plates," http://photon.bu.edu/PRIDE/SC570 /labs/lab1/theory.htm

In the alignment process, the shear plate was placed in the semi-collimated beam reflected from the paraboloid. The shear axis of the plate was aligned with the radial axis of the segment being tested (i.e. the pitch axis). The height of the point source was first adjusted to eliminate the tilt in the interference fringes, so that they were parallel to the reference line. The shear plate was then rotated 90° so that its shear axis was perpendicular to the previous orientation. Any tilt observed in the fringes (see Fig. 7) would indicate that the beam was astigmatic. To reduce the astigmatism, the "pitch" translation axis of the waveguide mount was adjusted to attempt to achieve an equal amount (magnitude and sign) of tilt in the interference fringes for both

orientations of the shear plate. Once equalized, that axis was stabilized and (with the shear axis again aligned to the pitch axis of the segment) the focus error again minimized with the height adjustment. The process was then repeated using the "yaw" translation axis to attempt to remove the astigmatism by equalizing (for all shear plate orientations) any focus error that was observed. The highly iterative process consisted of first establishing a near focus condition, then identifying any astigmatism and removing it by making the amount of defocus equal in the two orthogonal shear plate orientations (and in between), then removing the residual focus. The process continued until the defocus and astigmatism were minimized.

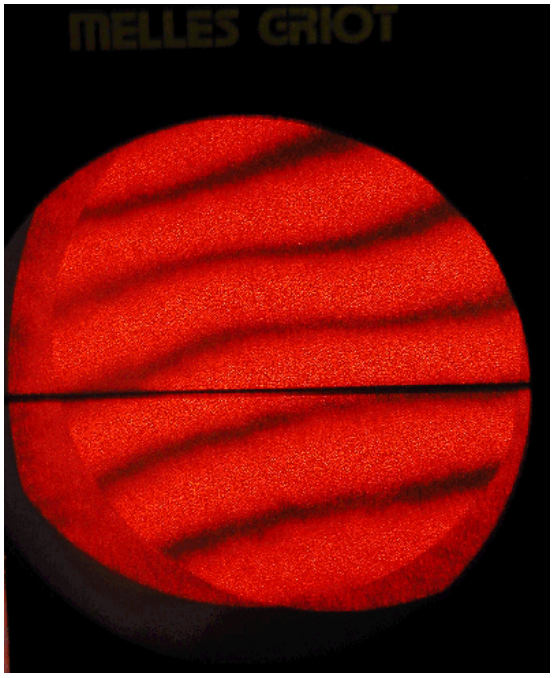

Fig. 7. Shear plate interferogram revealing moderate focus error along with wavefront distortion

The second method for identifying and removing aberrations in the beam reflected from the paraboloid employed a large aperture (63mm) corner cube retroreflector. A corner cube retroreflector has the useful property that it returns light rays along a path exactly parallel to the path from which it received them. Thus, when it was placed in the semi-collimated beam reflected from the paraboloid it returned the light back to the same portion of the paraboloid from whence it came. That light was then re-focused onto the end of the single mode fiber. A beamsplitter and a CCD camera (just the CCD array with no lens) were used to sample part of the returned light to evaluate the quality of the focused spot. A microscope cover slip was used for the beamsplitter, making its cost negligible but creating a double image of the focused spot (due to the reflection from both surfaces of the cover slip). The camera and beamsplitter were mounted on a single mounting structure that was attached to the aluminum rod containing the point source. This assembly, shown in Fig. 8, placed the beamsplitter at 45° to the returned beam and positioned the plane of the CCD array so that it and the point source were both equidistant from the beamsplitter. The output of the CCD array was observed on a black and white television monitor. As the height of the point source was adjusted, the focused spot on the camera could immediately be interpreted to see if the returned light was focused or not. The position of the point source could then be swiftly and intuitively moved to achieve the best focus of the returned light. It should be noted that this is tantamount to performing a star test, with the point source, paraboloid and corner cube functioning together to produce the source of the parallel light rays.

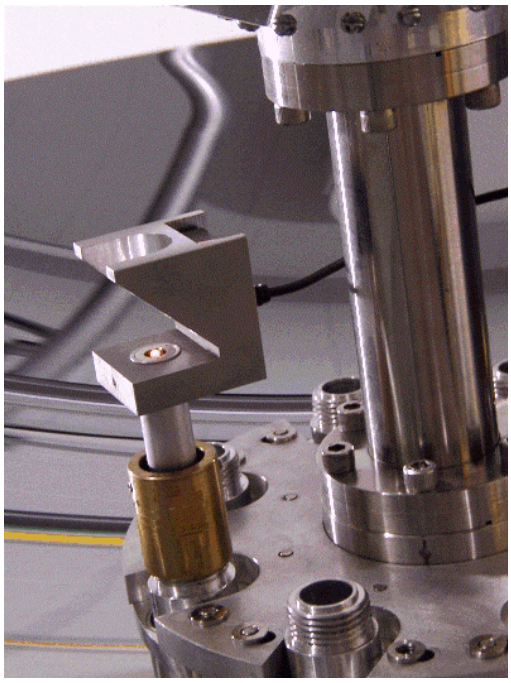

Fig. 8. Beamsplitter/camera mount attached to single mode fiber adapter in waveguide mounting structure

It is the interpretation of the alignment information contained in the focused spot that makes this technique particularly useful. Initially the best focus will probably be observed to be somewhat elongated, indicating astigmatism. The nature of the interaction between the paraboloid and the retroreflector enables the elongation of the focused spot to be systematically evaluated to align the system. The beamsplitter/camera mount must first be oriented so that the camera is pointing outward along the radial (pitch) axis of the segment being adjusted. In that orientation, the following procedure can be followed.

Observing the focused spot, note whether the elongated spot is either perfectly vertical or horizontal. If it is tilted with respect to either axis, it indicates the presence of pitch error as shown in Fig. 9a. Adjust the pitch translation of the waveguide mount to force the elongation into alignment with either the vertical or horizontal axis as shown in Fig. 9b. The remaining elongation indicates yaw error and may be removed by adjusting the yaw translation axis to produce a round focused spot. The height of the point source is then adjusted once again to produce the best (smallest) focused spot. If the spot is round (as in Fig. 9c) and shows no further elongation, the alignment is optimized. Otherwise, the same methods of interpretation and

adjustment should be applied to eliminate any residual elongation in the focused spot.

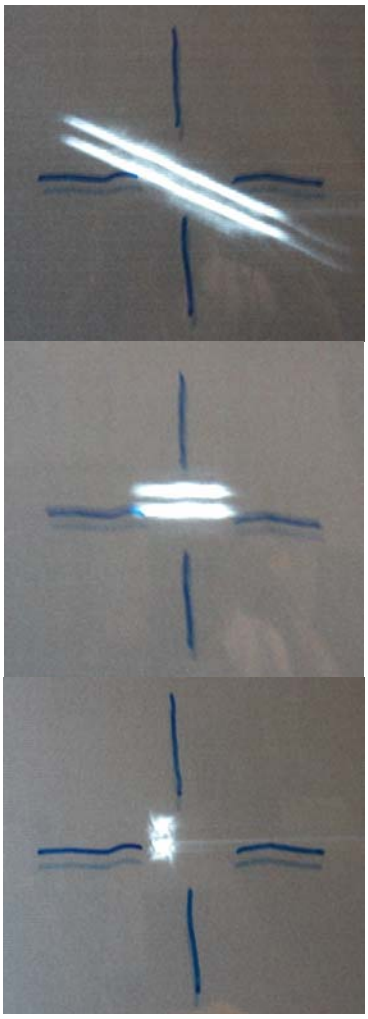

Fig. 9. Alignment sequence showing:
a. prior to adjustment, dominant pitch error;
b. pitch error removed, revealing only yaw error;
c. yaw error removed revealing final well focused un-aberrated spots

DISCUSSION AND RESULTS

Both the shear plate method and the corner cube method of alignment proved to be effective, however, the corner cube method was faster, easier, and more reliable. The shear plate revealed some information about local surface irregularities in the mirror that were less obvious in the focused spots obtained with the corner cube method.

Some segments of the mirror showed greater irregularities than others. The focused spots for some segments were almost perfectly circular, while others had residual astigmatism that could not be eliminated through further alignment. Particularly in those cases, determining when the alignment was optimized would have been much more difficult with the shear plate method. During the alignment process, the segments that seemed to have significant distortion in the mirror were noted. During the "on-sun" final alignment, the majority of the spots could be centered in the waveguide apertures by adjusting the azimuth and elevation of the solar tracker. Minor additional adjustments using the translation adjustments on the waveguide mounts were necessary to optimize the alignment into the remaining waveguides.

ACKNOWLEDGMENTS

Research at ORNL was sponsored by the Energy Efficiency and Renewable Energy Office of the U.S. Department of Energy and the Public Power Institute of the Tennessee Valley Authority.

This document has been prepared by the Oak Ridge National Laboratory, Oak Ridge, Tennessee 37831-6472, managed by UT-BATTELLE for the U.S. DEPARTMENT OF ENERGY under contract DE-AC05-00OR22725.

REFERENCES

1. Muhs, J. D., "Hybrid Solar Lighting Doubles the Efficiency and Affordability of Solar Energy in Commercial Buildings," CADDET Energy Efficiency Newsletter December 2000, p. 6.
2. Muhs, J.D., "Design and Analysis of Hybrid Solar Lighting and Full-Spectrum Solar Energy Systems," *Solar 2000, July 16-21, 2000,* American Solar Energy Society
3. "Star Tests," Optical Shop Testing, Chapter 11, Edited by Daniel Malacara, John Wiley and Sons Inc., 1978
4. Maxey, L. Curt, "Novel Technique for Aligning Paraboloids," Proc. SPIE 1531, 147-155, 1991
5. Maxey, L. Curt, et al., "Automated Alignment System for Aspheric Mirrors," Proc. SPIE 1776, 130-139, 1992
6. "Theory and uses of shear plates," http://photon.bu.edu/PRIDE/SC570/labs/lab1/theory.htm

APPENDIX E

CHARACTERIZATION OF TRANSMISSION PROPERTIES OF 3M LF120C PLASTIC OPTICAL LIGHT GUIDE

M. R. Cates, S. L. Jaiswal, L. C. Maxey, D. D. Earl
Oak Ridge National Laboratory
Oak Ridge, Tennessee

ABSTRACT

Transmission studies of 3M optical light guide, type LF120C with nominal 12.6 mm core diameter, were performed to characterize the material for use in hybrid solar lighting applications, in particular for the transport of sunlight from a collector to discrete lighting fixtures (luminaires). The light guide properties studied included: total transmission (in lumens) per unit length, transmission as a function of input angle and wavelength, transmission as a function of bend radius, and transmission through two bends. The preliminary value for total transmission is 96.6 % per meter. Angular input begins to drop significantly at angles greater than 25 degrees. Wavelength transmission has significant minima at about 643 and 750 mm. Losses through bends are much greater for light input at large angles. In addition to the data compilations and detailed summaries of measurement findings, the measurement system and error sources are described.

INTRODUCTION

As the United States moves into the 21st century and the post-September 11th era, our efforts to increase energy efficiency and minimize dependence on foreign oil take on increasing importance. In our active, industrialized society one of the leading energy costs continues to be lighting. The peak electric lighting bill, ironically, occurs when the sun is highest, near midday, and therefore, when solar light is maximally available. The Hybrid Solar Lighting (HSL) program, [1] centered at Oak Ridge National Laboratory and involving a number of industrial and government partners, conceived to take advantage of available solar light, is dealing directly with the challenge to produce lower-cost, higher quality lighting that can be included in new construction and retro-fit into older facilities. An important part of the HSL approach is the transport of solar light, collected by systems exterior to the buildings involved, or light from centralized artificial sources. Large-core plastic light guides are good candidate materials for this purpose because of their light-carrying capacities, relatively low cost, and flexibility. In this study, a commercial plastic guide has been evaluated both qualitatively and quantitatively in the attempt to determine its degree of utility for use in HSL systems.

Light Guide Characteristics

The plastic light guide used in this study, manufactured by 3M Corporation, is identified as type LF120C. Its core diameter is nominally 12.6 mm. Our random checks of the core diameters of various pieces of the material showed that it could vary between about 12.0 and 13.0 mm. The core index of refraction, n_1, is given as 1.498. The material is polymethacrylate (PMA). It was designed to be flexible down to 0 degrees centigrade. The cladding is a polyfluorocarbon similar to Teflon, with an index, n_2, of 1.35. In addition to this work, other investigations of the 3M light guide are focusing on improving coupling, surface polish, index matching materials, temperature dependent behavior, and other related properties. [2]

Applying Snell's Law to the two materials, the core and the cladding of the light guide, we can write

$$n_1 \sin\theta_1 = n_2 \sin\theta_2,$$

where θ_1 is the angle from the normal to the two surfaces made by the light ray in the core, and θ_2 is the angle from the normal to the two surfaces made by the light ray in the cladding. The critical angle, θ_c, is reached when the light approaching the interface from within the core refracts 90 degrees to the normal, that is, when θ_2 reaches 90 degrees, its sine therefore, reaching unity. Solving the Snell's Law equation for those conditions gives the critical angle as

$$\theta_c = \sin^{-1}[n_2/ n_1].$$

For this material, then, the critical angle would be sin-1[0.901] or 64.3 degrees. The numerical aperture is a practical measure of the angle of acceptance (or output) of the light guide. The numerical aperture, NA, is written

$$NA = [n_1^2 - n_2^2]^{1/2}.$$

For the 3M LF120C light guide, the NA computes to about 40.5 degrees. This is the half angle of the full cone of light the fiber can accept or will produce when light exits it. The measure of the half angle is from the normal to the end surface, which corresponds to incidence angles for light described below. Were the material to be a perfect waveguide with no surface irregularities, it could be expected that no light with angle greater than 40.5 degrees could enter or exit the light guide. As it turned out, incident light in excess of 40.5 degrees was coupled into the core, but with very low efficiency, as will be shown.

Visible Light Transport Efficiency

The arrangement for measuring the total light through a light guide was comprised of a stable broad-band xenon light source, [3] a length of 3M light guide, an integrating sphere,[4] and an optical multi-channel analyzer (OMA). Both ends of the light guide were polished. The light-input end was pressed into a tapered aperture where the light exited the source. The light source with fiber pressed into the aperture is shown in Fig. 1. The process of pressing the fiber into the aperture was repeated a number of times under identical conditions to determine the repeatability of the process. It was found to vary by only around 1%. Other sources of error, described below, were somewhat more significant.

Fig. 1. Photograph of 3M light guide pressed into tapered aperture of light source

We tested a length of 3M LF120C light guide (core diameter about 12.6 mm) to determine the amount of light transported per unit length. Figure 2 shows a section of 3M plastic light guide attached to the integrating sphere, used to measure the light exiting the end of the guide. The light guide, at the onset of the measurements, was about 2.8 m long. Input light was supplied by a broad-band xenon lamp that provided a significant amount of light for each of the visible wavelengths. Spectra were recorded from the integrating sphere using the OMA. The measured spectra were then mathematically overlapped with the human-eye-response curve [5] to produce the total number of lumens collected. A series of measurements was made, beginning with the full length, followed by measurements after approximately 0.5 m was cut from the previous lengths, down to a final section less than 1 m long. In each case, the cut fiber end was polished to about a 0.5 micron finish [3] with the goal of providing uniform optical conditions for each input and output surface. We stress that this is a preliminary study. A larger scale study, using longer lengths of fiber has begun, and is expected to produce higher precision data. The current study, however, was able to give both a good estimate of the material performance and an increased understanding of the types of errors that plague measurements of this kind.

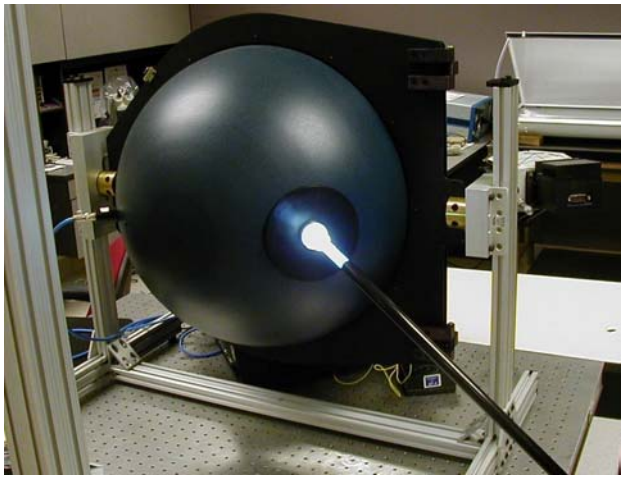

Fig. 2. Photograph of 3M light guide attached to integrating sphere

Figure 3 is a plot summarizing the data taken in the total transport study. Shown is the measured light as a function of wavelength that was transported through the various lengths of fibers, as indicated in the legend of the graph. The curve labeled "0 m" is light directly into the integrating sphere from the light source, normalized to an extrapolation of the light through the various lengths. The extrapolation was required to put the zero-length data into the same geometry as the measurements with the light guides themselves. Three different output settings on the xenon source were used, so that three different measurements were made for each fiber length. Data were normalized so that each measurement was associated with a single input power (in this case, the lowest setting of the source), both to improve the statistics of the measurements and to look for inconsistencies that could be corrected before averaging the data. In Fig. 4 are plots of the ratio of data through a particular length of fiber to a zero length, that is, the fraction of the total light transported through the fiber. In the figure, the large absorption at 750 nm is clearly seen, as well as the significant absorption at about 643 nm. Note that between 350 and 450 nm the 0.69 and 1.15 m data are sometimes above unity. These values are artifacts both of the low signal-to-noise ratio of the data signal and the process of normalizing the zero length data to conform to the light guide optics. In general, however, the trends are shown clearly. Even these short lengths of material show significant loss in the visible near 645 nm and in the near infrared around 750 nm.

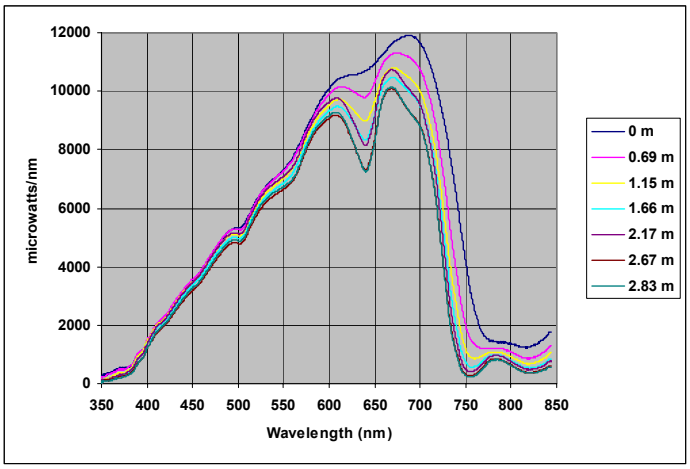

Fig. 3. Transmitted light versus wavelength for various lengths of 3M light guide

Each spectral measurement through the various light guide lengths was folded with the human eye response to determine the lumens transported into the integrating sphere for that particular set of conditions. The overlap calculation had been checked with measurements made with a calibrated integrating photodiode that viewed the averaged light in the integrating sphere. Table 1 gives the numbers of lumens obtained for each case. In Table 2 the ratio of the values to the zero length cases are shown. These values illustrate the statistical variation that can be expected for data of this type. When the averages of the transport fractions are taken and normalized to one meter of length, we arrive at the average transport fraction of 0.966 per meter. The number involves lumens; consequently, the losses in the red and infrared are not weighted as heavily as the yellow-green region that is the peak of the human eye response.

Several sources of error were present in the measurements described. Included are: (1) variations in the quality of the light guide surface (polish) at the input end, (2) drift of the light source intensity, (3) characteristic signal to noise ratio (SNR) of the OMA, and (4) possible variations in attaching input light source to light guide input. In particular, we found that the polish variations and the drift of the light source can each cause up to 2 or 3 percent uncertainty. The other two, the SNR and the light-input attachment variation, give less uncertainty. The SNR is unimportant because the lumen extraction of the data comes from a region where the SNR is quite large. When all these possible errors are folded into a single measurement, variations of 5 percent or more can be common; however, when the 18 separate measurements are averaged the reliability of the results becomes significantly higher.

Transmission As A Function Of Input Angle

To efficiently couple solar light into a light guide, it can be required for large-area solar collectors, to focus the light, thereby distributing it into a distribution of approaching angles. The greater the angle, with zero degrees defined as the normal to the surface, the higher the likelihood that the light ray will reflect at the surface rather than be transmitted through it. For any optical surface, such as the polished end of a light guide, the numerical aperture limits the angle of incidence. However, surface polish, uniformity, and perhaps other optical properties of the light guide material can affect the transmission of the light at the incidence angles allowed by the numerical aperture. With this in mind we assembled a measurement system to allow us to impinge a narrow column of light at any selected incidence angle on the end of a light guide. The assembly consisted of the broad-band xenon source, used in the previously described measurements, focused through a collimating lens and variable aperture, all mounted in a fixed geometry on a moveable platform. The input end of a length of 3M light guide was clamped into a holder so that the guide end surface was fixed, allowing the light source assembly to be positioned at any selected angle with respect to the normal to that surface. We facilitated the angle selection by scribing angle reference lines on the surface to which the light guide end clamp arrangement was attached. The light source assembly and light guide end clamp arrangement are shown in Fig. 5.

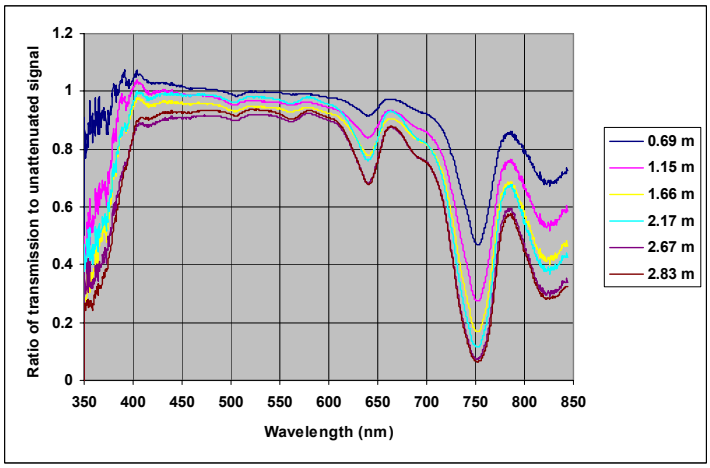

Fig. 4. Ratio of transmitted light through various lengths of 3M light guide to input light, as a function of wavelength

Because the xenon lamp was an extended source, the simple lens and collimator system used did not produce a perfectly collimated parallel beam of light for input into the light guides. However, the light-spread out of the collimator was low enough that a great majority of the light was centered on the selected incidence angle. Except at about 25 degrees, when the roll-off in the signal began to be significant, the less-than-perfect collimation had little effect on the measurement. Near 25 degrees, however, the input rays on the low side of the nominal angle would be transported somewhat better than the nominal, and those on the high side of the nominal 25 degrees would be transported significantly poorer. The upshot would be a slight rounding the curve, depressing the values slightly. These variations, however, are probably less than the variations in the measurements arising from the same four types of errors previously discussed.

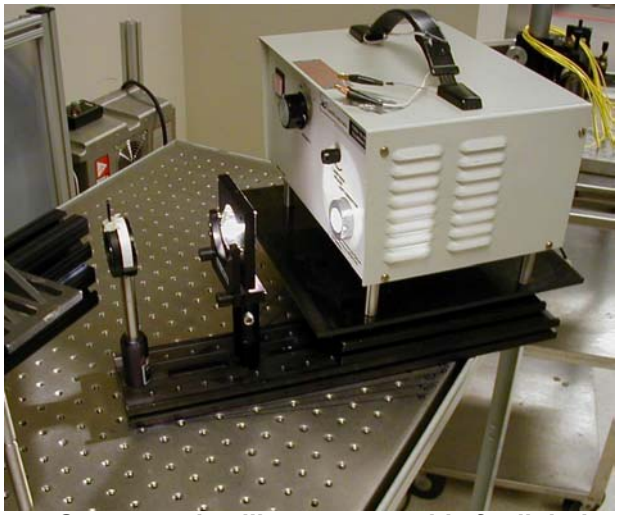

Fig. 5. Source and collimator assembly for light input at various angles and clamp arrangement to hold the input end of the 3M light guide.

Angle study of a short length of light guide. The angle study was begun by examining a short length of 3M light guide, 21 inches (0.53 m) long. The goal of using a short length was to minimize the variation in losses that might occur in the guide from material absorption of the light propagated over the varying length light paths that result from variations in incidence angle. In other words, with a relatively short section of light guide the light transported into the integrating sphere would show losses that were dominantly caused by the angle of incidence. Surface reflections, then, would be the primary attenuators of the measured light, not the aggregate absorption losses along relatively long transport paths. Figure 6 summarizes the measurements made. The collimated input beam was approximately 3-mm diameter. For each measurement, a spectrum was recorded by the OMA and folded with human eye response to give a single lumen value. Little attenuation occurs until the angle of incidence exceeds 20 degrees, after which the drop-off is rapid until, at the maximum incidence angle measured (46.3 degrees), the fractional transport is only about 8 percent of the zero-degree value. Also, as the incidence angles increased the SNR of the data decreased; consequently, the uncertainties were greater at the higher incidence angles.

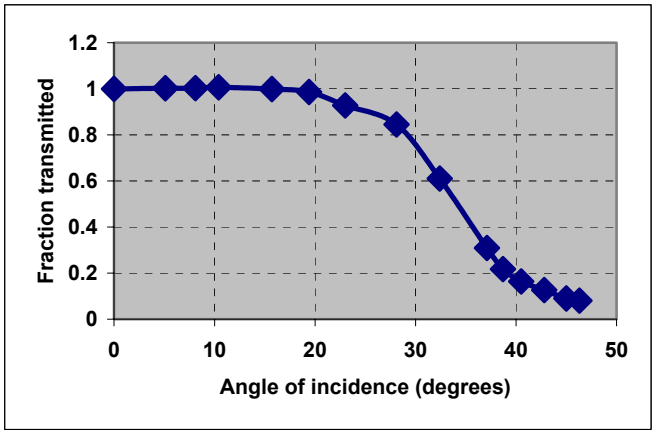

Fig. 6. Relative light transported through a 21-inch length of 3M light guide as a function of incidence angle

Angle study of a light guide with a 90-degree bend. A 5.0 meter (197 inches) length of 3M light guide was also studied, both to observe the material-dependent transport losses and to provide enough material so that a 90-degree bend could be imposed on the light guide, without the bend being too close to either end. Several bend radii were measured, in addition to no bend (infinite bend radius). An earlier preliminary evaluation of the effects of bends, done with a filtered diode (to approximate eye response) measuring the integrating sphere, indicated that bends of about a 6-inch radius or less were required to produce any significant effects on the light guide transport properties. In other words, only sharp bends made any appreciable difference in the transport properties of the light guide. Figure 7 is a graph of the incidence-angle dependent transport through each of the bend radii. The transmitted light was normalized to the zero degree data for the straight (no-bend) measurement. All data were taken as spectra by the OMA and overlapped to give an answer in lumens. Expressing data in terms of lumens, while useful for applications such as lighting where human vision is concerned, does not clearly illustrate the wavelength dependence of the phenomenon being measured. The trend of the data, however, clearly shows that tighter bends limit the total transmission. Because of the range of possible errors for individual measurements it is hard to quantify the total loss as function of bend radius. Future studies are planned to make similar measurements with higher precision so these trends can be better quantified.

Figure 8 shows the same data plotted as ratios of the transmitted light, at various angles of incidence for each bend radius, to the no-bend data for each angle of incidence. Plotted this way, it is easy to see the trend of lower transmission for higher incidence angles as the bend radius is reduced. The data for incidence angles greater than 40 degrees are not reliable, so the ratio tending to go up between 40 and 45 degrees is probably an artifact of the data.

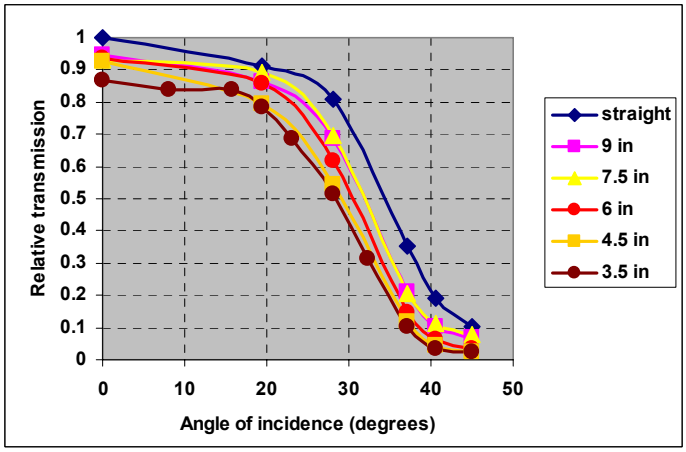

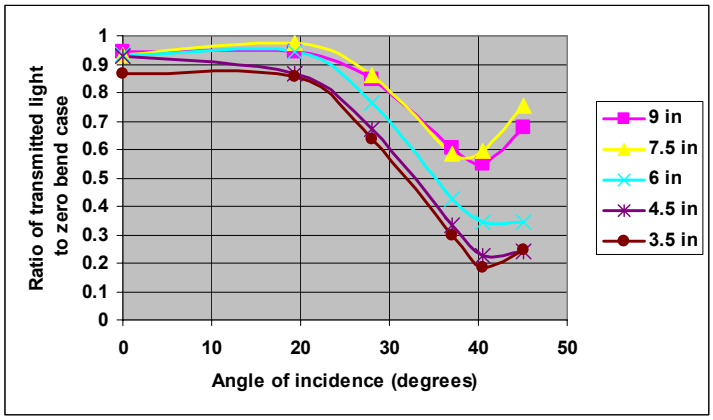

Fig. 8. Ratio of transported light at various bend radii to no-bend case, as a function of incidence angle

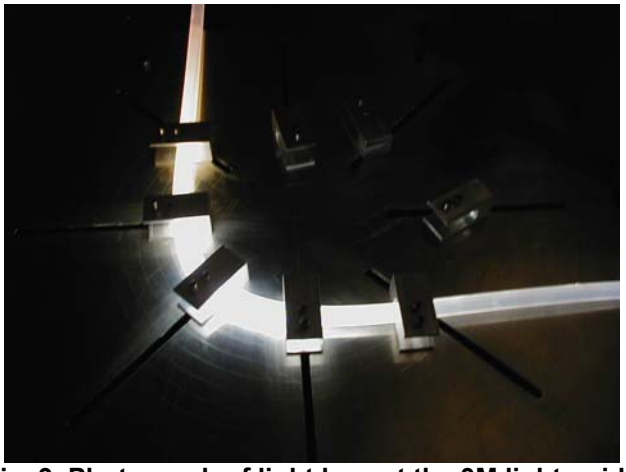

Fig. 9. Photograph of light loss at the 3M light guide bend

Light Transport Study Of 7.5-Meter 3m Light Guide

A 7.5-meter (295-inch) section of 3M light guide was configured so that it could be aligned into a straight path from the light source, pass through a single 90-degree bend, or pass through two 90-degree bends, to the integrating sphere. It was noted during the measurements that when light was introduced at larger angles the bends showed significantly increased light leakage. Figure 9 is a photograph showing the effect. These light leaks are the expected result of rays of light approaching the core-cladding interface at angles that are reasonably close to the critical angle. Any irregularity in the optical surface can allow scattering, absorption, or losses from light exiting the core. The central beam of the quasi-collimated light source appears to be preserved for all the light guide lengths studied, maintaining the angle of internal scattering pattern corresponding to the incident angle.

Figure 10 is a compilation of data from the straight, one-bend, and two-bend conditions of the 7.5-m light guide. Both bend radii were 4.0 inches (100 mm). As expected, the first bend causes considerable loss of light at the larger incidence angles, while the additional bend makes a less significant additional effect. For these data we used a photodiode to monitor the output of the light source; consequently, the drift in light intensity of the source was removed as a significant cause of error. Another important source of error, the input surface characteristics of the light guide, was also reduced for these measurements, because the same section of light guide, with no required cutting and polishing, was used for all three cases.

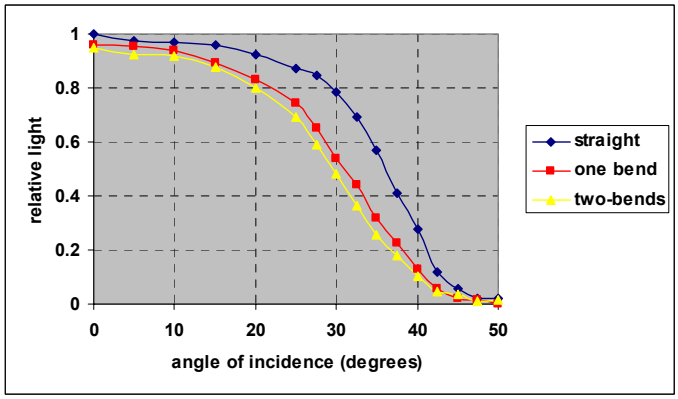

Fig. 10. Relative light transported through a 7.5-meter 3M light guide in three conditions: straight, containing one 90-degree bend, and two 90-degree bends, all as a function of incidence angle

Transmission As A Function Of Both Angle Of Incidence And Wavelength

A 6.5-meter (256-inch) straight length of 3M light guide was studied to evaluate the transmission characteristics as a function of both angle of incidence and wavelength. For this evaluation, the data measured by the OMA, comprised of 992 wavelength values extending from 350 to 844 nm, were compared by wavelength segment for angles of incidence out to 45 degrees. The data illustrate the influence of angle of incidence on the color characteristics of the transported light. Figure 11 is a compilation of the data taken. Data at each end of the wavelength range (below 400 nm and above 750 nm) are not plotted because of their low SNR for this light source. The numbers are the signal at any particular wavelength segment divided by signal from the corresponding segment for the zero-degree incidence case (with the light source centered on the center line of the light guide). These data represent only one of several lengths of 3M fiber measured in this way. In future work added data will improve the accuracy and allow for a determination of these wavelength-dependent properties per unit length of light guide.

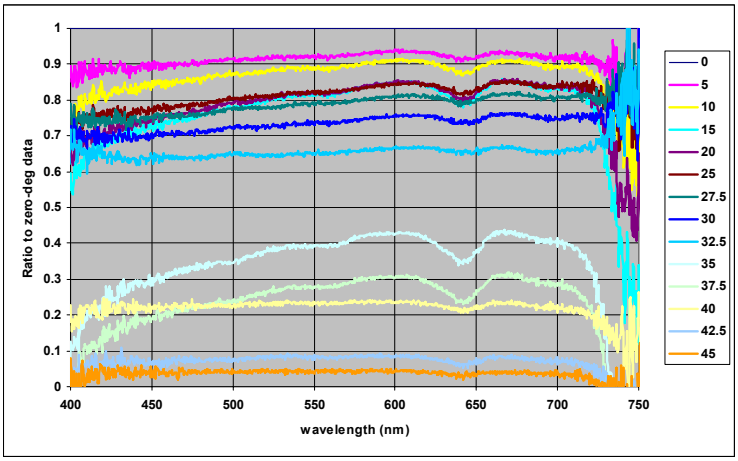

Fig. 11. Light guide transmission as a function of incident angle and wavelength

CONCLUSIONS

The 3M LF120C light guide studied has important potential as a light distribution medium for HSL applications. The preliminary value of total transmission per unit length, 96.6 percent per meter, is consistent with the numbers quoted by the manufacturer, and is marginally adequate for many aspects of the prospective applications. Lengths of more than ten meters represent losses of 25% or more, thereby limiting some types of use. Investigation of other materials and types of light guide should continue, in the hope of finding guides that can transport with higher efficiency.

The absorption bands in the spectral transmission of the material may lead to the necessity for color correction in some instances. Other materials that have flatter color transmissions should be sought out and evaluated. The importance of angle of incidence on transport properties has to be taken into account with solar collectors, beam-splitters, and in laying lengths of the light guide for building applications. Continuing measurements on the 3M product, and other products as they become available, will help establish limits and types of use, and will be important in coordination with remote source and artificial lighting that is expected to be coupled with solar light in many future configurations.

ACKNOWLEDGMENTS

The authors are especially grateful to Jeff Muhs whose enthusiasm and effective coordination has been a major factor in the growing success of HSL technology. We also wish to acknowledge the helpful laboratory support given us by Robert Thomas, David Beshears, Mike Jenkins, and Steve Allison here at Oak Ridge National Laboratory.

REFERENCES

1. Muhs, J. D., "Design and Analysis of Hybrid Solar Lighting and Full-Spectrum Solar Energy Systems," *Solar 2000, July 16-21, 2000,* American Solar Energy Society
2. Maxey, L. C., et al, "Efficient Optical Couplings For Fiber-Distributed Solar Lighting," ORNL-TM (2002)
3. AO Scientific Instruments, 1185B 150 watt illuminator
4. Labshere 21" integrating sphere with SC-5500 Controller
5. Wyzecki G. and Stiles, W. S., *Color Science,* 2nd Edition, John Wiley and Sons, pp. 256-259 (1982).

LIST OF FIGURES

APPENDIX F

EFFICIENT OPTICAL COUPLINGS FOR FIBER-DISTRIBUTED SOLAR LIGHTING

L. C. Maxey, M. R. Cates, and S. L. Jaiswal
Oak Ridge National Laboratory
Oak Ridge, Tennessee

ABSTRACT

Although the concept of transmitting the sun's light through an optical fiber for illumination is simple, lighting systems based on this approach will be somewhat more complex. The sun's light must first be collected and launched into a fiber. From there, it must be transmitted, perhaps divided and ultimately allowed to flow into a luminaire for useful distribution into the area to be lighted.

Large core (12.6mm) plastic optical fiber is being used in the development of hybrid lighting systems [1, 2] that will combine natural and artificial light. What is, for simplicity, called an optical fiber is actually configured as an optical waveguide, with a central core surrounded by cladding material of lower index of refraction. The deployment of efficient hybrid lighting systems will require the ability to connect all of the various subsystem components in a way that minimizes any degradation of luminous efficiency. When the sun's energy is collected and launched into a fiber, any subsequent connection of that fiber to another system component (e.g. another fiber, a splitter or a luminaire) will cause some of the light to be lost. The quality of the systems that are ultimately deployed will directly depend on the ability to connect all of the components in a way that wastes as little of the collected light as possible.

INTRODUCTION

Although the concept of transmitting the sun's light through an optical fiber for illumination is simple, lighting systems based on this approach will be somewhat more complex. The sun's light must first be collected and launched into a fiber. From there, it must be transmitted, perhaps divided and ultimately allowed to flow into a luminaire for useful distribution into the area to be lighted.

Large core (12.6mm) plastic optical fiber is being used in the development of hybrid lighting systems that will combine natural and artificial light. What is, for simplicity, called an optical fiber is actually configured as an optical waveguide, with a central core surrounded by cladding material of lower index of refraction. The deployment of efficient hybrid lighting systems will require the ability to connect all of the various subsystem components in a way that minimizes any degradation of luminous efficiency. When the sun's energy is collected and launched into a fiber, any subsequent connection of that fiber to another system component (e.g. another fiber, a splitter or a luminaire) will cause some of the light to be lost. The quality of the systems that are ultimately deployed will directly depend on the ability to connect all of the components in a way that wastes as little of the collected light as possible.

Optical couplings and their associated losses

In order to develop methods for minimizing connection losses, it is important to first understand why they occur. In a fiber-distributed lighting system, the minimum amount of loss that can occur is the small amount of absorption that takes place as the light passes through a straight section of un-interrupted fiber. Here the light is completely contained by the core and cladding of the fiber and it is only the material properties of the fiber core and cladding that cause a little of the light to be absorbed along the way.

A casual observation of almost any fiber connection will look almost like a continuous section of fiber. If we could take a microscopic look at the connection, however, we would see a very different situation. At every coupling of a fiber to another fiber (or to another component) the containment of the light crossing that interface is momentarily lost. The light completely exits one fiber, passes through the free space between the two fibers and must re-enter the other fiber. Unlike a continuous section of fiber, this introduces several ways in which light can escape and also creates additional resistance to the flow of the light. To minimize the optical losses, the coupling must approximate an uninterrupted fiber as closely as possible. The ends must be in intimate contact, the axial alignment of the two ends must be preserved and the optical index variation across the gap between the fibers must be negligible.

Endface preparation

The first step in making an optical fiber coupling is the preparation of suitable fiber endfaces. Each endface must have shape that enables it to mate well with another similarly prepared endface and it must be polished to reduce the scattering of light as it passes through the surface. The best shape for reliable coupling and reduced losses is a flat endface that is perpendicular to the axis of the fiber. Figure 1 illustrates the benefits of preparing this type of endface and the losses that can occur with other types of fiber ends.

In addition to furthering the objective of achieving flat and perpendicular endfaces fixtured polishing methods are also more repeatable and less dependent upon the skill level of the individual performing the polishing. The endface profile measurements presented in the graph in Fig. 3 show quantitatively, the improvement in profile and repeatability.

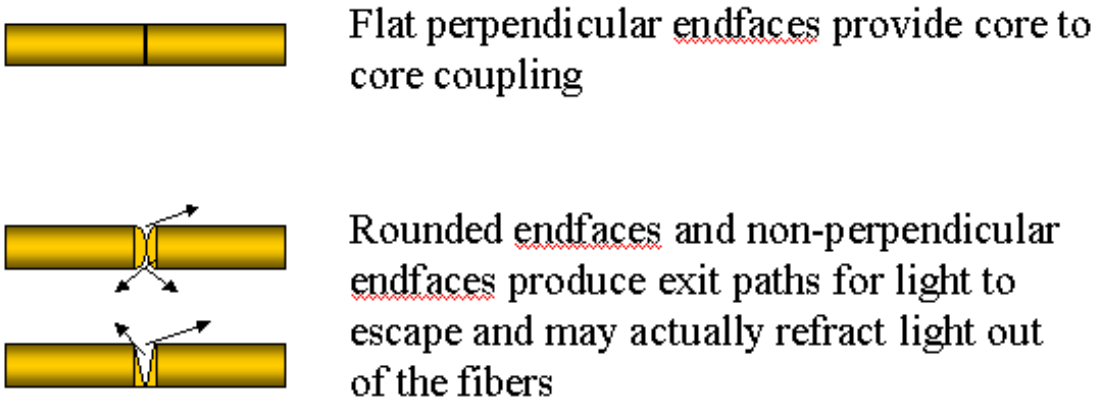

Fig. 1. Effects of endface shape on optical couplings

Hand polishing is commonly used to produce fiber ends that are adequate for getting light into or out of a length of fiber. However, hand polishing produces less than optimum results for fiber couplings. Fixtured polishing that produces flat and perpendicular endfaces can facilitate the production of low-loss couplings. A hard aluminum lap with adhesive backed aluminum oxide abrasive sheets applied to it provides a suitable surface for generating good quality endfaces. The fixture that maintains the fiber perpendicular to the surface of the lap is aligned with a digital displacement gauge to ensure perpendicularity across the range of travel across the lap. A very coarse abrasive is used to grind the initial surface and progressively finer abrasives are used to remove the surface damage produced in the grinding step. Once the flat and perpendicular end is well developed, final polishing can be achieved in very brief unfixtured hand polishing steps using very fine aluminum oxide abrasives on a soft rubber-polishing pad mounted in an electric drill. The material removal in the polishing steps is minimal and does not significantly degrade the surface geometry. A comparison of the endfaces produced with a freehand polishing method and a fixtured polishing method is shown in the photo in Fig. 2.

In addition to furthering the objective of achieving flat and perpendicular endfaces fixtured polishing methods are also more repeatable and less dependent upon the skill level of the individual performing the polishing. The endface profile measurements presented in the graph in Fig. 3 show quantitatively, the improvement in profile and repeatability.

Axial alignment and connector design considerations

Although all of the examples in Fig. 1 are shown with good axial alignment, it is intuitive that any axial misalignment will also create an opportunity for light loss to occur. The manufacturing processes for the large core plastic fiber products allow a fairly large tolerance (about 1mm total) in the variation in the fiber diameter. This complicates the process of maintaining alignment within a connector. Fortunately the variations within a given batch of fiber are usually much smaller than the manufacturer's specified maximum tolerance. However, they are significant enough to require some effort to ensure axial alignment.

Some of the commercial connectors that have been used failed to provide enough mechanical support to the coupling to maintain the axial alignment. One method for improving the performance of these connectors has been the addition of an elastomeric bushing. Heavywalled vinyl tubing was used for one version of this bushing and offered promising results. The tensile properties of the bushing tended to hold the fibers in alignment. Also, the bore of the connector was modified to provide a mild interference fit when the fibers and bushing were in place. The elasticity of the bushing combined with the interference fit tended to provide a self-centering means of placing the two fiber ends into good axial alignment.

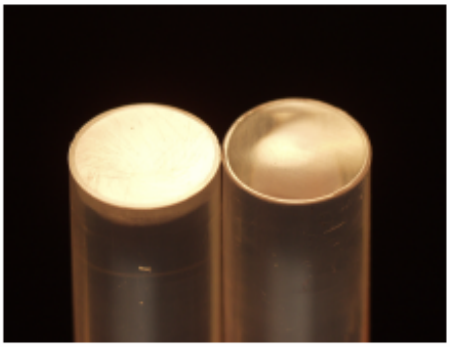

Fixture polished endface (left) is noticeably flatter than the freehand polished surface (right)

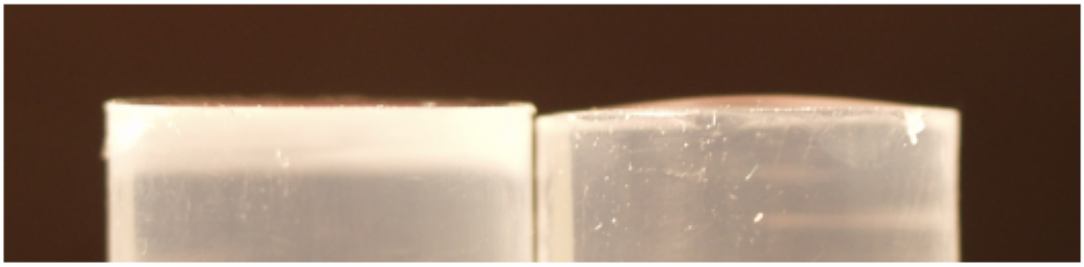

Fig. 2. Endfaces prepared using fixtured (left) and freehand (right) methods

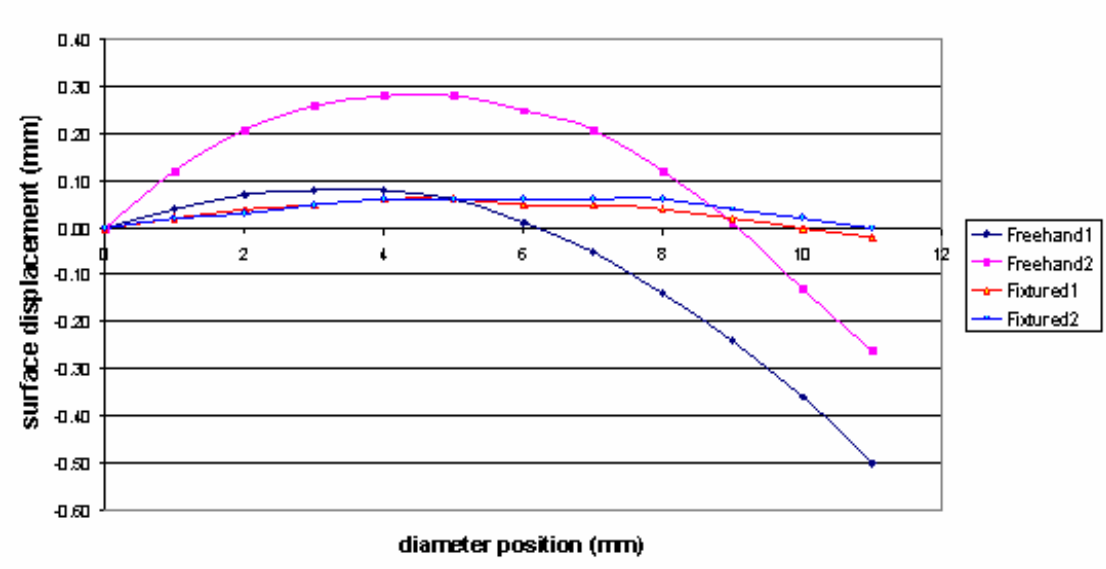

Fig. 3. Measured surface profiles of freehand and fixtured polishing results

There is another aspect of the large core plastic fibers that complicates the axial alignment. That is the lack of straightness in the fiber. The fibers are typically shipped in coils and tend to retain curvature from the coiling process. Even over a short section this can be significant enough to affect the axial alignment. One improvement over the commercial connectors that have been tested so far is to increase the length of the connector body. Some prototypes with this modification have been produced and initial tests indicate significant improvement in the axial alignment and resistance to lateral strain once assembled.

Reflective losses and index matching media

There is another loss mechanism that occurs due to material properties and can contribute significantly to coupling losses. No matter how well the fiber endfaces are prepared, there will still be some gap between the two coupled fibers. Whether the gap is less than one micron or more than one

hundred microns, there will be about a 4% loss as the light leaves the first fiber and enters the air gap. There will be another 4% loss of the remaining light as it enters the second fiber. These losses are due to the difference in the optical properties (specifically the index of refraction) of the air and the fiber core material and are referred to as "Fresnel reflection" losses. These reflections alone will cause about 8% of the light to be lost at each connection, no matter how well the endfaces are prepared and no matter how well they are aligned. Any other losses due to misalignment and scattering will result in still more attenuation.

The only way to avoid the reflective losses is to make the gap between the fibers look as much like the fiber core material itself as possible. There are commercially available compositions designed to perform just this task. These are known collectively as "index matching media" and can be purchased as fluids or gels, which are used to displace the air in the gap between the fibers. If an index matching medium can be found that exactly matches the index of refraction of the fiber core, theoretically the reflective loss would be zero. In optical fiber communications systems it can be extremely important to eliminate even the smallest of reflections that occur at the fiber coupling interfaces. Consequently, great effort and expense is justified to obtain an index matching medium with an exact match to the fiber core. In practice, however, even a relatively poor match is sufficient to make the losses negligible for lighting applications. The core of the fibers used in the hybrid lighting research have an index of refraction of about 1.50. Figure 4 shows the calculated reflective losses as a function of the number of couplings. The calculated losses with no index matching medium are compared with the calculated losses using a commercially available gel with an index of 1.46. The gel with an index of 1.46 lowers the fresnel reflection loss per coupling from 7.8% down to 0.03%. Over 99% of the light is maintained after eight couplings with the gel. By contrast, without an index matching medium, the same number of couplings would cause almost half of the light to be lost due to fresnel reflections.

The actual choice of an appropriate index matching medium for lighting applications is dictated more by its mechanical properties than its index of refraction. Many media, from glycerin to super-glue, would provide an acceptable index match and offer significant flexibility in coupling design options.

Preliminary tests have been conducted with three types of index matching media, fluids, gels and adhesives. All of the materials show good optical characteristics but vary in their ease of use and mechanical properties. The fluids appear to be the least useful for most hybrid lighting applications because they can seep out of the connections unless some reservoir is provided around the coupling to reliably contain them. The gels, by comparison, stay in place and are very easy to work with. There are a variety of adhesive options with different properties. Both cyanoacrylates and epoxies have been tested with good results for permanent or semi-permanent applications.

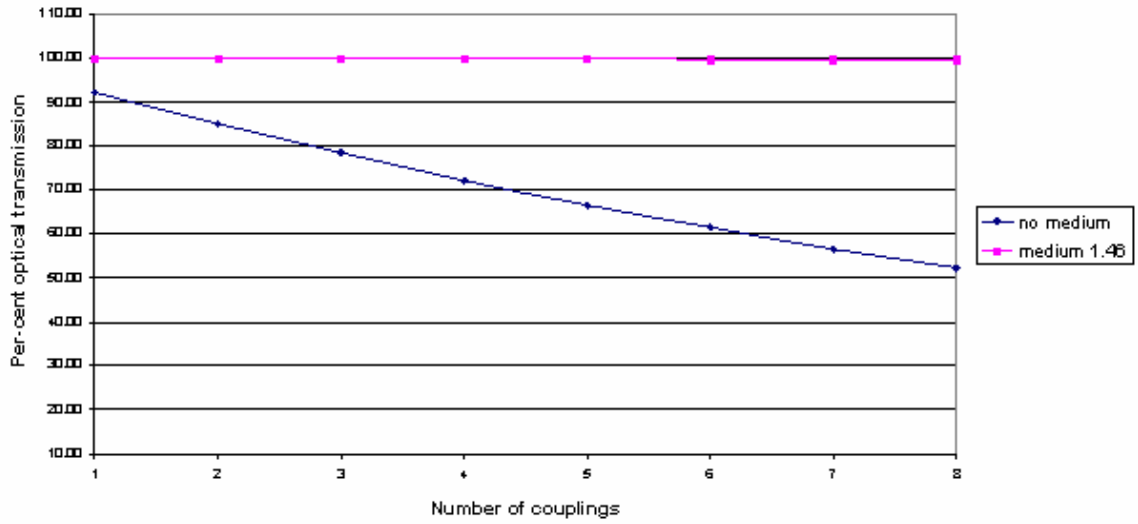

Fig. 4. Comparison of calculated losses with and without index matching gel

CONCLUSIONS

The losses associated with the use of couplings for fiber distributed solar lighting systems are largely attributable to the combined effects of endface geometry, axial alignment and Fresnel reflection loses. Significant progress has been made in the development of polishing methods that rapidly, reliably and repeatably result in high quality endface surfaces. This is expected to significantly reduce the amount of light that can escape at the fiber couplings. Similarly, the use of improved connectors to reduce axial misalignment of the fiber ends appears to be reducing the losses associated with that loss mechanism.

There has been an initial learning curve associated with the effective use of the index matching media but the results that are presently being obtained with these products are extremely encouraging. The effectiveness of the index matching media is so impressive that it may reduce the amount of polishing that is required. Experiments have shown that even endfaces that have only a preliminary polish (resulting in a frosted appearance) look perfectly clear and perform as well as highly polished endfaces, when mated to a similarly prepared endface surface with an index matching medium in between.

It has been difficult to reliably quantify the isolated impacts of each of the individual mechanisms associated with coupling losses. This is largely due to the variability in the results obtained with uncontrolled endface geometries, axial alignments and reflective losses. Prior to taking steps to control these various losses, connector losses on the order of 15% per coupling were common. The collective measures that have been taken to control these losses have, however, led to a measurable reduction of in coupling losses. With the existing degree of development in endface preparation, connector designs and the use of index matching media, losses are routinely being contained to between 2% to 5% per coupling.

ACKNOWLEDGMENTS

Research at ORNL was sponsored by the Energy Efficiency and Renewable Energy Office of the U.S. Department of Energy and the Public Power Institute of the Tennessee Valley Authority.

This document has been prepared by the Oak Ridge National Laboratory, Oak Ridge, Tennessee 37831-6472, managed by UT-BATTELLE for the U.S. DEPARTMENT OF ENERGY under contract DE-AC05-00OR22725.

REFERENCES

1. Muhs, J. D., “Hybrid Solar Lighting Doubles the Efficiency and Affordability of Solar Energy in Commercial Buildings,” CADDET Energy Efficiency Newsletter December 2000, p. 6.
2. Muhs, J. D., “Design and Analysis of Hybrid Solar Lighting and Full-Spectrum Solar Energy Systems,” *Solar 2000, July 16-21, 2000,* American Solar Energy Society

APPENDIX G

THERMAL MANAGEMENT OF THE POLYMETHYLMETHACRYLATE (PMMA) CORE OPTICAL FIBER FOR USE IN HYBRID SOLAR LIGHTING

Murat Tekelioglu*
tekeliog@unr.edu
Ph: (775) 784-6735
Fx: (775) 784-1701

Mechanical Engineering – 312
University of Nevada, Reno
Reno, NV 89557

Byard D. Wood
bdwood@unr.edu
Ph: (775) 784-6931
Fx: (775) 784-1701

Mechanical Engineering – 312
University of Nevada, Reno
Reno, NV 89557

* Corresponding author

Key Words: Optical Fiber, Day Lighting, Concentrator/Receiver, Thermal Analysis

ABSTRACT

This work is part of a team effort to develop a hybrid solar lighting (HSL) system that transports day light from a paraboloidal dish concentrator to a luminaire via a large core polymer fiber optic. For example, the luminaire can be a device to distribute sunlight into a space or it can be a device that is a combination of day lighting and florescent lighting. In this project, the sunlight is collected using a one-meter paraboloidal concentrator dish with two-axis tracking. The secondary mirror consists of eight planar-segmented mirrors that direct the visible part of the spectrum to eight fibers (receiver) and subsequently to eight luminaires. This results in about 8,200 lumens incident at each fiber tip.

This paper is concerned with predicting the radial and axial temperature distribution in the entrance region of the fiber in light transmission. Thermal management of the plastic optical fibers (POFs) is crucial to prevent melting or deformation of the fiber. Several filtering techniques have been investigated to minimize the effect of IR portion of the solar spectrum at the fiber entrance tip surface as well as the whole-spectrum absorption of solar energy inside the fiber. According to the analysis results, the use of fused quartz glass attachment was proven to be cheaper, more cost effective and feasible among other proposed
solutions.

In the present study, we used the SMARTS v2.9 program, a Fortran code, to predict the terrestrial direct normal solar spectral irradiance. Ray tracing software TracePro was used to describe the incident radiation at the fiber tip and as it passes through the fiber. A 3-D thermal model was developed using ANSYS v6.1, an FEA software.

Depending on the mirror/filter specifications, the first 8 mm of the fiber was found to be critical based on 5 m/s air speed across the lateral surface of fiber. Modes of heat transfer taken into account included thermal conduction, convection and radiation on the first 5 cm of the polymethylmethacrylate (PMMA) core and Teflon-FEP cladding fiber. A case-basis comparison was made with the experimental result.

1. INTRODUCTION

Figure 1 shows the "Full-Spectrum Hybrid Solar Lighting System Design". Full spectrum in this definition is the utilization of entire solar spectrum except ultraviolet and hybrid solar lighting is the use of electricity as backup whenever the sunlight is unavailable (night time), or partially available (cloudy sky conditions).

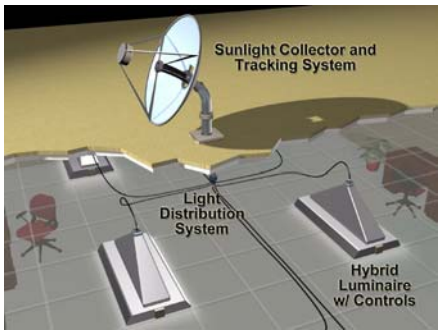

Figure 1. Adaptive full-spectrum hybrid solar lighting system design showing collector/tracker system, distribution system and hybrid luminaires.

Figure 2 shows the solar collector-receiver system. In this system, electricity is produced through GaSb silica cells that collect the IR (infrared) solar spectrum between 0.7 and 1.8 microns located behind the secondary mirror and fiber bundles transmit the VIS (visible) light between 0.4 and 0.7 microns into the spaces where daylighting is needed.

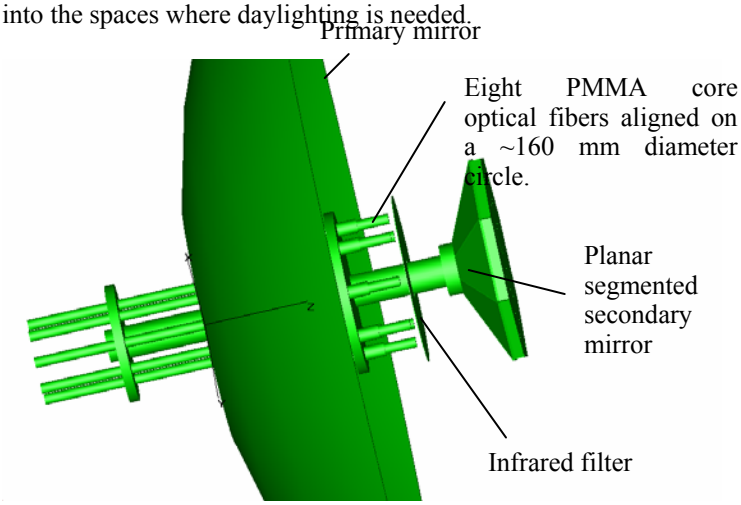

Figure 2. Schematic cut of the main body of collector-receiver: the solar dish, secondary mirror and eight large-core PMMA fibers.

2. PROBLEM STATEMENT

Solar irradiance coming from the sun has three spectral components: Ultraviolet, visible, and infrared. In typical solar collectors, the solar radiation is absorbed from all of the three spectral regions. The net outcome of solar radiation absorption is temperature rise on the absorbing medium. The level of temperature rise of the medium depends primarily on the absorptivity of the medium, which in turn is a function of wavelength, source temperature and direction of the incoming rays. If absorptivity of a surface is poor or can be neglected in comparison to its optical reflectivity and transmissivity, temperature rise on that surface can only be explained by the heating effect of infrared part of the solar spectrum. Thus, infrared part of the solar spectrum differs from ultraviolet and visible spectrums in that it also has a direct surface heating effect when the surface absorptivity is negligible. Then, the medium's thermal mass and energy storage capacity together with possible heat transfer mechanisms such as conduction and convection determine the temperature distribution on the medium. In the present work, infrared part of the solar spectrum has a direct surface heating effect at the fiber tip and gives off heat to the surroundings in the form of convection (tip and lateral surface). It was determined that any radiation effect from the lateral surface and the fiber tip would be negligible. The tip radiation from the infrared was eliminated because of the negligible absorption on this surface. The lateral surface infrared emissivity is negligibly small since most of the rays that enter the fiber core are trapped in the core and the part that are refracted into the cladding are negligible. Also, the type of fibers analyzed herein is named as end-light type and do not allow infrared -as well as visible- part of the spectrum to escape from the cladding surface to the surroundings.

In order to investigate the effect of infrared spectrum at the entrance region tip and ultraviolet and visible spectrums absorption inside the fiber on the temperature of the fiber entrance region, finite element model was applied on ANSYS 6.1. A triple boundary conduction consisting of heat flux, convection and radiation off the entrance region fiber tip was once applied as case basis.

The first part of the thermal management deals with the forced air-cooling of the fiber tip and lateral surface of fiber. Air speed values of 5, 10, and 15 m/s were set and results were compared. Second part of the thermal management proposes the use of infrared filter before the fiber inlet. Infrared filter, made of special glass, is highly reflective in the infrared and highly transmittive in the visible. Third part of the study investigates the use of the fused quartz glass (vitreous silica-SiO_2 glass) before the fiber instead of forced air-cooling or infrared filter. Fourth part of the study recommends the use of white paint at the fiber tip having high emissivity (0.6 and 0.8), thus, absorptivity in the infrared. Lastly, eight-fiber bundle system is recommended to be put into a local surroundings such as a cylindrical cover, highly transmittive, that will help keep the local surroundings temperature at 0 and –5°C instead of ordinary ambient temperature of 25°C. Such coverage of eight fibers with cooling will augment the convective heat transfer from both lateral and tip surfaces of fiber while allowing transmission of the light into the fibers. Proposed solutions were compared in terms of the application cost and feasibility and a recommendation was made depending on the results.

3. REVIEW OF FIBER STUDIES (POLYMER AND SILICA)

Diverse aspects of plastic and silica fibers were studied by several researchers. For example, a ray tracing model was applied for the multimode silica core optical fiber. The numerical aperture (NA) characterizes the light collection capacity of a fiber and is a function of surrounding medium, core and cladding refractive indices (See Eq. 11). The bending loss versus bending radius of three fibers with the same NA-numerical aperture (0.37) but different fiber diameters (200 μm, 400 μm, and 600 μm) were measured and plotted in comparison with the authors' own theoretical prediction. Similarly, fibers with the same diameter but different NAs (0.37 and 0.22 respectively) were also studied [1]. POF optical transparency, light scattering, optical bandwidth, and refractive index control along with polymer loss limit were studied [2]. Intensity (angular) distribution, illuminance (spatial) distribution, and total heat flux at the output of the bent fiber were investigated using the state-of-the-art illumination design software. Three different fiber types investigated had no clad, clad with outer surface of the clad absorbing, and clad with bulk attenuation [3]. In another paper, it was stated that for the same diameter fiber, NA and λ both affected the fiber attenuation. It was shown, however, that NA dominated the attenuation loss. A 150 W illuminator with different diameter LCP (Liquid Crystalline Polymer) fibers was used to determine the transmittance versus fiber length. It was noted that the light loss, and color shift for a white, broad-band source would vary for different reflector designs in illuminator systems [4]. In order to examine the effect of heating the fibers, the thermomechanical performance of a commercial fiber jacketed with a UV-cured acrylate was measured and partial delamination of the jacket materials between the primary and secondary coatings was found. The application of cyclic force applied axially along optical fibers at elevated temperatures was found to cause separation of the secondary jacket from the primary jacket [5]. Another cited reference investigated the thermal degradation of plastic optical fibers. In that paper, measured α (attenuation) included α_e, α_v, α_R, and α_i where α_e is the electronic transition absorption, α_v is the higher harmonic absorption loss of C-H molecular vibration, α_R is the Rayleigh scattering loss due to the fluctuation of density and refractive index (anisotropy in the polarization of the core material), and α_i is the scattering loss due to imperfections in the POF structure. Among others, α_e was found to have greater increase with temperature. This was attributed to very small amount of conjugated carbonyl groups formed by the thermal oxidation reaction of core polymer. Thus, it was concluded that α of POFs increased with temperature. In the case of POFs, the light transmits in a long optical path so that even very small chemical and physical changes due to thermal degradation greatly influence the attenuation loss [6]. Loss mechanisms in optical light pipes were described through five

instead of four loss mechanisms. These were intrinsic absorption, bulk scattering, losses due to roughness at the core-cladding interface, losses due to large-scale defects at the core-cladding interface and losses that are due to absorption in the cladding material. The primary conclusion made in that paper was that the transmission in high quality light pipes could be severely degraded by roughness at the core-cladding interface. Losses due to absorption and scattering in the cladding were proven to be negligible. Cladding absorption was ruled out because of small extinction coefficient of cladding. In the paper, intrinsic absorption loss was determined from laser calorimetry where the fiber was illuminated by a laser beam of known power and temperature rise versus time was recorded. Bulk scattering losses were measured by shining a He-Ne laser beam through the axis of a 40-mm-long section of Lumenyte type fiber and measuring the intensity emitted into a band of 3 mm around the pipe. Since the intensity loss through this small (40 mm) section of the fiber was negligible, the Rayleigh scattering loss coefficient was given by $\alpha_{scatt} = I_s/(I_0 w)$ where α_{scatt} is the bulk scattering loss coefficient which is due to density and refractive index variations inside the core, I_s is the total scattered intensity into a bandwidth of $w = 3mm$ and I_0 is the intensity inside the pipe. Interface effects were determined by comparing rays that enter the light pipe axially with $d = 0$. After that, the angle between core-cladding normal and the incoming rays, φ, was fixed and the attenuation was given versus core diameter. To find σ (root-mean-square roughness) in the evaluation of fiber attenuation, core and cladding were separated and atomic force microscopy (AFM) was applied on five different locations of the inner surface of cladding [7].

Although diverse aspects of plastic or silica fibers were studied by several researchers, the effect of concentrated sunlight on the melt or deformation of plastic optical fibers was not well established.

The present study evaluates the thermal manageability of PMMA (polymethylmethacrylate) core optical fiber to be used in hybrid solar lighting via finite element modeling. The selection of finite element scheme was made for two reasons: First, due to the temperature dependence of physical properties of core and cladding materials, exact-analytical solutions can not be found easily due to non-linearity of the partial differential equations. Second, the heat flux profile at the fiber entrance tip is not uniform rather has spatial differences on the surface that are not suited to analytical modeling. Nevertheless, problems of non-linear partial differential equations and non-uniform heat flux profiles can easily and accurately be modeled using finite element techniques.

4. ANALYSIS

The solar radiation reaching onto the earth's surface has two components: Direct part and diffuse part. Direct solar radiation is the part received from the sun without having been scattered by the atmosphere (beamlike) and diffuse solar radiation, also called sky or solar sky radiation, is the part received from the sun after its direction has been changed by scattering by the atmosphere [8]. The paraboloidal solar dish shown in Fig. 2 collects the beamlike or direct part of the solar radiation and focuses it onto a focal point. Practically, there is no diffuse part of the solar radiation utilized with such paraboloidal dishes. The paraboloidal dish analyzed in this study has 46.5" outer diameter, 16.5" focal length, 12" diameter center hole, and 0.25" thickness. The active area of the solar dish after counting central hole is nearly 1 m^2. The secondary mirror has eight planar segments each tilted by 25° and has a surface area of about 69.4 cm^2.

Air mass is defined as the ratio of the mass of atmosphere through which beam radiation passes to the mass it would pass through if the sun were at directly overhead. Thus, at sea level when the sun is overhead (solar noon), air mass is one. To a good approximation, the air mass is given for zenith angles (θ) between 0° and 70° by 1/cos(θ) [8]. One exception to the air mass definition is the air mass zero which is reserved to name the extraterrestrial solar irradiance outside the earth atmosphere as measured, for example, by high flying balloons [9]. In the present study, terrestrial direct normal solar spectral irradiance for air mass 1.5 was obtained from SMARTS v2.9, a FORTRAN 77 code [10]. U.S. Standard Atmosphere (USSA) used in the SMARTS code assumes rural aerosol, precipitable water vapor column of 1.42 cm, total ozone thickness of 0.34 cm, and atmospheric turbidity (base e, lambda = 0.5 microns) of 0.27. A total of 19 species including H_2O, O_2, O_3, and CO_2 that absorb solar radiation through the layers of atmosphere are included in this atmospheric model. In this code and elsewhere [11] air mass (AM) 1.5 together with an atmospheric turbidity of 0.27 is considered to be representative average atmosphere in the 48 contiguous states of the U.S over a one-year period. The direct normal solar spectral irradiance in the present code is the same as that measured with a 5.8° field-of-view normal irradiance pyrheliometer which allows a small amount of circumsolar (diffuse) radiation to be detected. This circumsolar radiation adds approximately 1% to the measured direct normal solar irradiance. Figure 3 shows the spectral regions from SMARTS code. Shown in this figure are the visible direct normal solar irradiance, 293.2 W/m^2, which is about 38.6% of total direct normal solar irradiance, the infrared part, 445.4 W/m^2, which is about 58.6% of total direct normal solar irradiance, and the ultraviolet part, 21.1 W/m^2, which is about 2.8% of total direct normal solar irradiance falling onto earth's surface.

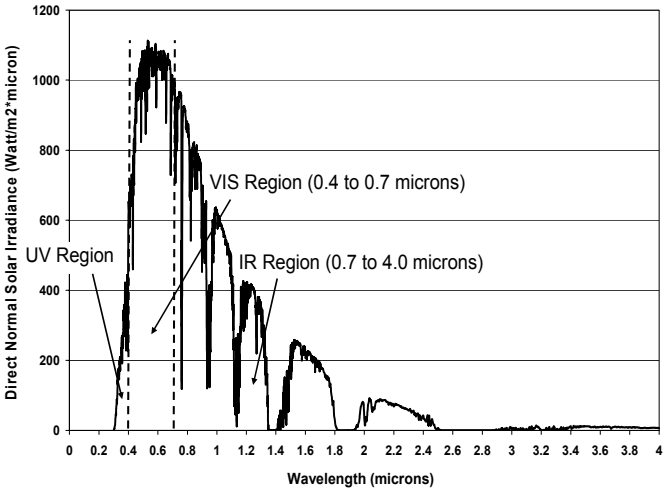

Figure 3. Terrestrial direct normal solar spectral irradiance for air mass 1.5 from SMARTS v2.9.

Figure 4 shows the primary and secondary mirror reflectivities as measured with an integrating sphere. The measured reflectivity is directional-hemispherical or hemispherical-directional as both are taken equal in practice [9].

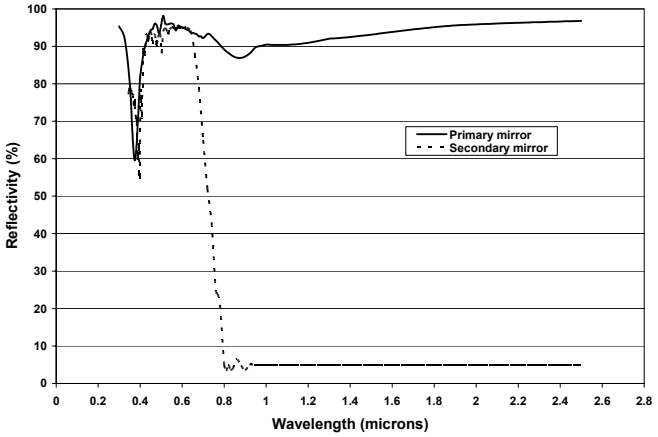

Figure 4. Spectral reflectivities of primary and secondary mirrors at room temperature.

The primary mirror is made of glass and coated with enhanced aluminum by Flabeg Inc. The secondary mirror is coated with a silvered polymer from Navitar Coating Labs. Inc. The average reflectivity in the VIS is about 90%. Although there is no delamination of this coating, there is not a lot of data concerning longevity of the coating. The secondary mirror reflectivity was obtained after measuring the transmissivity of the mirror, with 15% absorption up to 0.4 microns and 5% absorption beyond 0.4 microns up to 2.5 microns. On the secondary mirror, it was estimated a maximum off-normal angle of about 45° for the incident rays (from the outer rim of the secondary mirror) and taken that the angle of incidence dependence on transmissivity was not significant.

Figure 5 shows the infrared filter located before the fiber that reflects the IR spectrum of solar radiation and transmits the VIS spectrum. The angle dependence of transmissivity was assumed not to be significant although incoming rays that hit the infrared filter surface makes a maximum off-normal angle of about 28°. The infrared filter used in the study has the almost same average transmissivity for 0° and 45° of incidences although a slight shift is realized centered nearly at 420 nm [12].

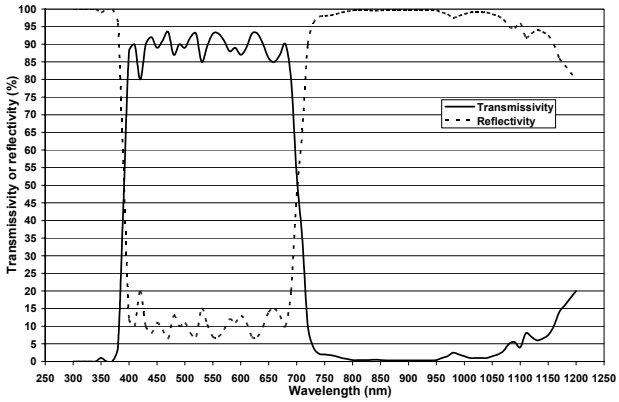

Figure 5. Infrared filter reflectivity and transmissivity.

A finite element model which incorporates the solar irradiance data of SMARTS v2.9 code, primary and secondary mirror reflectivities, and the heat flux profile of TracePro [13] was implemented on ANSYS 6.1 [14].

Initially, a constant-property analytical model applied on a laterally insulated PMMA rod with left end subjected to heat flux input and right end insulated showed that temperature at the entrance region tip can go up indefinitely precluding the presence of any steady-state [15]. This was not the actual case of the deformed entrance region tip of fiber by looking at the experiment results made at ORNL. In parallel to the experiment results, it was decided that there must be convection loss from the fiber entrance region tip surface as well as the fiber lateral surface. In the nature of modeling, the tip radiation loss was negligible: The reason to assume negligible radiation is the small value of absorptivity thereby emissivity on the transparent tip surface. Volumetric heat generation inside the fiber was taken into account through the ultraviolet and visible spectrums absorption. ANSYS 6.1 simulation used Newton-Raphson iterative algorithm with solid90 type elements each having 20 nodes and an approximate length of 3 mm in the fiber axis direction.

Encountered heat transfer mechanisms and boundary conditions included isotropic conduction inside the core, cladding and between core and cladding, forced convection from the fiber tip and cladding surface to the surroundings, entrance region fiber tip heat flux input and entrance region tip radiation that is due to selective surface coating. Figure 6 shows the nature of forced air cooling on the optical fiber where v_∞ is the average air speed at the fan exit and taken as 5, 10 and 15 m/s in the present analysis.

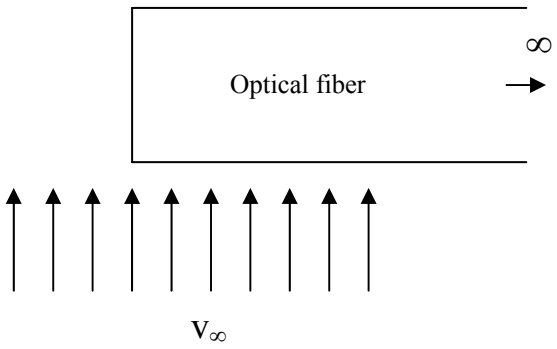

Figure 6. Forced air flow of a centrifugal air fan over the entrance region fiber tip and across the cylindrical fiber surface.

The lateral surface convective heat transfer coefficient was found from the correlation given for forced flow across a solid cylinder [16]

$$\overline{Nu}_{d,f} = 0.3 + \frac{0.62 \cdot \mathrm{Re}_d^{\frac{1}{2}} \cdot \mathrm{Pr}^{\frac{1}{3}}}{\left[1 + \left(\frac{0.4}{\mathrm{Pr}}\right)^{\frac{2}{3}}\right]^{\frac{1}{4}}}$$

$$\text{for } \mathrm{Re}_d < 10^4, \mathrm{Pr} > 0.5 \qquad (1)$$

$$\overline{Nu}_{d,f} = \left[0.3 + \frac{0.62 \cdot \mathrm{Re}_d^{\frac{1}{2}} \cdot \mathrm{Pr}^{\frac{1}{3}}}{\left[1 + \left(\frac{0.4}{\mathrm{Pr}}\right)^{\frac{2}{3}}\right]^{\frac{1}{4}}}\right]\left[1 + \left(\frac{\mathrm{Re}_d}{282{,}000}\right)^{\frac{1}{2}}\right]$$

$$\text{for } 2 \cdot 10^4 < \mathrm{Re}_d < 4 \cdot 10^5,\ \mathrm{Pr} > 0.5 \qquad (2)$$

where $\overline{Nu}_{d,f}$ is the average forced Nusselt number based on fiber cladding diameter, Re_d is the Reynolds number based on fiber cladding diameter, Pr is the Prandtl number given by $\mathrm{Pr} = \frac{\upsilon}{\alpha}$ where υ is the kinematic viscosity (m^2/s) and α is the thermal diffusivity of air (m^2/s). Re_d number is defined by

$$\mathrm{Re}_d = \frac{\nu \cdot d}{\upsilon} \qquad (3)$$

where ν is the average velocity of forced air flowing across the cylinder (m/s), d is the fiber cladding diameter (m), υ is the kinematic viscosity for air (m^2/s). Thus, the average forced-convection heat transfer coefficient on the lateral fiber surface is given by

$$\overline{h}_f = \frac{k}{d}\overline{Nu}_{d,f} \qquad (4)$$

where $\overline{h}_f$ is the average forced convective heat transfer coefficient on the cylinder surface (W/m^2K) and k is the thermal conductivity of air (W/mK).

Similarly, for the forced convection from the entrance region fiber tip, we assumed a flate-plate approximation on the circular geometry of fiber tip. This approximation was satisfied as long as 13.5 mm diameter circular shape was estimated by 13.5 mm long side of flat plate. Since the surface area was not too large, only about 1.43 cm^2, this approximation was found to be reasonable. The forced convection correlation was given by [16]

$$\overline{Nu}_{d,f,tip} = 0.664 \cdot \mathrm{Re}_d^{1/2} \cdot \mathrm{Pr}^{1/3} \qquad (5)$$

where $\overline{Nu}_{d,f,tip}$ is the average forced-convection Nusselt number at the tip surface, Re_d is the Reynolds number based on the fiber cladding diameter as given by Eq. 3, and Pr is the Prandtl number. Thus, the average forced-convection heat transfer coefficient at the fiber entrance tip surface is given by

$$\overline{h}_{f,tip} = \frac{k}{d}\overline{Nu}_{d,f,tip} \qquad (6)$$

In Eqs. 2 through 6, the kinematic viscosity υ, Prandtl number Pr, and thermal conductivity k, are surface temperature dependent provided that the ambient temperature is constant. As a result, Eqs. 4 and 6 are fluid properties dependent and become function of surface temperature of fiber.

It was noted that the fiber attenuation characterized by 3M is not because of absorption alone inside the fiber but also because of Rayleigh scattering due to density and refractive index variations, core-cladding surface roughness, and impurities. Thus, substitution of attenuation curve for the absorption inside the fiber gives an upper limit for any possible heat generation inside the fiber.

To find the volumetric heat generation inside the fiber, we apply the power decay law over ultraviolet and visible spectrums at a specific z location given by [7]

$$\overline{P_{out}}(z) = P_{in} \cdot 10^{-\frac{\overline{\alpha}_{UV,VIS} \cdot z}{10}} \qquad (7)$$

where z is the distance from the fiber inlet (m), $\overline{\alpha}_{UV,VIS}$ is the average attenuation from the ultraviolet and visible spectrum (dB/m), P_{in} is the power input at the fiber entrance region tip from the entire spectrum (W), and $\overline{P_{out}}(z)$ is the fiber power output from the ultraviolet and visible spectrums at the end of distance z (W). Note that Eq. (7) can also be written in terms of heat flux by replacing P_{in} and $\overline{P_{out}}(z)$

by the heat flux at fiber tip and at the end of distance z, respectively. Average loss over distance z is given by

$$\overline{Loss}(z)(\%) = \frac{P_{in} - \overline{P_{out}}(z)}{P_{in}} 100 \quad (8)$$

where $\overline{Loss}(z)$ is the average of power loss at the end of distance z from ultraviolet and visible spectrum (%), P_{in} is the power input of fiber from ultraviolet and visible spectrums (W), and $\overline{P_{out}}(z)$ is the average power output at the end of distance z (W). Introducing Eq. 7, Eq. 8 takes the form

$$\overline{Loss}(z)(\%) = \frac{P_{in} - P_{in} \cdot 10^{-\frac{\overline{\alpha}_{UV,VIS}}{10} z}}{P_{in}} 100 \quad (9)$$

or

$$\overline{Loss}(z)(\%) = \left(1 - 10^{-\frac{\overline{\alpha}_{UV,VIS}}{10} z} \right) 100 \quad (10)$$

Thus, the percent power loss at a specific z location is independent of power input and depends solely on the average value of attenuation constant (which is a function of numerical aperture, fiber core diameter, and wavelength). Spectral absorption is shown in Fig. 7 as determined by cut-back method after applying Eq. 10 on per wavelength basis. Attenuation data was measured with 350 W Sumitomo 3M LBM130H Illuminator having a source NA ~ 0.4. Fiber numerical aperture is a refractive index dependent property and defined as

$$NA = n_0 \sin\theta = (n_1^2 - n_2^2)^{1/2} \quad (11)$$

where n_0 is the refractive index of air ($n_0 = 1$), n_1 is the refractive index of PMMA core ($n_1 = 1.498$), n_2 is the refractive index of Teflon-FEP (fluorinated ethylene propylene) cladding ($n_2 = 1.35$), θ is the half-cone maximum acceptance angle of PMMA core optical fiber ($\theta \cong 41^\circ$), and NA is the numerical aperture ($NA \cong 0.65$). As far as the source NA is less than the fiber NA, all rays that enter the fiber are trapped in the PMMA core and refracted part of rays into the cladding is negligible.

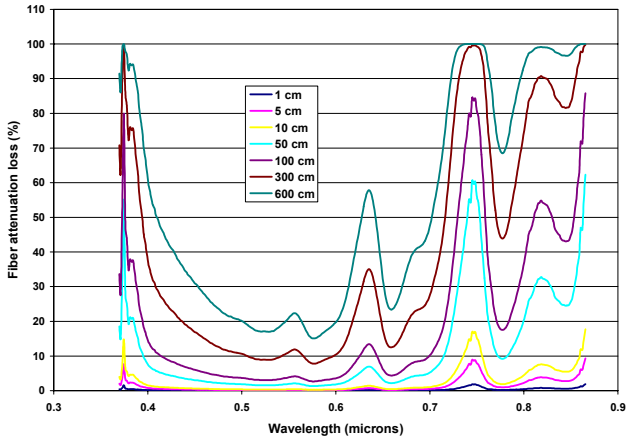

Figure 7. Fiber attenuation loss (%) versus wavelength (microns) in the range 0.37 to 0.865 μm with fiber length (Published with written permission of 3M).

The physical properties of PMMA (polymethylmethacrylate) core material and Teflon-FEP (fluorinated ethylene-propylene) cladding material were taken from several references. Table 1 lists the basic properties and Fig. 8 shows the specific heat with temperature taken for core and cladding materials.

Table 1. PMMA core and Teflon-FEP cladding material properties.

	Section			
	Core [17]		Cladding [18]	
Material	PMMA		Teflon-FEP	
Diameter (mm)	12.6		13.5	
Refractive index (-)	1.498		1.35	
Melting point (°C)	60		264	
Density (kg/m^3)	25°C	1188	25°C	2140
Thermal conductivity (W/mK)	0-50°C	0.193	25°C	0.2
	100°C	0.25	-	-

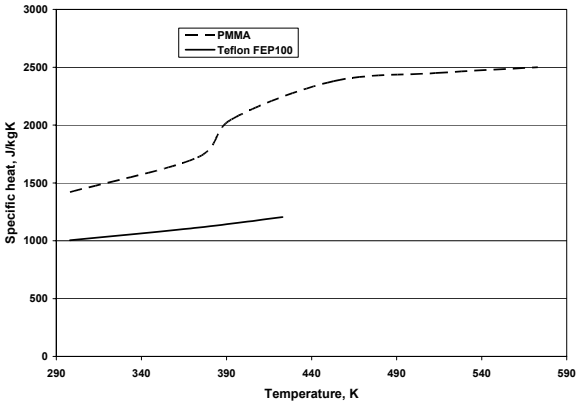

Figure 8. Specific heat of PMMA core [17] and Teflon FEP cladding [18] with temperature.

Table 2 lists the density and melting point and Figs. 9 and 10 show the specific heat and thermal conductivity with temperature of the quartz glass, respectively.

Table 2. Density and melting point of the fused quartz (vitreous silica-SiO_2) glass [19].

Section	Melting point (°C)	ρ (kg/m^3)
Vitreous silica-SiO_2	1410	2200

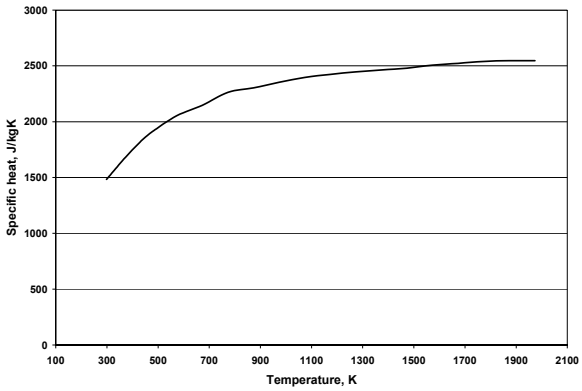

Figure 9. Specific heat of fused quartz glass [19] with temperature.

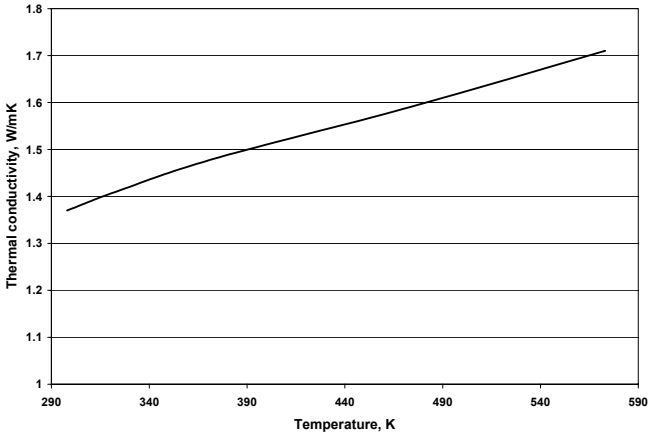

Figure 10. Thermal conductivity of fused quartz with temperature [19].

Figures 11 and 12 show, respectively, the heat interaction with and without infrared filter. The darker angular ring surrounds the core shown in lighter color.

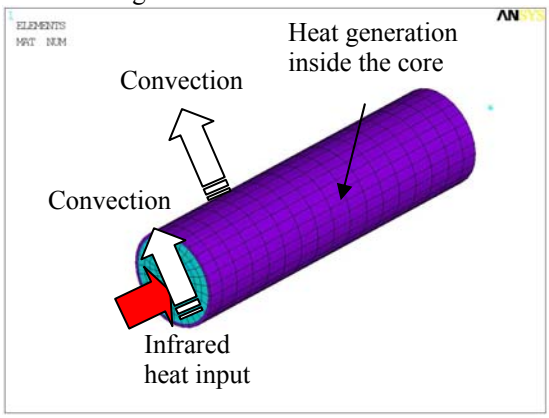

Figure 11. Meshed structure of the first 5-cm of fiber showing the infrared power input without infrared filter.

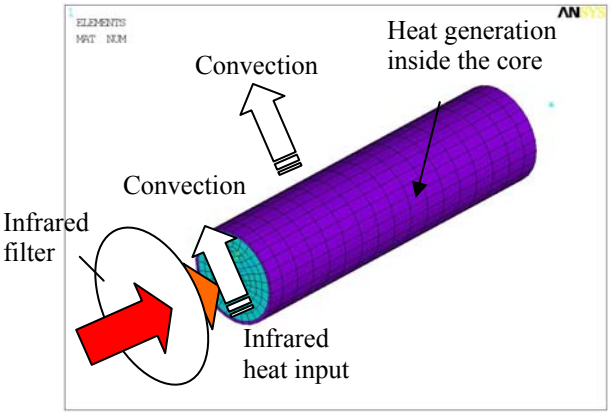

Figure 12. Meshed structure of the first 5-cm of fiber showing the infrared power input with infrared filter.

Figures 13 through 16 show the infrared (IR) solar radiation with infrared filter present and without infrared filter. It is seen from Figs. 13 and 15 that after the use of infrared filter, the solar power from the infrared spectrum decreases by 96% from 4.6 W to 0.2 W. Base plane is a 13.5x13.5 mm square that encompasses the 13.5 mm diameter of the fiber. Integration of local heat flux values over all 128x128 = 16,384 parcels yields 4.6 W in Fig. 14 and 0.2 W in Fig. 16.

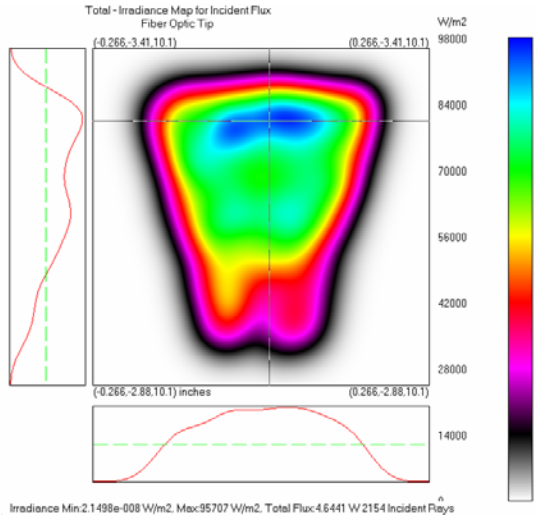

Figure 13. TracePro output of infrared (IR) solar radiation at the entrance region fiber tip without infrared filter.

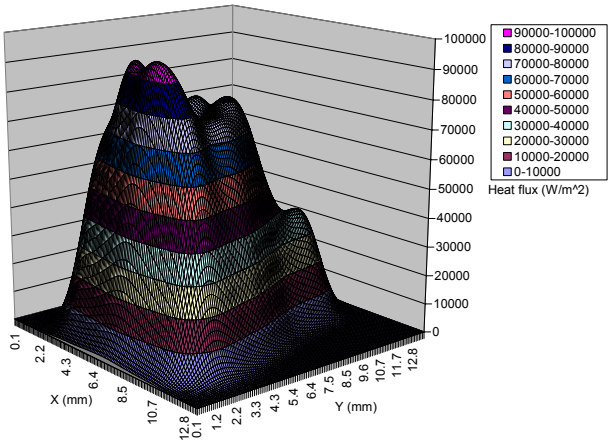

Figure 14. 3-D representation of the infrared (IR) solar radiation at the entrance region fiber tip without infrared filter as given by Fig. 13.

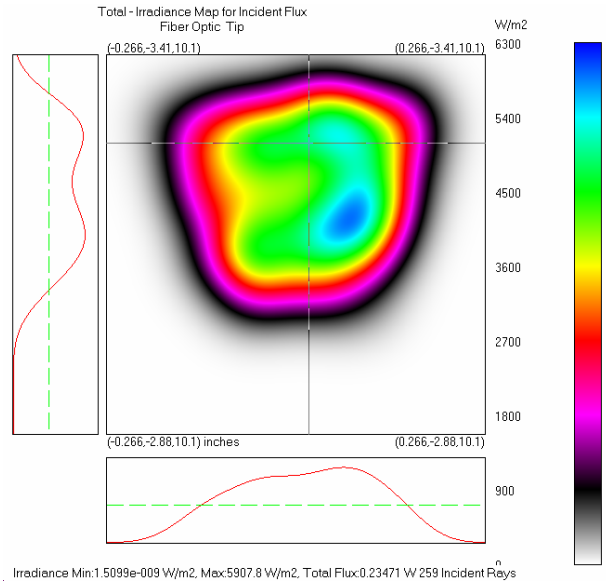

Figure 15. TracePro output of infrared (IR) solar radiation at the entrance region fiber tip with infrared filter.

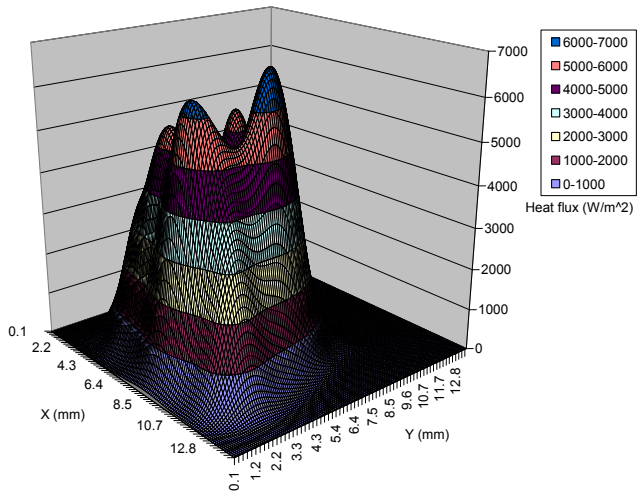

Figure 16. 3-D representation of the infrared (IR) solar radiation at the entrance region fiber tip with infrared filter as given by Fig. 15.

Figure 17 shows the deformed fiber tip after exposition to sunlight long periods of time as obtained from the experiment made at ORNL [20]. The experimental setup of ORNL was comprised of parts given in Fig. 2. In addition to the fiber tip burn, the other thing observed was the burn of the fiber protection case (that covers the fiber cladding) after fiber is bent beyond its critical bending radius of 108 mm. The explanation of the fiber entrance region tip burn is the "surface heating effect" of the infrared radiation (heat flux boundary condition) and that of the protection case is the "ultraviolet and visible spectrums absorption" of the solar radiation. Surface heating effect of the infrared spectrum substantiates the entrance region fiber tip deformation because after counting 3-4% fresnel reflectivity at the fiber tip, transmissivity is ~100% with ~0% absorptivity at the fiber tip. In the deformation of protection case, although incident rays get refracted into the cladding, no deformation on cladding material is realized.

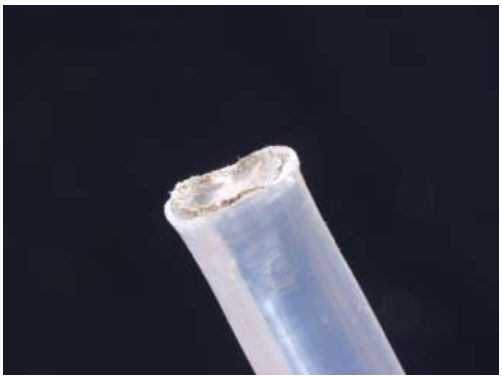

Figure 17. The fiber tip burnt after exposition to 7,500 lumens for almost 3 hours.

5. RESULTS

Figures 18-20 show, respectively, the temperature distribution with forced convective cooling when the air speed over the entrance region fiber tip and across the cylindrical surface of fiber is 5 m/s, 10 m/s, and 15 m/s with no infrared

filter or quartz glass attachment based on 12 hours of simulation. Figure 21 shows the results with infrared filter present with 5 m/s air speed over the entrance region fiber tip and across the fiber lateral surface based on 12 hours of simulation. In Figs. 18-26, the lateral surface and tip surface convective heat transfer coefficients have surface temperature dependence as given by Eqs. 4 and 6, respectively.

Figure 18 shows with 5 m/s air speed and without infrared filter and glass attachment that the temperature at the fiber inlet could reach about 668°C, which is substantially greater than the upper limit of safe operation temperature of 60°C given for the PMMA core material. The critical distance from the fiber inlet was determined to be about 7.8 mm. Thus, the use of some methods for deformation free operation is important for the safety of fiber. Figure 19 shows that with 10 m/s air speed, temperature at the fiber inlet drops by 105°C to 563°C making the first 5.7 mm critical and Fig. 20 shows that with 15 m/s air speed, the temperature drops by 163°C attaining 505°C at the fiber tip compared to the 5 m/s case making the first 4.6 mm critical. Figure 21 shows with infrared filter and an air speed of 5 m/s that the temperature at the fiber tip drops by 604°C to 64°C compared to the no infrared filter case at the same air speed, yet, causing fiber deformation at the entrance region tip. Figure 22 shows that using 20-mm-thick fused quartz glass just before the fiber inlet instead of infrared filter prevents the fiber burn based on 12 hours of simulation. It is found that an approximate fused quartz glass thickness of 14.0 mm will ensure safe operation of the fiber. The refracted light loss off the glass lateral surface to the surroundings was estimated to be negligible and a small amount of light loss was estimated due to the interface between glass and the fiber. On the other hand, infrared filter use may reduce the visible (VIS) power input to the fiber by almost 12% (See the transmission curve in Fig. 5). Thus, the use of quartz glass attachment was seen to be cheaper and more effective compared to the infrared filter use case at 5 m/s air speed. Figure 23 shows that the joint application of the infrared filter and the fused quartz results in uniform temperature of 40°C on the glass and the fiber.

Figure 24 shows the temperature distribution when the selective tip surface emissivity is 60% in the infrared and Fig. 25 when it is 80%. It is seen that application of a selective coating having an infrared emissivity of 80% results in reduction of temperature at tip of about 230°C, from 668°C to 438°C, compared to the case without radiation of Fig. 18. The difference in tip temperatures when the selective tip surface emissivity is 60% and when it is 80% is 33°C.

Figures 26 and 27 show, respectively, the temperature distribution when the ambient temperature is 0°C and -5°C without application of infrared filter or glass. It is seen from Fig. 26 that when T_∞ = 0°C, the entrance region tip temperature drops only by 23°C and from Fig. 27 when T_∞ = -5°C it drops by 27°C compared to the T_∞ = 25°C case of Fig. 18.

In Figures 18, 19, 20, 24, 25, and 26, the heat generated inside the core was 77,633 W/m^3, in Fig. 21 it was 50,686 W/m^3, in Fig. 22 it was 67,776 W/m^3 in the glass and 77,472 W/m^3 in the PMMA core, and in Fig. 23 it was 44,360 W/m^3 in the glass and 50,530 W/m^3 in the PMMA core.

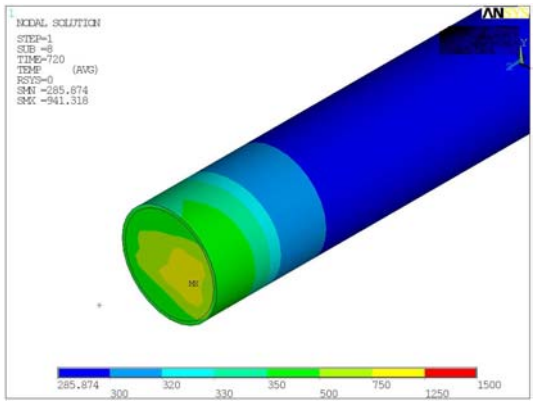

Figure 18. Temperature distribution at the fiber entrance region (first 5 cm of the fiber) without tip radiation and with 5 m/s air speed.

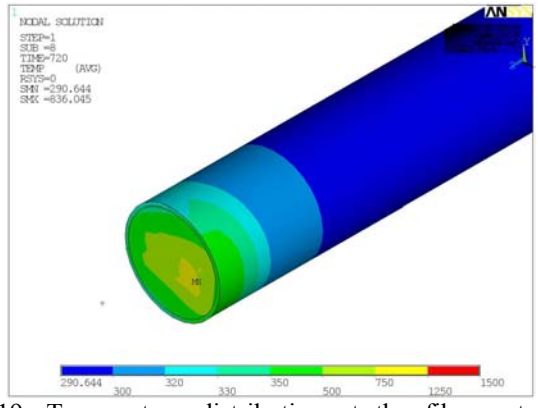

Figure 19. Temperature distribution at the fiber entrance region (first 5 cm of the fiber) without tip radiation and with 10 m/s air speed.

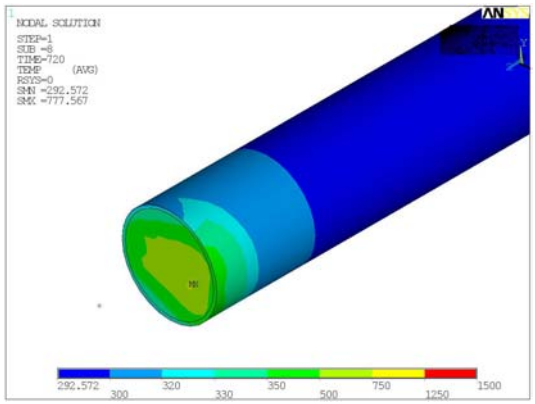

Figure 20. Temperature distribution at the fiber entrance region (first 5 cm of the fiber) without tip radiation and with 15 m/s air speed.

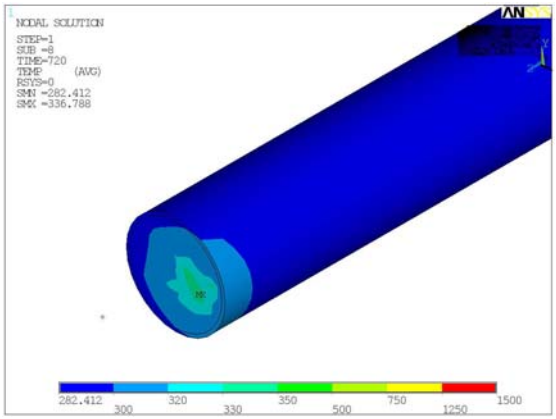

Figure 21. Temperature distribution at the fiber entrance region (first 5 cm of the fiber) without tip radiation, with 5 m/s air speed and with infrared filter before the fiber.

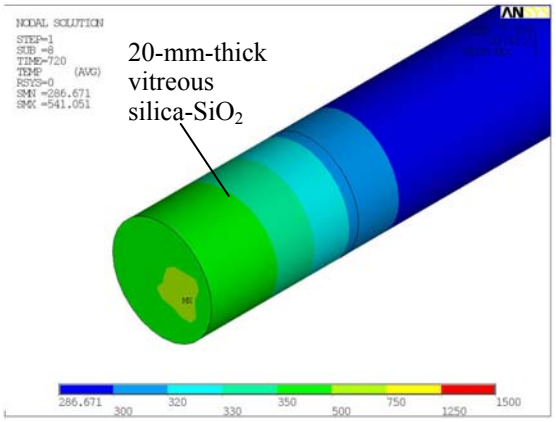

Figure 22. Temperature distribution at the fiber entrance region (first 5 cm of the fiber) without tip radiation, with 5 m/s air speed and with 20-mm thick fused quartz glass attachment before the fiber.

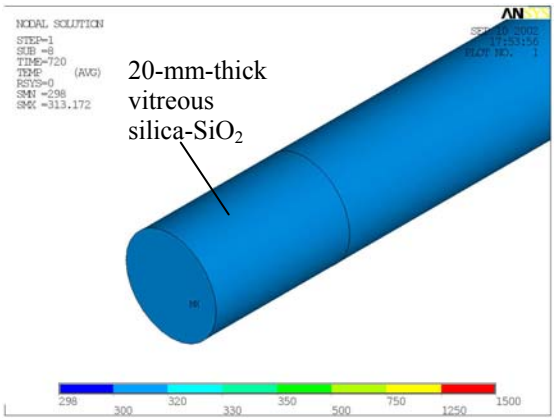

Figure 23. Temperature distribution at the fiber entrance region (first 5 cm of the fiber) without tip radiation, with 5 m/s air speed, with infrared filter and with 20-mm thick fused quartz glass attachment before the fiber.

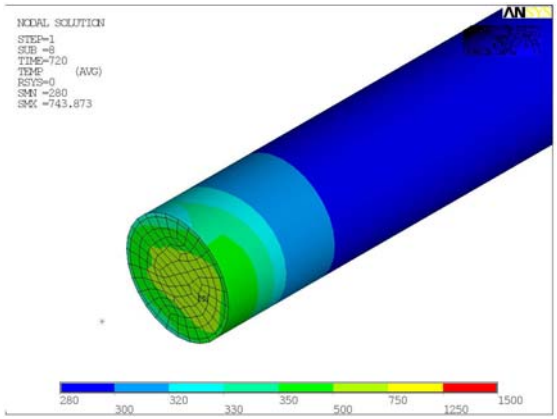

Figure 24. Temperature distribution at the fiber entrance region (first 5 cm of the fiber) with 60% tip surface emissivity, with 5 m/s air speed, and without infrared filter.

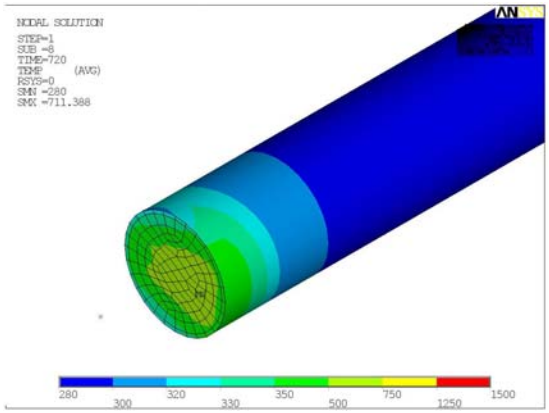

Figure 25. Temperature distribution at the fiber entrance region (first 5 cm of the fiber) with 80% tip surface emissivity, with 5 m/s air speed, and without infrared filter.

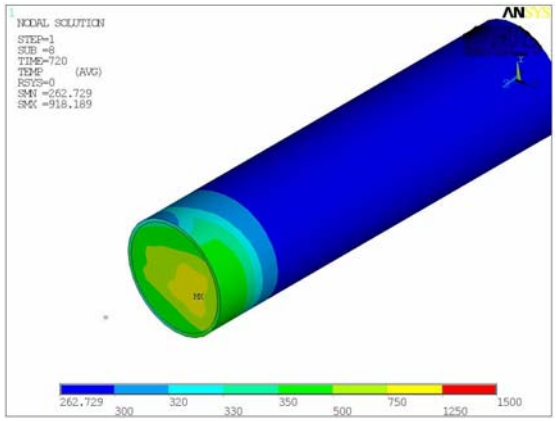

Figure 26. Temperature distribution at the fiber entrance region (first 5 cm of the fiber) without tip radiation, with 5 m/s air speed, with $T_\infty = 0°C$, and without infrared filter.

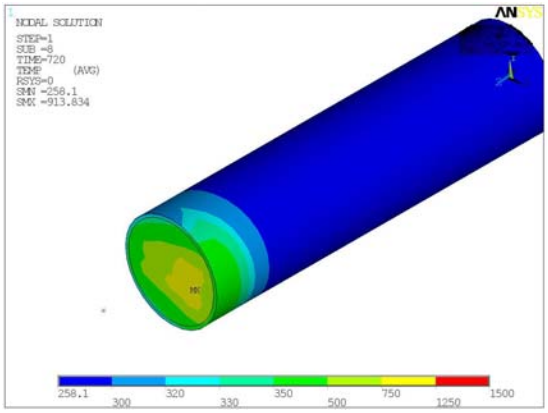

Figure 27. Temperature distribution at the fiber entrance region (first 5 cm of the fiber) without tip radiation, with 5 m/s air speed, with T_∞ = -5°C, and without infrared filter.

6. DISCUSSION AND CONCLUSIONS

The application of fused quartz glass attachment would be cheaper than the application of infrared filter or cooling fan. Fan application at the beneath of fibers will require maintenance and weather protection due to severe conditions such as storm, rain, etc. Also, it will require additional power (about 1.9 W) which will add as loss to the generated electricity of photovoltaic cells. The application of fused quartz glass attachment would be more feasible than the application of cooling fan, which would require a design space of about 80x80x25.4 mm. Infrared filter, if purchased, can be used to further reduce the required thickness of fused quartz glass which in turn helps reduce the refracted loss of the rays from the glass lateral surface.

7. ACKNOWLEDGMENT

Support of National Energy Technology Laboratory through the United States Department of Energy under cooperative agreement DE-FC26-01NT41164 is acknowledged.

8. REFERENCES

[1] Hao Liu and Paul Yager, **"Modeling of optical bending losses in multimode waveguides"**, Proceedings of Biomedical Optoelectronic Instrumentation: San Jose, CA, 7-9 February 1995, 120-129.

[2] Toshikuni Kaino, **"Plastic optical fibers"**, 164-187.

[3] T. L. Davenport, R. L. Hansler, T. E. Stenger, W. J. Cassarly, G. R. Allen, R. F. Buelow, **"Changes in Angular and Spatial Distribution Introduced into Fiber Optic Headlamp Systems by the Fiber Optic Cables"**, International Congress and Exposition, Detroit, Michigan, February 23-26, 1998.

[4] Andrew Biermann, Nadarajah Narendran and Nishantha Maliyagoda, **"How to report light loss values for optical fibers used in fiber-optic lighting applications"**, Proceedings of the SPIE, Vol. 3428, July 1998, 62-72.

[5] Hirotoshi Nagata, **"Effect of Heating on Jacketed Optical Fibers"**, Optical Fiber Technology 6, 192-198, 2000, 192-198.

[6] Yoshitaka Takezawa, Seikichi Tanno, Noriaki Taketani, Shuichi Ohara, Hideki Asano, **"Analysis of thermal degradation for plastic optical fibers"**, May 1991, v 42, issue 10, 2811-2817.

[7] J. T. Remillard, M. P. Everson and W. H. Weber, **"Loss Mechanisms in Optical Light Pipes"**, Applied Optics, Vol. 31, No. 34, 1992, 7232-7241.

[8] John A. Duffie and William A. Beckmann, **"Solar Engineering of Thermal Process"**, John Wiley&Sons Inc., 2nd edition, NY, 1991, p 10.

[9] Michael Modest, **"Radiative Heat Transfer"**, McGraw-Hill, Inc., 1993, p 7 and p 88.

[10] SMARTS v2.9, "Terrestrial Direct Normal Solar Spectral Irradiance for AM = 1.5". This program is available as Fortran 77 code at http://homepage.mac.com/smarts2

[11] Roberta A. Priemon-Storer (Managing Standards Editor), ASTM standard E891-82, **"Terrestrial Direct Normal Solar Spectral Irradiance Tables for Air Mass 1.5"**, ASTM, MD, 1985, p 692.

[12] Edmund Industrial Optics, **"Optics and Optical Instruments Catalog"**, 2002, p 85 and p 106.

[13] TracePro, Lambda Research Corporation, Littleton, MA 01460-4400. World-wide at http://www.lambdares.com.

[14] ANSYS v6.1, Release April 2002.

[15] Glen E. Myers, **"Analytical Methods in Conduction Heat Transfer"**, 2nd edition, AMCHT Publications, WI, 1998, p 78.

[16] A. F. Mills, **"Heat Transfer"**, 2nd edition, Prentice Hall, Inc., NJ, 1999, p 313-319.

[17] J. Brandrup and E. H. Immergut Eds., **"Polymer Handbook"**, 3rd edition, John Wiley&Sons Inc., 1989, v/77-v/79.

[18] DuPont catalog, **"Product and Properties Handbook-Teflon FEP (FEP 100)"**, 1998, p 3.

[19] Narottam P. Bansal and R. H. Doremus, **"Handbook of Glass Properties"**, Academic Press, Orlando, 1986.

[20] Oak Ridge National Laboratory, Oak Ridge, TN.

APPENDIX H

PERFORMANCE OF NEW HYBRID SOLAR LIGHTING LUMINAIRE DESIGN

Dennis D. Earl, Curt L. Maxey, and Jeff D. Muhs
Oak Ridge National Laboratory
2360 Cherahala Blvd.
Knoxville, TN 37932

Robert R. Thomas
Pennsylvania State University
University Park, PA 16802

ABSTRACT

We report on the performance of a new hybrid luminaire designed to blend light from a fiber optic solar source with electric fluorescent lamps. The luminaire design studied involves a commercially-available fluorescent luminaire that had been modified to include optical elements for efficiently dispersing two fiber optic solar light sources. Quantitative measurements of the hybrid luminaire's optical efficiency and spatial intensity distribution/deviations are discussed. The effects of static differences and dynamic fluctuations in spatial intensity distribution are qualitatively discussed and potential design improvements examined.

INTRODUCTION

Oak Ridge National Laboratory is developing an energy-efficient Hybrid Solar Lighting System which uses large-core plastic optical fiber to permit direct utilization of visible solar light for internal lighting[1,2], see Fig. 1. A major step toward the realization of fiber optic solar lighting for internal lighting purposes is the development of a hybrid luminaire to seamlessly balance electric and fiber optic illuminants. Fluctuations in the intensity of collected solar light, due to changing cloud coverage or solar collector movement, requires rapid compensation by electric lamps to maintain a constant room illumination. If the spatial intensity distribution of a hybrid luminaire's electric lamps does not closely match the spatial intensity distribution of the luminaire's fiber optic illuminants, then the shift between artificial and solar lighting will be noticeable, and potentially distracting, to the occupant. In addition, because this technology is primarily aimed at reducing energy usage, any potential hybrid luminaire designs must maintain high optical efficiencies.

To develop an optically efficient hybrid luminaire that exhibits a static spatial intensity distribution, regardless of which lighting source dominates, various light dispersing techniques have been developed and studied[3]. Among these techniques, one dispersion device and corresponding luminaire are providing encouraging results. The construction details of this luminaire and a quantitative measurement of its optical performance are reported in this paper.

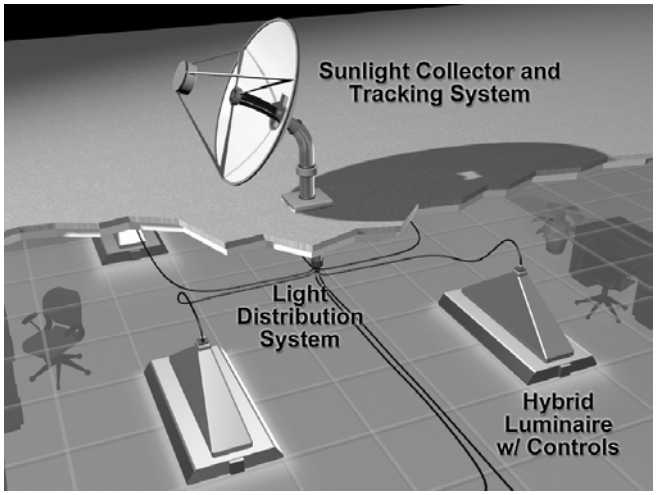

Fig. 1 - Hybrid Solar Lighting System

SELECTION AND MODELING OF COMMERICIAL LUMINAIRE

A wide variety of commercially-available luminaires exist which can be adapted for use as hybrid luminaires. However, to limit design efforts, a single Lithonia four-tube T8 fluorescent luminaire was selected for retrofitting. The Lithonia General Purpose T8 Luminaire was chosen because of its high electrical and optical efficiency, relative low cost, and easily integrated design. The GT8 luminaires also utilize an acrylic diffuser that assists in masking/merging two internal light sources. To aid in the design, construction, and testing of a hybrid luminaire, a high-detail optical model of the luminaire was first constructed using ZEMAX ray-tracing software. This model allowed the luminaire to be simulated under various configurations. The modeled luminaire was simulated within a six-foot cube, to provide intensity distribution data at various positions and working distances. An example of one such simulation is shown in Fig. 2.

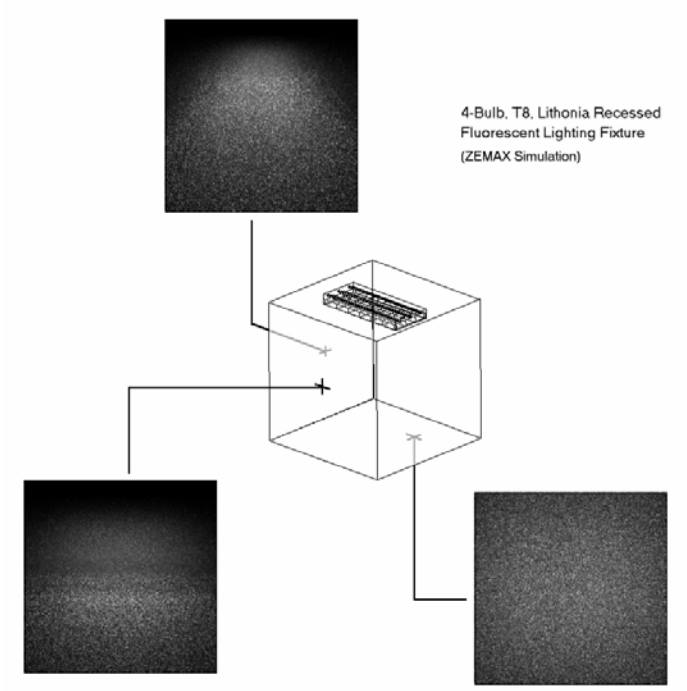

Fig. 2 - Spatial Intensity Distribution of Selected Commercial Fixture

From these simulations, it was verified that the natural conic intensity distribution of an optical fiber was highly incompatible with the intensity distribution of a fluorescent 4-tube luminaire designed for large-area lighting. It was determined that the conversion of the natural fiber optic light distribution into a into a long, uniform, cylindrical source distribution would permit the most effective blending of fiber optic lighting with fluorescent lamps.

HYBRID LUMINAIRE USING 3M SIDE-EMITTING ROD

Past attempts to develop an efficient means of converting the conic distribution of fiber optic lighting into a cylindrical distribution had resulted in less than desirable results. A partially scattering acrylic diffuser, shown in Fig. 3, had provided less than 40% efficiency and had resulted in a non-uniform intensity distribution. A search for alternative techniques revealed a new product developed by 3M. The 3M Side-Emitting Rod (Part #: LF-180-EX-D-1M), shown in Fig. 4, was similar in design to past attempts, but utilized precision machined grooves to more accurately control scattering along the length of the rod.

Fig. 3 - Early Attempt to Construct a Cylindrical Diffusing Rod

Preliminary investigations revealed that the one-meter long, side-emitting rod appeared suitable for use in a hybrid luminaire but would require additional measurements to determine the final effectiveness and efficiency of the device.

Fig. 4 - 3M Side-Emitting Rod Design

To further improve the efficiency of the side-emitting rod, a flat mirror was attached to one end of the rod. The mirror served to reflect and diverge any co-axial light that was not scattered on an initial pass through the rod. The rod was mounted within a

custom-machined acrylic holder that allowed a large-core optical fiber to mate with one end of the rod. The assembly of the optical fiber, acrylic holders, and side-emitting rod are shown in Fig. 5 for one side of the rod.

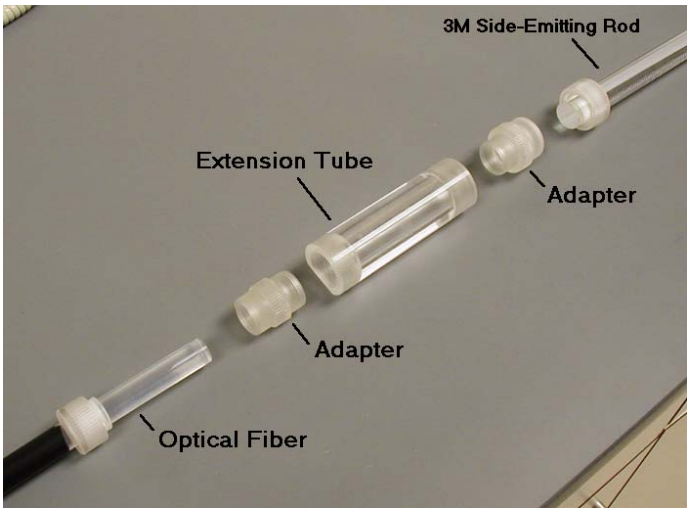

Fig. 5 - Side-Emitting Rod and Holders

Two assembled rods were mounted within a 4-tube fluorescent fixture, as shown in Fig. 6. The two side-emitting rods were located on each side of the ballast cover, directly between the two corresponding fluorescent tubes.

Fig. 6 - Hybrid Luminaire with Side-Emitting Rods (Diffuser Removed)

The hybrid luminaire was mounted, and its performance tested, within ORNL's Illumination Cell (see Fig. 7). ORNL's Illumination Cell is a six-foot cube equipped with mounts in the ceiling for attaching a fluorescent luminaire. A re-locatable, spectrally neutral, white wall within the cube allows the intensity distribution at various positions to be observed. A Prometric CCD colorimetry system allows the intensity and color distribution, incident on the white wall, to be precisely mapped.

Fig. 7 - ORNL Illumination Cell

The finished hybrid luminaire was mounted within the Illumination Cell and its optical performance measured (see Fig. 8).

Fig. 8 - Mounted Hybrid Luminaire with Fiber Optic and Fluorescent Sources On

RESULTS

The spatial intensity distribution on each of the five walls of the Illumination Cell was measured for the hybrid luminaire. Because we were concerned with effectively blending two different lighting sources, the distribution measurements of the luminaire were performed twice; once with all fluorescent lighting on and fiber optic lighting off, and once with fiber optic lighting on and fluorescent lighting off. The measurements produced ten intensity distribution maps, which were cropped and normalized so that they could be easily compared.

Under ideal conditions, the intensity distribution of the fluorescent lighting and the fiber optic lighting would be identical. In such a situation, any rapid change from one source to the other would be non-perceivable to the occupant. Actual measurements of the hybrid luminaire, however, revealed significant differences in intensity distribution

between the fluorescent and fiber optic sources. For a nearby side-wall, the hybrid lighting fixture exhibited two "hot spots" near the center and top corner of the wall (see Fig. 9). A maximum percent difference of 12% was measured for a patch of wall roughly one square foot in area.

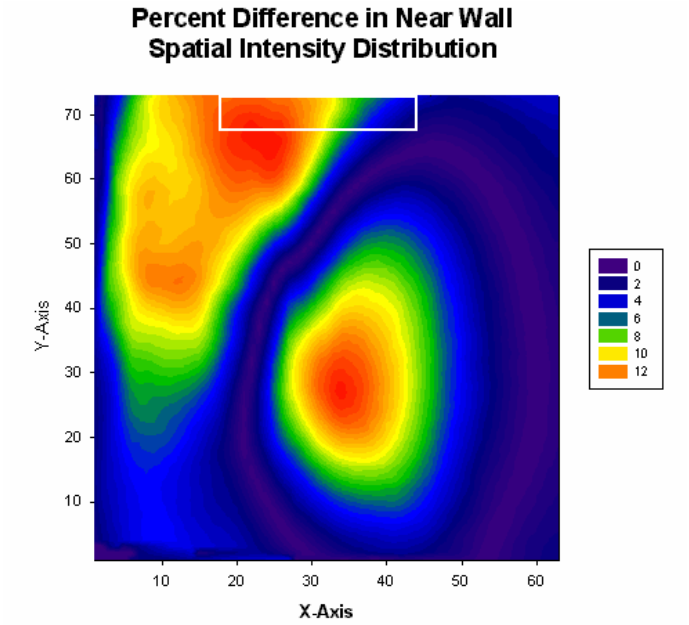

Fig. 9 - Differences in Spatial Intensity Distributions for Near Side Wall (White Box Indicates Orientation of Luminaire)

The largest difference, however, was measured at the floor of the Illumination Cell, directly beneath the hybrid luminaire. The percent differences in intensity between the fiber optic and fluorescent sources are shown graphically in Fig. 10. A significant portion of the floor area, roughly six square feet, has an intensity difference of greater than 20%. The highest measured percent difference was 27% and occurred slightly off-center of the luminaire's mounted position.

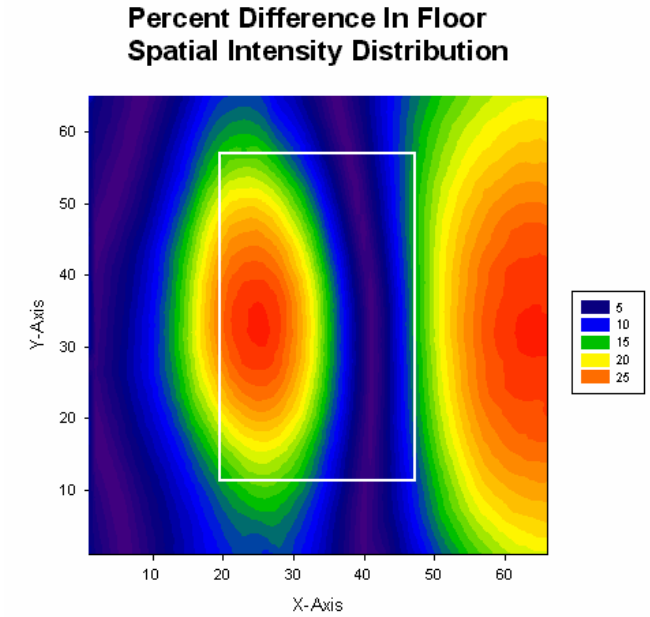

Fig. 10 - Differences in Floor Spatial Intensity Distribution (White Box Indicates Orientation of Luminaire)

The non-symmetric nature of the distribution was somewhat unexpected and may be the results of differences in total flux between the two 3M side-emitting rods. Potentially, the non-symmetry could also be due to slight variations in the mounting of the side-emitting rods. Because the current mounting did not rigidly position the side-emitting rods within the luminaire, there was some opportunity for positional variation.

The final efficiency of the 3M side-emitting rods, within the fluorescent lighting fixture, was determined by integrating all of the mapped intensity distributions for the fiber optic source and dividing by the known output of the optical fibers. The measured efficiency was approximately 58.4%. For the Hybrid Solar Lighting System to be economically feasible, it has been estimated that a hybrid luminaire design is needed which is 85% efficient. Obviously, the current luminaire efficiency is significantly lower than desired. However, it is suspected that a significant portion of the fiber optic light (≈20%) was lost due to coupling losses. Since this experiment was conducted, an improved method for coupling large core optical fibers has been developed with coupling losses as low as 3%. Given these improvements, the efficiency of the 3M side-emitting rod, within the hybrid luminaire, could potentially approach 75%. Such an increase, if confirmed, would make this technique a viable candidate for use with the Hybrid Solar Lighting System.

CONCLUSIONS

The hybrid luminaire presented in this paper still requires a significant amount of additional testing, modeling, and re-design before its physical implementation can realize its full potential. It is hoped that the incorporation of improved coupling connections and rigid mounts will significantly

improve the efficiency of the hybrid luminaire to greater than 75%, while also increasing its effectiveness at blending fluorescent and fiber optic sources. In addition, there is still much research which needs to be conducted to determine the effects of small-area intensity fluctuations. With the current Hybrid Solar Lighting System, and hybrid luminaire, a small-area intensity fluctuation of 27% would be experienced over a four to five second period. Whether or not this slow fluctuation would be distracting to an occupant still remains to be determined and is expected to be the focus of future research.

ACKNOWLEDGMENTS

Research at ORNL was sponsored by the Energy Efficiency and Renewable Energy Office of the U.S. Department of Energy and the Public Power Institute of the Tennessee Valley Authority.

REFERENCES

1. J. D. Muhs, "Hybrid Solar Lighting Doubles the Efficiency and Affordability of Solar Energy in Commercial Buildings", CADDET Energy Efficiency Newsletter December 2000, p. 6.
2. J. D. Muhs, "Design and Analysis of Hybrid Solar Lighting and Full-Spectrum Solar Energy Systems", *Solar 2000, July 16-21, 2000,* American Solar Energy Society.
3. D. D. Earl, J. D. Muhs, "Preliminary Results on Luminaire Designs for Hybrid Solar Lighting Systems", *Solar 2001, April 21-25, 2001,* American Solar Energy Society.

APPENDIX I

MODELING AND EVALUATION OF CHROMATIC VARIATIONS IN A HYBRID SOLAR/ELECTRIC LIGHTING SYSTEM

Prepared by

D. D. Earl and J. D. Muhs
Oak Ridge National Laboratory

ABSTRACT

This report describes recent efforts, conducted by ORNL, to develop, test, and evaluate a computational model capable of accurately predicting the chromaticity values of collected and fiber-optically distributed sunlight. This effort is in support of ongoing research towards developing a Hybrid Lighting System, capable of utilizing direct sunlight to supplement artificial lighting for the purpose of reduced energy consumption. The seamless integration of solar and electrical illuminants into a single Hybrid Lighting System requires the careful color matching of two spectrally different sources. Due to the high variability of solar spectra with time, day, year, and location, combined with the significant absorption effects associated with collection and distribution optics (mirror coatings, fiber optic transmission, etc.) an extensive chromaticity model is required to predict the final output spectrum and color values (CRI, CCT, and CIE x-y, u-v, u'-v' values) of collected and distributed sunlight. This report characterizes the spectral properties of unmodified direct sunlight in North America, evaluates the spectral modification of sunlight due to a proposed solar collector design, and evaluates the severity of color shifting due to the fiber optic transport of sunlight. The effects of fiber optic launch angles on spectral shifting are examined using data known about the current Hybrid Lighting Solar Collector design and transport optical fibers. The color matching between fluorescent and unfiltered sunlight is addressed and the design of a filter to improve color matching between solar and electric illuminants is discussed. Conclusions related to the applicability and energy efficiency of the final system are presented.

TABLE OF CONTENTS

1.0 Introduction

Lighting of commercial and residential buildings accounts for a significant amount of energy consumption in the United States, as well as worldwide. As a nation, we spend approximately one-quarter of our electricity budget on lighting alone. In an effort to reduce the energy consumption associated with lighting, Oak Ridge National Laboratory is investigating the feasibility of using large-core optical fibers to capture and distribute sunlight as a supplement to artificial lighting. Successful development of an economically-feasible hybrid solar/electric lighting system, hereafter referred to as the Hybrid Lighting System, would offer the potential for improved lighting quality combined with *significant* energy savings. To be widely accepted, it is anticipated that a Hybrid Lighting System would need to seamlessly blend solar and electric illuminants such that alternations between the two sources would not result in reduced occupancy comfort or productivity. However, seamlessly blending two spectrally-differing sources is a non-trivial task. Efforts must be taken to ensure that the perceived color of the two sources match to within some permissible value, thereby ensuring that rapid alternations between the two sources do not produce undesirable effects. Because the Hybrid Lighting System is a multi-component system, with each component altering the spectrum/color of the collected sunlight, it is necessary to fully model the spectral modifications that each system component imparts on the original solar spectrum. Given an accurate prediction of the final output spectrum of the collected solar light, comparisons of the collected sunlight chromaticity with selected electric illuminants can then be made.

This report details the results of a computational chromaticity model specifically developed to analyze the chromatic performance of a complete Hybrid Lighting System. An analysis of solar spectra variations due to physical phenomena (variations with time, date, and location), collector optics, and fiber optic transmission properties is presented. Chromatic performance is measured in terms of standard chromaticity values (CRI, CCT, CIE x-y, u-v, u'-v' values) and full spectral contents, when appropriate. A comparison of the final color agreement between commercially available electric illuminants and unfiltered collected sunlight is made and the design of a filter or additive LED lighting element, to improve color matching between solar and electric illuminants, is presented. Concluding remarks pertaining to the applicability, energy efficiency, and future research and development requirements of the Hybrid Lighting System are discussed.

2.0 Overview of Hybrid Lighting System and Components

The Hybrid Lighting System is a novel energy efficient lighting system that combines solar lighting and artificial lighting into one single system[1,2] to provide increased energy savings. As shown in Figure 1, the Hybrid Lighting System utilizes a large solar collector to collect and distribute sunlight into multiple large-core optical fibers. The optical fibers transport the sunlight to hybrid luminaries that blend the solar light with electric illuminants. The fiber optic transported solar light is dispersed, by the hybrid luminaire, in a manner well suited to interior lighting and matching the spatial intensity distribution of the luminaire's electric illuminants. Fluctuations in the intensity of the collected solar light are compensated for by the electric illuminants in the hybrid luminaire to maintain a constant room illumination.

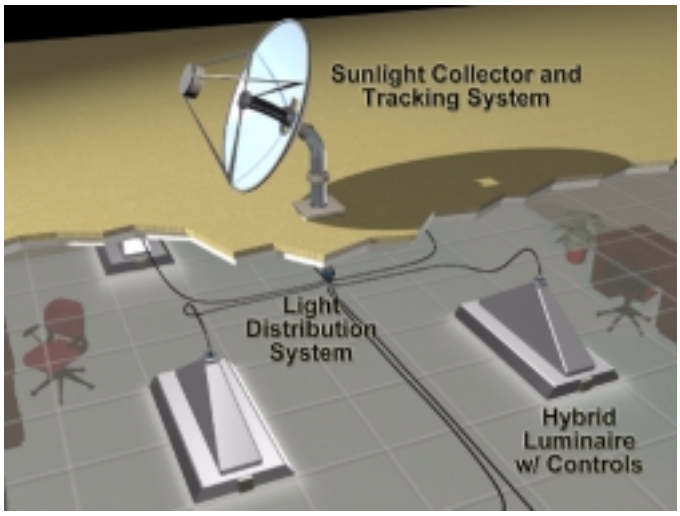

Figure 1. Hybrid Lighting System

Research is currently underway to design and construct a **Solar Collector** and tracker system that will provides low-cost, high-efficiency concentration of solar light (see Figure 2). Critical design features and construction details are already available which facilitates the accurate modeling of chromatic effects due to the solar collector optics.

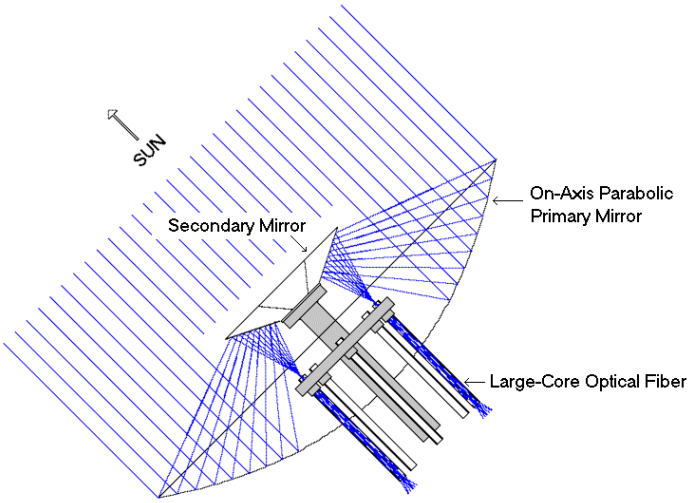

Figure 2. Solar Collector Design

Likewise, the characterization of selected large-core **optical fibers** has been conducted to provide information critical to calculating the effects of fiber optic transport on chromaticity. The measurement of bulk absorption, bulk scatter, and anomalous transmission losses within an optical fiber (due to manufacturing defects), has be conducted and utilized in the modeling calculations presented in this report.

Equally as important are the efforts to develop a **Hybrid Luminaire**, which have resulted in the construction of two potentially viable designs that retrofit commercially available

luminaries (see Figure 3). Each Hybrid Luminaire design has been accurately modeled using ZEMAX ray-tracing software allowing computer-based simulations of design performance. Various light sources are possible for use as an electric illuminant, with much design emphasis being placed on T8 fluorescent tubes (Sylvania Octron 841).

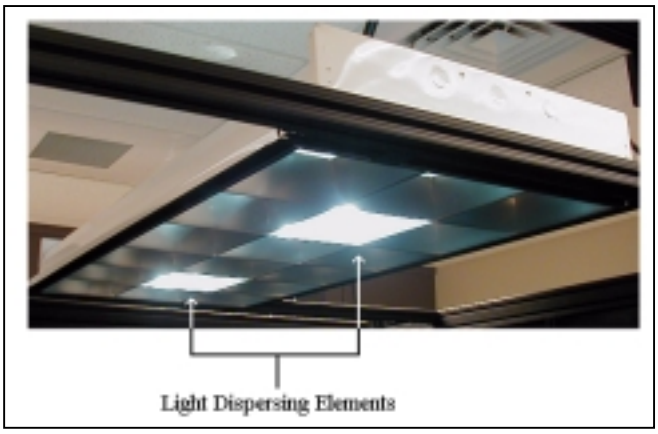

Figure 3. Hybrid Luminaire

The Hybrid Lighting System's Solar Collector, large-core optical fibers, and Hybrid Luminaire (with electric illuminant) represent the three critical components of the Hybrid Lighting System. Each component's chromatic performance is modeled and simulated in the following sections using commercially available modeling tools, custom-written code, and experimentally acquired component data. In addition, the chromatic properties of the sun are modeled and used as input data for all measurements.

3.0 Algorithm Development/Usage for Chromaticity Calculations

This section describes the tools used to model the chromatic performance of a complete Hybrid Lighting System. When possible, commercially available tools and pre-existing source code were employed. However, for certain specific modeling measurements, such as modeling optical fiber loss at varying launch angles, custom-written software was developed. The development of these custom-written programs is not described in detail but an overview of their function is presented and any chromatic calculations utilized by the program are referenced at the end of this report.

3.1 Algorithms for Calculating Solar Spectral Power Distributions

Calculations of solar spectra and power were accomplished using the Simple Solar Spectral Model for direct irradiance on horizontal and tilted planes at the Earth's surface, developed by R. Bird and C. Riordan[3]. The model assumes a cloudless atmosphere and provides terrestrial spectra between 300-4000 nm with a resolution of approximately 10 nm. Inputs to the model include the solar zenith angle, the collector tilt angle, atmospheric turbidity, the amount of precipitable water vapor and ozone in the atmosphere, surface pressure, and surface temperature. Past evaluations of the Simple Solar Spectral Model have shown that it agrees well with more rigorous solar spectral models and experimental data. The results of these past evaluations are well documented by Bird and Riordan (Technical Report No. SERI/TR-215-2436). Figure 4 gives an example comparison (data collected by Bird and Riordon) between the predicted and actual measured direct solar irradiance (data for Boulder, CO, 08/19/1981). For purposes of evaluating the chromatic performance of the Hybrid Lighting System, this level of accuracy is sufficient.

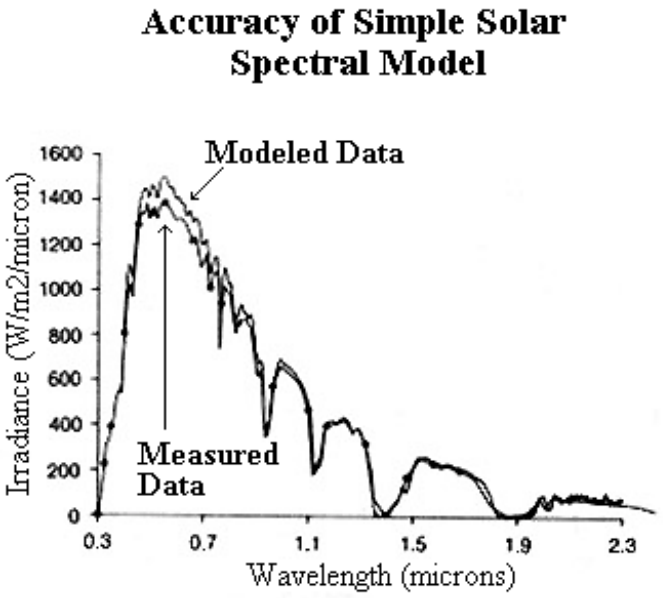

Figure 4. Bird and Riordan Measurement of Simple Solar Spectral Model Accuracy

A program previously written in C code, by Martin Rymes, was available from the National Renewable Energy Laboratory webpage[4] and computed the solar spectrum and power based upon Bird and Riordan's Simple Solar Spectral Model. Given the desire time, date, longitude, latitude, and timezone, Rymes' code made the necessary solar position calculations needed to determine the solar zenith angle required by the Simple

Solar Spectral Model. To provide improvements to the user interface and to more easily integrate the code with other pre-existing software (written in Visual Basic and Visual C++), the original C code was ported to Visual C++. A linear interpolation function was added to the original code that allowed the resolution of the terrestrial spectra to be increased to 1.0 nm increments. The final code allowed the user to select a city, state and the desired date and time at which to calculate the solar spectrum. The solar spectral power distribution (SPD) would be returned as a text file in units of Watts per meter^2 per nanometer.

Using the solar SPD algorithm, a large database of solar spectra was created for three cities in North America; Spokane, WA, Topeka, KA, and Miami, FL. As can be seen in Figure 5, these three cities span the full extent of the continental United States and serve as good test locations for evaluating the performance of the Hybrid Lighting System.

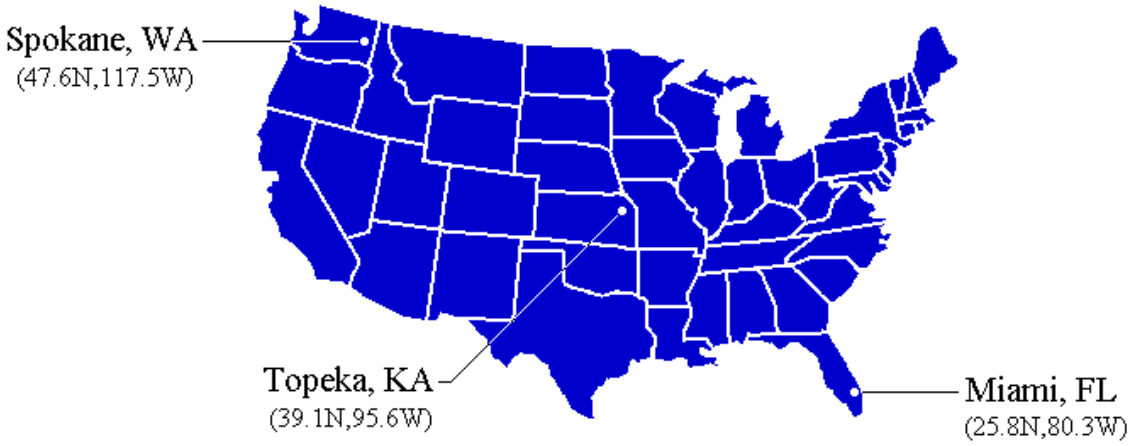

Figure 5. Test Locations Used For Simulations

These three cities were chosen purely for their longitude and latitude values and are not intended to imply the optimal location for installation of a Hybrid Lighting System

Database files were calculated for every 30-minute increment from 01/01/2001 – 12/31/2004. All calculations assumed the following general atmospheric parameters:

Surface Temperature = 27º C
Surface Pressure = 1006 millibars
Atmospheric Turbidity = 1.14 (Power on Angstrom Turbidity)
Amount of Precipitable Water Vapor = 1.36 cm.
Aerosol Optical Depth at 0.5 Microns, Base e = 0.2
Aerosol Assymetry Factor = 0.65

Although these constant parameters could have been made variable for given dates and times (i.e. the Surface Temperature is more likely to be 15º C than 27º C in January), the

errors that resulted from using the static atmospheric parameters were assumed to not be significant during projected peak usage times (10:00 a.m. – 6:00 p.m.).

3.2 Software for Evaluating Solar Collector Performance

A commercially-available optical ray-tracing program was used to evaluate the chromatic performance of the Hybrid Lighting System's Solar Collector. ZEMAX (version 10.0a) was used to model the Solar Collector design and all associated mirror coatings. Because the Solar Collector design utilizes a cold-mirror coating for the removal of unwanted infrared radiation, it was necessary to perform a ray-tracing analysis of the propagation of incident sunlight as it travels through the collector design. The reflectivity of a cold-mirror coating is dependent upon both incident angle and wavelength, therefore, both the design of the collector as well as the selection of coating materials play an important role in determining the chromatic properties of the solar collector. Coating data was represented as a real and imaginary index of refraction based on manufacturer provided data.

ZEMAX is an established, commercial program that is used extensively by optical engineers throughout the world. The accuracy of the software has long been established and can be considered accurate for geometric ray-tracing calculations.

3.3 Algorithms to Predict Color-Shifting During Fiber Optic Transport

Large-core optical fibers are used in the Hybrid Lighting System to distribute collected sunlight to Hybrid Luminaires. Optical fibers, like all transparent materials, have an associated absorption and transmission curve and a bulk material scattering coefficient. Optical fibers consist of a core material, which the collected light propagates through, and a cladding material, which serves the function of providing a higher index of refraction boundary needed to support total internal reflection within the fiber. Often large-core optical fibers can develop a localized separation between the core and the cladding of the optical fiber. This undesirable separation may be the result of improper manufacturing or acute stress applied to the unprotected optical fiber. Regardless of the cause, the effect is a large optical loss located around the position of the core-cladding separation. Core material absorption and bulk core material scattering, plus localized separation of the core-cladding interface, compose the three principle components responsible for loss and color-shifting within a large-core optical fiber.

To calculate the spectral modifications that occur during fiber optic transport, it was necessary to measure the three principle components of loss in the optical fiber selected for use with the Hybrid Lighting System. The fiber, 3M LF120B, was characterized by Rensellaer Polytechnic Institute. The spectral transmission properties of the fiber were measured for various fiber lengths and source launch angles. An increased launch angle results in a lengthened optical path plus the increased probability of encountering a core-cladding separation. Therefore, it was expected that the attenuation and chromatic

variation exhibited by the optical fiber would increase with increasing launch angle. Figure 6 shows a plot of the optical fiber transmission data vs. wavelength for increasing angles of incidence.

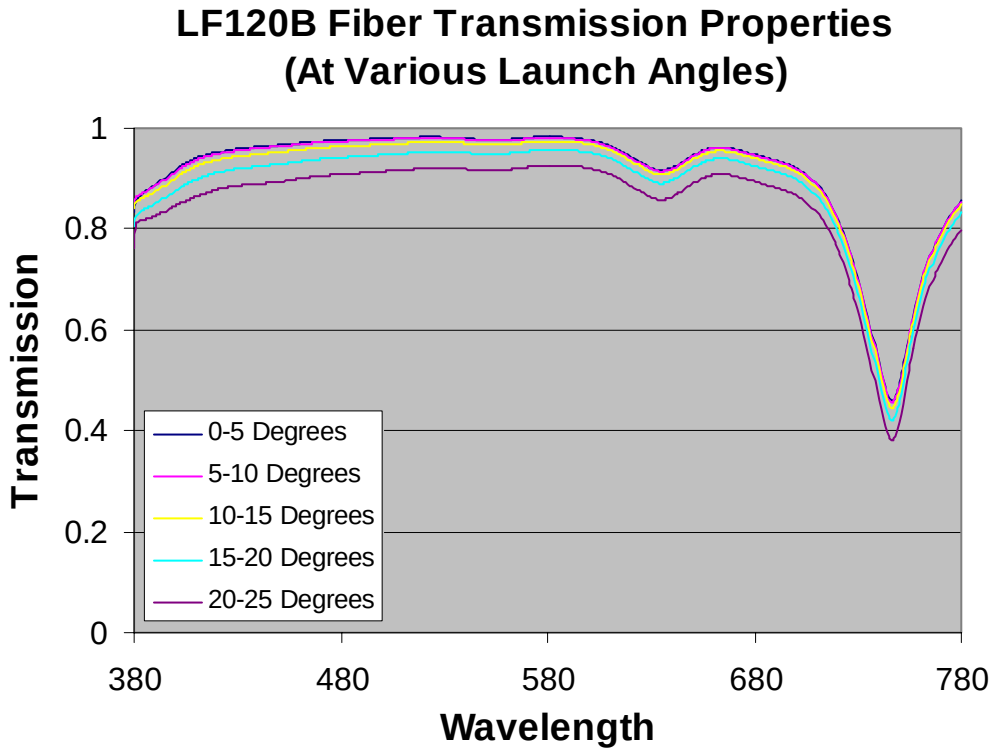

Figure 6. Optical Transmission Properties of 3M Fiber

As is evident in Figure 6, the attenuation exhibited by the fiber does indeed increase with increasing launch angle. The transmission spectrum of the fiber, however, does not appear to shift with increased launch angle.

The data shown in Figure 6 was used to establish the cornerstone of a larger software program to estimate the output spectra of a fiber of defined length and defined launch conditions. Given an input spectrum, the launch angle flux distribution, and the appropriate optical fiber data (Figure 6), a prediction of the output spectrum could be made. Standard color-value algorithms were written to convert the output spectrum to CIE coordinates (x-y, u-v, u'-v')[5-7]. The program was written in MATLAB code by Rensellear Polytechnic Institute, and later converted to C++ by ORNL for improved user interface.

3.4 Experimental Verification of Fiber Optic Chromaticity Program

To verify that the Fiber Optic Chromaticity (FOC) program was accurately predicting shifts in color, the FOC program needed to be experimentally verified. A Prometrics® CCD-based Photometric system was used to measure the u'-v' coordinates of light

emitted from a 10-meter length LF120B optical fiber. A metal halide lamp, manufactured by Cogent Inc., coupled approximately 3000 lumens into the optical fiber under test. The color of the light, after being transmitted through 10 meters of optical fiber, was measured with the Prometrics® system. Both the entrance and exit faces of the optical fiber were polished. After measurement at 10 meters, the fiber was reduced by one meter, polished, and again measured. This continued until a length of 2 meters was reached. Cutting, polishing, and measuring the light emitted from less than 2 meters of fiber posed a significant physical challenge and, therefore, experimental data was only taken from 2 to 10 meters. The resulting experimental data is shown in Figures 7 and 8:

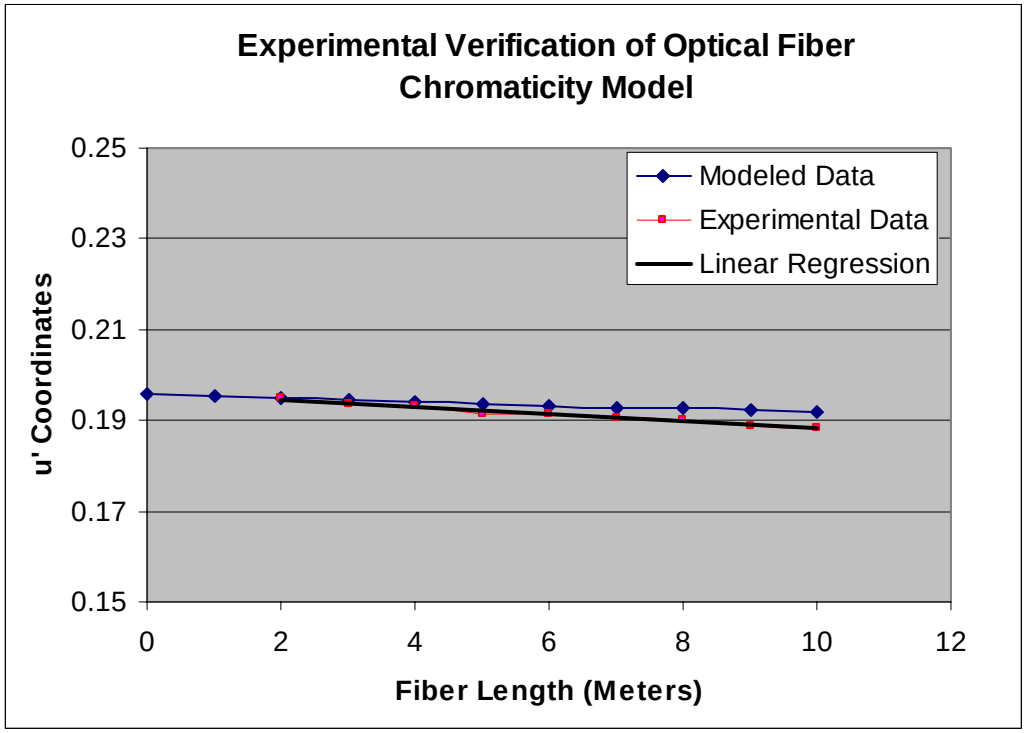

Figure 7. Experimental Variation in u' Coordinate With Increasing Fiber Length

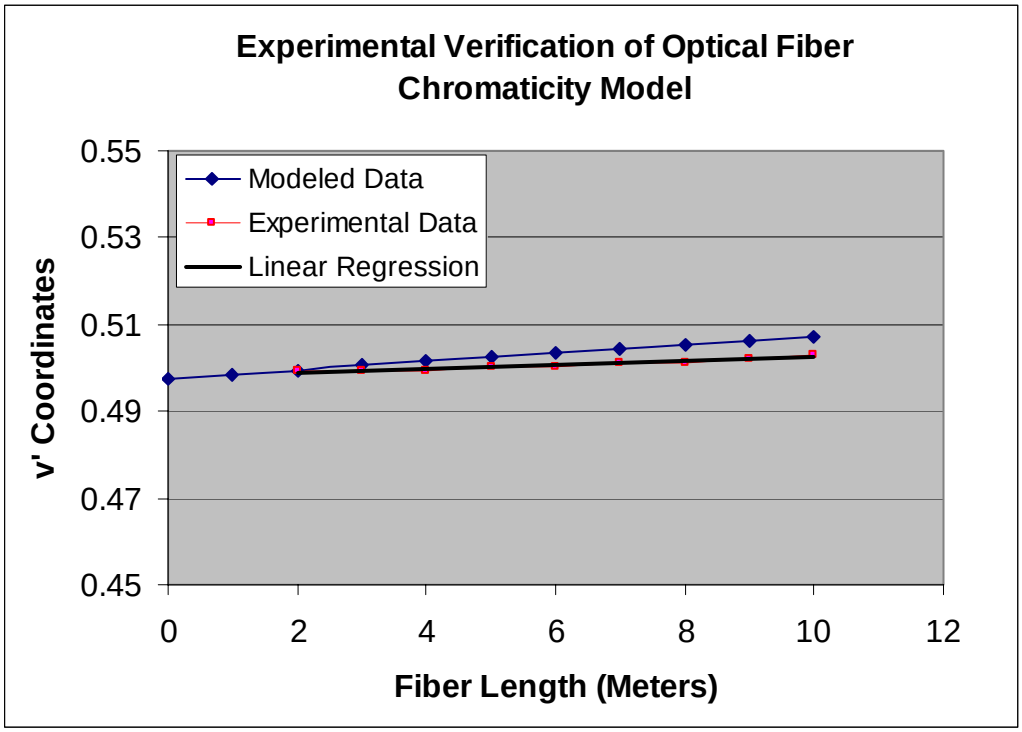

Figure 8. Experimental Variation in v' Coordinate With Increasing Fiber Length

The slight disagreement between the calculated and measured color values, in Figure 7 and 8, is within the uncertainty limits of the experiment. Uncontrolled color shifting was observed in the source over time and represented the most significant measurement error. Disagreement between the modeled and experimental data is less than can be perceived with the human eye (< 1-step MacAdam ellipse).

4.0 Evaluation of Chromaticity Characteristics of Direct Sunlight

As mentioned previously, successfully matching the color of a solar illuminant to an electric illuminant requires the characterization of variations in the collected and distributed sunlight's spectral content. Effectively matching a solar illuminant with an electric illuminant will only be possible if the spectral fluctuations in the collected sunlight can be kept to a minimum. Natural variations in solar spectra occur depending upon the time of day, time of year, geographic location, and atmospheric conditions. This phenomenon is easily observed at the solar sunrise and sunset of every day. At sunrise or sunset, the spectral content of the direct solar irradiance is strongly shifted toward the red portion of the spectrum and, therefore, exhibits a noticeably reddish-orange color. This is the result of an increased optical path length through the atmosphere combined with the effects of atmospheric contaminants. At midday, the spectral content of the direct solar irradiance is more evenly distributed across the visible spectrum and appears more yellowish/white in color. The spectral shift is illustrated in Figure 9, where all solar calculation were made using the Simple Solar Spectral Model described in Section 3.1:

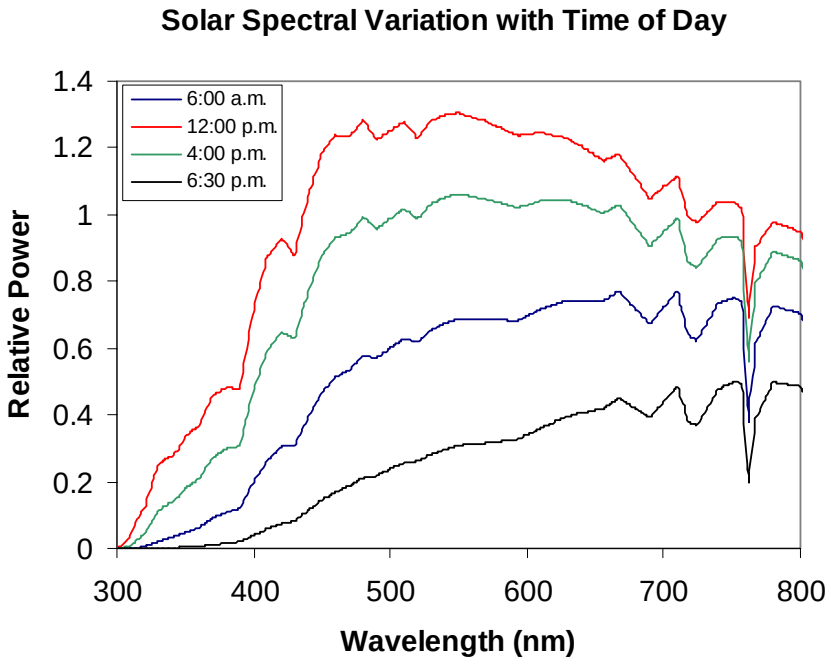

Figure 9. Solar Spectral Variation (Data for June 01, 2001/Spokane, WA)

A Hybrid Lighting System, which blends the highly variable-colored sunlight shown in Figure 9 with an electric illuminant, would most definitely exhibit a noticeable color difference between its solar and electric illuminants. By itself, the difference in color does not actually present a serious illumination deficit. However, because a sudden change in the intensity of the collected sunlight (due to cloud coverage or tracking errors – wind gust, etc.) would be compensated for by an increase in the intensity of the electric illuminant, the alternation between the two sources would potentially produce a

noticeable and undesirable strobe-like color effect. Therefore, the fluctuation in solar spectral content should be minimized to avoid this undesirable effect.

Figure 9 only shows the spectral change for one particular location on one particular day. To fully investigate the effects of the changing color of direct sunlight, it is convenient to switch to the more compact notation, and human response oriented, CIE tri-stimulus color coordinate values (u', v'). Using the Simple Solar Spectral Model described previously, the u'-v' color coordinate values were computed for direct sunlight for one whole year at three separate locations within the continental United States. The changes in the perceived color of direct sunlight, for every hour of every day of one full year (2001), is charted in Figure 10:

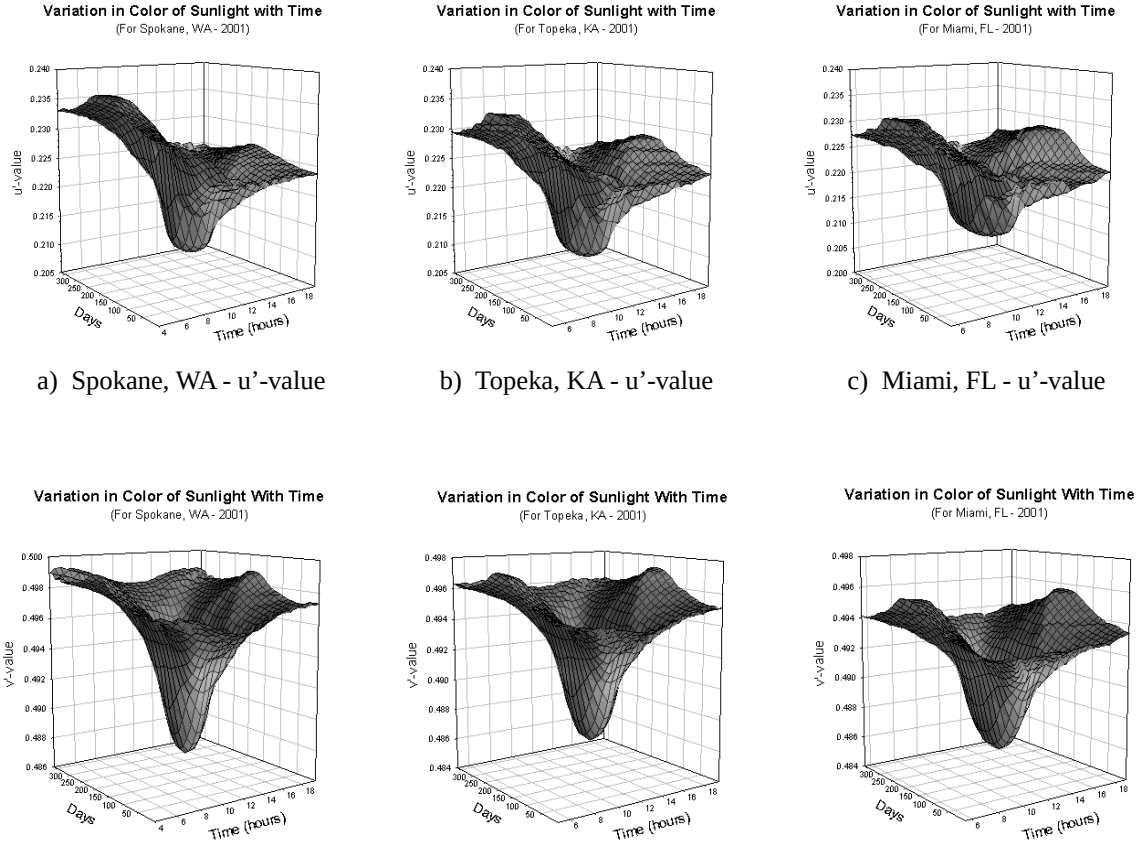

a) Spokane, WA - u'-value b) Topeka, KA - u'-value c) Miami, FL - u'-value

d) Spokane, WA - v'-value e) Topeka, KA - v'-value f) Miami, FL - v'-value

Figure 10. u'-v' Coordinate Representation of Solar Variations Throughout Year

Figure 10 expresses the change in solar chromaticity with "time of day and year." This is useful for investigating ***when*** the largest chromatic shifts are observed (morning vs. afternoon, winter vs. summer, etc.). Likewise, Figure 10 also allows us to compare various longitudes and latitudes to determine how different locations might experience different fluctuations in color with time. For example, in Figure 10a and 10c, we can observe that Spokane, WA is expected to exhibit a greater chromatic fluctuation in the morning than would be observed in Miami, FL. This information can later be used to

help identify the optimal operating times for a Hybrid Lighting System given a particular location.

To help visualize the sunlight's shift in color with time of day, and to compare this with the amount of available sunlight at those times, Figure 11a,b shows the solar intensity and color versus time of day for two different days (Location: Miami).

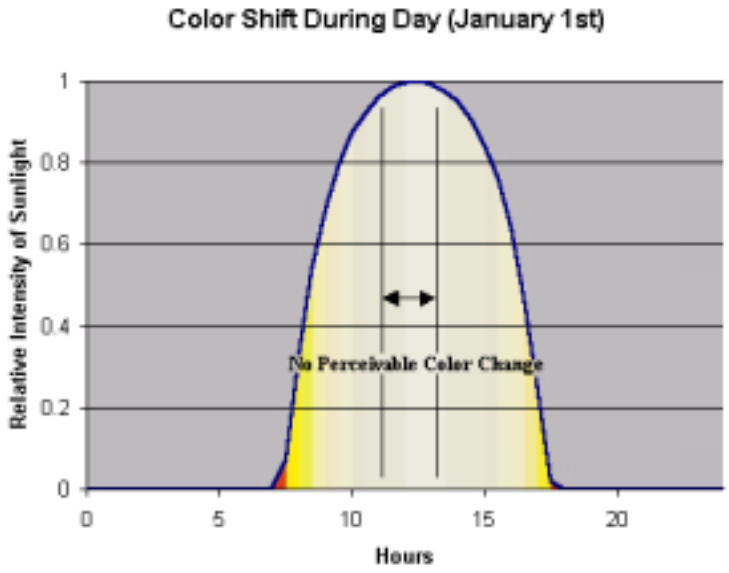

(a)

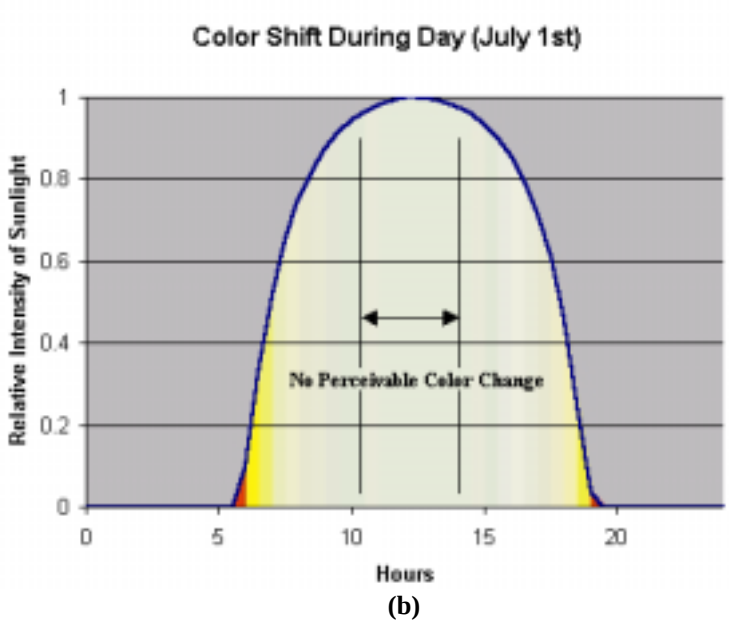

(b)

Figure 11. Joint Representation of Solar Intensity and Color Shift with Time of Day

Figure 11a,b also indicates the range of times that would exhibit colors perceived to be identical (within a 1-step MacAdam). For January 1st, this is a 2½ hour period and for July 1st, a 4½ hour period.

Another useful way to visualize these variations in solar color is shown in Figure 12a:

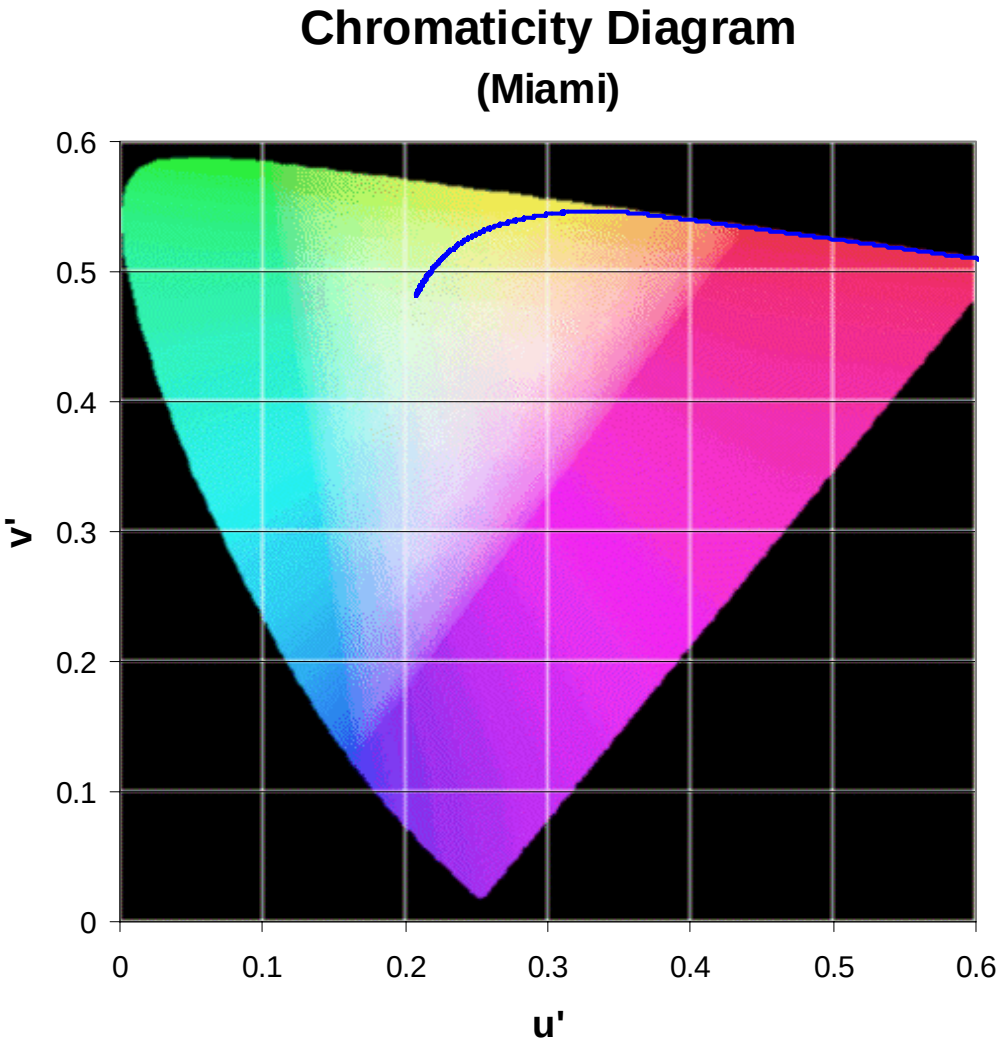

Figure 12a. u'-v' Coordinate Representation of Solar Variations (u'-v' Color Space)

Here the solar chromaticity values for a full year are represented simultaneously in u'-v' color space. The CIE u'-v' color map is shown behind the graphed data to provide an estimate of the approximate color associated with each point on the curve. Due to color printer limitations, this background map should only be considered a rough approximation of the actual solar color. Although this graph does not provide us with any information concerning the temporal fluctuation in solar color it does allows us to quickly visualize the extent of the fluctuation in chromaticity.

As can be seen in Figure 12b-d, the chromaticity curve is approximately the same for various longitude and latitudes within the continental United States. Therefore, from this point on, when representing data in u'-v' color space only one location will be chosen for graphing.

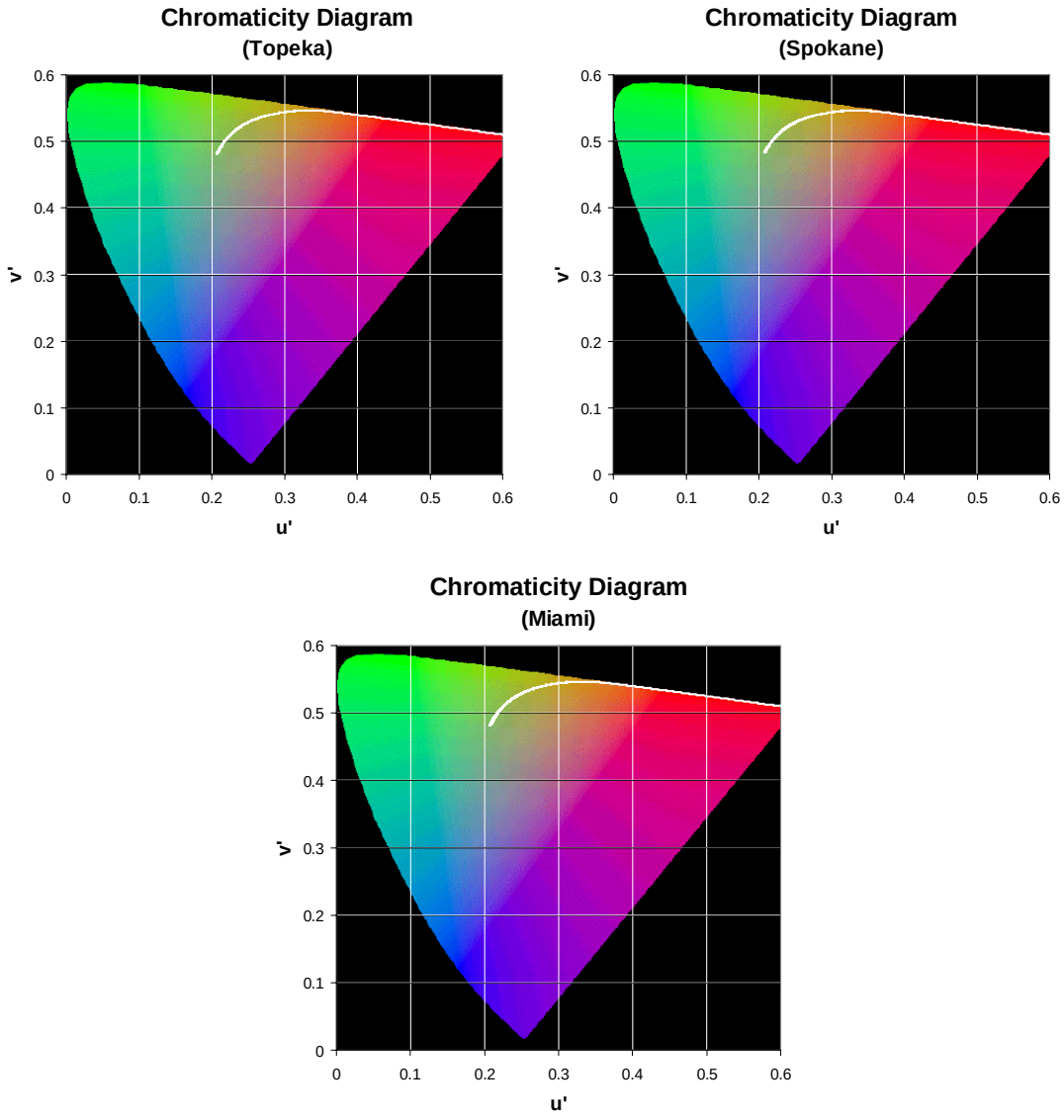

Figure 12b,c,d. Comparison of Solar Variations at Difference Locations

The u'-v' color space was chosen based on its improved representation of color differences. Although not a truly uniform color space, equal distances between u'-v' chromaticity points space represent approximately equal "differences" between perceived color. Therefore, we can quantitatively specify a color difference as being the distance between two color coordinates in u'-v' space. Equation 1 describes the traditional measurement of color difference between two color points (u_1',v_1') and (u_2',v_2'):

$$color\_difference = \sqrt{(u_2'-u_1')^2 - (v_2'-v_1')^2} \qquad \text{Equation 1}$$

Therefore, for the values graphed in Figure 12a-d, the following information can be deduced (see Table 1):

Table 1: Full Color Variation of Sunlight in One Year

CITY	Average (u',v')	Standard Deviation	Maximum Color Distance
Spokane, WA	(0.232, 0.500)	(±0.061,±0.0170)	0.4163
Topeka, KA	(0.231, 0.498)	(±0.065,±0.0165)	0.4160
Miami, FL	(0.230, 0.496)	(±0.067,±0.0162)	0.4159

Among each of the three locations, the average color and maximum color deviation is very nearly the same.

To reduce the spectral variation of collected sunlight in a Hybrid Lighting System, limiting the allowable "collection" times appears to represent the simplest, most effective, and inexpensive solution to reducing spectral fluctuations in sunlight. Limiting the "collection" times of a Hybrid Lighting System would simply entail the enforced/programmed inactivity of the solar collector system during portions of the day when chromatic variations are high (i.e. sunrise and sunset). It is expected that system inactivity during the early morning and late afternoon may already be required in a number of roof-mounted environments due to mechanical restrictions present at the installation site. Primarily, obstruction of the sun, at low angles, by other nearby roof-mounted structures is expected to be a common occurrence.

Since inactivity of the solar collector will obviously reduce the potential energy savings per year for a Hybrid Lighting System, an optimal balance is sought between maximum energy savings and minimal solar spectral variations. Figure 13 illustrates the reduction in yearly solar spectral variation that occurs as a result of imposed inactivity (given in hours) after sunrise and before sunset. In the same figure, the total amount of light collected in a year, given the reduced operating time, is compared. The maximum amount of collectable light obviously occurs when there is no system inactivity, and the graph is scaled such that this point represent 100% collected sunlight. Similarly, the maximum amount of solar spectral fluctuation will occur when there is no system inactivity and the data is likewise scaled such that this will be the point of 100% chromatic fluctuation.

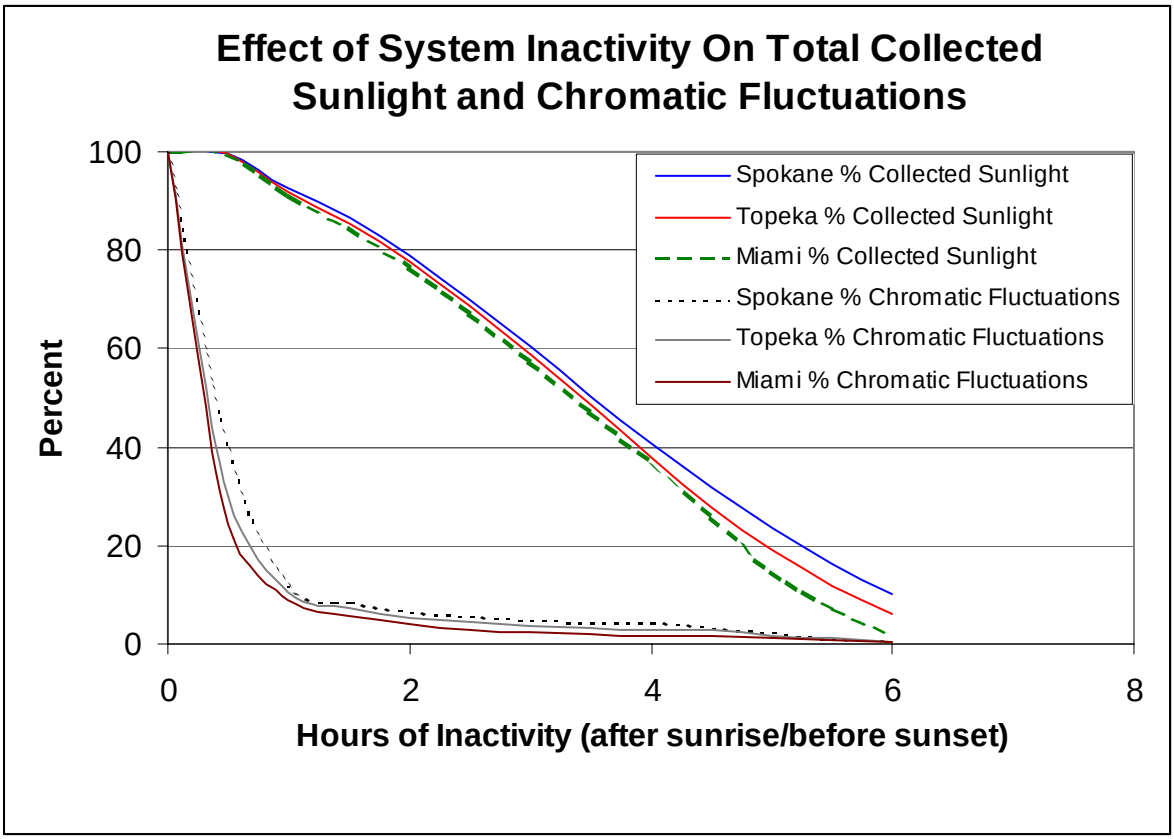

Figure 13. Competing Chromatic Fluctuation Reduction and System Usage Factors

From Figure 13, it would appear that 1½ hours of inactivity, after sunrise and before sunset, might produce a nice balance. However, additional system requirements are going to eventually determine the optimal balance between the two competing processes and the data shown in Figure 13 will be useful for weighing those future effects. The effect of reduced chromatic fluctuations due to system inactivity is approximated in Equation 2.

$$\text{Maximum Color Difference} = 0.0005x^6 - 0.0111x^5 + 0.0919x^4 - 0.3804x^3 + 0.8285x^2 - 0.9045x + 0.4163$$

Equation 2

Where x is the hours of inactivity and the maximum color difference is the maximum distance between u'-v' coordinates in a u'-v' color space

5.0 Evaluation of Chromaticity Variations Due To Solar Collector Design

5.1 Overview

The Hybrid Lighting System's Solar Collector tracks the sun and focuses sunlight into multiple large-core optical fibers. Because the reflective coatings used on the various components of the collector design are sensitive to wavelength and incidence angle, some chromatic modification to the collected sunlight is expected. The current design uses a high-quality parabolic primary mirror with a segmented secondary reflector element to precisely split and focus incident solar radiation into eight large-core optical fibers. This system is designed to couple light into each optical fiber with high total system efficiency in the visible portion of the spectrum. The main optical components of the system are illustrated in Figure 14:

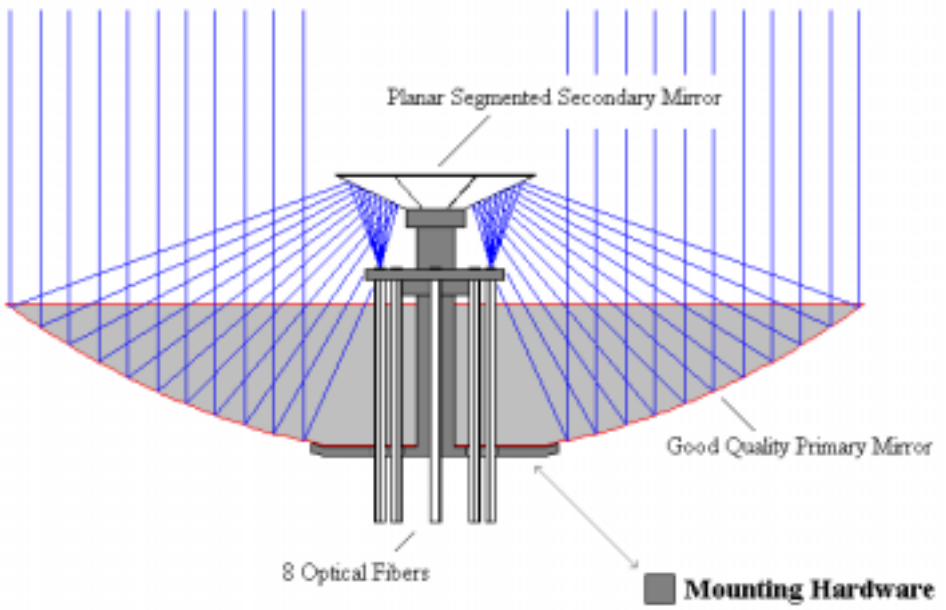

Figure 14. Current Solar Collector Design

As can be seen in Figure 14, the collimated sunlight is collected and focused using a large parabolic mirror, hereafter referred to as the primary mirror. The focused light is redirected toward the optical fibers through an 8-sided segmented-planar mirror, hereafter referred to as the secondary mirror. The chromatic performance of this optical system was modeled using ZEMAX ray-tracing software and its simulated performance is described below.

5.2 Primary Mirror

The primary mirror is a 46.5” diameter parabolic mirror with a focal length of 16.5”. The mirror was manufactured by ROC Glassworks and consists of a glass substrate prepared with a front-surface reflective coating. A 12” hole is bored in the center of the mirror to accommodate mounting for a secondary mirror and fiber optic holding apparatus. The exact dimensions of the finished primary mirror are shown in Figure 15:

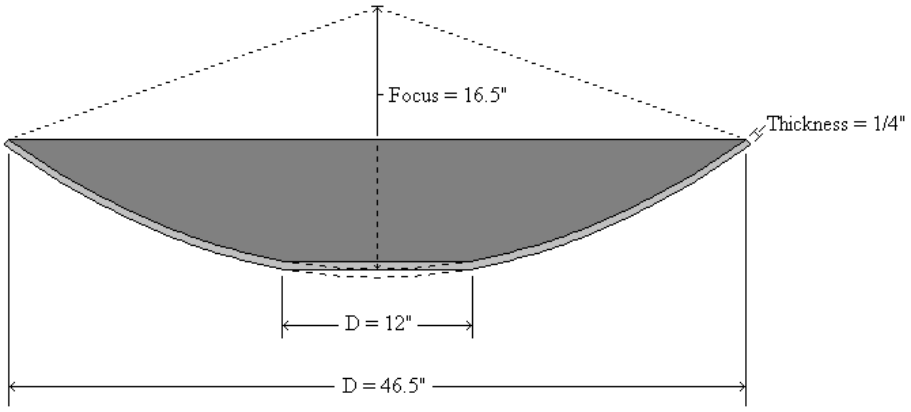

Figure 15. Dimensions of High Quality Parabolic Primary Mirror

The current specification of the primary mirror is based primarily on availability and cost, not on design optimization. Future optimization of the primary mirror design is anticipated.

The mirror was coated, by FLABEG Inc., with an enhanced aluminum coating. The coating provides high reflectivity across the visible spectrum and is a durable coating suitable for the environmental conditions expected. The spectral reflectivity characteristics of the coating are shown in Figure 16.

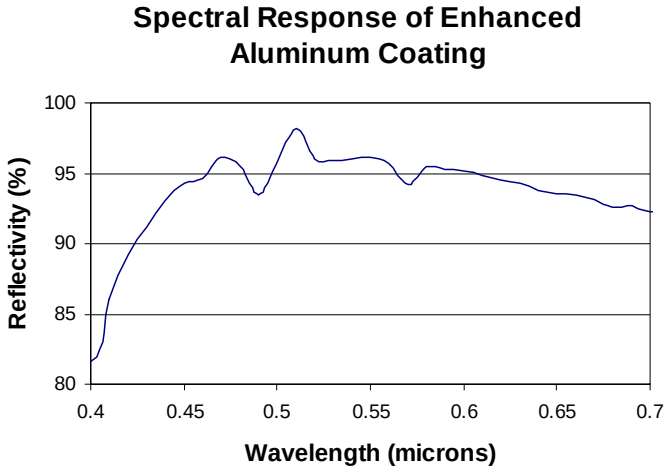

Figure 16. Reflectivity vs. Wavelength of Primary Mirror Coating

The finished primary mirror, with front-surface coating, is shown in Figure 17:

Figure 17. Finished Primary Mirror with Coating

To accurately simulate the chromatic performance of the Solar Collector design, it was first necessary to precisely determine the surface deviations present in the finished primary mirror, since these surface defects affect the angular distribution of the collected sunlight (which later affects the reflectivity of the secondary mirror). The surface of the primary mirror was mapped using the National Renewable Energy Laboratory's (NREL) VSHOT measurement system. The VSHOT measurement system measured the deviation of the primary mirror's surface slope from a true parabolic shape. A vector plot showing the measured residual error of multiple data point's slope relative to a true parabolic fit is shown in Figure 18:

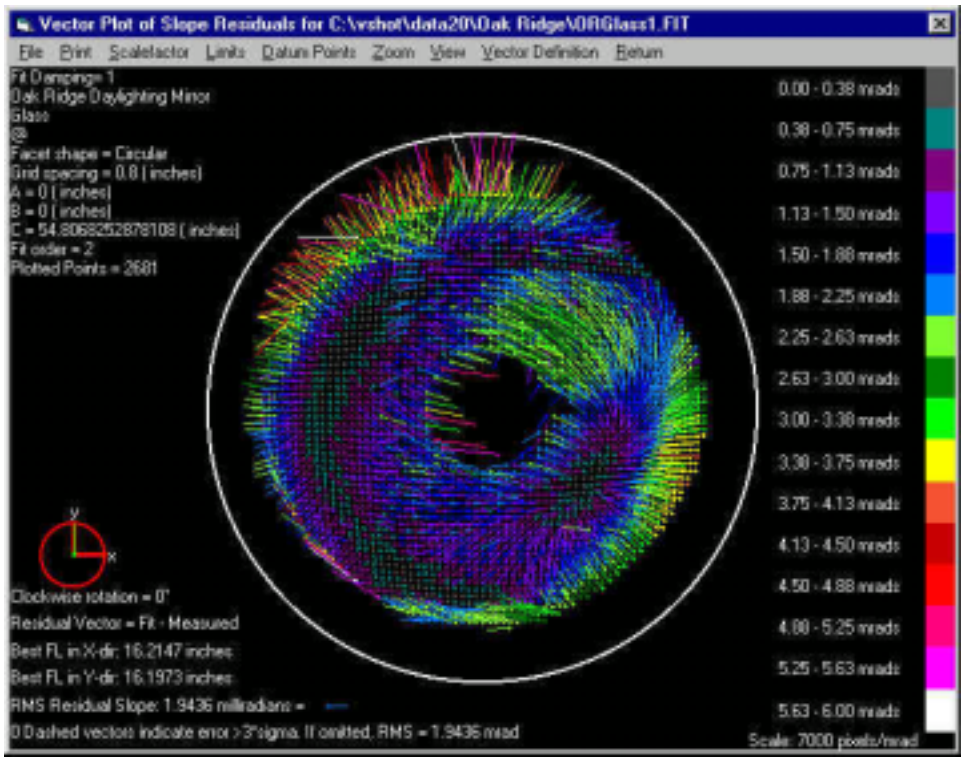

Figure 18. VSHOT Data Vector Plot of Surface Slope Deviations

The primary mirror's surface characterization data was input into SolTrace, an NREL developed Monte Carlo ray trace code, to predict the flux distribution at the focus of the primary mirror. The data was refit to an 8th order Zernike equation to minimize the residual slope error and obtain increased-accuracy flux predictions. The residual slope error in both cases was on the order of 0.5 milliradians. The focal spot flux distribution, predicted by SolTrace, was compared against the approximated surface deviation of a ZEMAX model to develop an accurate represent of the physically constructed primary mirror. This data, combined with the coating spectral response shown in Figure 16, fully described the chromatic contribution of the primary mirror

5.3 Secondary Mirror

Modeling the performance of the secondary mirror proved to be a more challenging effort. The purpose of the secondary mirror is two fold. First, the secondary must function to redirect focused light toward multiple large-core optical fibers and, second, it must separate out infrared light for photovoltaic conversion (which also helps to reduce unwanted heating effects in the polymer optical fibers).

To redirect the light focused by the previously described primary, a segmented planar secondary mirror was designed and is described in Figure 19.

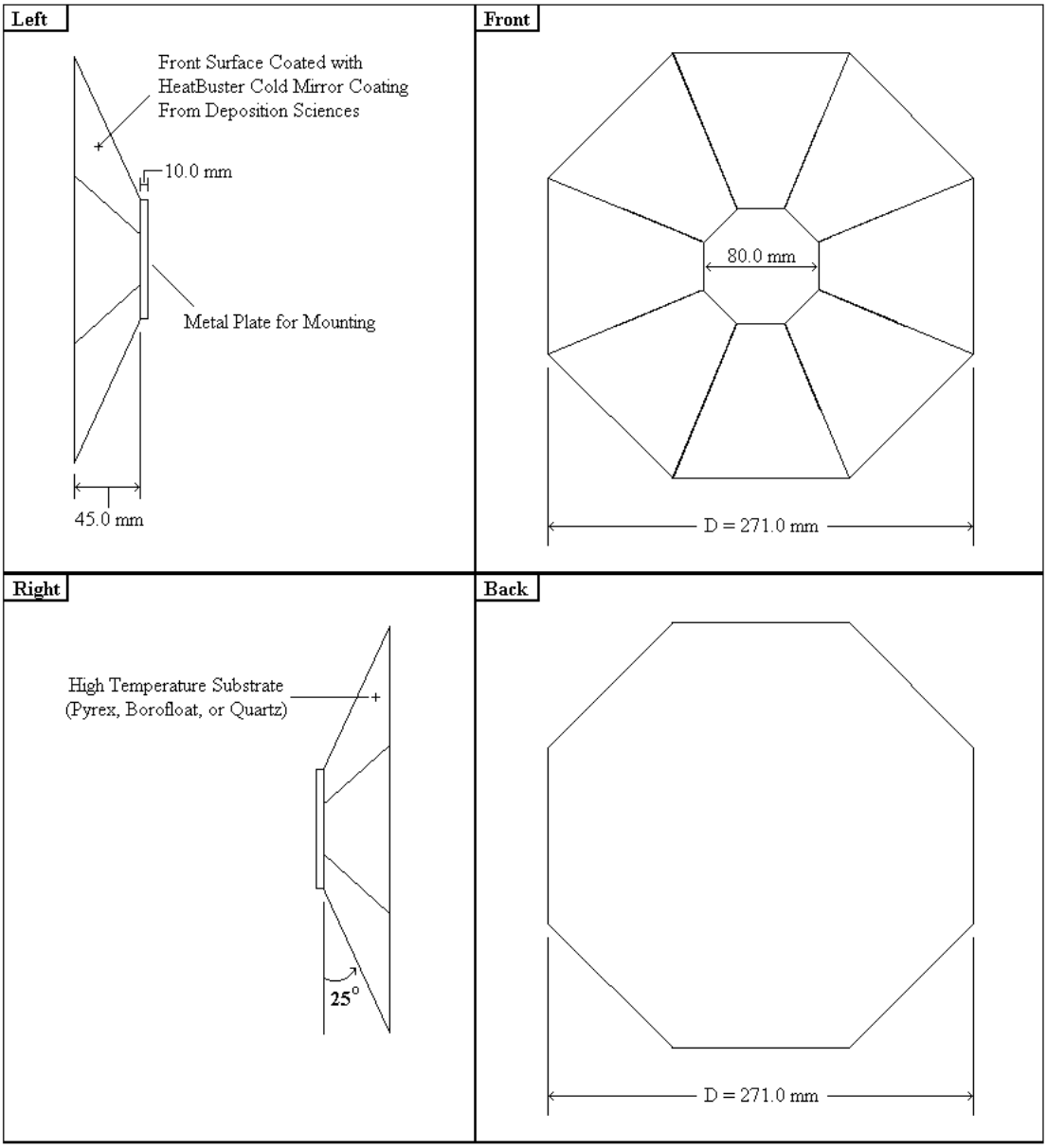

Figure 19. Segmented Planar Secondary Element for Current Solar Collector Design

The secondary mirror utilizes a cold mirror coating to separate the infrared from the visible portion of the spectrum. The HeatBuster® cold mirror coating, developed by Deposition Sciences Inc., is a typical cold mirror coating that reflects ultraviolet and visible light while transmitting IR. Applied using a MicroDyn sputtering technique, the coating can operate up to a maximum temperature of 500°C. It is anticipated that the secondary mirror, due to optical absorption in the mirror substrate, will need to operate at a temperature near 300°C.

The spectral reflectivity of the HeatBuster® cold mirror coating, at normal incidence, is shown in Figure 20:

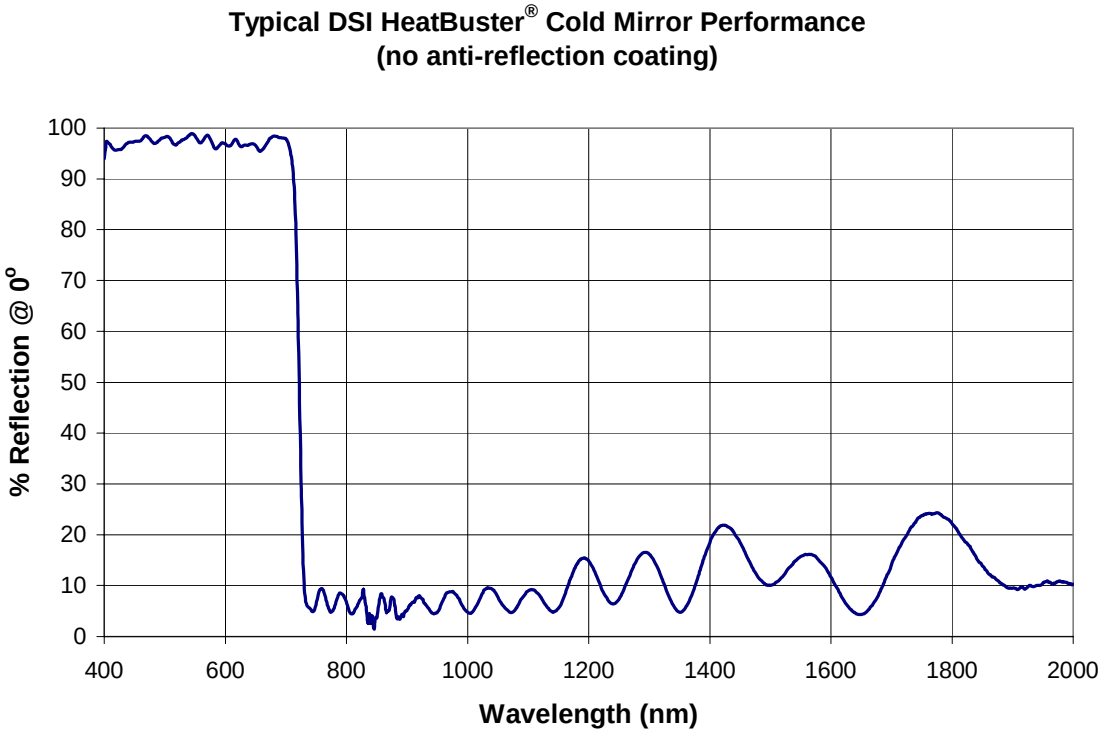

Figure 20. Reflectivity of HeatBuster® Cold Mirror Coating for Secondary Mirror

In addition to wavelength dependency, thin film cold mirror coatings exhibit a reflectivity that is also dependent upon incidence angle. The theoretical spectral shift with incidence angle for the HeatBuster® cold mirror coating is shown in Figure 21.

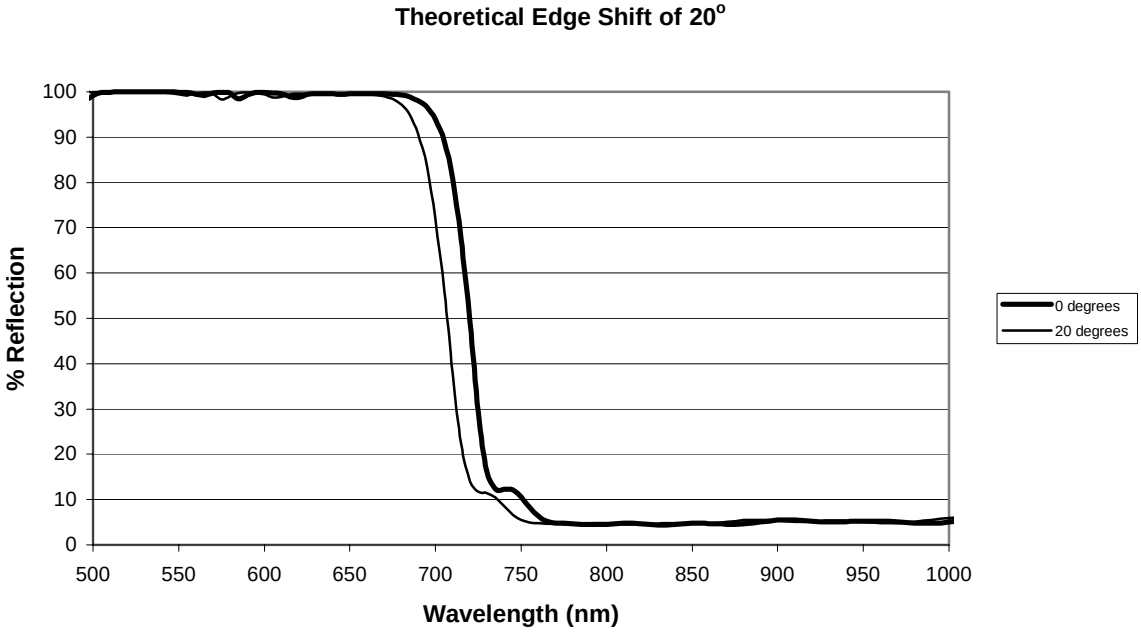

Figure 21. Dependency of Cold Mirror Coating's Reflectivity on Incidence Angle

Since the segmented planar secondary mirror is redirecting a focused beam, a variety of incidence angles (± 25°) are encountered at the surface of the secondary. Future optimizations of the Solar Collector design will be aimed at increasing the primary mirror's f/d, thereby reducing this large angular range.

Due to the cold-mirror coating's angular sensitivity, the reflectivity of the secondary mirror must be evaluated using ray-tracing analyses in combination with spectral reflectivity data. Given the coating data in Figures 20 and 21, and a ZEMAX ray-tracing model of the secondary mirror design illustrated in Figure 19, the chromatic performance of the secondary mirror could be fully described and tested.

5.4 Results of Full Solar Collector Design Simulation

Using the coating data previously presented for the primary and secondary mirror, and the final design configuration of the system (Figure 14), an analysis was performed using ZEMAX ray-tracing software to determine the chromatic performance of the full collector design. The resulting combined effect of the primary mirror and secondary mirror coatings can be summarized as a filter with the transmission spectrum shown in Figure 22.

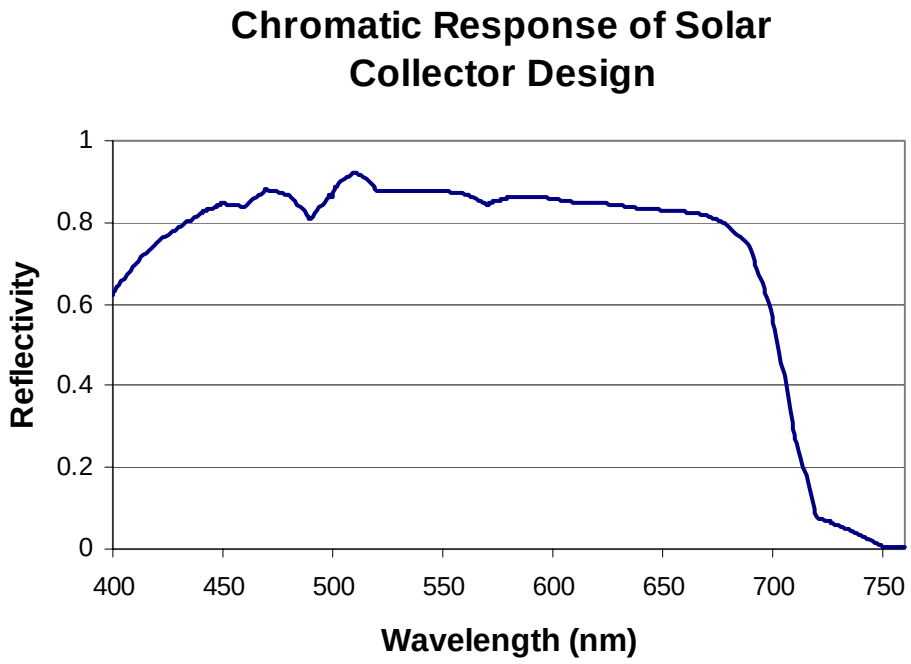

Figure 22. Combined "Filtering" Effect of Primary and Secondary Mirror Coatings

The result this "filter" has on the color of the collected sunlight is shown in Figure 23, which shows the chromatic variation of collected sunlight over a one-year period in Topeka, KA.

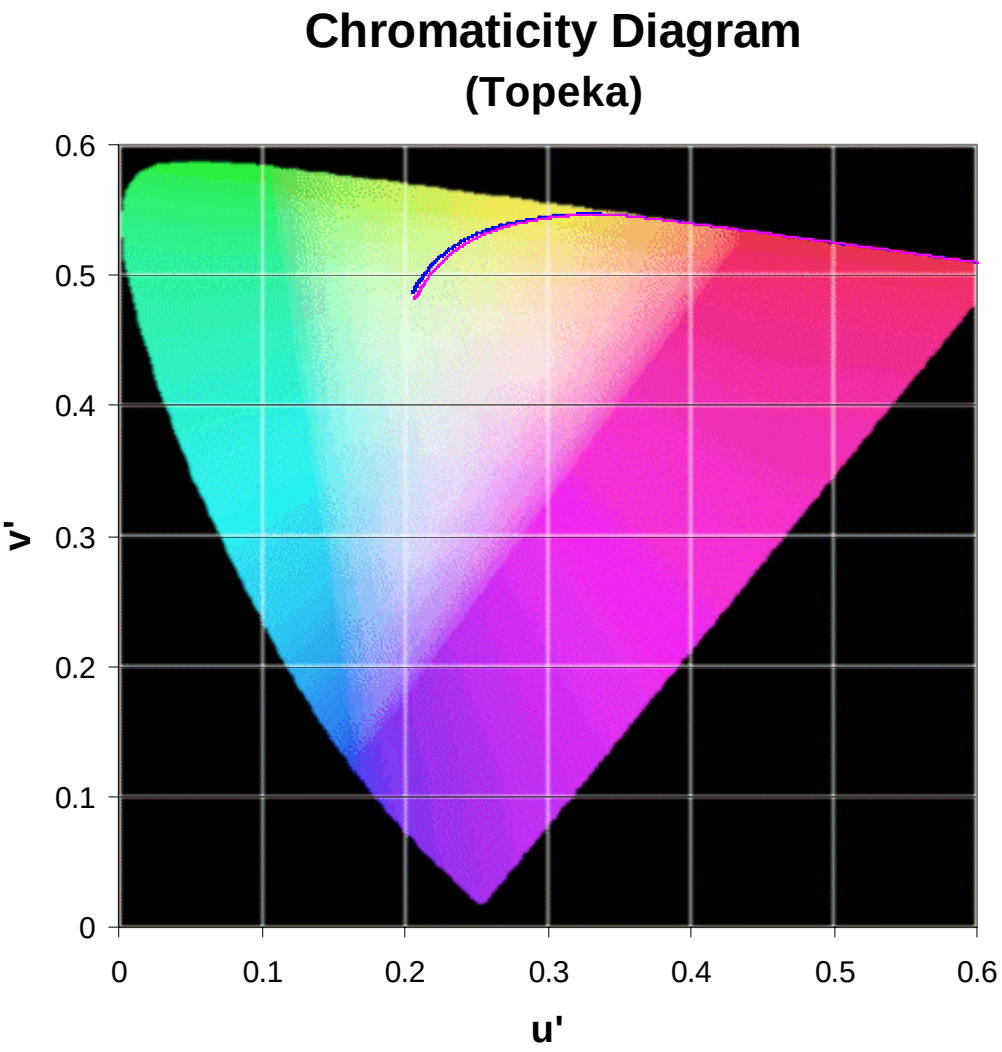

Figure 23. Chromatic Shift Resulting From Collector Optics

Figure 23 shows both the sunlight *before* collection (lower curve) and the sunlight *after* collection. Two important observations can be made from the data graphed in Figure 23. First, the full ***range*** of the data (total chromatic fluctuation) is unmodified by the collector optics. The collector neither improves nor worsens the extent over which the sunlight/collected light fluctuates. Secondly, only a small color shift toward the green portion of the spectrum is observed due to the collector optics. Although future modifications to the collector design warrant a re-evaluation of its chromatic performance, it is expected that small changes to the collector design will have only minimal effects on the final color value of the collected sunlight.

Given the physical configuration of the primary and secondary mirror, it is prudent at this time to evaluate another critical design parameter associated with the design of the collector optics. The collector design, shown in Figure 14, produces eight equivalent-intensity images of the sun at a distance of 60 mm from the end of the secondary. The

relative placement of these multiple images, in the plane of the optical fibers, is shown in Figure 24.

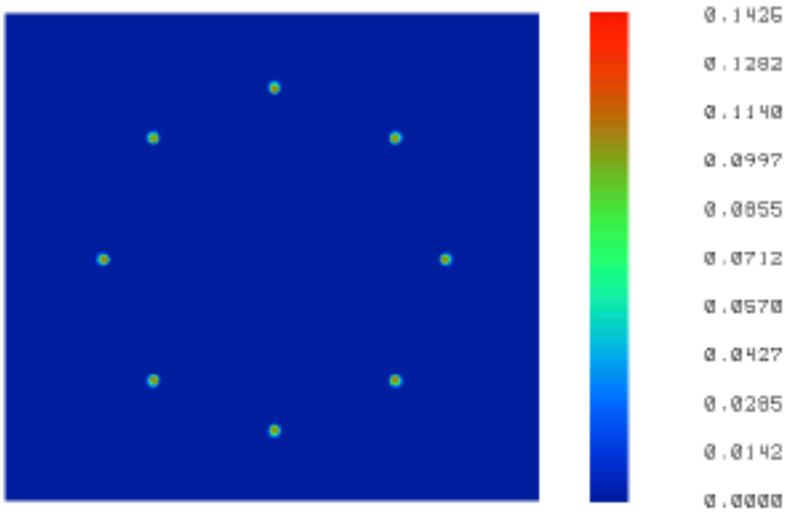

Figure 24. Footprint of Focused Light on Optical Fiber Plane (Image Width ≈ 200 mm)

Each of the eight individually focused images is launched into a single optical fiber. The footprint of the focused image at the fiber face is shown in Figure 25:

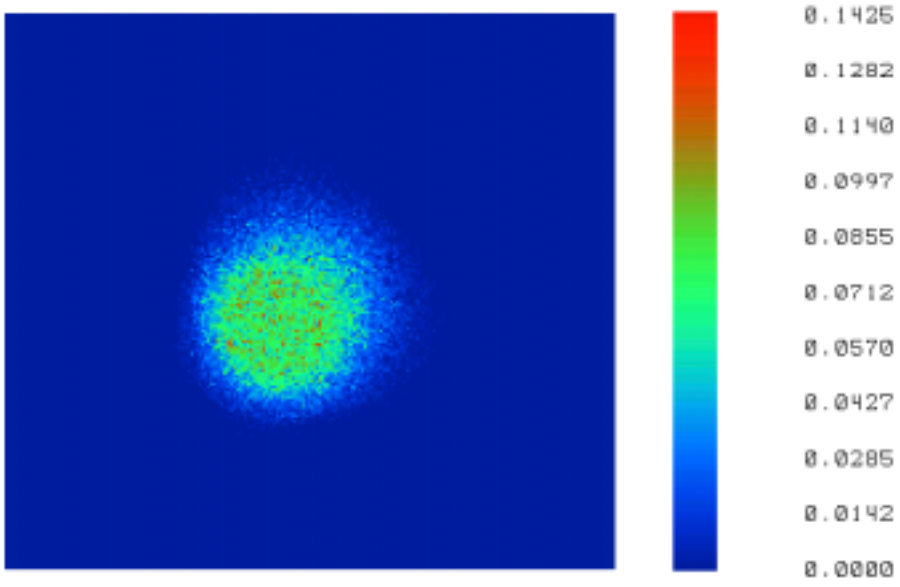

Figure 25. Image of Sun on Optical Fiber Face (Image Width = 20 mm)

The focused image results in light being launched into the fiber at slightly varying angles. As was shown in Figure 6, the launch angle affects the amount of absorption exhibited by the large-core optical fiber. Therefore, the distribution of launch angles at the fiber face is an important parameter in modeling the final absorption characteristics of the optical

fiber. Figure 26 shows the distribution of launch angles at one optical fiber face (the top image spot in Figure 24). The data is expressed in x-y Cartesian coordinates.

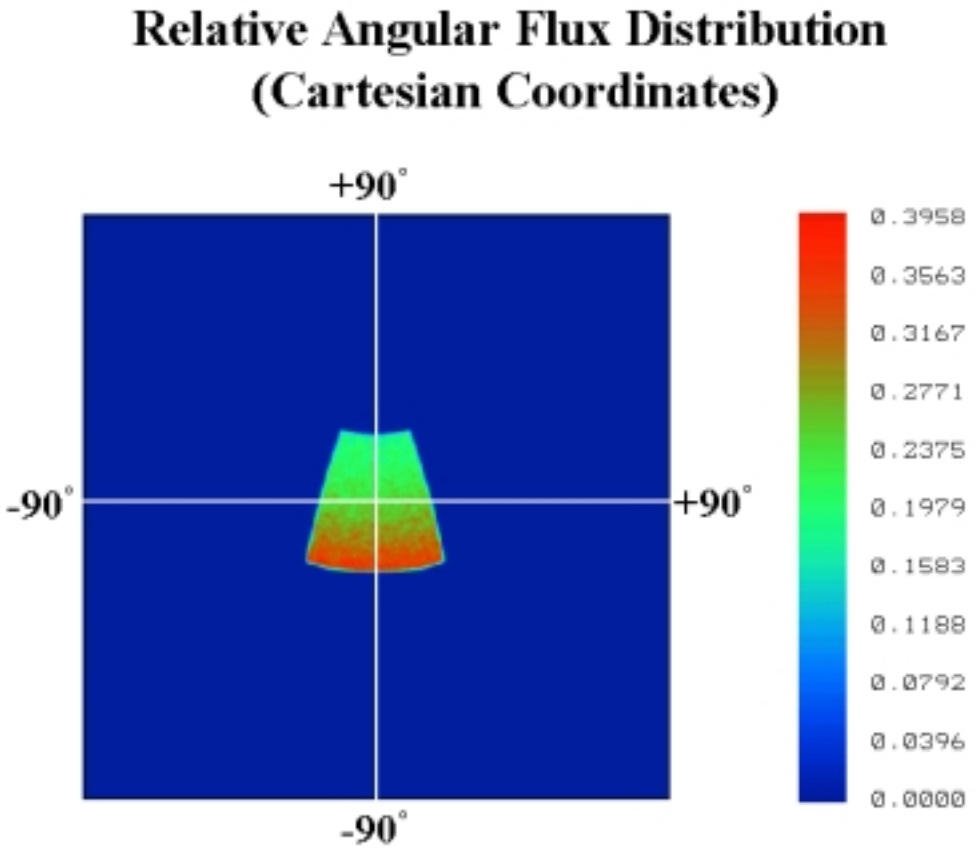

Figure 26. Angular Distribution of Rays Launched into Optical Fiber

From this data, it is evident that a significant portion of the collected light is launched into the optical fiber at an angle of approximately -15°. Figure 27 re-represents the data as the total flux within a symmetric angular "band":

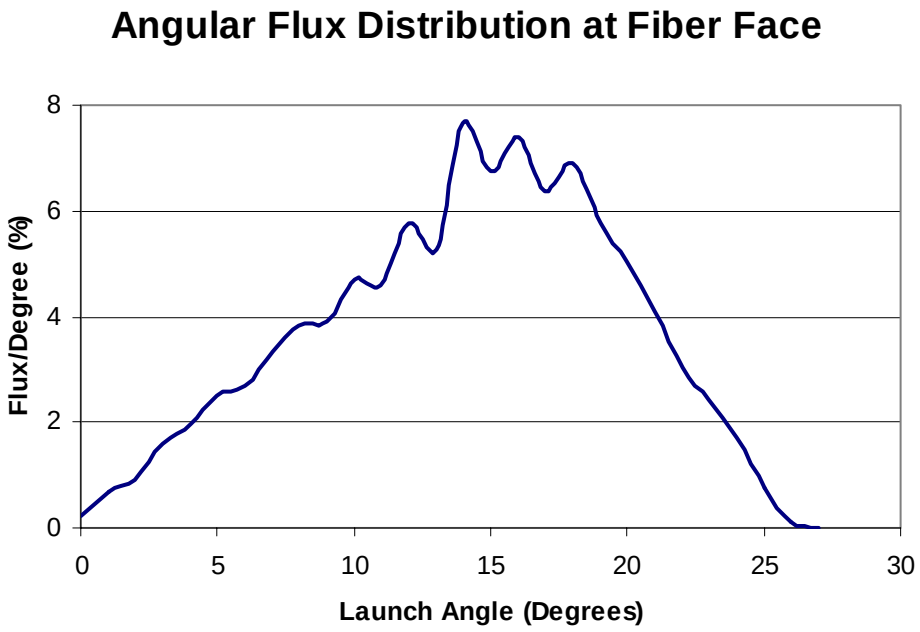

Figure 27. Symmetric Angular Flux Distribution of Rays Launched into Optical Fiber

And this data can be further broken down into larger discrete angular bands (bandwidth = 5°), which is more useful for modeling purposes (see Table 2).

Table 2. Discrete Angular Flux Distribution

Angular Range	Percent Flux (%)
0 to 5 degrees	6
5 to 10 degrees	16
10 to 15 degrees	28
15 to 20 degrees	33
20 to 25 degrees	16
25 to 30 degrees	1
30 to 90 degrees	0

From this data, we can note that the collector design, with it's non-optimized primary mirror, creates a large number of high-angle launch rays. Therefore, increased absorption within the optical fibers is expected. The launch conditions shown in Table 2 will be used in the following section to estimate the chromatic effects of this increase in fiber optic absorption.

6.0 Evaluation of Chromaticity Variation Due to Fiber Optic Transport

Light collected with the Hybrid Lighting System's Solar Collector must be distributed to Hybrid Luminaires through large-core optical fibers. As already discussed, these optical fibers have a transmission value that is dependent upon wavelength and launch angle. This transmission curve acts as a filter that further modifies the previously collected sunlight.

To estimate the color-shift associated with fiber optic transport, calculations were made using the spectrums of solar data after passing through the collector. Custom-written software, described and verified in Section 3, was used to calculate the u'-v' values of light emitted from various lengths of optical fiber. For most system configurations, past design studies have indicated that an optical fiber length of six to ten meters will be optimal for light distribution. Therefore, the chromaticity values of light resulting from collection by the solar collector and transported through 6 meters of fiber and 10 meters of fiber were calculated and are shown in Figure 28 and 29.

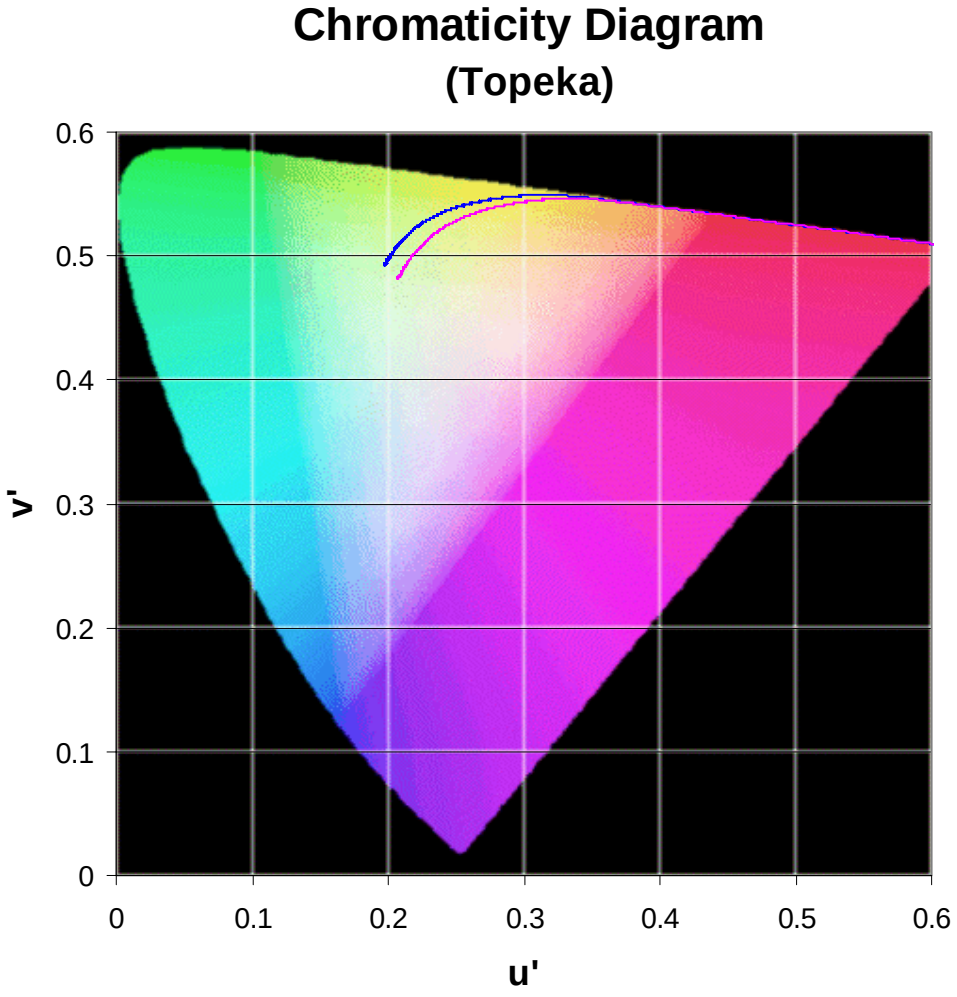

Figure 28. Color-Shift Resulting from 6-Meters of Fiber Optic Transport

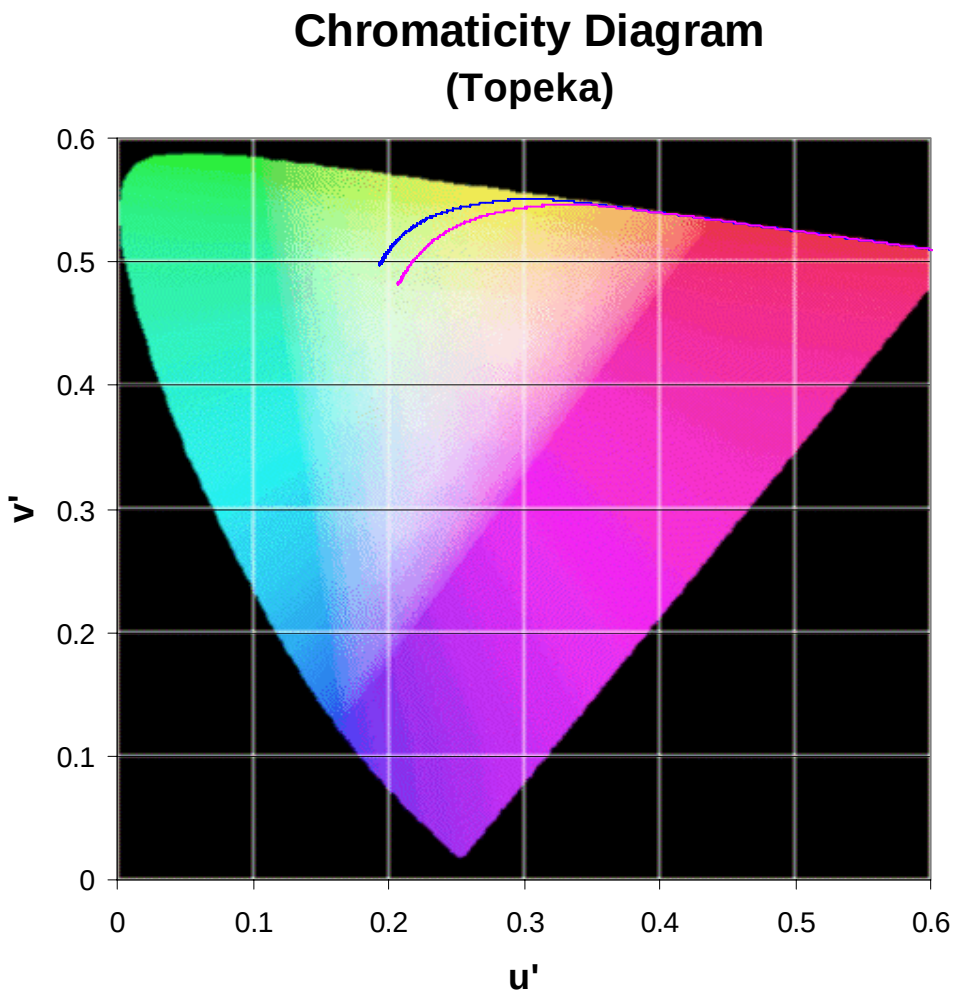

Figure 29. Color-Shift Resulting from 10-Meters of Fiber Optic Transport

As before, Figures 28 and 29 show both the sunlight *before* collection (lower curve) and the sunlight *after* collection and transmission through the optical fiber (upper curve). The chromatic shift is significant in both cases and a noticeable shift toward the green portion of the spectrum can be easily observed.

7.0 Final System Performance

7.1 Final System Specifications: Average Color Value and Color Deviation

The final chromatic performance of the complete Hybrid Lighting System is summarized in Figure 30.

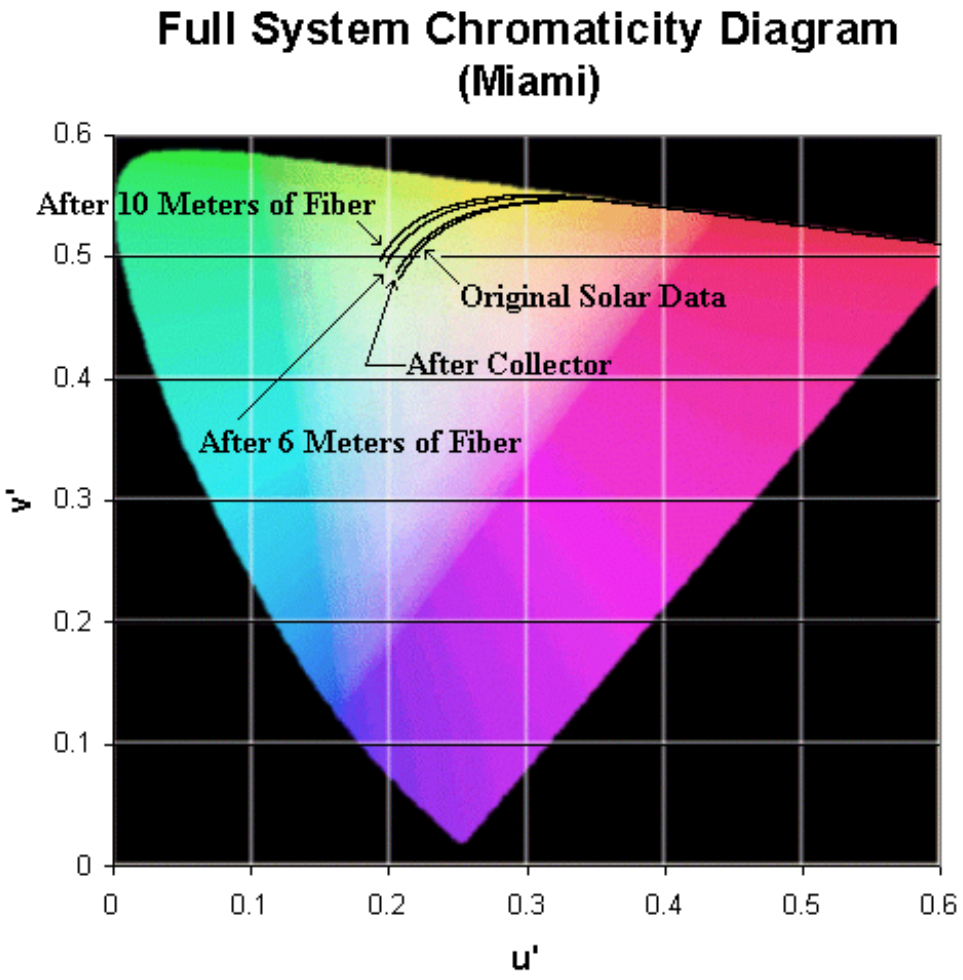

Figure 30. Summary of Hybrid Lighting System's Chromatic Performance

As was stated earlier in Section 4.0, the large color range exhibited by the full operation system is highly undesirable. To reduce fluctuations in collected/distributed sunlight, a "reduced operation" system is preferred. Figure 31 illustrates the color range associated with a 1-hour "reduced operation" system (starts 1 hours after sunrise, ends 1 hour before sunset).

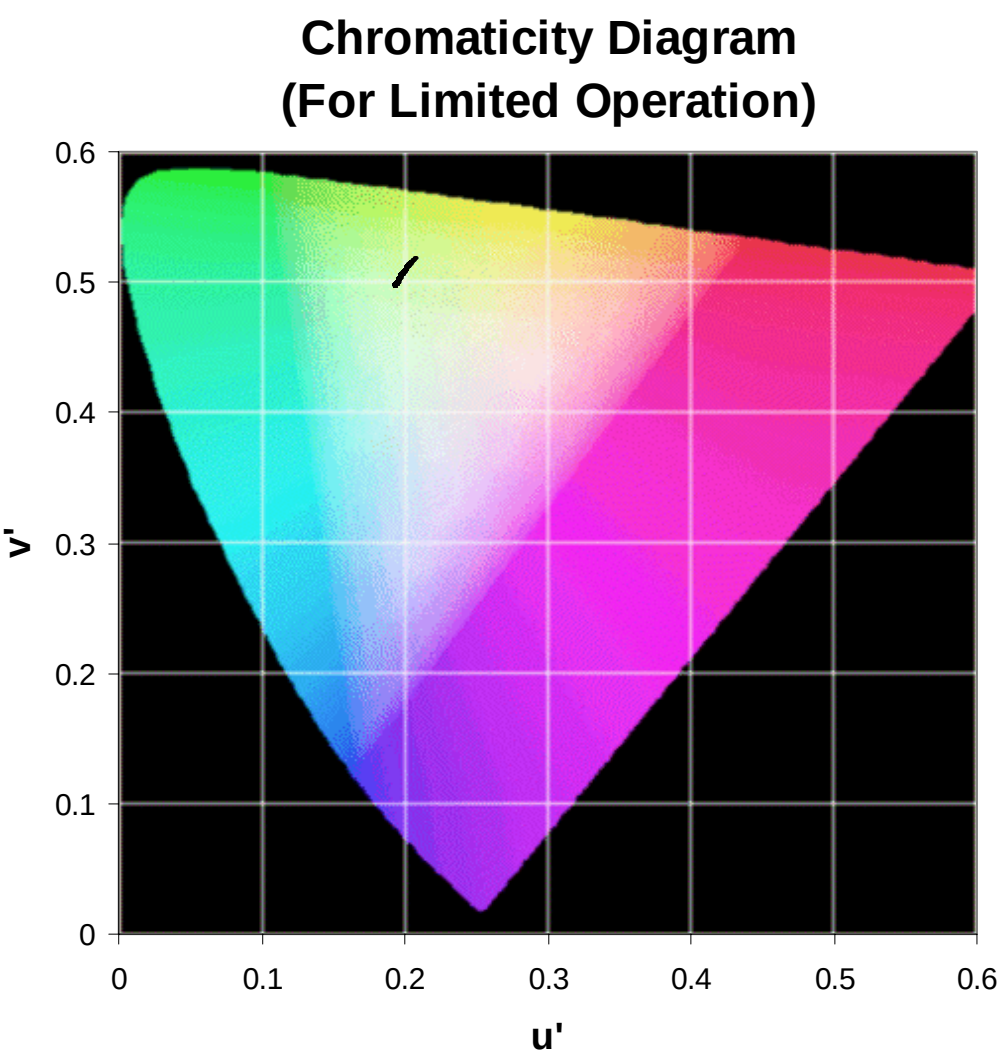

Figure 31. Chromatic Variations in 1-Hour "Reduced Operation" Hybrid Lighting System

Such a system has a noticeably smaller color range compared with Figure 30, and from the data presented in Figure 13, we can estimate that only 10% of the available sunlight is being lost due to system inactivity. The mean color of the 1-hour "reduced operation" system's collected and distributed light is:

Mean Chromaticity (u', v') = (.195838, .501733).

Unfortunately, even with the reduced operating time, the range of colors exhibited by the system will still be noticeable to an occupant. Figure 32 shows the range of colors experienced with a 2-hour reduced operation system. The color range is further reduced but only 80% of the total available sunlight is now being collected. The figure superimposes a 1-step MacAdam ellipse (charted in u'-v' space) around the mean chromaticity point to provide a measure of color discrimination. All colors lying within the 1-step MacAdam ellipse would be perceived as identical colors by an occupant.

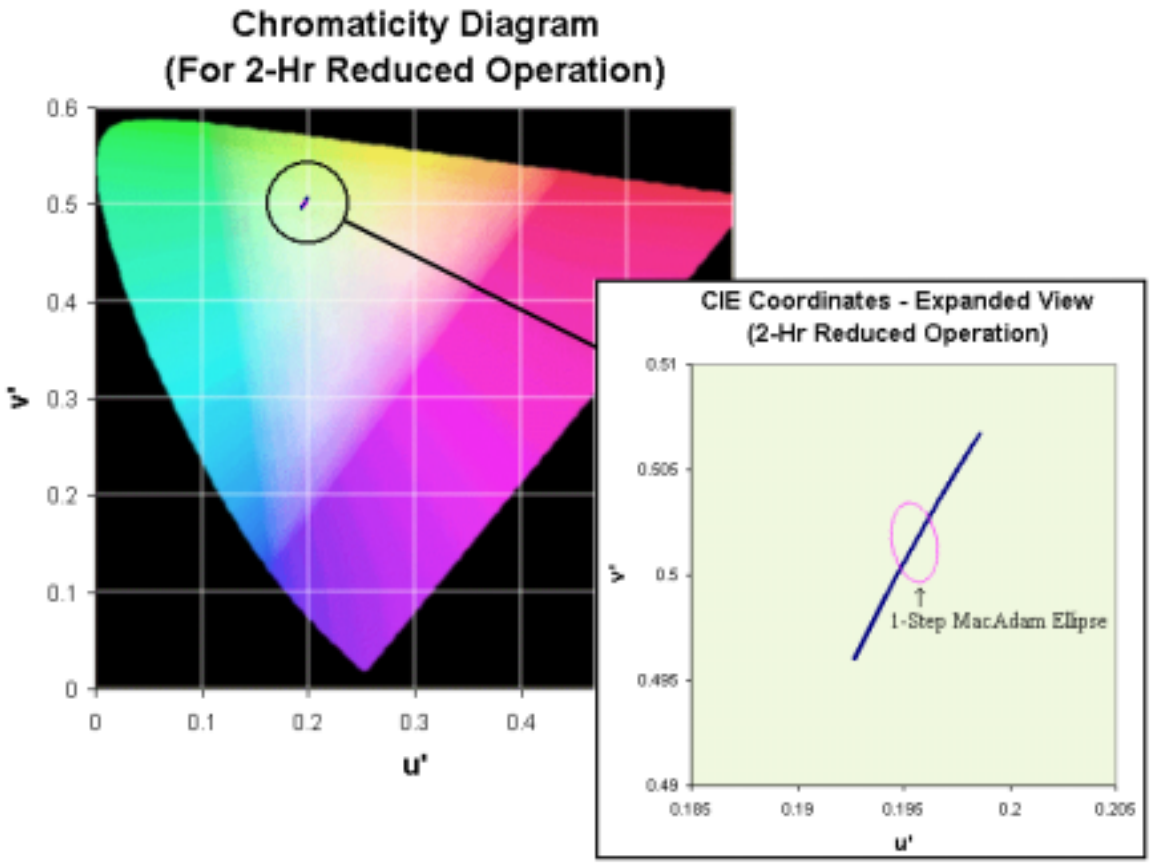

Figure 32. Chromatic Variations with 1-Step MacAdam Ellipse

From Figure 32, we can see that the color variations in a 2-hour "reduced operations" Hybrid Lighting System will still exceed the limits on perceivable color difference. These color differences represent the full range of colors that would be experienced in one solar year.

7.2 Comparison to Electric Illuminants

When compared with currently available electric illuminants, the collected and distributed sunlight is close to several potential sources (see Figure 33).

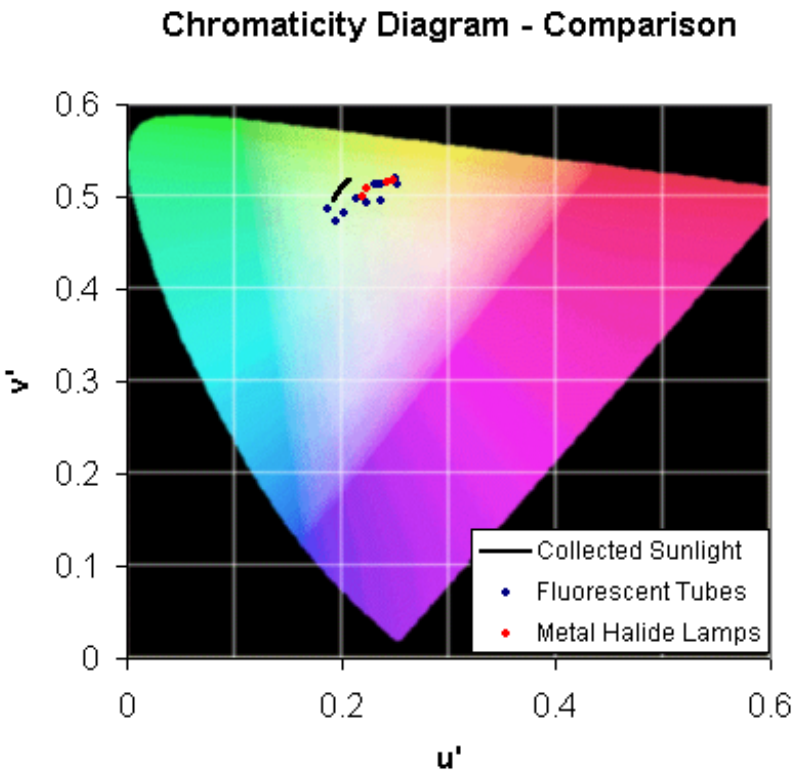

Figure 33. Comparison of Collected and Distribution Sunlight To Ellectric Illuminants

Figure 33 compares the color of collected sunlight, after being transported through ten meters of optical fiber, with several commercially available metal-halide lamps and fluorescent tubes (ranging from 3000°K - 6500°K). Numerous electric illuminants exist on today's market and Figure 33 represents only several of the most popular illuminants.

7.3 Design of a Chromatic "Compensating" Filter

To improve the color matching between collected/distributed sunlight and a selected electric illuminant, a color filter can be used to alter the center location of the chromatic range shown in Figure 33. A thin-film chromatic filter can be designed to produce nearly any final desired mean color. The thin-film filter would be applied as a custom coating to the Solar Collector's primary mirror, allowing the color of the collected/distributed sunlight to more accurately match that of an electric illuminant.

From the chromaticity diagrams of Figures 30-32, it is estimated that a "compensating" filter that slightly reduced the amount of green light present in the collected sunlight would be advantageous. Construction of such a filter would not reduce color deviation but it would allow the collected sunlight curve of Figure 31 to be shifted to a more agreeable location on the CIE color diagram.

Design of the chromatic "compensating" filter is challenging because many variables affect its design and performance. Because of this multi-variable, multi-local optimum

problem, the solution is best obtained using an evolutionary algorithm approach that efficiently searches for a global optimum. Research is currently underway to develop a chromatic "compensating" filter that provides the optimal filter design for matching to a desired electric illuminant. The optimum filter design would provide maximum optical collection and minimal color deviation between distributed sunlight and electric illuminant.

APPENDIX J

Daylighting and Productivity
A Literature Review

Submitted by:

Charles Fay
Lighting Research Center
Rensselaer Polytechnic Institute

Reviewed by:

Mark S. Rea, Ph.D.
Mariana Figueiro, MSc
Lighting Research Center
Rensselaer Polytechnic Institute

Submitted to:

ADAPTIVE FULL-SPECTRUM SOLAR ENERGY SYSTEMS

Cross-Cutting R&D on adaptive full-spectrum solar energy systems for more efficient and affordable use of solar energy in buildings and hybrid photo-bioreactors.

Project Sponsor: US Department of Energy

August 1, 2002

Daylight and Productivity – A Literature Review

INTRODUCTION

In 1997, Norris and Tillet wrote, in their review of the literature:
People believe, and research generally supports, that daylight does not help their productivity. People strongly believe, and research generally does not support, that daylight is a better, healthier workplace light source than electric light. Research confirms that people overwhelmingly prefer windows. What they like best about windows is the view, particularly if it contains nature. (p. 213)

This review, written five years later, reports similar findings, which were generally reported in 1966 by R.G. Hopkinson (Hopkinson et al. 1966).

To date, very few studies have focused directly on daylighting and productivity, and none of these studies has established a causal relationship between daylighting and productivity. A study conducted in 1999 by the Heschong Mahone Group (p. 57) stated, " We have merely shown an association between the presence of daylight and higher student performance, not shown that daylighting causes students to learn more." The group has been lionized by various organizations, including the U.S. Department of Education[1]. Their study is widely cited as conclusive evidence that daylighting affects productivity directly.

No studies to date have demonstrated a causal relationship between daylighting and productivity, but this does not mean a mechanism does not exist. Light is not restricted to vision in its ability to affect people. There are three routes through which light (including daylight) might affect productivity[2]: the visual system, the circadian photobiological system, and the perceptual system.

The visual and the circadian photobiological systems are essentially discrete systems, each with its' own unique set of physiological processes[3]. Each system is essentially consistent, with normal variation, in its functioning among the human population. This consistent functioning allows for direct investigation of the underlying mechanisms of these systems.

We have a good understanding of how light affects the visual system. Quantitative models have been developed allowing the prediction of lighting conditions on visual performance. Since there is no evidence that daylight is inherently[4] different from electric light in its effect on the visual system (McColl and Veitch, 2001; Rea, et al., 2002), we can use these models to reliably predict daylight's impact on visual performance.

---

[1] Specifically through the National Clearinghouse for Educational Facilities (NCEF), which provides information about K-12 school planning, design, financing, construction, operations and maintenance.
[2] More precisely, individual performance.
[3] The visual system and circadian system respond differently to the fundamental characteristics of light: quantity, spectrum, spatial distribution, timing and duration; each system has its own unique biophysical responses to these characteristics.
[4] While daylight differs from electric light commonly used in offices, technology allows for electric light to mimic daylight.

While our knowledge of the visual system is fairly complete, our understanding of the circadian system is in its infancy. We know that light is the primary stimulus for synchronizing the daily rhythm of the system to its surroundings and that the sensitivity of the system changes over the course of the day. We also know that light must actually enter the eye for it to be effective, and that the quantity of light required for proper functioning of the circadian system is much greater than the quantity of light required by the visual system. Whereas daylight offers nothing unique to the circadian system, it may offer an efficient means of maintaining circadian rhythmicity in the built environment (offices, factories, etc.). This is especially likely during the winter months when availability to daylight is limited on the commute to and from work.

Unlike the other two systems, the perceptual system is not simply a function of certain physiological events. It is inherently complex and unique to each individual in a population. The perceptual system, being idiosyncratic to individual experience, temperament, education, etc., responds to many variables in many combinations. It does not readily lend itself to scientific investigation, except in the most general sense. This means that the interpretations of lighting installations are unique to each individual in a population. This individuality makes a systematic study of daylighting's effect on productivity via the perceptual system quixotic; at the end of the research day, we will likely be no further in our conclusions of the relationship between daylighting and productivity than we were in the 1960's.

There is nothing magical about daylight. The distinct requirements of the visual system and the circadian system can be served by electric lighting through proper specification of the characteristics of that light (quantity, spectrum, spatial distribution, timing and duration). Daylight can, however, provide a practical source of light able to serve both the visual and circadian system in a highly efficient manner.

This is a complex issue. Therefore, before examining studies dealing specifically with daylighting and productivity, we will investigate the topics of 1) **How we light** – the various sources used to light an interior office space, 2) **Productivity** – contemporary thoughts, and 3) **Why we light** – the various ways visible light can affect people.

LITERATURE REVIEW

Background: How do we light?

There are two ways to light an indoor space during the day: through electric lighting and/or through daylighting.

Electric Lighting

Electric light sources are categorized into three broad classes: incandescent, low intensity discharge, and high intensity discharge. LEDs are not included because they are not yet a suitable technology.

Incandescent light sources produce light by heating a filament, with the light spectrum determined by the filament temperature. Discharge light sources produce light by passing an electric current through an ionized gas, with the light spectrum determined by the type of gas, the gas pressure, the other elements in the discharge, and the presence or absence of a phosphor coating. Incandescent lamps have a continuous spectrum in the visible region that is dominated by the long wavelengths. Discharge lamps (such as fluorescent) typically have a spectrum consisting of strong single wavelengths amid a continuous background (IESNA, 2000).

One category of fluorescent lamps is specially designed to simulate daylight. These are the so-called full-spectrum fluorescent lamps (FSFL). FSFLs have been compared to daylight, based on their high correlated color temperature (CCT), the high CIE General Color Rendering Index (CRI), and the deliberate inclusion of an element of near ultra-violet (UV) radiation in the spectral emission (McColl and Veitch, 2001). The CCT specifies the apparent color of light emitted by the lamp—the higher the CCT, the cooler (or more blue) the apparent color of the light. The CRI quantifies the ability of the lamp to render colors as well as a standard lamp with the same color temperature or CCT.

Boyce defines FSFL as having "spectral emissions in all parts of the visible spectrum and some emission in the ultra-violet, mainly the near ultra-violet" (Boyce, 1994, p. 30). Since several other kinds of fluorescent lamps have similar spectrums, it is only the UV component that distinguishes a FSFL from any other fluorescent lamp (Boyce, 1994). It should be noted that UV does not directly stimulate the retina; radiation below a wavelength of 380 nanometers is absorbed by the cornea and lens of the eye.

Daylighting

As *sunlight* passes through the atmosphere, a portion is scattered[5] by dust, water vapor, and other suspended particles. This scattering, acting in concert with clouds, produces *skylight*. Sunlight that directly enters an office space is a potential problem, and usually elicits the use of

[5]There are two types of scattering: Rayleigh scattering and Mie scattering. Rayleigh is strongly wavelength dependent and produces the 'blue' sky, which is why daylight has a high CCT; Mie is not strongly wavelength dependent and is commonly seen as a white 'haze' around the sun.

window blinds (Rea, 1998). Daylight is light entering in a more indirect manner, and is produced by a combination of skylight and sunlight reflected from the ground as well as surrounding buildings. "Physically, daylight is simply electromagnetic radiation in the wavelength range that is absorbed by the photoreceptors of the human eye. In this respect it is the same as all other light sources" (Boyce, 1998, p.360). However, electric light sources produce a fairly stable spectrum, whereas daylight's spectrum varies throughout the day and the season, depending on the latitude of the location, the elevation of the sun in the sky, and the amount of water vapor/cloud cover in the atmosphere. Daylight varies in CCT from 5000 to 10,000 Kelvin (K) (Thorington, 1985). See Figure 1.

The quantity of light is perhaps a more important key to distinguishing daylighting from electric lighting. Electric light levels in today's offices range from 300-500 lx on the workplane. Outside, daylight is on the order of 2000-100,000 lx. Inside, daylighting near a window can deliver over 2000 lx on the workplane, depending on the atmospheric conditions. (Rea, et al., 2002). It should be noted that the two means of delivering daylight into an interior space, skylights and windows, are quite different in the way they can potentially affect people. A skylight provides illumination alone, while a window provides a view, as well as illumination.

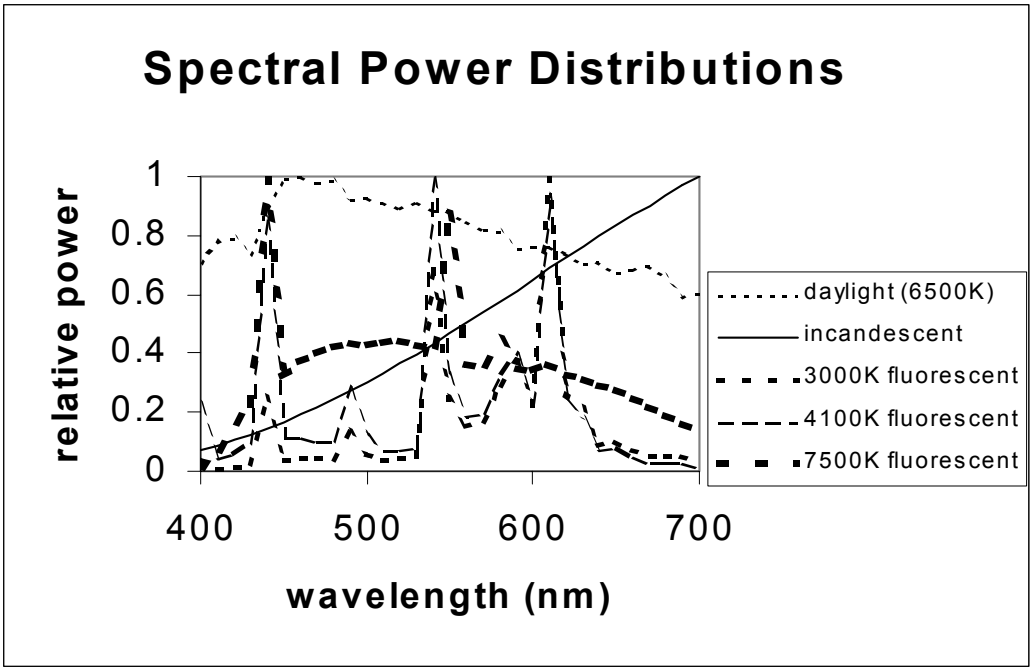

Figure 1 - Spectral power distributions of several light sources: daylight, incandescent lamps, and rare earth phosphor fluorescent lamps. [Figure courtesy of Rea et al. (2002)].

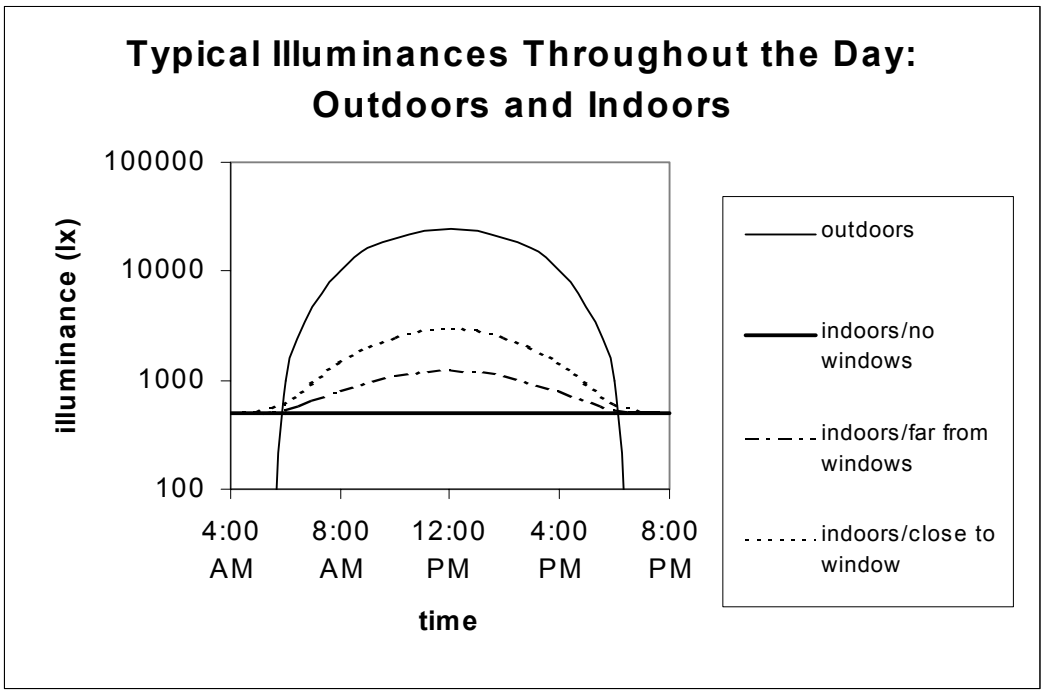

Figure 2 - Typical illuminances experienced outdoors in open country, indoors in a windowless space, and indoor spaces approximately 3 meters from windows (daylight factor 3%) and immediately adjacent to windows (daylight factor 10%). Daylight is assumed from a partly cloudy sky with no direct sunlight. [Figure courtesy of Rea et al. (2002)].

What is Productivity? Does environment affect Productivity?

The question of productivity is an extremely complicated issue. It is therefore helpful to look at what contemporary thought on this topic reveals. Productivity is not simply the number of widgets produced per unit of time or cost. As the unit of work becomes more information and service based, productivity becomes increasingly difficult to measure (Aronoff and Kaplan, 1995; Ferguson, 2000).

According to Aronoff and Kaplan (1995),
…there simply may be no way to measure whether separate changes in equipment, tools, management style, or physical office setting have improved the productivity of an individual or a work group. …difficulties in objectively quantifying change are not proof of its absence. Organizations support training and education programs, counseling services, substance abuse rehabilitation programs, and other employee benefits with the expectation that worker performance will be enhanced even though such gains are not readily quantified.

On an organizational level, productivity measures have expanded beyond the industrial input/output model to include innovation, quality of products and services, efficiency of resource use, and customer satisfaction. In addition, many organizations track a number of indirect measures of overall productivity, such as quality of work life, absenteeism, health care

costs, ability to attract high quality workers, and turnover (Aronoff and Kaplan, 1995; Hedge, 2000).

On an individual level, "a person's work environment directly affects the quality and quantity of work they are able to produce" (Aronoff and Kaplan, 1995). The fields of organizational psychology and environmental psychology have found that physical environmental factors, such as lighting, temperature, ventilation, and workspace design, can influence employee attitudes and behavior significantly.

Individual performance is widely viewed as a function of two factors: ability and motivation. Ability deals with whether a person can perform a task, while motivation is a measure of whether a person wants to do it. We cannot accurately predict a lighting installation's capacity to motivate an individual. We can, however, make reliable predictions of how lighting installations will affect visual ability. In addition, the disruption of circadian rhythmicity has the potential of producing harmful effects on ability and performance. Research has begun to reveal how light is able to maintain circadian rhythmicity, and thereby promote the potential for high productivity.

Why do we light? How does lighting affect performance?

The answer to this first question initially seems simple: we light to see. However, research into the circadian photobiological system, and its potential role in our everyday functioning, indicates the answer to the second question may not be so simple.

Boyce and Rea (2001) define three routes through which visible light can affect people: the visual system, the circadian photobiological system, and the perceptual system. How can each of these routes affect an individual's performance? A few select quotes from their report on Lighting and Human Performance help to explain these various routes.

Visual System

The visual system is devoted to detecting differences in the visual environment. These differences can occur in both brightness and color, and can vary over both time and space. It is the interaction between the object to be seen, the background against which it is seen and the lighting of both object and background that determine the stimuli for the visual system and its operating state. The aspects of lighting likely to be important for visual performance are the amount of light, the spectrum of the light and the distribution of the light on and around the object. (p.2-1)

It should be noted that visual performance and task performance are not necessarily the same. Task performance is the performance of the complete task. Visual performance is the performance of the visual component of the task. Task performance is needed in order to measure productivity and to establish cost/benefit ratios for determining the effectiveness of

providing a lighting installation. However, visual performance is the only component of task performance that can be directly affected by changing the lighting conditions. (p.2-3)

How changes in the amount of light, the spectral content of light and the distribution of light alter either the stimuli a specific task presents to the visual system or the operating state of the visual system are well understood (Boyce, 1994); the effects of these changes on the performance of the visual component of a task can be predicted through models of visual performance (Boyce and Rea, 2001).

Circadian system

Another means whereby lighting conditions can affect work is through the circadian photobiological system. The most obvious evidence for a circadian system in humans is the existence of the sleep / wake cycle, but this cycle represents only a small part of the activity of the circadian system. Variations in many different hormonal rhythms occur over a 24-hour period. The aspects of lighting that influence the circadian system are[6]: light spectrum and illumination reaching the retina, which in turn depend on the light spectrum of the light source used, the light distribution, the spectral reflectances of the surfaces in the space, the spectral transmittance of the optic media and where the observer is looking. Light operating through the circadian system can alter human performance by changing the "platform" from which the rest of the body functions. This means that light can influence human performance in all its aspects; cognitive as well as visual. (p.2-3)

Light is the primary stimulus for synchronizing the circadian system. Each morning, the sleep wake cycle is reset by light to "be in concert with the night-day cycle"(Rea, et al., 2002).

Perceptual system

The third means whereby lighting conditions can affect work is through the perceptual system. The perceptual system takes over once the retinal image has been processed by the visual system. The simplest output of the perceptual system is a sense of visual discomfort, which may change the observer's mood and motivation, particularly if the work is prolonged.

Lighting conditions in which it is difficult to achieve a high level of visual performance will be considered uncomfortable, as will conditions in which the lighting leads to distraction from the task, which can occur when glare and flicker are present. But perception is much more sophisticated than just producing a feeling of visual discomfort. In a sense, every lighting installation sends a 'message' about the people who designed it, who bought it, who work under it, who maintain it, and about the place where it is located. Observers interpret the 'message' according to the context in which it occurs and their own culture and expectations.

The importance of this 'message' is sometimes enough to override conditions that might be expected to cause discomfort. For example, lighting conditions that would be considered

[6] In addition to spectrum and quantity, the characteristics of light that influence the circadian system are timing and duration.

extremely uncomfortable in an office are positively desired in a dance club. According to what the intended or perceived 'message' is, the observer's mood and motivation can be changed.

It is important to appreciate that each of these routes can also interact. For example someone who is asked to work while sleep-deprived will be fatigued. This fatigue will affect task performance through both its cognitive and visual components. Conversely, people who are performing a task that is visually difficult for a long time will experience fatigue, even if they are not sleep-deprived. Another example would be a situation where the lighting provides poor task visibility, so that visual performance is poor. If the worker is aware of the poor level of performance and it fails to meet his or her expectations, then the worker's mood may be altered. Multiple interactions of this type can occur. To further complicate the picture, it is necessary to appreciate that while visual performance for a given task is determined by the lighting conditions alone, a worker's motivation can be influenced by many different factors apart from lighting conditions. As for the circadian system, this can be influenced by such factors as the timing of exercise and social cues as well as light exposure. It is this complex pattern of interacting effects that has made the study of the relationship between lighting and human performance so prolonged and difficult. (p.2-4)

No studies were found detailing daylighting's effect on visibility tasks[7]. What we do know has been extrapolated from studies conducted with FSFL (McColl and Veitch, 2001). McColl and Veitch, after conducting an extensive literature review on FSFL stated, "For most people, and most tasks, there is no evidence that any particular lamp type is better than any other in its effects on people." (p.13)

A frequently quoted study by Berman et al. (1993) claimed that a 'cool' light source (towards the short end of the spectrum), through its effects on pupil size, would lead to better visual performance. However, experiments and field studies with more naturalistic viewing conditions and white lamps of varying spectral power distributions (SPD) have failed to find comparable effects (Veitch, 2001). Boyce et al. (2002) concluded that spectrum may indeed impact task performance under extreme laboratory conditions, but "such conditions will rarely be of practical interest." (p.14) The visual system simply does not care whether the light is delivered through daylighting or an electric lighting installation.

What daylight (and electric light sources of similar CRI) does offer is good color rendering[8]. This will be important for any task where color discernment is critical (for example, matching dental ceramics). We should note two more attributes of daylight: 1) daylight delivered through a window differs from most overhead lighting installations in its ability to model 3-dimensional objects. In an office environment, especially those that utilize computer screens this has no effect on visual performance; and 2) light levels delivered by daylight (see section on light sources) may be a component critical to the synchronized functioning of the circadian system.

Disruption of normal circadian rhythmicity has been linked to several clinical conditions, including abnormal sleep-phase disorders and Seasonal Affective Disorder (SAD) (Rusak et al.,

[7] Any lighting installation, be it daylighting or electric lighting, can hinder ability by acting as a glare source and reducing contrast.
[8] Good color rendering also can make objects, such as retail merchandise, look appealing.

1997; Rusak, 2001). A sub-clinical form of SAD ("winter blues") has been identified, and is considered to be more prevalent than the clinical form (Rusak et al., 1997). Bright light therapy is now well established as an effective treatment for SAD. Evidence also supports its use for people with the sub-clinical form (Rusak et al., 1997).

In summary, the visual system is well understood. Daylight offers no unique characteristic that cannot be duplicated by electric light as it relates to visual performance. The circadian system has the potential to affect both ability and mood, and therefore, 'the platform' from which an individual operates. The characteristics of light that are important to the circadian system (as well as the visual system) are: quantity, spectrum, spatial distribution, timing, and duration. Daylight offers the quantity and spectral content of light necessary for proper circadian functioning, and if received by the eye at the critical time and for the right duration, will enable the circadian clock to synchronize to its environment, thereby promoting the potential for high performance**.** The perceptual system is infinitely complex. Studies addressing mood have produced conflicting results, and due to the idiosyncratic nature of this system, will continue to do so.

Few studies have dealt directly with daylighting and productivity, and those frequently are anecdotal reports. Literature pieces that promote a direct link between daylighting and productivity frequently cite studies dealing with windows and daylight preference as support for their argument.

The literature strongly supports people's preference for windows and daylighting (Markus, 1965; Ruys, 1970; Jackson and Holmes, 1973; Ne'eman and Longmore, 1973; Collins, 1975; Ludlow, 1976; Cuttle, 1983; Heerwagen and Heerwagen, 1986; Leslie and Hartleb 1990; Leslie and Harleb, 1991; Boubeki et al., 1991). While these studies have shown a preference for daylighting, they have not separated daylighting from the elements commonly associated with windows.

Windows not only provide illumination, they present a view, which is highly desirable but very complex in terms of its psychological impact. Most notably, views have been appreciated for the information they present regarding the weather and time of day (Hopkinson, 1966; Ne'eman and Longmore, 1973; Collins, 1975; Heerwagen, 1986; Butler and Biner, 1989). Therefore, window studies have an inherent flaw when it comes to studying daylighting's impact on productivity. Having said that, we will attempt to review the literature that directly addresses the topic of daylighting and productivity.

Two studies conducted in the 1960's assessed the impact of windowless schools on scholastic performance, physical health, and mental health. While the authors found no effect on performance, the measures used in these studies (as well as studies showing changes in performance) have been criticized as not being highly sensitive.

Larson (1965) conducted a three-year study of elementary school children in Michigan. This study allowed for students to experience both the windowless classroom, as well as the windowed classroom. The authors found no significant effect on scholastic performance or absenteeism. Demos et al. (1967) in a California study, compared achievement and personality scores, school health records, and grade point averages of elementary children in windowed

and windowless classrooms. The authors found no significant difference in performance or health.

Tognoli (1973) looked at short-term memory of subjects placed in a windowless room, in relation to subjects in a room with windows. The author found no significant effect on short-term retention. Brill et al. (1985) in a general survey of the office environment, briefly examined performance at various distances from a window. They found no evidence that windows had an effect on performance.

Stone and Irvine (1991) measured the performance of a managerial task in a room with a window, and a room without a window. No statistically significant effects of having a window were found for task performance or mood. Leslie and Hartleb (1991) looked at the effect of windows on the performance of an anagram task. While they were able to show an effect, the authors concluded that windows have a relatively minor influence on productivity, mood, and decision-making.

A study by Kuller and Lindstrom (1992) looked at health and behavior of children in classrooms with and without windows for an entire academic year. The study followed the children's production of cortisol, a stress hormone whose output is governed by the body's biological clock. On the basis of cortisol measurements they concluded that "work in classrooms without daylight may upset the basic hormone pattern and may in turn influence children's ability to concentrate or cooperate and also eventually impact annual body growth and sick leave" (Kuller and Lindstom, 1992). This study has met with some criticism based on interpretation of the results (Rusak et al., 1997). In addition, the authors failed to show any negative impact on the children's performance or health.

Hedge (1994) looked at performance using a simulated computer task in two rooms lit with electric lights. One room had windows, and one did not. He found a small but statistically significant improvement in task performance when windows were present. It is not clear whether this occurred because the presence of windows improved the stimuli the tasks presented to the visual system, or changed the operating state of the visual system, or because the subjects were in a better mood.

The Rocky Mountain Institute (1994/1998), whose goal is to foster the efficient and sustainable use of resources, presented two anecdotal studies showing an increase in productivity, and/or a decrease in absenteeism. Both studies concerned newly built facilities with many amenities, including an atrium space. One such facility was the International Netherlands Group (ING) Bank, where absenteeism dropped 15% and remains 15% lower than in the bank's old building. The other was a frequently quoted study, the Lockheed Martin Building 157 in Sunnyvale, California.

The Lockheed Martin Building 157, with its 15-foot-high window walls, has been described "as a beautiful space…a space the employees love". (p.8) Lockheed itself has never published the figures concerning the improvements in absenteeism and productivity. This information was relayed to the Institute by the chairman of the Department of Environmental Studies at San Jose State, who said "Lockheed moved a known population of workers into the building and absenteeism dropped 15 %." (p.9)

We do not doubt the decrease in absenteeism and the perception of an increase in productivity. However, these new, well-designed buildings present a host of variables, aside from daylighting, that could contribute to the findings.

The next three school studies are frequently grouped together in a discussion of the positive effects of daylighting on productivity. The first study by Hathaway (1995) is not a daylighting study, but rather a FSFL study. The Bailey study (1997) was conducted by the architecture firm that designed the schools being analyzed. The third study was conducted in 1999 by the energy-consulting firm, Heschong Mahone.

The Hathaway study (1995) is the only one of these three to actually set up an experiment with controls. The author looked at 4th graders from five schools in Alberta, Canada.
Over a two-year period, children attending elementary schools with full spectrum lights with varying amount of UV were compared with children in classrooms with cool white fluorescent lights. The author concluded that students under FSFL with enhanced UV developed fewer dental cavities, and had better attendance, achievement, growth, and development than students under other lights. This study has been critiqued by several researchers in the lighting community (Levin, IRC Internal Report No. 659) as well as from other disciplines (Rusak et al., 1997). The study is viewed as having a number of confounding factors. Rusak states: "the study was flawed in design, execution, and analysis, and essentially no reliable conclusions can be reached based on it" (Rusak et al., 1997, p.75). Since this study did not control for the daylight in the classrooms, there was no population to compare performance against; everyone had daylight. In addition, no records were kept of daily light exposure during recess.
The Bailey study (Nicklas and Bailey, 1997) was not a controlled experiment; rather it was an analysis of achievement scores collected over four years. They were able to compare test scores for grades 3-5 in three different schools. The daylight schools were built because the 'old' schools burned to the ground. While the new schools were being built, the students were in mobile units and other temporary facilities.

While they did find an increase in student performance in relation to both the 'old' school and the temporary school, they did not conduct a statistical analysis of the data. The study should be examined with reservation since: 1) they compared test scores of grades 3-5 from year to year and, therefore were comparing different student populations against each other. 2) teacher ability and motivational capabilities were not considered. 3) the amenities of the new school provided more than daylight and are potentially confounding factors. 4) no mention was made of the lighting installations in the new schools in relation to the "old" schools. 5) they state, "windows were also incorporated for view" – a known confound. It should be noted that student performance while in the portable school was consistently less than the performance in both the 'old' school and the new daylight school.

The Heschong study (1999) is quite possibly the most quoted study on this topic. They analyzed standardized tests for approximately 21,000 students, grades 2-5, in Capistrano, Ca., Seattle, Wa., and Fort Collins, Co.

The California district provided the most thorough data from approximately 8000 students. The authors found that students with the most daylighting in their classrooms progressed 20% faster on math tests and 26% on reading tests. The tests for California were given at the beginning of the school year as well as the end of the school year. They report that students in classrooms with the largest window areas were found to progress 15% faster in math and 23% faster in reading than those with the least. In addition, students in rooms with operable windows (allowing for ventilation) were found to progress 7-8% faster than those in fixed window rooms.

The authors stated that their original intention was to isolate skylights from windows. However this did not come to fruition, and the data for rooms with skylights always included a window component. Some spaces had no windows, some had windows only, and some had both windows and skylights.

Forty percent of their data set for California was from portable classrooms. These had only one small window[9] (please see note below). The authors stated, "Because every school site had at least a handful of portables, and because of their uniformity across schools, the portables served as something of a 'placebo' in our analysis." (p.26) They found that students in rooms with both skylights and windows progressed 19% to 20% faster. The authors stated a high (99%) statistical certainty on all measures.

The Seattle and Fort Collins school districts administer only one standardized test per year. In both districts students with the most daylighting were found to have 7% to 18% higher scores than those with the least—again with a statistical certainty.

The authors, in a re-analysis (Heschong Mahone, 2002) found that physical classroom characteristics (daylighting, operable windows, air conditioning, portable classrooms) do not have an effect on student absenteeism. The re-analysis addressed earlier criticism concerning teacher bias – they found no bias. The Heschong Mahone study has gained a considerable amount of attention. This can be attributed to the fact that they 1) provided a large sample size to be statistically analyzed, and 2) claimed a statistical certainty in their findings.

Analyzing such a large sample size is bound to show a significant effect. They do show a significant improvement in scholastic performance over a year, however they fail to show a correlation between daylighting and improved performance. The authors show a 99% statistical certainty that there was an increase in performance, but the correlation value, R^2, was 0.25-0.26. This is the real value of interest, and it is too small to make any claims that daylighting was responsible for the increase in performance. In fact when the correlation value is looked at closely, the apparent reason the students performed better on reading and math tests at the end of the year (grades 2 and 3), was simply because they stayed in school for the year. Daylighting contributed very little.

[9] The authors mention that 60-80% of the time, the door to these portable rooms was opened for ventilation throughout the school year. In fact they state that the opened door provided enough daylight to increase it one rank, on a scale of 0-5. Originally the portables were given the rating of 1 (minimal daylighting, small token window), they were upgraded to 2 (poor daylighting, illumination is always inadequate without electric lights). While traditional classrooms had fairly consistent electric lighting, the portables' electric lighting was highly variable.

It is also important to point out that the results showing an increase on math tests and on reading test were found when comparing classrooms with no daylight (rank 0) to classrooms with the 'best' daylighting (rank 5). If daylighting did contribute to increased productivity, we should expect to see a trend of increased performance when comparing the classrooms of the middle ranks (rank 1, 2, 3, and 4). Unfortunately these data were not provided. In addition, as with the studies already reviewed, this study has not addressed environmental confounds that might have contributed to the results.

Based on the idea that daylight will not have a consistent effect on productivity via the visual system or the perceptual system, Figueiro et al. (2002) looked at daylighting and productivity through the framework of circadian disruption. The authors hypothesized that in winter months (when bright light exposure is limited on the commute to and from work) people occupying interior windowless offices, would be less productive than a matched group of people in windowed offices. Operationally, it was reasoned that people in interior offices would spend less time in their offices (due to illness or self-medication[10] in bright locations) and less time working on their computers than their colleagues in windowed offices. It is important to emphasize that occupants of both windowed and interior offices held similar job positions.

The authors found no difference in occupancy, but people in windowed offices spent significantly more time working on the computer (t_7, $p<0.001$) and significantly less time talking to people (t_7, $p<0.003$) or talking on the telephone (t_7, $p<10^{-7}$) than people in interior offices. The authors hypothesize, that during the summer months (when individuals are exposed to bright light on the commute to and from work) these differences in behavior will disappear. While these studies need to be replicated in a larger population, the authors have established a plausible framework of investigation into why daylighting might affect productivity.

[10] Studies by Schaap and Meijer (2001) have shown that circadian disruption can be counteracted through social interaction (such as talking on the phone, etc.), as well as through bright light exposure.

REFERENCES

Aronoff, S., Kaplan, A. (1995). *Total Workplace Performance: Rethinking the Office Environment*. WDL Publ. Ottawa, CN.

Berman, S.M., Fein, G., Jewett, D.L., and Ashford, F. (1993). "Luminance-controlled pupil size affects Landolt C task performance." *Journal of Illuminating Engineering Society*, 22, 150-165.

Boubekri, M., Hull, R.B., and Boyer, L.L., (1991). "Impact of window size and sunlight penetration on office workers' mood and satisfaction: A novel way of assessing sunlight." *Environment and Behavior*, 23:(4), 474-493.

Boyce, P.R. (1998). "Why daylight?" Conference Proceedings: International Daylighting Conference 1998, May 10-13, 1998 Ottawa, CN.

Boyce, P.R. (1994). "Is full-spectrum lighting special?" In J.A. Veitch (Ed)., *Full-spectrum lighting effects on performance, mood, and health* (IRC Internal Report No 659, 30-36). Ottawa, ON: National Research Council of Canada, Institute for Research in Construction.

Boyce, P.R., and Rea, M.S. (2001). *Lighting and Human Performance II: Beyond Visibility Models Toward a Unified Human Factors Approach to Performance*, EPRI, Palo Alto, CA, National Electrical Manufacturers Association, VA, and U.S. Environmental Protection Agency Office of Air and Radiation, DC: 2001. 1006415.

Boyce, P.R., Akashi, Y., Hunter, C.M., and Bullough, J.D. (2002). "The impact of spectral power distribution on task performance." *Lighting Research and Technology*. submitted for publication.

Brill, M., Margulis, S., and Konar, E., with BOSTI. (1985). Using Design to Increase Productivity, vol.1 "Lighting." *Workplace Design and Productivity*, Inc., New York.

Butler, D. L., & Biner, P. M. (1989). "Effects of setting on window preferences and factors associated with those preferences." *Environment and Behavior*. 21.17-31.

Collins, B.L. (1975). *Windows and People: A Literature Survey: Psychological Reaction to Environments with and without Windows*; National Bureau of Standards Building Science Series 70, U.S. Department of Commerce.

Cuttle, C. (1983), "People and windows in workplaces." Proceedings of the People and Physical Environment Research Conference, Wellington, New Zealand.

Demos, G., D., Davis, S., and Zuwaylif,, F.F.(1967). "Controlled physical environments." *Building Research*, 4, 60-62.

Ferguson, E. D. (2000). *Motivation: A Biosocial and Cognitive Integration of Motivation and Emotion*. New York: Oxford University Press.

Figueiro, M.G., Rea, M.S., Rea, A.C., and Stevens, R.G. (2002). "Daylight and productivity : A field study." ACEEE Conference Proceedings, Summer 2002.

Hathaway, W. (1995). "Effects of school lighting on physical development and school performance." *The Journal of Educational Research,* 88:(4).

Hedge, A. (1994). " Reactions of computer users to three different lighting systems in windowed and windowless offices." *Work and Display Units*, '94. B54-B56.

Hedge, A. (2000). "Where are we in understanding the effects of where we are?" *Ergonomics*, 2000, 43:(7) 1019-1029.

Heerwagen, J.H. (1986). "Windowscapes: The role of nature in the view from the window." Conference Proceedings: International Daylighting Conference 1986, November 4-7, 1986 Long beach, California, U.S.A.

Heschong Mahone Group(1999). "Daylighting in schools: An investigation into the relationship between daylighting and human performance." Pacific Gas and Electric.

Heschong Mahone Group (2002). "Daylighting in schools: Additional analysis." New Buildings Institute.

Hopkinson, R.G., Petherbridge, P., Longmore, J.(1966). Daylighting. London: Heinemann.

IESNA Lighting Handbook, ninth edition.(2000). Illuminating Engineering Society of North America. M.S. Rea (Ed.).

Jackson, G. J., and Holmes, J. G. (1973). "Let's keep it simple – what we want from daylight." *Light and Lighting*, (12) 80-82.

Kuller, R., and Lindstren, C. (1992). "Health and behavior of children in classrooms with and without windows." *Journal of Environmental Psychology*, 12, 305-317.

Larson, C. T. (1965). " The effect of windowless classrooms on elementary school children." Architectural Research Laboratory, Department of Architecture, University of Michigan.

Leslie, R., and Hartleb, S. (1990)."Windows, variability, and human response." Proceedings, International Daylighting Conference, Moscow, 1990.

Leslie, R., and Hartleb, S. (1991). "Some effects of the sequential experience of windows on human response", *Journal of the Illuminating Engineering Society*, 91-99, Winter 1991.

Levin, R.E., "Full-spectrum lighting." In J.A. Veitch (Ed)., *Full-spectrum lighting effects on performance, mood, and health* (IRC Internal Report No 659, 127-128). Ottawa, ON: National Research Council of Canada, Institute for Research in Construction.

Ludlow, A. M. (1976). "The functions of windows in buildings." *Lighting Research and Technology.* 6(2). 57-68.

Markus, T. A. (1967). "The function of windows: A reappraisal." *Building Science,* 2, 97-121.

McColl, S.L., and Veitch, J. A. (2001). "Full- spectrum fluorescent lighting: A critical review of its effects on physical and mental health." *Psychological Medicine*, 31, 949-964.

Ne'eman, E., and Longmore, J. (1973). "Physical aspects of windows: Integration of daylight with artificial light." Proceedings of CIE Conference, Istanbul on 'Windows and their function in architectural design', October 1973.

Nicklas, M. and Bailey, G. (1997). "Analysis of the performance of students in daylit schools", Proceedings of the 1997 Annual Conference, ASES.

Norris, D. and Tillett, L. (1997). "Daylight and productivity: Is there a causal link?" Proceedings, Glass Processing Days Conference, Tampere, Finland.

Rea, M.S., Rutledge, B., Maniccia, D. (1998). "Beyond daylight dogma." Conference Proceedings: International Daylighting Conference 1998, May 10-13, 1998 Ottawa, Ontario, Canada.

Rea, M. S., Figueiro, M. G., and Bullough, J.D. (2002). "Circadian photobiology: An emerging framework for lighting practice and research." *Lighting Research and Technology,* in press.

Romm, J.J., Browning, W.D. (1994; revised 1998). "Greening the building and the bottom line: Increasing productivity through energy-efficient design." Rocky Mountain Institute.

Rusak, B., Eskes, G.A., and Shaw, S.R. (1997). "Lighting and human health: A review of the literature." Canada Mortgage and Housing Corporation, Ottawa.

Rusak, B.(2001)."Health effects of disrupted sleep and circadian rhythms." in Final Report to the Canadian Institutes of Health Research, December 8-9, 2001, Halifax, Nova Scotia.

Ruys. (1970).Windowless Offices (M.A. Thesis, University of Washington, Seattle, Washington**.**

Schaap, J., and Meijer J. (2001)."Opposing effects of behavioural activity and light on neurons of the suprachiasmatic nucleus." *European Journal of Neuroscience*13,1955-1962.

Stone, N., and Irvine, J.(1991). "Performance, mood, satisfaction and task type in various work environments: A preliminary study." *Journal of General Psychology*. 120, 489-497.

Thorington, L. (1985)."Spectral irradiance and temporal aspects of natural and artificial light" in R.J. Wurtman (Ed)., *Annals of the New York Academy of Sciences* vol. 453: 'The medical and biological effects of light.' 28-54.

Tognoli, J.(1973). " The effect of windowless rooms and unembellished surroundings on attitudes and retention." *Environment and Behavior*, 5, 191-201.

Veitch, J.A. (2001). "Lighting quality contributions from biopsychological processes." *Journal of the Illuminating Engineering Society*, 30(1), 3-16.

8.0 Conclusions and Future Research Efforts

The research efforts to develop, test, and evaluate a computational model capable of accurately predicting the chromaticity values of collected and fiber-optically-distributed sunlight have, for the most part, been successful. Although significant system design questions still remain, and additional research and experimental verification are required, a comprehensive model of the chromatic performance of the complete Hybrid Lighting System has been developed.

In Section 7.0, a prediction of the full color deviation for the current Hybrid Lighting System design was described. Future research efforts are being planned to address the concerns these predictions may pose. Improvements to the Hybrid Lighting System's hybrid luminaire design are being considered which permit greater flexibility in color matching of dual illuminants. A hybrid luminaire design that includes a variable-color source to counterbalance color drifting in collected sunlight represents one potential means of correcting the solar color-shifting.

Future research efforts must eventually focus on the human perception of the various chromatic fluctuations identified in this report. It is not known, with any great certainty, what effect slight chromatic variations in collected sunlight will have on human performance and comfort. Human factors research into the effects of dynamic dual-source illumination must be performed to fully interpret the data presented in this report. The temporal and spectral data already computed and described should serve as a guideline for identifying variable ranges in any future human-subject experiments.

All future design improvements will be evaluated using the chromaticity model described in this report. With the possibility of some additional revisions, the chromaticity model developed provides an accurate representation of the complete Hybrid Lighting System.

ACKNOWLEDGEMENTS

The computations presented in this report were performed on a four-year solar spectra database generated using R. Bird and C. Riordan's Simple Solar Spectral Model for Direct Irradiance. Special thanks to Timothy D. Mowrer for his conversion of the original C-code Solar Spectra Program into a C++ program with an advanced graphical user interface and automation capabilities. This improvement enabled the speedy generation of multiple databases for various model parameters. The improved code is now being adapted for use as the main computation engine of an evolutionary development program aimed at finding an optimal "compensating" filter design.

Additional thanks to Tim Wendelin of NREL for his assistance in measuring the optical performance of the Hybrid Lighting System's Solar Collector primary mirror. Without his knowledge and expertise in Video Scanning Hartmann Optical Testing (VSHOT), verification of the primary mirror's ZEMAX model parameters would not have been possible.

REFERENCES

1. J. D. Muhs, “Hybrid Solar Lighting Doubles the Efficiency and Affordability of Solar Energy in Commercial Buildings”, CADDET Energy Efficiency Newsletter December 2000, p. 6.

2. J. D. Muhs, “Design and Analysis of Hybrid Solar Lighting and Full-Spectrum Solar Energy Systems”, *Solar 2000, July 16-21, 2000,* American Solar Energy Society.

3. Bird, R.E., and C. Riordan, Simple Solar Spectral Model for Direct and Diffuse Irradiance on Horizontal and Tilted Planes at the Earth's Surface for Cloudless Atmospheres, Technical Report No. SERI/TR-215-2436, Golden, CO: Solar Energy Research Institute, 1984

4. Rymes, Martin, *Solar Codes & Algorithms: SPECTRL2*, http://rredc.nrel.gov/solar/codes_algs/spectral/

5. Wyszecki, G. and Stiles, W. S., Color Science: Concepts and Methods, Quantitative Data and Formulae, 2nd ed. New York: Wiley, 1982

6. Macadam, D.L., Colour Measurement, Springer Verlag, Berlin, 1985

7. Hunt, R.W.G., Measuring Colour, Ellis Horwood, New York, 1991

APPENDIX K

RESULTS FROM AN EXPERIMENTAL HYBRID SOLAR LIGHTING SYSTEM INSTALLED IN A COMMERCIAL BUILDINGS

Jeff Muhs, Duncan Earl, Dave Beshears, and Curt Maxey
Oak Ridge National Laboratory
2360 Cherahala Blvd.
Knoxville, TN 37932

ABSTRACT

This paper describes preliminary results from research on a new hybrid solar lighting (HSL) system being developed to reduce electric lighting in commercial office buildings. A physical description of HSL system components along with preliminary results from an experimental system deployed in a commercial building in Knoxville, TN are provided. Results from a systems-level, computer-based chromaticity model are compared with experimental data. A total lumen distribution efficiency of over 50% was recorded for the initial prototype having optical fibers an average of 6 m (19.5 ft) in length. The total electrical power displacement of the 1 m^2 HSL proof-of-concept prototype is estimated to be between 522 – 2350 watts per 1000 W/m^2 of incident solar radiation depending on the type of electric lights being used in conjunction with the solar lighting system. By adding the reductions in heat gain associated with reduced electric lamp use and predicted performance improvements achieved by a system redesign, the electrical power displaced in a commercial prototype could rise to between 702 – 3160 W (peak)/m^2 not including any additional electrical power that can be generated using the otherwise wasted IR energy. The color temperature of the distributed sunlight emerging from the optical fibers is approximately 5100^{o}K and the chromaticity values in uniform color space (u'v') are approximately (.2010, .4977). These values match well with modeled results and will vary slightly depending on the day, time, atmospheric conditions, and system configuration. The paper concludes with a discussion of new value propositions that HSL provides architects, energy providers, building owners, and occupants.

INTRODUCTION

Throughout the 1900s, use of the sun as a source of energy has evolved considerably. Early in the century, the sun was the primary source of interior light for buildings during the day. Eventually, however, the cost, convenience, and performance of electric lamps improved and the sun was displaced as our primary method of lighting building interiors. This, in turn, revolutionized the way we design buildings, particularly commercial buildings, making them minimally dependent on natural daylight. As a result, electric lighting now represents the single largest consumer of electricity in commercial buildings. [1]

During and after the oil embargo of the 1970s, renewed interest in using solar energy emerged with advancements in daylighting systems, solar hot water heaters, and photovoltaics. Today, daylighting approaches are designed to overcome earlier shortcomings related to glare, spatial, and temporal variability, difficulty of spatial control, and excessive illuminance. In doing so, however, they waste a significant portion of the visible light that is available by shading, attenuating, and or diffusing the dominant portion of daylight, i.e., direct sunlight, which typically represents well over 80% of the light reaching the earth on a sunny day. Further, they do not use the remaining half of energy resident in the solar spectrum (mainly infrared radiation beyond 0.7), often add to building heat gain, require significant and expensive architectural design modifications, must be oriented properly to maximize solar utilization, and are not easily reconfigured. These drawbacks continue to limit the use of conventional daylighting approaches, and led Oak Ridge National Laboratory (ORNL) to pursue HSL system development.

Previous attempts to harness and use sunlight directly for interior lighting via fresnel lenes collectors, reflective light-pipes, and fiber-optic bundles, have been plagued by significant losses in the collection and light distribution system, ineffective use of nonvisible solar radiation, and a lack of integration with collocated electric lighting systems required to supplement solar lighting on cloudy days and at night. Another of ORNL's motivations for this research was to develop new sunlight collection, distribution, and control strategies that alleviate most, if not all, of these problems.

Similar deficiencies exist in photovoltaics, solar thermal electric systems, and solar hot water heaters. For example, the conversion efficiency of traditional silicon-based solar cells in the ultraviolet and short wavelength visible region of the solar spectrum is low and the solar energy residing beyond ~1.1 um is essentially wasted, see Fig. 1. To overcome this and address other economic barriers, one approach has been to develop utility-scale PV and solar thermal concentrators. The rationale being that the cell area and, consequently, the cell cost can be reduced by approximately the same amount as the desired concentration ratio. Unfortunately, this cost-savings is typically offset by the added cost and complexity of the required solar concentrator and tracking system. As such, the final motivation for this research is to comparatively assess the feasibility of HSL and existing solar options used in

commercial buildings, and determine if HSL is a more cost-effective alternative.

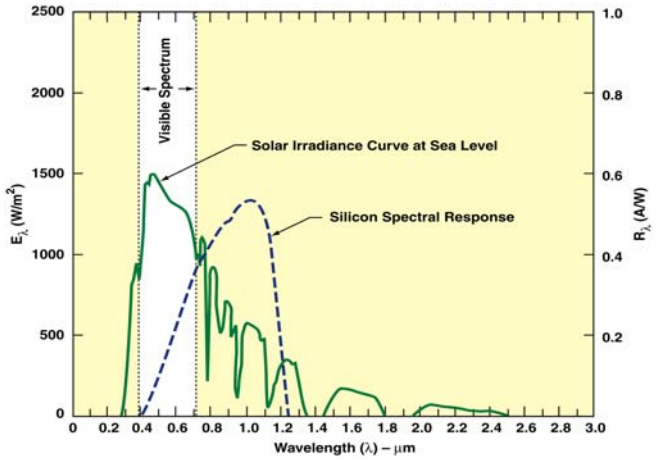

Fig. 1. Approximate Spectral Radiance E_l of the Sun at Mean Earth-Sun Separation and Silicon Spectral Response (R_l)

Physical description of HSL system components

Initial hybrid solar lighting systems consist of three primary components, as illustrated in Fig. 2. The sunlight collector consists of a 1.1 m diameter parabolic primary mirror with a 0.3 m hole in the center and a nominal 94% reflective enhanced aluminum surface. This equates to a total collection area of 1 m^2. The segmented secondary mirror consists of eight planar facets designed to separate and focus the visible portion of sunlight into eight large core optical fibers while simultaneously transmitting the ultraviolet and infrared energy. For the engineering prototype collector shown in Fig. 3, each segment of the secondary mirror (nominal 92% reflectivity) redirects ~.0125 m^2 of the visible portion of sunlight into a large core (12.6 mm) optical fiber. A schematic representation of the optical design of the collector/concentrator is provided in Fig. 4.

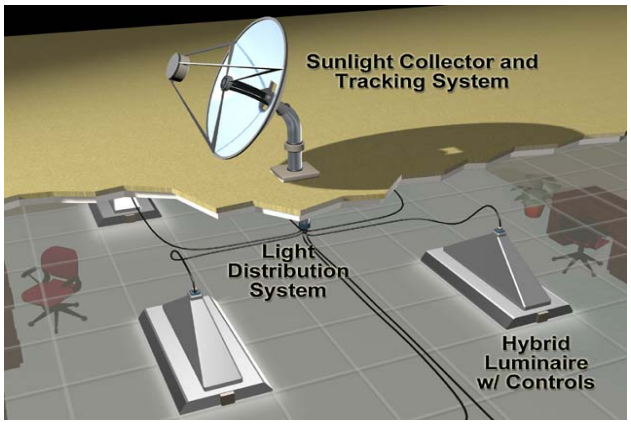

Fig. 2. Hybrid lighting combines sunlight and electric light sources into integrated, energy-efficient "hybrid" lighting system

Fig. 3. Prototype Collector installed at the NTRC Facility in Knoxville, Tennessee

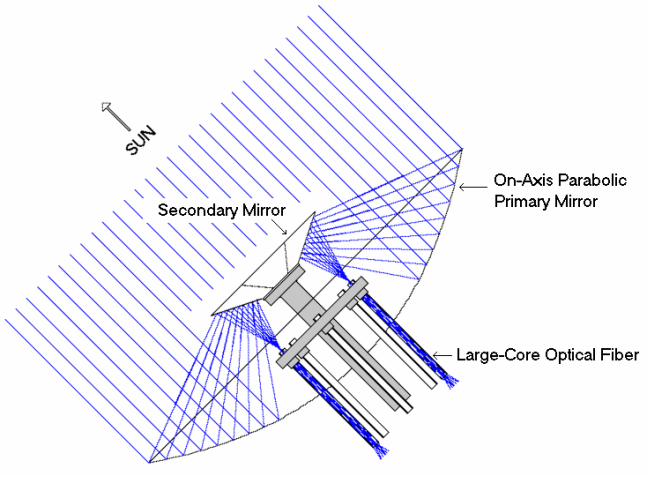

Fig. 4. Solar Collector Design

In addition to the optical components, each collector includes a two-axis tracker with associated precision open-loop controls (provided by Enhancement Electronics Inc.), optical filters, and mounting hardware for the mirrors and optical fibers. The collector is mounted on a 4-inch schedule 80 pipe that penetrates the building roof. These components and their effect on the overall system performance are described by Beshears, et. al. [2]

The large core polymer optical fiber used to transport the light from the rooftop to fixtures was manufactured by 3M (product number LF120C). Cates et. al., describes the spectral-dependent loss characteristics of the fiber as a function of launch angle, bend radii, number of bends, and fiber length. [3] For a single story application, the fibers used range from 4 to 9 m in length depending on the location of the collector relative to the hybrid luminaries discussed below. The average length of each fiber is 6 m.

Initially, each luminaire consists of a traditional 2x4 foot light fixture containing four fluorescent lamps (Lithonia GT8 Fixture – 2GT8-4-32-A19). The fixtures have been slightly modified to accommodate two sunlight diffusing rods (see Fig. 5) or a fresnel lens/holographic optical element (see Fig. 6) that spatially distribute the sunlight similar to co-located electric lamps. Preliminary results from initial luminaire designs are discussed by Earl, et. al. [4]

Results from HSL chromaticity and efficiency system performance model

Each component in the system exhibits its own spectral response. To predict the overall spectral response of the experimental system, a HSL chromaticity model was developed by ORNL and RPI-LRC to determine the chromaticity values in C.I.E. uniform color space, correlated color temperature (CCT), and color rendering index (CRI) of distributed sunlight emerging from the hybrid luminaires. The model allows users to input the spectral characteristics of: a) the solar light source based on time, date, location, temperature, and general atmospheric conditions, b) the primary mirror and C) secondary mirror. It also allows users to input the launch conditions of light entering the optical fiber, the spectral attenuation rate of the fiber being used, and the length of the optical fibers. The model predicts the spectral power distribution, CCT, and chromaticity values. Table 1 shows the results of the HSL model given the input parameters associated with the experimental system using fibers from 4.5 – 10.5-m in length.

Table 1. Model Results for Oct. 17, 2002 (1:00pm)

Fiber Length (m)	Chromaticity Value (u',v')	CCT (K)
4.5	(.2019, .4957)	5098
5.5	(.2007, .4967)	5123
6.5	(.1995, .4977)	5147
7.5	(.1984, .4986)	5169
8.5	(.1972, .4995)	5190
9.5	(.1961, .5005)	5210
10.5	(.1951, . 5014)	5229

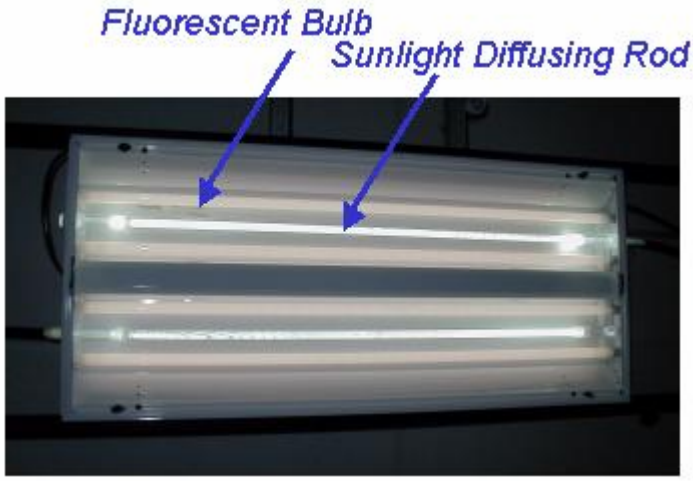

Fig. 5. Luminaire Accommodating Two Sunlight Diffusing Rods

Fig. 6. Fresnel Lens/Holographic Optical Element

Preliminary results from the HSL commercial building experimental system

On Oct. 17, 2002, between 11:00 am – 2:00 pm, data was taken on the experimental system described earlier to compare and verify the accuracy of the above model. Multiple measurements of the delivered lumens, chromaticity, and correlated color temperature were taken using a 50-cm. diameter-integrating sphere coupled to a spectrometer (Oriel Multispec). It should be noted that the primary and secondary mirrors had not been cleaned prior to the measurements

Table 2 summarizes the chromaticity values, correlated color temperature, and system efficiency from the same fiber at lengths of 7.5, 8.5, 9.5, and 10.5 meters, respectively on Oct. 17 from 11:00 a.m. to 2:00 p.m. The results match well with the chromaticity model results summarized earlier. Table 2 also includes extrapolated data for shorter lengths of fiber used in the experimental system, however, measurements at floor level in the experimental facility could not be taken at these fiber lengths because of physical limitations.

For a fiber length of 10.5 meter, Figure 7 compares the spectral power distribution predicted by the HSL chromaticity model with the measured spectral data acquired from the HSL system. The two curves differ only slightly over most of the visible range, with differences at higher wavelengths (700-780nm) being attributed to spectral differences in the actual and modeled cold mirror coatings of the secondary mirror.

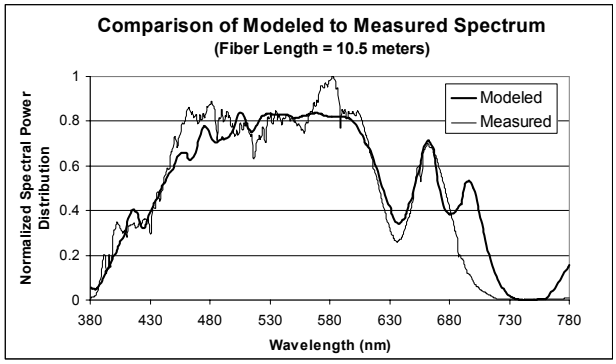

Fig. 8. Comparison of Modeled and Experimental Data

Table 2. Experimental Results w/ extrapolated data points

Fiber Length (m)	System Efficiency (%)	Chromaticity Value (u',v')	CCT (K)
4.5*	53.5	(.2026, .4979)	5033
5.5*	51.7	(.2016, .4978)	5073
6.5*	49.9	(.2006, .4976)	5111
7.5	48.1	(.1996, .4975)	5150
8.5	45.8	(.1987, .4978)	5182
9.5	44.9	(.1975, .4976)	5243
10.5	42.6	(.1965, .4981)	5268

* Denotes values extrapolated from data at longer fiber lengths

To evaluate system efficiency, the total optical flux delivered by the eight optical fibers was measured. The delivered flux value was then divided by the simultaneously measured direct-beam solar flux, recorded using a normal incidence pyrheliometer (NIP sensor) placed near the solar collector. It is estimated that measurement errors of ±5% could be expected in the above data as a result of optical misalignments, variable atmospheric conditions during the measurements, and or calibration errors in the NIP Sensor. Further measurements are planned to more accurately evaluate the efficiency of the system under more suitable measurement conditions with fully calibrated detectors.

Nonetheless, using the preliminary measured efficiency of 50%**,** and assuming the sunlight diffusing rods and co-located fluorescent lamps (rated at ~90 l/w) result in an equivalent luminaire efficacy, the total electrical power displaced by the 1 m^2 experimental system is estimated to be 522 watts peak based on very preliminary estimates. These values jump to 2350 when incandescent lamps are used.

Since artificial lighting is exclusively an electric industry, this represents a 7X – 31X improvement over solar option available today for lighting the interior of buildings, e.g. photovoltaic cells. This assumes a total system efficiency of 7.5% for a low-cost, silicon-based PV system. Stated another way, between ~14 to 62 m^2 of commercially-available, silicon-based PVs would be required to displace the same amount of nonrenewable electricity as a 2 m^2 HSL system.

Methods of improving the performance of the experimental system

To improve performance of the HSL system, modifications to the secondary mirror and fiber mounting hardware are needed. In the current system, the visible portion of sunlight enters the fibers at an average angle of incidence of over 15 degrees, as illustrated in Fig. 9 and Table 3. By redesigning the above components so that the fiber is properly aligned with the incoming light, model results suggest a 17% improvement in distribution efficiency will be obtained.

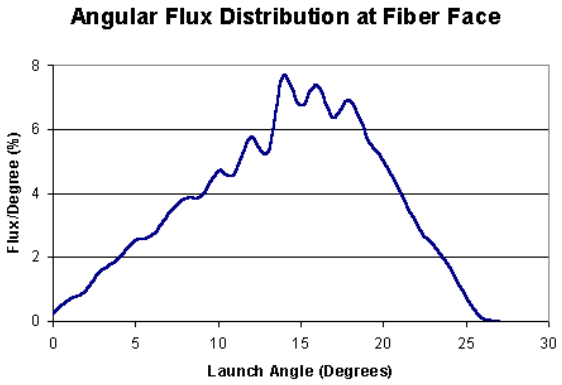

Fig. 8. Launch conditions in experimental HSL system

Angular Range	Percent Flux (%)
0 to 5 degrees	6
5 to 10 degrees	16
10 to 15 degrees	28
15 to 20 degrees	33
20 to 25 degrees	16
25 to 30 degrees	1
30 to 90 degrees	0

Table 3. Discrete Angular Flux Distribution

HSL Value Propositions

Unlike other renewable energy technologies that generate electricity, the tangible benefits of hybrid solar lighting can be easily understood and visualized by architects, building owners and workers and students using the light to perform visual tasks. From a global perspective, the value propositions of hybrid solar lighting are a lower cost, more-efficient solar alternative to photovoltaics, energy savings, a subsequent reduction in greenhouse gas emissions, and higher quality lighting.

Value propositions to architects and contractors – Initially, environmentally sensitive architects and contractors will likely view the use of hybrid solar lighting as a unique method of making a corporate statement towards environmental sustainability. As knowledge of the technology grows, architects and contractors will begin to appreciate the other value propositions HSL provides them. Architects wishing to incorporate daylighting strategies into their building designs are currently plagued by several problems. First, in order to maximize daylighting efficiency, site layouts dictate that windows, light shelves, and roof monitors face south in the U.S. This is not always possible given urban site constraints. Second, in order to eliminate glare and over-illumination and increase light penetration depth, expensive, labor-intensive additions such as mentioned above are required. In addition to being expensive, these additions take up space, require large roof and wall penetrations, cannot be easily reconfigured, often add significantly to the air-conditioning load, and often require higher ceilings. Hybrid lighting eliminates the above problems and offers architects and building contractors the convenience of efficient, easy to install, "plug-and-play" daylighting. In the retrofit market, architects and contractors can more readily incorporate HSL into existing buildings whereas other daylighting strategies typically cannot be incorporated. Last, because light from an HSL system emerges at the same location as co-located electric lamps, significant costs associated with properly commissioning daylight harvesting systems are significantly reduced or eliminated.

Value propositions to building owners - HSL minimizes a building owners operational risk because the units are removable and inherently have an electrical back up if the HSL system fails. Further, HSL requires fewer and smaller roof penetrations compared to traditional skylights. This translates into fewer and less severe leaks. For example, in a large retail store over 1000 linear feet of roof penetration is required to install typical skylights. Using HSL, this value can be reduced to less than 50 linear feet of roof penetration. In one business model being contemplated, installed HSL systems may be partially- or fully-owned by an energy service provider or utility with the resultant light sold like electricity is today in a $/klumh basis. Under such a scenario, building owners will incur less up-front capital costs and will not be responsible for maintaining the equipment once installed.

Value propositions to users - Users of HSL include all building occupants (tenants and their employees, customers, patients, students, etc.). The value proposition to building occupants is primarily the glare-free, even distribution and use of desirable, full-spectrum sunlight as opposed to electrically-generated light from such sources as fluorescent lamps and incandescent bulbs. Several credible scientific reports and studies detailing how sunlight increases worker health and productivity, improves patient health, boosts student test scores, and improves retail sales have been published. [1]

Value propositions to green power users – Green power users are organizations who agree to pay more (typically 15 – 20%) for a portion of their electricity in return for the satisfaction in knowing an equivalent amount of power is generated through clean energy means such as wind, PV's, and biomass. Ironically, green power demand is now surpassing available supply in most regions of the country. To these customers, HSL provides a tangible benefit in the form of higher quality lighting. In such programs, users of green power will likely be willing to pay a small premium for distributed sunlight because of the full-spectrum nature of the light being used.

CONCLUSION

This paper has described preliminary results from research on a new hybrid solar lighting (HSL) system being developed by the Oak Ridge National Laboratory and several university and industry partners. Based on initial results, the total electrical power displacement of the initial HSL on a per square meter basis is estimated to be 522 – 2350 watts (peak), depending on a number of factors associated with the electric lighting system being used in combination with the solar lighting system. By adding in reductions in heat gain associated with less use of electric lamps (an expected 15% savings) and modeled performance improvements that can be achieved by directing sunlight into the optical fibers at lower angles (an expected 17% improvement based on ray-tracing models), the electrical power displaced in a commercial prototype could rise to between 702 – 3160 W peak. New value propositions that HSL provides architects, building owners, occupants, and green power users have also been detailed in the paper.

ACKNOWLEDGEMENTS

The authors thank colleagues John Jordan, Gary Capps, Mike Cates, Supriya Jaiswal, Leesa Laymance, John Turner, and Steve Allison, for their hard work and commitment to the HSL program. They also thank the sponsors of this work at the U.S. Dept. of Energy's Office of Energy Efficiency and Renewable Energy (EERE) and the Tennessee Valley Authority (TVA). The authors also thank their many university and industry partners associated with the EESI Project. Finally, the lead author wishes to thank ORNL's Art Clemons for his dedicated commitment and shared leadership of the HSL vision.

REFERENCES

1. Loisos, G., "*Skylighting and Retail Sales, An Investigation into the Relationship Between Daylighting and Human Performance*," Design Initiative, California Board for Energy Efficiency Third Party Program, August 1999.
2. Beshears, D. L, et. al., "*Tracking Systems Evaluation For The 'Hybrid Lighting System'*," ASME/JSME, Proceedings of ISEC 2003, March 2003
3. Cates, M. R., et. al., "*Characterization Of Transmission Properties of 3m Lf120c Plastic Optical Light Guide*," ASME/JSME, Proceedings of ISEC 2003, March 2003
4. Earl, D. D., et. al., "*Performance Of New Hybrid Solar Lighting Luminaire Design*," ASME/JSME, Proceedings of ISEC 2003, March 2003